

**PROCESS PLANNING FOR THICK-FILM MASK PROJECTION MICRO
STEREOLITHOGRAPHY**

A Thesis
Presented to
The Academic Faculty

by

Xiayun Zhao

In Partial Fulfillment
Of the Requirements for the Degree
Master of Science in Mechanical Engineering

Georgia Institute of Technology

May, 2009

Process Planning for Thick-film Mask Projection micro Stereolithography

Approved by:

Dr. David W. Rosen, Advisor
School of Mechanical Engineering
Georgia Institute of Technology

Dr. Martha A. Grover
School of Chemical and Biomolecular
Engineering
Georgia Institute of Technology

Dr. Suman Das
School of Mechanical Engineering
Georgia Institute of Technology

Date Approved: March 26, 2009

ACKNOWLEDGEMENTS

I take this opportunity to express my sincere appreciation to my advisor Dr. David W. Rosen for his understanding, support, patience, inspiration and confidence in my abilities. His generous offer to admit me into Georgia Tech helped me fulfill my wish of studying together with my boyfriend here. His rich experiences and insights have navigated me through the completion of my Master's work. I will be grateful to his nice personalities and excellent guidance forever.

I would like to thank CIBA Vision Corporation for the financial supports to the project. I would also like to thank the Chemical Engineering collaborators, in particular, Dr. Martha A. Grover, Dr. Victor Breedveld, and Dr. Cliff Henderson, who have provided a lot of rewarding advice and assistance in the teamwork.

I was fortunate to have colleagues Dr. Fei Ding and Amit S. Jariwala, my super teammates, without whose diligent contributions, the work presented in this thesis is impossible. I am grateful to their tremendous efforts in improving the TfMP μ SLA setup, in doing numerous experiments as well as in helping me with the documentation and experimental validations.

Dr. Ameya Limaye, one previous teammate who worked on the same project before I came, is acknowledged for his significant research achievement.

I was also fortunate to be a part of the Systems Realization Laboratory at Georgia Tech. The diverse group of people, intellectual lab meetings and joyous extracurriculum activities enriched greatly my graduate student life.

I am thankful to Dr. Suman Das for being one of my committee members.

I am grateful to my former advisor Dr. Yan Deng in Tsinghua University. Without her generosity, insights and support, I would never achieve where I am today. Moreover, I want to thank Dr. C. Richard Liu and Dr. Vincent G. Duffy in the School of Industrial Engineering at Purdue University, who guided me through my first semester in US. I am greatly indebted to my three former graduate advisors above. Thanks to their selflessness, encouragement and understanding, I could pursue my desired life freely.

I thank all my friends at home and abroad for their friendship. They have been providing me an enjoyable social atmosphere.

I especially cherish the love from my boyfriend Yanjun Zhao. I have no words to express the profound love and respect that I have for him, not just as my soul mate, but also as my mentor.

Finally, I wish to express my endless gratitude to my parents and other members in my family.

TABLE OF CONTENTS

ACKNOWLEDGEMENTS	III
LIST OF TABLES	VIII
LIST OF FIGURES	IX
LIST OF SYMBOLS AND ABBREVIATIONS	XIV
SUMMARY	XVI
CHAPTER 1 INTRODUCTION	1
1.1 Framing: mask projection micro stereolithography (MP μ SLA) as an approach to micro stereolithography (μ SLA).....	2
1.1.1 Stereolithography (SLA).....	3
1.1.2 Micro-Stereolithography (μ SLA)	5
1.1.3 Mask projection micro stereolithography (MP μ SLA).....	9
1.2 Motivation for Study: MP μ SLA through transparent substrate.....	11
1.2.1 An example product by EnvisionTec.....	11
1.2.2 MEMS-based stereolithography for fabricating micro-optical components	13
1.2.3 Summary	14
1.3 Research Objective	15
1.4 Organization of the Thesis	17
CHAPTER 2 LITERATURE REVIEW AND RESEARCH PROBLEM STATEMENT	20
2.1 Definition of Process Planning	20
2.2 Existing Process Planning Methods for μ SLA	21
2.2.1 Overview of conventional process planning methods for μ SLA	22
2.2.2 Use of parameter estimation for scanning μ SLA process planning.....	22
2.2.3 Multi-objective process planning method for MP μ SLA	25
2.2.4 Development of Projection-based μ SLA Adapted to Large Surface and Microstructure Fabrication for Human Body Application.....	32
2.3 Summary and Research Gaps Analysis	37
2.4 Research Questions and Hypothesis	40
2.5 Chapter summary	43
CHAPTER 3 FOUNDATIONS OF PROCESS PLANNING METHOD FOR TFMP μ SLA	44
3.1 Introduction of the TfMP μ SLA	44
3.1.1 Basic setup of the TfMP μ SLA system	44
3.1.2 Need to modify the system setup.....	48
3.1.3 Modified experimental setup	51

3.2	Modelling the Process Planning Method for TfMP μ SLA	54
3.3	Geometrical Module	56
3.3.1	Developing the Geometrical Module.....	56
3.3.2	Application Scope of the Geometrical Module	59
3.4	Chemical Module.....	60
3.4.1	Underlying chemistry of resin curing	61
3.4.2	Modeling the chemical resin cure behavior	63
3.4.3	Developing the Chemical Module	66
3.5	Optical Module	74
3.5.1	Ray-tracing method.....	75
3.5.2	Calculation of single ray power	78
3.5.3	Irradiance Matrix	78
3.5.4	Optical Module Developed.....	79
3.5.5	Analysis of the ray-tracing density effect	80
3.6	Chapter summary	86
CHAPTER 4 MATHEMATICAL MODULE.....		87
4.1	Mathematical Formulation.....	87
4.1.1	TfMP μ SLA parameter estimation formulation example	88
4.1.2	Problem formulation – optimizing z	89
4.1.3	Problem formulation – optimizing E	93
4.2	Proposed Algorithms	96
4.2.1	Optimization	97
4.2.2	Clustering Algorithm	98
4.3	Developing the mathematical module	101
4.3.1	The initial 2.5D process planning method	101
4.3.2	Improving the process planning method.....	109
4.3.3	The mathematical module developed	112
4.4	Validating the mathematical module	113
4.5	Analyzing the mathematical module	120
4.5.1	Effects of the number of bitmaps.....	121
4.5.2	Optimize z vs Optimize E	124
4.6	Chapter summary	130
CHAPTER 5 PHYSICAL MODULE - EXPERIMENTAL VALIDATION.....		132
5.1	Validation strategy for the TfMP μ SLA process planning method.....	132
5.2	Applying the TfMP μ SLA process planning method	134
5.2.1	Case 1: curing a spherical profile on a cylinder base.....	138
5.2.2	Case 2: curing microchannels	143
5.2.3	Case 3: curing micro lens array	153
5.2.4	Summary	159
5.3	Error analysis of the TfMP μ SLA process.....	160
5.3.1	Modeling Loss 1: perception and measurement	162
5.3.2	Modeling Loss 2: model simplification	163
5.3.3	Modeling Loss 3: solution approximation	164
5.3.4	Modeling Loss 4: implementation	166

5.4 Chapter summary	169
CHAPTER 6 CLOSURE AND RECOMMENDATIONS.....	171
6.1 Answering the research questions (Evaluation of Hypotheses).....	171
6.2 Contributions.....	177
6.3 Scope and limitations of this research	180
6.4 Future work.....	185
APPENDIX A CODE FOR RESIN WORKING CURVE	190
APPENDIX B CODE FOR THE OPTICAL MODULE	194
APPENDIX C CODE FOR THE MATHEMATICAL MODULE.....	197
APPENDIX D STUDYING THE EFFECTS OF THE NUMBER OF BITMAPS	206
APPENDIX E CODE AND RESULT FOR “OPTIMIZE Z” PROBLEM.....	211
REFERENCES	213

LIST OF TABLES

Table 2.1	Research Gaps Analysis.....	37
Table 3.1	Specifications of the TfMP μ SLA system at Georgia Tech	47
Table 3.2	Comparison of exposure profile in original and current systems	53
Table 3.3	Effect of the sampling density in the ray-tracing method.....	85
Table 4.1	Comparison on dimensions of desired part and part from experiments – curve feature	105
Table 4.2	original 2.5D process planning system vs current 3D process planning system	109
Table 4.3	effects of the number of bitmaps.....	122
Table 4.4	compare the results from “optimize z ” and that from “optimize E ”	130
Table 5.1	Validation strategy of the TfMP μ SLA process planning method	134
Table 5.2	Comparison on dimensions of desired and cured part – spherical profile on cylinder base	142
Table 5.3	Comparison on dimensions of desired and cured part – microchannels.....	147
Table 5.4	Error analysis for curing microchannels	152
Table 5.5	Error analysis and comparison on dimensions – micro lens array.....	157
Table 5.6	Validating the spatial repeatability	158

LIST OF FIGURES

Figure 1.1	Stereolithography process [2].....	4
Figure 1.2	micro stereolithography (μ SLA) system and principle of operation [4].....	6
Figure 1.3	Schematic of the Scanning micro stereolithography apparatus [25].....	8
Figure 1.4	Schematic of the mask projection micro stereolithography apparatus (MP μ SLA) [25].....	9
Figure 1.5	Schematic Diagram of a Mask Projection micro stereolithography (MP μ SLA) [9].....	10
Figure 1.6	MP μ SLA through Transparent Substrate – EnvisionTec’s Perfactory System [26]	12
Figure 1.7	Scheme of the MEMS-based Stereolithography for fabricating micro-optical components [28].....	14
Figure 1.8	Cross-section of Microchannel.....	16
Figure 1.9	Organization of the thesis.....	17
Figure 2.1	Difference between intended and cured profiles [35]	23
Figure 2.2	SLA parameter estimation formulation example [35].....	24
Figure 2.3	Math form of SLA problem in Sager’s work [35]	25
Figure 2.4	Scheme of the MP μ SLA system by Limaye [1]	26
Figure 2.5	Structure of the Inverse Layer Cure Model [24].....	27
Figure 2.6	Detailed structure of Inverse Layer cure model [24]	28
Figure 2.7	Process planning method for MP μ SLA [1].....	31
Figure 2.8	Schematic of the DMD-based μ SLA [25].....	33
Figure 2.9	the 3D model of STL file [25].....	34
Figure 2.10	the 3D model of sliced section file [25]	34
Figure 2.11	Pseudo code for bitmap generation [25].....	35

Figure 2.12	Example of binary bitmap generation [25].....	36
Figure 3.1	Schematic Diagram of the TfMP μ SLA system in this research	44
Figure 3.2	Exploded View of the resin vat (designed by Amit S. Jariwala, 2008)	46
Figure 3.3	using a CCD camera to detect the actual exposure profile on substrate	49
Figure 3.4	irradiance line profile plot from CCD	50
Figure 3.5	effects of irradiance variations on the cured part	50
Figure 3.6	modified experimental setup - TfMP μ SLA	52
Figure 3.7	a more uniform exposure profile on the substrate obtained by rotating diffuser	52
Figure 3.8	Grayscale plots of the exposure profiles obtained by static and rotating diffuser	53
Figure 3.9	Model of the Process Planning System for TfMP μ SLA	55
Figure 3.10	(a) Irradiation on the flat substrate from center micromirror; (b) Irradiation on the flat substrate from an edge micromirror	57
Figure 3.11	the flowchart of the geometrical module.....	59
Figure 3.12	the scheme of the photo-polymerization process [51].....	61
Figure 3.13	Exposure Threshold model VS. Complex SL Cure Process model [52]	65
Figure 3.14	Modeling resin curing as a transient phenomenon [43]	68
Figure 3.15	Deduction of a closed-form solution to the resin cure model as a transient process	69
Figure 3.16	Working curve of Huntsman 5510 resin with the TfMP μ SLA system.....	72
Figure 3.17	the flowchart of the chemical module	73
Figure 3.18	Schematic of ray tracing algorithm [43].....	76
Figure 3.19	the flowchart of the optical module.....	80
Figure 3.20	(a) the exposure profile for 1 second generated by the sparse ray-tracing; (b) the exposure profile for 1 second generated by the dense ray-tracing	82
Figure 3.21	box plot of the irradiation distribution generated by the sparse and dense ray-tracing	83

Figure 3.22	the target geometric profile in demonstrating the ray-tracing density effect	84
Figure 3.23	energy exposure profile estimation with (a) sparse ray-tracing (b) dense ray-tracing	85
Figure 4.1	TfMP μ SLA parameter estimation formulation example	88
Figure 4.2	brief introduction of “lsqin” (MATLAB help document)	97
Figure 4.3	(a) The CAD model (desired cured shape); (b) The cross-section view of the desired cured shape for example: curing a curve feature	102
Figure 4.4	optimizing E for example: curing a curve feature	103
Figure 4.5	Bitmaps displayed on DMD for example: curing a curve feature	104
Figure 4.6	Cured shape from experiments for example: curing a curve feature	105
Figure 4.7	edge pixels get better irradiation with more micromirrors	107
Figure 4.8	MATLAB code to solve the exposure profile optimization problem in 2.5D process plan	111
Figure 4.9	MATLAB code to solve the exposure profile optimization problem in 3D process plan	112
Figure 4.10	the flowchart of the mathematical module	113
Figure 4.11	the desired geometric profile (discretized) for validating the mathematical module	114
Figure 4.12	resin working curve used in validating the mathematical module	115
Figure 4.13	resultant bitmaps and exposure time from the mathematical module	116
Figure 4.14	desired energy exposure vs estimated profile returned by the mathematical module	117
Figure 4.15	the estimated geometric profile returned by the mathematical module	118
Figure 4.16	the residuals between the estimated and desired geometric profile	119
Figure 4.17	the effects of the number of bitmaps	123
Figure 4.18	brief introduction of “lsqnonlin” (MATLAB help document)	125
Figure 4.19	Desired geometric profile – example in comparing “optimize z ” with “optimize E ”	127

Figure 4.20	bitmaps and exposure time generated by the “optimize E ” method.....	128
Figure 4.21	bitmaps and exposure time generated by the “optimize z ” method	129
Figure 5.1	Process planning method for Thick-film Mask Projection micro Stereolithography	135
Figure 5.2	working curve for the chemical resin PEGDA MW 700	137
Figure 5.3	CAD model (desired cured shape) for Case 1: curing a spherical profile on a cylinder.....	138
Figure 5.4	desired energy exposure profile for Case 1: curing a spherical profile on a cylinder.....	139
Figure 5.5	Bitmaps displayed on DMD for Case 1: curing a spherical profile on a cylinder.....	140
Figure 5.6	estimated energy exposure profile for Case 1: curing a spherical profile on a cylinder.....	141
Figure 5.7	TfMP μ SLA part built for Case 1: curing a spherical profile on a cylinder	142
Figure 5.8	CAD model for Case 2: curing a part of microchannels (a) desired part (b) desired dimensions	143
Figure 5.9	Bitmaps displayed on DMD for Case 2: curing a part of microchannels...	144
Figure 5.10	estimated energy exposure profile for Case 2: curing a part of microchannels.....	145
Figure 5.11	TfMP μ SLA part built for Case 2: curing a part of microchannels.....	146
Figure 5.12	the simulated irradiance profile on the substrate.....	149
Figure 5.13	Simulated geometric profile: microchannels.....	150
Figure 5.14	CAD model for Case 3: curing a micro lens array (a) top view (b) front view	153
Figure 5.15	Bitmaps displayed on DMD for Case 3: curing a micro lens array	154
Figure 5.16	Estimated exposure profile for Case 3: curing a micro lens array	155
Figure 5.17	TfMP μ SLA part built for Case 3: curing a micro lens array	156
Figure 5.18	Simulated geometric profile: micro lens array	158
Figure 5.19	TfMP μ SLA process modeling loss [56].....	161

Figure 5.20	(a) Irradiation on the flat substrate from center micromirror; (b) Irradiation on the flat substrate from one edge micromirror.....	167
Figure 6.1	Validating Hypothesis 2 (a) bitmap displayed on the DMD (b) irradiance profile on the substrate	175
Figure 6.2	Irradiance on pixels consistent with estimated values.....	176
Figure 6.3	the dose calculation function [61]	188
Figure 6.4	Optimization cycle for improving the fabricated topology	189
Figure D.1	Desired geometric profile (side view – XZ dimensions)	206
Figure D.2	Estimated geometric profile resulted from 5 bitmaps (side view – XZ dimensions)	207
Figure D.3	Estimated geometric profile resulted from 10 bitmaps (side view – XZ dimensions)	207
Figure D.4	Estimated geometric profile resulted from 15 bitmaps (side view – XZ dimensions)	208
Figure D.5	Estimated geometric profile resulted from 20 bitmaps (side view – XZ dimensions)	208
Figure D.6	Estimated geometric profile resulted from 25 bitmaps (side view – XZ dimensions)	209
Figure D.7	Estimated geometric profile resulted from 30 bitmaps (side view – XZ dimensions)	209
Figure D.8	Estimated geometric profile resulted from 50 bitmaps (side view – XZ dimensions)	210
Figure D.9	Estimated geometric profile resulted from 100 bitmaps (side view – XZ dimensions)	210

LIST OF SYMBOLS AND ABBREVIATIONS

B	a set of bitmaps in the TfMP μ SLA process
B_i	the i^{th} bitmap in the TfMP μ SLA process
$B_i^{(j)}$	the j^{th} pixel of the i^{th} bitmap in the TfMP μ SLA process
c	power of a single ray in ray-tracing method (mW)
C_d	Thickness of the part cured
D_p	Depth of penetration for light propagation in chemical resin
D_{pS}	Depth of penetration for a cured (solid) part
D_{pL}	Depth of penetration for liquid resin
E_c	Critical (threshold) exposure value of SLA resin (unit: mJ/cm^2)
E_z	Energy exposure at a depth of z (unit: mJ/cm^2)
E_0	Desired energy exposure profile: a vector of desired exposure values
E	Estimated energy exposure profile: a vector of estimated exposure values
f_{ET}	Function to compute energy exposure profile
f_{zE}	Working curve function of exposure dose E to compute cured height z
f_{Ez}	Transfer function of cured height z to compute exposure dose E
H	Irradiance matrix (unit: mW/cm^2)
H_{ij}	Cell of H : irradiance on Pixel i (p_i) by Micromirror j (m_j)
K	Number of bitmaps in the TfM μ PSLA process
N_{ij}	Number of rays striking a substrate pixel p_i by a micromirror m_j
N	Number of pixels for a given geometric profile on the substrate
M	Number of micromirrors used in the TfMP μ SLA
$R_a(z-z_0)$	an arithmetic average of the geometric profile roughness
RMS ($z-z_0$)	RMS value of deviation in estimating geometric profile

RMS $(E-E_0)_{abs}$	RMS value of the absolute error in estimating exposure profile
RMS $(E-E_0)_{rel}$	RMS value of the relative error in estimating exposure profile
RMS $(T-Bt)$	RMS value of the intra-variance in clustering bitmaps
t	a vector of exposure times for bitmaps in TfMP μ SLA process
t_i	exposure time of the i^{th} bitmap
T	a vector of exposure time of each micromirror
$\ x\ $	2-norm distance of vector x
z_0	Desired geometric profile: a vector of desired heights of all voxels
z	Estimated geometric profile: a vector of estimated heights of all voxels
RP	Rapid Prototyping
SLA	Stereolithography
μ SLA	micro stereolithography
MP μ SLA	Mask Projection micro Stereolithography
TfMP μ SLA	Thick film Mask Projection micro Stereolithography
UV	Ultra Violet
2.5D	Two and half-dimensional
3D	Three-dimensional
DMD	Digital Micromirror Device
DOC	Degree of Cure
RMS	Root Mean Square

SUMMARY

Mask Projection micro Stereolithography (MP μ SLA) is an additive manufacturing process used to build physical components out of a photopolymer resin. Existing MP μ SLA technology cuts the CAD model of a part into slices by horizontal planes and the slices are stored as bitmaps. A layer corresponding to the shape of each bitmap gets cured. This layer is coated with a fresh layer of resin by lowering the Z-stage inside a vat holding the resin and the next layer is cured on top of it.

In our Thick-film MP μ SLA (TfMP μ SLA) system, incident radiation, patterned by a dynamic mask, passes through a fixed transparent substrate to cure photopolymer resin. The existing MP μ SLA fabrication models can work only for controlling the lateral dimensions, without any control over the thickness of the cured part. The proposed process plan controls both the lateral dimensions and the thickness of profile of the cured part.

In this thesis, a novel process planning method for TfMP μ SLA is developed, to fabricate films on fixed flat substrate. The process of curing a part using this system is analytically modeled as the “Column cure model”. It is different from the conventional process - “Layer cure model”. “Column” means that a CAD model of part is discretized into vertical columns instead of being sliced into horizontal layers, and all columns get cured simultaneously till the desired heights. The process planning system is modularized into geometrical, chemical, optical, and mathematical modules and validated by curing test parts experimentally. The feasible process planning method provides a strong basis for continued investigation of TfMP μ SLA technology in microfabrication.

CHAPTER 1

INTRODUCTION

Today, many researchers are studying 3D fabrication in smaller sizes or more complex shapes, as mechanical, chemical, and photochemical fabrication technologies have been advanced. To realize the fabrication of 3D structures, additive methods are superior to removal methods, because they can avoid tool interference. These 3D fabrication technologies have been advanced toward 3D microfabrication and the development of microsystems. Miniaturization on a micron scale results in more integrated components and the production of highly functional systems.

RP (Rapid Prototyping) technology has been widely used in the fabrication of complex 3D structures. Compared with RP technology, MEMS (MicroElectroMechanical System), which evolved from semiconductor production technology, has better resolution. It is capable of producing highly functional parts through the integration of actuators, sensors, and so on, with a maximum resolution of several tens nanometers. To make up for the weak points of MEMS, which is restricted to the fabrication of microstructures without high-aspect ratios, LIGA technology, which is a German acronym for Lithographie (Lithography) Galvanoformung (Electroplating) Abformtechnik (Molding), was developed. However, MEMS and LIGA technologies cannot fabricate complex 3D microstructures due to the increasing costs accompanied with the fabrication of a number of masks, complexity of 3D models and characteristics of the process.

Micro stereolithography is a micro-manufacturing method that can fabricate complex 3D microstructures by curing liquid photosensitive resin in a layer-by-layer process. By this method, small 3D objects with micron resolution can be fabricated rapidly and this method has attracted more attention. At present, Mask projection micro stereolithography (MP μ SLA) is considered to be the most promising Micro stereolithography (μ SLA) technique to fabricate micro parts.

This thesis will develop a process planning method for the Thick film Mask Projection micro stereolithography apparatus (TfMP μ SLA) in the author's laboratory. Instead of using a movable Z-stage to translate the resin vat vertically, the TfMP μ SLA is different from previous MP μ SLA due to the fixed transparent resin substrate. This chapter will frame the issues at hand by presenting background information about MP μ SLA as a μ SLA process. In Section 1.1, an introduction to MP μ SLA has been provided. In Section 1.2, the motivation of study in MP μ SLA and in process planning for MP μ SLA has been reviewed and the areas where research is needed are identified. In Section 1.3, the research objective for this thesis is scoped out. In Section 1.4, the organization of this thesis is presented.

1.1 Framing: mask projection micro stereolithography (MP μ SLA) as an approach to micro stereolithography (μ SLA)

Stereolithography is a common rapid manufacturing and rapid prototyping technology for producing parts with high accuracy and good surface finish. A device that performs stereolithography is called an SLA or Stereolithography Apparatus.

When stereolithography is used to fabricate micro-parts, it is called micro stereolithography. The principle of micro stereolithography is the same as

stereolithography; however, the resolution required of a micro stereolithography process is much finer.

Micro stereolithography (μ SLA) technologies developed so far can be divided into three categories [1]:

1. Scanning Micro stereolithography
2. Two photon polymerization
3. Mask projection micro stereolithography (MP μ SLA).

The stereolithography process is explained in Section 1.1.1. Section 1.1.2 and 1.1.3 outline the relationships between MP μ SLA and other μ SLA technologies and highlights why MP μ SLA may have the potential to surpass other processes in the future and is thus worthy of investigation.

1.1.1 Stereolithography (SLA)

The term “stereolithography” was coined in 1986 by Charles (Chuck) W. Hull. Stereolithography was defined as a method and apparatus for making solid objects by successively “printing” thin layers of the ultraviolet curable material one on top of the other. Hull described a concentrated beam of ultraviolet light focused onto the surface of a vat filled with liquid photopolymer. The light beam draws the object onto the surface of the liquid layer by layer, causing polymerization or crosslinking to give a solid.

Stereolithography is an additive fabrication process utilizing a vat of liquid UV-curable photopolymer "resin" and a UV laser to build parts a layer at a time. On each layer, the laser beam traces a part cross-section pattern on the surface of the liquid resin. Exposure to the UV laser light cures, or, solidifies the pattern traced on the resin and adheres it to the layer below.

After a pattern has been traced, the SLA's elevator platform descends by a single layer thickness, typically 0.05 mm to 0.15 mm (0.002" to 0.006"). Then, a resin-filled blade sweeps across the part cross section, re-coating it with fresh material. On this new liquid surface the subsequent layer pattern is traced, adhering to the previous layer. A complete 3-D part is formed by this process. After building, parts are cleaned of excess resin by immersion in a chemical bath and then cured in a UV oven. The SLA process is illustrated in Figure 1.1

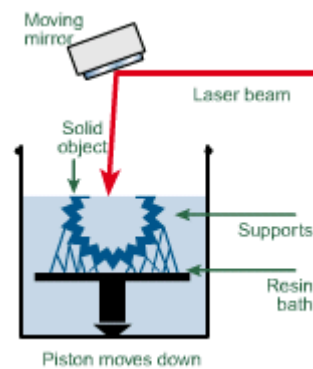


Figure 1.1 Stereolithography process [2]

Stereolithography requires the use of support structures to attach the part to the elevator platform and to prevent certain geometry from not only deflecting due to gravity, but to also accurately hold the 2-D cross sections in place such that they resist lateral pressure from the re-coater blade. Supports are generated automatically during the preparation of 3D CAD models for use on the stereolithography machine, although they may be manipulated manually. Supports must be removed from the finished product manually; this is not true for all rapid prototyping technologies.

Stereolithography has many common names such as: 3D printing, optical fabrication, photo-solidification, solid free-form fabrication, and solid imaging. One of the appealing aspects about SLA is that a functional part can be created within one day which becomes useful when working in a “time is money” environment. However the amount of time to produce any one part depends on the size and complexity of it and can take anywhere from a few hours to more than a day. Many SLA machines can produce parts with a maximum size of 20” × 20” × 24”. To date, larger SLA machines are commercially available, for example, the iPro™ 9000 XL SLA product by 3D Systems can build multiple large parts or one extra-large part with the extra-large build platform (59” × 30” × 22”) [3]. Prototypes made by SLA can be very beneficial as they are strong enough to be machined and can be used as master patterns for injection molding, thermoforming, blow molding, and also in various metal casting processes.

1.1.2 Micro stereolithography (μSLA)

The commercialization of new products integrating many functions in a small volume requires more and more often the rapid prototyping of small high-resolution objects, having intricate details, small openings and smooth surfaces. To give an answer to this demand, the stereolithography process has started to evolve towards a better resolution.

Micro stereolithography (μSLA) has been developed to produce highly precise, three-dimensional (3D) microstructures from broad selection of functional materials, especially bio-compatible materials. Figure 1.2 schemes a typical μSLA. In principle, μSLA utilizes focused light to scan over the surface of a photo-curable resin, which undergoes photo-polymerization and forms solid microstructures. It provides an

engineering platform for various applications, such as Microelectromechanical Systems (MEMS), integrated photonics, tissue engineering, and THz metamaterial synthesis. The μ SLA fabricated devices, containing complex engineered microstructures which are covered with self-assembled functional groups, can work as a unique interface between the nanometer scale functional group and macro-scale bio-medical samples, therefore can find applications in Bio-MEMS.

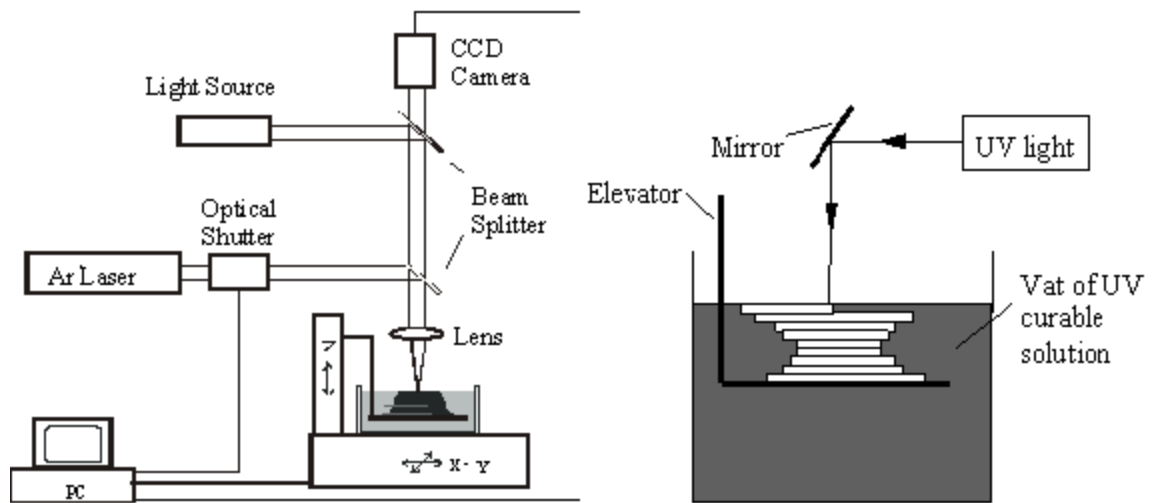


Figure 1.2 micro stereolithography (μ SLA) system and principle of operation [4]

Micro stereolithography (μ SLA), a technique with resolution about an order of magnitude better than conventional stereolithography, is studied by different academic research groups as below [5].

Ikuta et al. introduced micro stereolithography technology and developed several types of micro stereolithography apparatus [6]. They also proposed a means of applying micro stereolithography in mass-production using an optical fiber array so that multiple microstructures could be fabricated in a single process [7, 8]. However, the substrate was

moved in the x - y - z directions in the UV-curable liquid photopolymer, which could cause the fabricated microstructures to collapse in the photopolymer. Bertsch et al. developed a micro stereolithography apparatus employing a pattern generator in which a UV laser and dynamic LCD pattern generator were used to generate the cross section of a 3D structure [9 - 13]. While the substrate did not move in the x - y direction in the liquid photopolymer, an LCD pattern generation system was necessary and the resulting diffraction had to be considered. Lee et al. developed a micro stereolithography apparatus using a UV laser and a complex optical system [14 - 16].

On the other hand, Kawata et al. developed raster scanning based nano-stereolithography technology using two-photon absorption of photopolymer [17, 18]. This nano-technology makes it possible to fabricate nanoresolution 3D structures. Ikuta introduced vector scanning based nano-stereolithography technology [19], too. Nowadays, many researchers have applied this technology to various areas such as memory, biotechnology, and optical systems [20 - 23]. However, this system shows its promise only to fabricate the micro-structures. Moreover, the technology needs expensive femto-second-pulsed laser systems, complex optical systems, and nano-stage systems.

As a summary, different research teams around the world have studied the improvement of the resolution of the stereolithography process and developed micro stereolithography apparatuses (μ SLA). Up to now, all these micro stereolithography machines have been developed with primarily academic objectives. They can be classified in two main categories, depending on the way the layers are built [24]:

(1) In vector-by-vector scanning micro stereolithography processes as shown in Figure 1.3, the polymerization of each layer is obtained by moving a focused light beam on the surface of the photopolymerizable liquid medium.

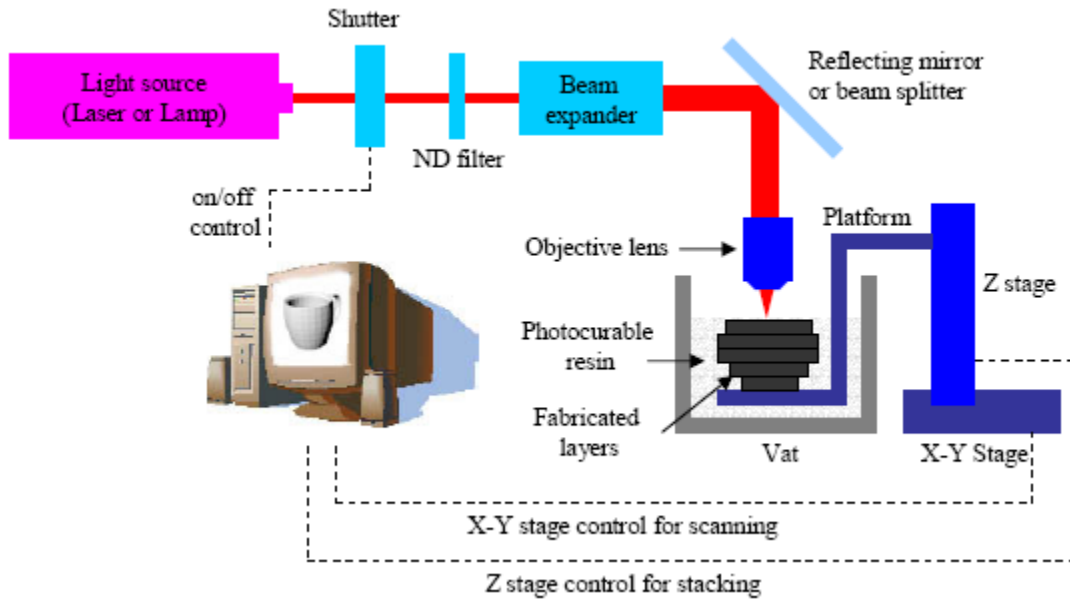


Figure 1.3 Schematic of the Scanning micro stereolithography apparatus [25]

This kind of micro stereolithography machine is directly inspired from conventional stereolithography. To obtain a high resolution, the light beam is no longer deflected by scanning mirrors but it is statically and very precisely focused on the surface of the chemical medium, and the object to be built is moved together with the photoreactor, in order to create the layers. Each layer is obtained in an incremental building method, which means long manufacturing times for complex-in-shape layers composed of many vectors.

(2) In mask projection micro stereolithography (MP μ SLA) or integral micro stereolithography processes as schemed in Figure 1.4, a complete layer is polymerized in

one irradiation only. In this case, layers are cured over their entire surface in one step, whatever their shape may be, and the time needed to polymerize one layer is independent of its complexity.

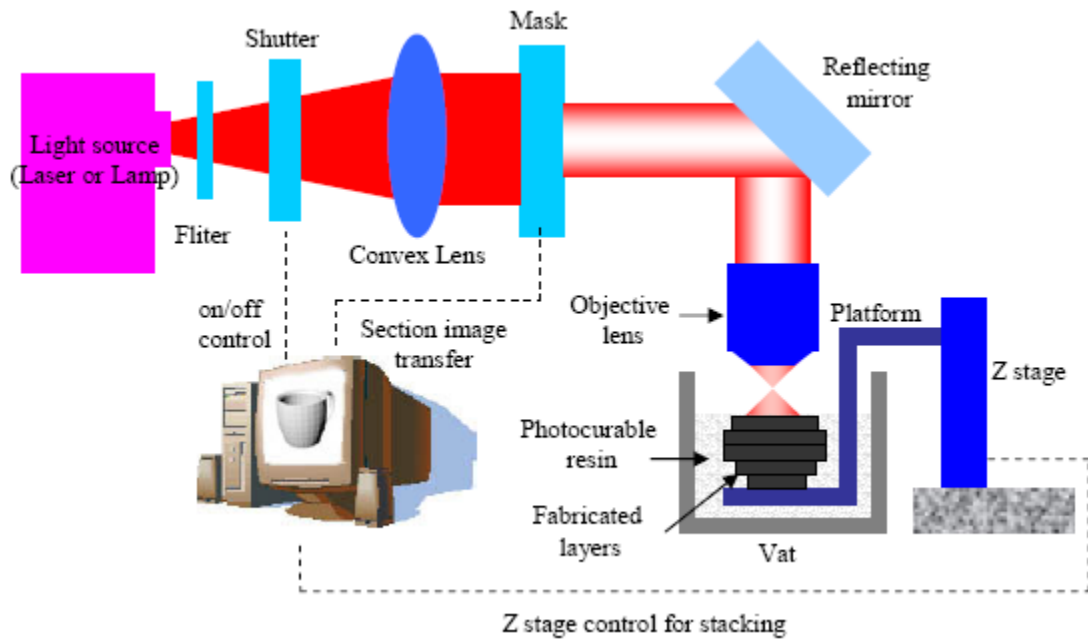


Figure 1.4 Schematic of the mask projection micro stereolithography apparatus (MP μ SLA) [25]

1.1.3 Mask projection micro stereolithography (MP μ SLA)

In mask projection micro stereolithography, also called integral micro stereolithography, a complete layer is polymerized in a single radiation. The principle of MP μ SLA is shown in Figure 1.5.

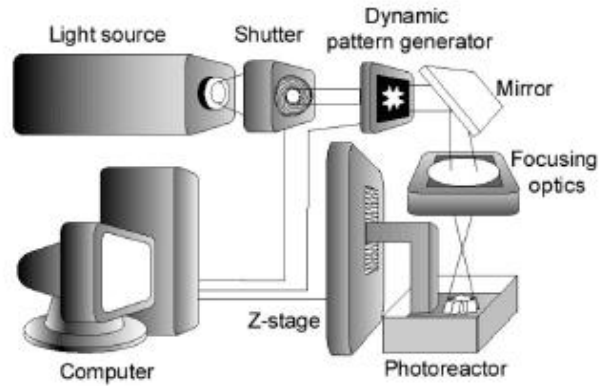


Figure 1.5 Schematic Diagram of a Mask Projection micro stereolithography (MP μ SLA) [9]

As shown in Figure 1.5, the MP μ SLA is used to project and focus the patterned light, which is formed by a mask on the resin surface according to the binary image generated from the sliced 2D section. In this process, the light source, a laser or a UV lamp, is enlarged and illuminated to the mask. A shutter controls the duration of the irradiation step. Each layer is cured according to a sliced 2D section, and then the cured layer is immersed into resin and the refreshed resin is covered such that it reaches slicing thickness by the Z stage. The final 3D microstructure is produced through the accomplishment of these consecutive processes in all layers.

There are two kinds of projection micro stereolithography [25], LCD-based and DMD-based. LCD transmits or blocks incident light by the direction of the arrangement of crystal liquid according to the electric signal. On the other hand, DMD selectively reflects incident light by tilting each micromirror, which is about 13 μm on each side, according to electrostatic force by electric signal.

In MP μ SLA, the pattern generation part plays a distinguished role in making dynamic patterns without any physical masks. It takes a shorter time to cure each layer

compared to that of a scanning micro stereolithography apparatus because the later uses a slower vector-by-vector scanning process. Moreover, the accuracy of MP μ SLA is better, because it is free from the errors introduced by the X - Y translation.

Due to these advantages, current research on micro stereolithography (μ SLA) is focused on Mask Projection micro stereolithography (MP μ SLA).

1.2 Motivation for Study: MP μ SLA through transparent substrate

In this thesis, a mask projection micro stereolithography apparatus (MP μ SLA) adapted to fabricate complex 3D microstructures through transparent substrate is dealt with.

The principle behind the MP μ SLA through transparent substrate is similar to that mentioned in the papers above introducing MP μ SLA. One of the interesting aspects of the machine is that the irradiation from the DMD chip passes through a fixed transparent substrate into the resin vat, compared to irradiance from the top of the vat as in conventional MP μ SLA processes.

Through literature review, some similar MP μ SLA through transparent substrate have been identified.

1.2.1 An example product by EnvisionTec

Commercially available machines include Perfactory® range of machines from EnvisionTec [26], Germany. Figure 1.6 presents such an SLA product developed by EnvisionTec.



Figure 1.6 MP μ SLA through Transparent Substrate – EnvisionTec’s Perfactory System [26]

The Perfactory build process [27] employs an image projection technology called Digital Light Processing (DLP) from Texas Instruments, thus each layer is cured in a single shot. To build your part or parts slice by slice the system projects a bitmap version of each layer onto the upside of a shallow vat of resin. The models are built upside-down. The build platform rises up as the model is built and the mask is projected from underneath the build area, onto the bottom of a transparent and relatively shallow vat of raw material (called the basement). Once cured sufficiently, the basement is peeled away from the model (which, through a capillary action, also replaces the used resin), the build platform raises and another layer is built onto the bottom of the last. The whole cycle takes just 25 seconds and there’s no planarisation or levelling, which in some machines can cause problems in the stability of the parts being built.

The technologies mentioned above cure parts in a layer by layer fashion on a transparent substrate by irradiance from underneath the resin surface. Research has been

done on curing parts through transparent substrates, which may enable thin film coating, deposition of micro-channel or modifying a surface of an optical part.

1.2.2 MEMS-based stereolithography for fabricating micro-optical components

Erdmann et al. (2005) had shown the use of mask projection micro stereolithography (MP μ SLA) through transparent substrates for manufacturing of micro-lens arrays [28]. Actually speaking, the system is a MEMS-based lithography system employing a digital multimirror device (DMD) as a switchable projection mask.

The DMD is imaged into a photoresist layer using a Carl Zeiss lithography objective with a demagnification of 10:1 and a numerical aperture of 0.32 on the image side. The resulting pixel size is $1.368 \times 1.368 \mu\text{m}$. In comparison with laser direct writing with a single spot, Erdmann's method is a parallel processing of nearly 800,000 pixels (1024×768 pixels). This fabrication method can be applied to all MOEMS components.

Figure 1.7 shows the setup to fabricate micro-optical components. An illumination system generates a uniform intensity distribution on the DMD chip and the angular spectrum required to fill the entrance pupil of the objective. The photoresist layer is located in the image plane of the objective. To enable the stitching of single exposed rectangles, the photoresist coated substrate is attached to a mechanical stage. A computer controls the DMD chip and the stitching stage.

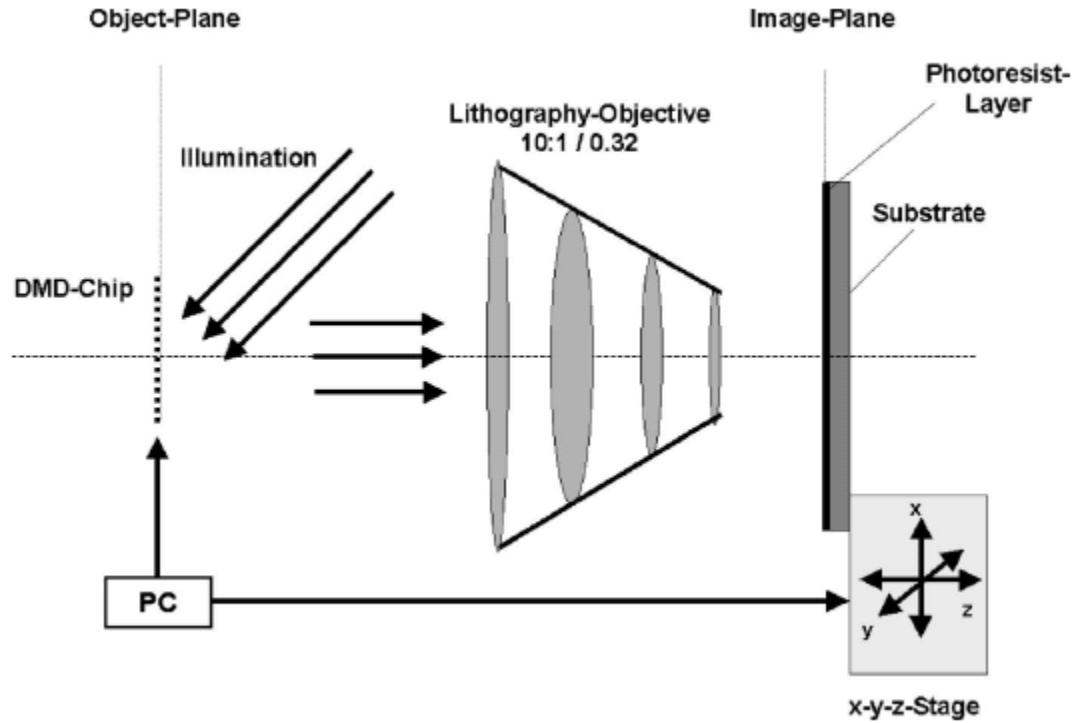


Figure 1.7 Scheme of the MEMS-based Stereolithography for fabricating micro-optical components [28]

1.2.3 Summary

The motivation for this study originates from tremendous interests in a series of novel designs in commercial SLA products and literatures, disclosing the potentiality of such a MP μ SLA technology in various micro fabrication areas, like micro-optics as presented above.

Although the MP μ SLA technologies mentioned above are common in receiving irradiance from underneath, the detailed designs and process planning methods varies in some extent. Our previous labmate, Dr. Ameya Limaye, developed a multi-objective process planning for conventional MP μ SLA with irradiance from the top of the vat [1]. Limaye's stereolithography setup was modified into our current MP μ SLA through transparent substrates; correspondingly, a process planning method needs to be

formulated for the new MP μ SLA through transparent substrates, which system is expected to be capable of fabricating microstructures like the aforementioned micro-optics and micro-fluidics components.

1.3 Research Objective

In this research, the author seeks to address the research area identified in Section 1.2, where the original motivating problem –MP μ SLA through transparent substrates was introduced. In this section, a more direct and specific motivating problem is provided that embodies the research area mentioned above.

Microchannels have numerous applications such as inkjet printers, lab-on-a-chip, chemical analysis systems, biological sensing, drug delivery, optical switching and molecular separation. Several reported techniques [29] to make microchannels include embossing (Juang et al. 2002), injection molding (Becker and Gartner 2000; Yu et al. 2004; Rudolf 2006), laser ablation (Mello 2002; Soper et al. 2000), soft lithography (McDonald and Whitesides 2002; Duffy et al. 1998), laser-based (Gaughan 2005; Said et al. 2004), and a combination of photolithography and etching (Malek et al. 2007). More advanced nanochannels can be achieved using nanoimprint lithography (Dumond et al. 2006). However, these fabrication techniques cannot fabricate microchannels with complex geometry conveniently and economically. Mask projection micro stereolithography (MP μ SLA) through transparent substrate can be used for this purpose, and would gain increasing popularity due to its inexpensive and time-efficient manner of prototyping microstructures.

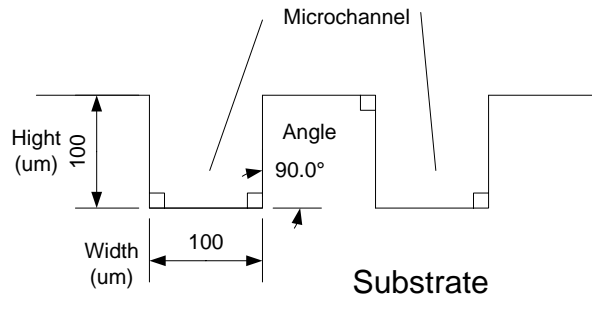


Figure 1.8 Cross-section of Microchannel

Example problem

The particular MP μ SLA through transparent substrate under consideration in this research is named as Thick-film MP μ SLA (TfMP μ SLA). A method for fabricating microchannels on glass substrate using the TfMP μ SLA is presented in this thesis. In contrast to conventional practice of fabricating microchannels as trenches or grooves in a substrate, microchannels are fabricated as thin walled raised structures on a substrate.

Typical overall microchannel sizes range from about 5-100 μ m wide and 5-100 μ m deep. As shown in Figure 1.8, the dimensions of the example microchannels here are 100 μ m wide and 100 μ m high.

The microchannel example presented here is representative of the class of parts whose fabrication would be enabled by this research. From the example problem, the following research objective has been abstracted.

To formulate a process planning method for thick-film mask projection micro stereolithography through a transparent substrate, that can be made to fabricate MP μ SLA parts with a given geometrical profile.

1.4 Organization of the Thesis

This thesis contains six chapters. A brief overview of the material covered in each chapter is presented here. The organization of this thesis is outlined in Figure 1.9.

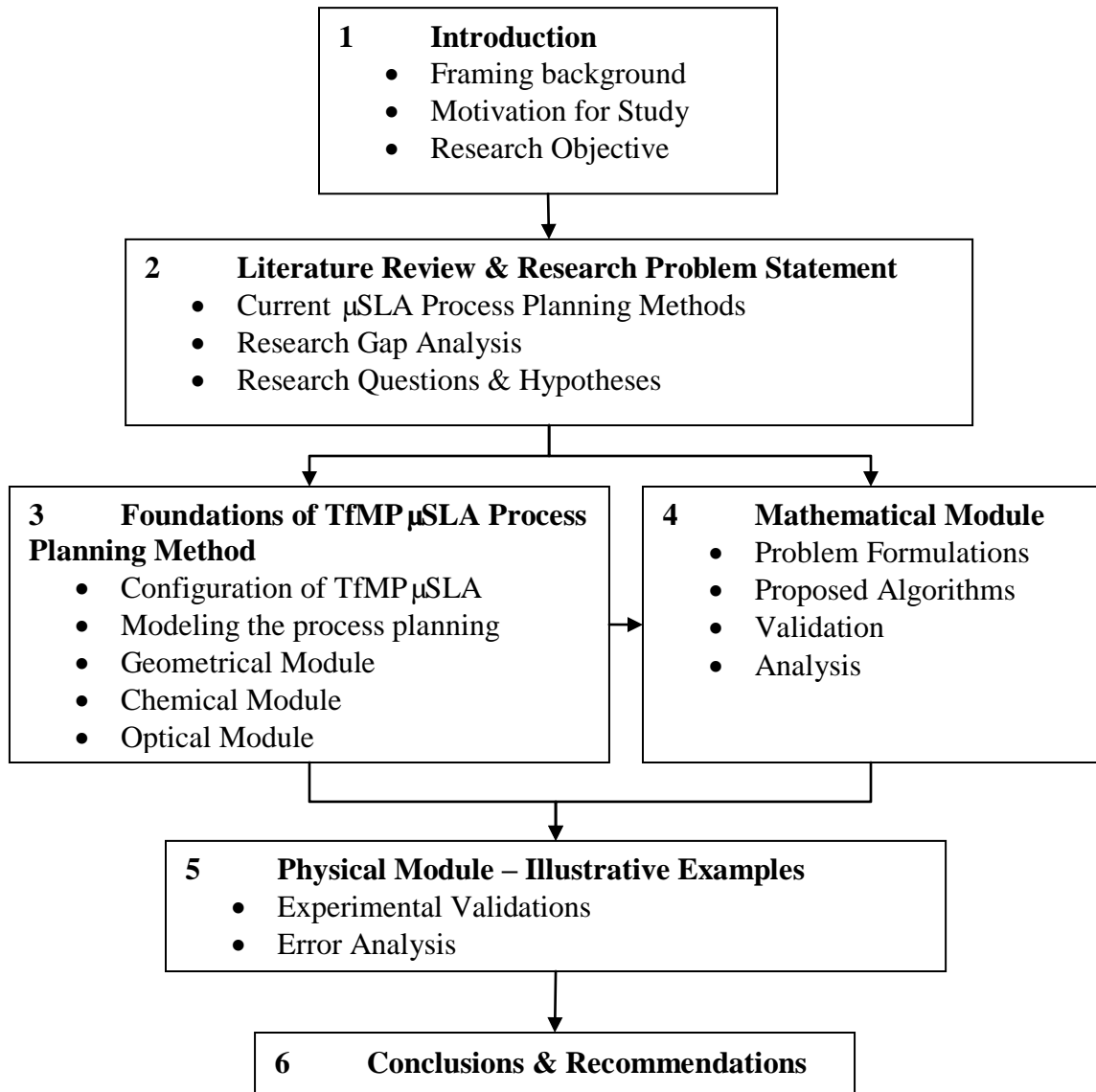


Figure 1.9 Organization of the thesis

This first chapter is intended to provide a framework for the remainder of the thesis. A brief introduction to MP μ SLA has been presented, along with the motivations for study that has been conducted. The research objectives have been expressed concisely via motivating rationale.

In Chapter 2, technical aspects of the existing process planning methods in μ SLA is reviewed, illuminating the achievements but also the limitations of current technologies. It is with this awareness of the current limitations that challenges can be identified, and improvements and progress can be made. Following the research gaps analysis, research questions have been formulated. Hypotheses have been put forth for each research question.

Chapter 3 begins to address the challenges identified in Chapter 2 on a more detailed level. The configuration of the TfMP μ SLA machine in this research is introduced. A model of the process planning system for the TfMP μ SLA under consideration is presented. The foundational modules include the geometrical module, the chemical module, and the optical module, which are detailed in this chapter. The three primary modules verify hypotheses to the first three research questions formulated in Chapter 2, and pave the way for the succeeding modules.

In the context of previous modules, Chapter 4 develops the mathematical module, to fulfill the process planning system. This module is the core of the process planning system, which behaves as a transfer function transforming the inputs from preceding modules into outputs of process data for curing physical parts. The particular problem for obtaining MP μ SLA process data, that is bitmaps and exposure time for each bitmap, is described mathematically. The related methods and algorithms used to solve the

mathematical problem are presented. Herein, the process planning method is complete, and ready to be validated.

Chapter 5 aims to validate the process planning method by physically curing some sample parts. This is the so called “Physical Module”. The first section introduces the validation strategy. The succeeding section reports on experimental testing of the process planning system, intended to illuminate the capability of the process planning system in curing complex 3D geometrical profiles using TfMP μ SLA. This involves testing various geometrical profiles with the hydrogel bio-material *PEGDA MW 700*.

Chapter 6 serves to bring together conclusions and understanding developed throughout the previous chapters. The research questions are re-visited and the contributions of this work are summarized. The thesis concludes with a discussion of limitations of the current work and suggestions for future investigation.

CHAPTER 2

LITERATURE REVIEW AND RESEARCH PROBLEM STATEMENT

In Chapter 2, firstly the foundational knowledge of process planning to achieve the research objective in Section 1.3 is presented.

A review of the current achievements in process planning methods for mask projection micro stereolithography (MP μ SLA) is presented in Section 2.2. Although the concern of this thesis is process planning for mask projection stereolithography, useful information can be gleaned from that for scanning stereolithography; these are therefore included as well.

Many problems exist in the process planning methods reviewed in this chapter. Research gaps analysis is presented in Section 2.3.

In Section 2.4, the research objective is broken down into research questions; hypotheses have been put forth for each research question and the approach used to verify those hypotheses has been identified.

2.1 Definition of Process Planning

Process planning translates design information into the process steps and instructions to efficiently and effectively manufacture products. It encompasses the activities and functions to prepare a detailed set of plans and instructions to produce a part.

A process plan specifies what raw materials or components are needed to produce a product, and what processes and operations are necessary to transform those raw

materials into the final product. It is the bridge between product design and manufacturing. The outcome of process planning is the information for manufacturing processes and their parameters, and the identification of the machines tools, and fixtures required to perform those processes.

2.2 Existing Process Planning Methods for μ SLA

In this section, an overview of conventional process planning for micro stereolithography (μ SLA) is presented, followed by several specific research cases on process planning methods.

Section 2.2.2 introduces a new process planning method for scanning μ SLA, based on parameter estimation (Sager, B., and D. W. Rosen, 2008). Although the main concern in this thesis is mask projection μ SLA, the process planning method by Benay Sager and David W. Rosen (2008) is very illuminating for process development in MP μ SLA; these are therefore included as well.

Section 2.2.3 presents a multi-objective process planning method for mask projection stereolithography (Ameya Shankar Limaye, 2007). Limaye put forward a novel method of modeling irradiance on the resin surface in the case of MP μ SLA, as well as a more rigorous Stereolithography cure model – transient layer cure model and the radical diffusion model. A process planning method that would guide a manufacturer through all steps of process planning, starting from the CAD model and ending with a finished part has been formulated.

Section 2.2.4 presents another process planning method used in “Development of Projection-based Microstereolithography Apparatus Adapted to Large Surface and Microstructure Fabrication for Human Body Application” (Choi Jae-Won, 2007).

2.2.1 Overview of conventional process planning methods for μ SLA

There are two types of micro stereolithography apparatus, one using the scanning method and the other using the projection method.

The former scans a fine spot through a focused beam or lamp on the resin surface according to the sliced 2D section, and is also called the vector-by-vector process. In this process, the making of the fine spot plays a key role, and it is controlled using the XY stage or galvano-mirror.

The latter is used to project and focus the patterned light, which is formed by a mask on the resin surface according to the binary image generated from the sliced 2D section, and is also called the integral process because of the one irradiation.

The main difference between the two processes is the curing method of each layer, but the other procedures are almost similar. That is, each layer is cured according to a sliced 2D section generated from the STL file, which is the standard format of conventional RP products, and then the cured layer is immersed into resin and the refreshed resin is covered such that it reaches slicing thickness by the Z stage. The final 3D microstructure is produced through the accomplishment of these consecutive processes in all layers.

2.2.2 Use of parameter estimation for scanning μ SLA process planning

In 2008, Benay Sager and David W. Rosen demonstrated that a new approach to process planning based on parameter estimation methods can improve greatly the surface finish of parts fabricated using scanning stereolithography [35]. The process planning method overcomes those limitations in traditional process planning for layer based

additive manufacturing technologies, like the build styles developed by the SLA machine manufacturer (3D Systems).

Parameter estimation is a method that finds a set of parameter values that minimize a measure of deviation. In the SLA process, exposure is the parameter that determines whether a point is solidified within the vat. The minimum exposure amount required to get liquid resin cured is called as the critical exposure or exposure threshold value (E_c), which is a property parameter for the resin material used in SLA. Therefore, exposure becomes the focus of the SLA parameter estimation formulation. In this work, the measure of deviation is the difference between the exposure received by points along down-facing surfaces and the stereolithography resin's critical exposure (E_c), which on the other hand embodies a measure of the difference between the intended and cured profiles as shown in Figure 2.1.

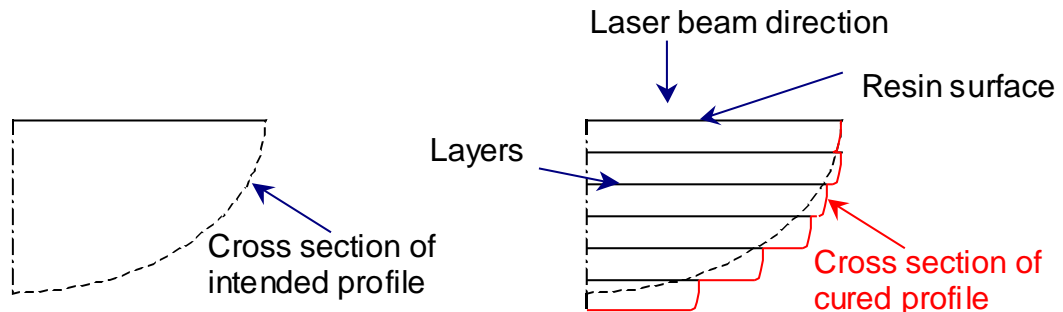


Figure 2.1 Difference between intended and cured profiles [35]

The basic idea of the proposed process planning method will be explained in the context of Figure 2.2. The outline of the surface of interest in the parameter estimation formulation can be expressed as a grid along which the exposure value should be equal to

the critical exposure. By specifying the shape and length of this grid, the surface finish of the cured outline can be controlled. For the points on this grid, the goal is to minimize the deviation of the exposure received from the critical exposure. The surface Sager's group was interested in is the down-facing surface, which has a quadratic shape. For the purposes of their work, they chose to use only the scan velocity as a variable, since it is the easiest process variable to control directly. Since points are cured as a result of laser beam scans, the goal is to estimate the scan velocity for each line. The laser power, the beam waist, and the spacing between each laser beam scan are kept constant.

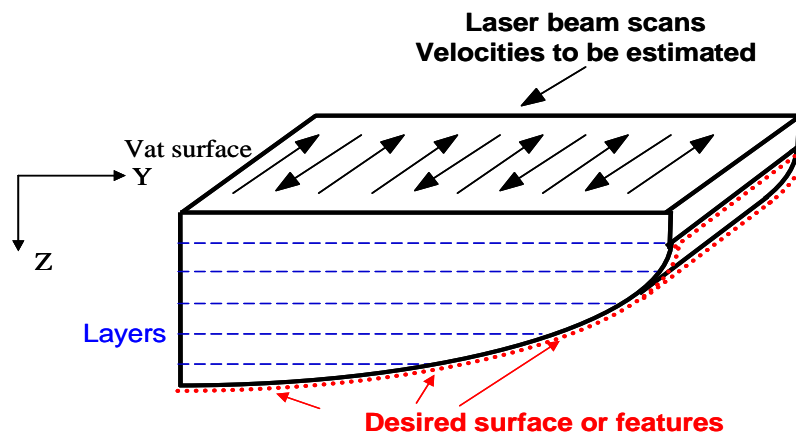


Figure 2.2 SLA parameter estimation formulation example [35]

For the SLA problem, the variables are the exposure levels along each scan vector to achieve the desired shape distribution. The grid of points serves as the measurement points for the inverse design methods. In typical SLA process plans, the number of scan vectors is greater than the number of measurement points M . As such, least-squares solution techniques are appropriate.

The desired exposure at each measurement point m_k is, of course, E_c . Let the estimated exposure at each measurement point be E_{ek} . Then, the least-squares fitting problem can be formulated as follows. The squared error term is given by Equation 2.1.

$$R = \sum_{k=1}^M (E_c - E_{ek})^2 \quad (2.1)$$

The mathematical form of the problem formulation for SLA parameter estimation is given in Figure 2.3. The non-linear least-squares solver in Matlab, lsqnonlin, was used to solve the problem.

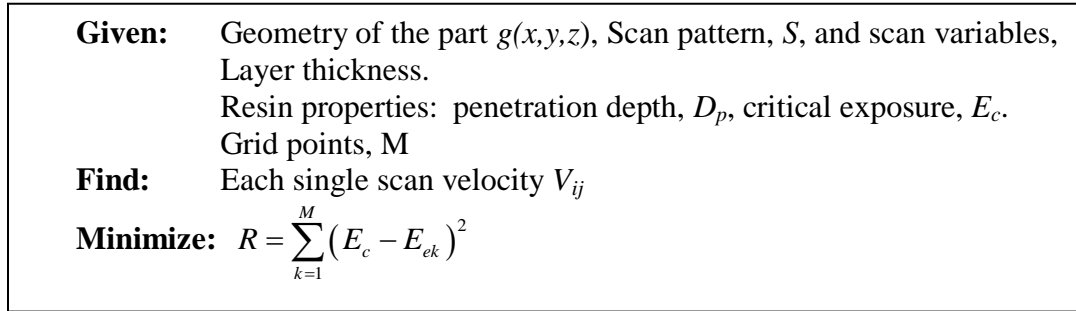


Figure 2.3 Math form of SLA problem in Sager’s work [35]

2.2.3 Multi-objective process planning method for MP μ SLA

In 2004, Limaye designed and analyzed a MP μ SLA using patterned irradiation rather than light beam scanning method as in Sager’s μ SLA presented above. The main difference is the curing method of each layer as explained in Section 2.2.1.

The primary modules of a MP μ SLA were identified in Ameya Limaye, (2004) as collimation system, imaging system, and build system. After three years’ work, Limaye

improved and complete the design of all these systems [1]. The schematic of the Limaye's system is shown in Figure 2.4.

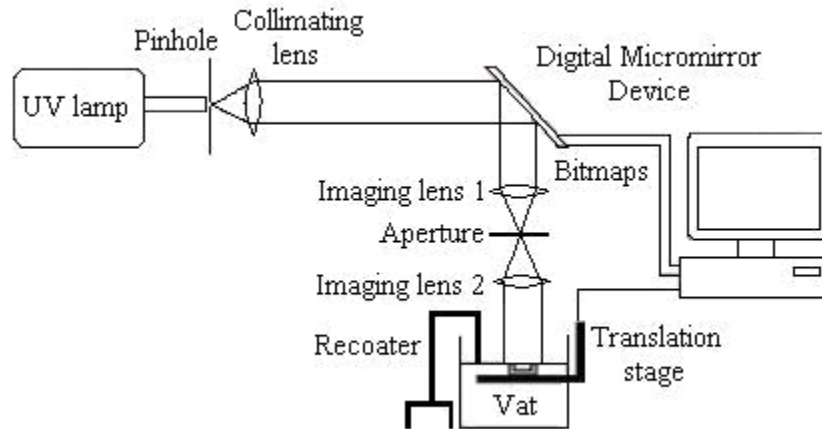


Figure 2.4 Scheme of the MP μ SLA system by Limaye [1]

2.2.3.1 Process planning method for curing one single layer

In his master thesis [24], Dr. Limaye developed a Layer Cure Model and an Inverse Layer Cure Model for his MP μ SLA. Using the Layer Cure model, the effect of the process variables, namely layer thickness (LT), time of exposure (TOE) and bitmap (B), on a cured layer's lateral dimensions is quantified. The Inverse Layer cure model returns the values of process parameters used to cure a layer of the required dimensions.

The Layer cure model computes the lateral dimensions of a layer in terms of the process parameters; while the Inverse Layer Cure Model computes the values of process parameters that would cure a layer of the intended dimensions. Hence, the inputs and outputs of the Inverse Layer cure model are opposite to those of the Layer cure model. The structure of the Inverse layer cure model is shown in Figure 2.5.

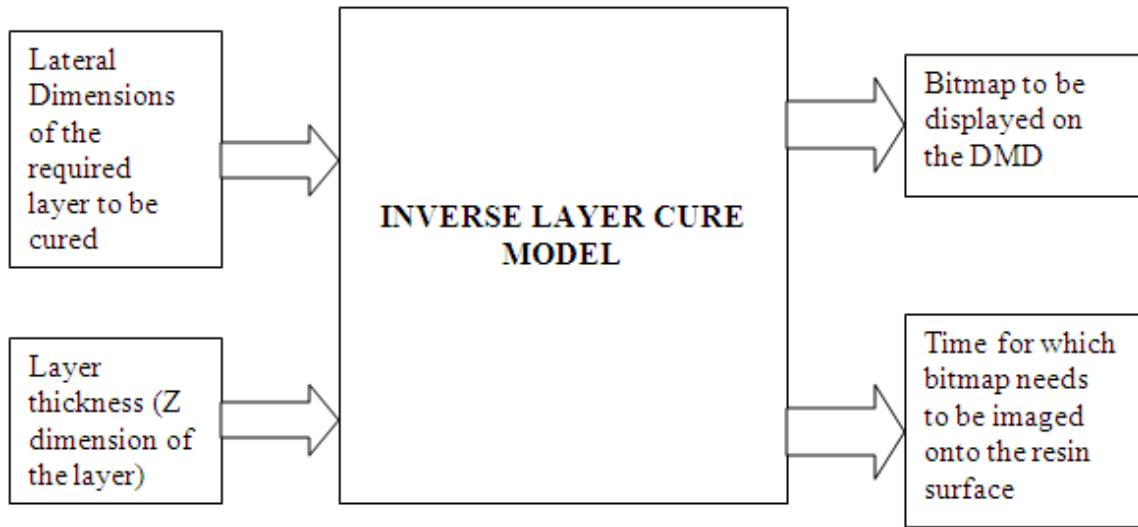


Figure 2.5 Structure of the Inverse Layer Cure Model [24]

The detailed structure of the Inverse Layer Cure Model is shown in Figure 2.6. The inputs to the Inverse Layer cure model are lateral dimensions of a layer and layer thickness. Using a Pixel mapping model, the bitmap to be displayed on the DMD in order to form an aerial image of the dimensions equal to those of the desired layer is generated.

The most important part of this model is the “Pixel-micromirror mapping database”, which relates the location of a micromirror on the DMD with the location of the pixel cured by it on the layer. Rays are traced from every micromirror on the DMD and the locations of their points of intersection with the resin surface are computed. The procedure of ray tracing is the one adopted while formulating the Irradiance model. The location of every point on the resin surface is documented against the location of the micromirror on the DMD irradiating it.

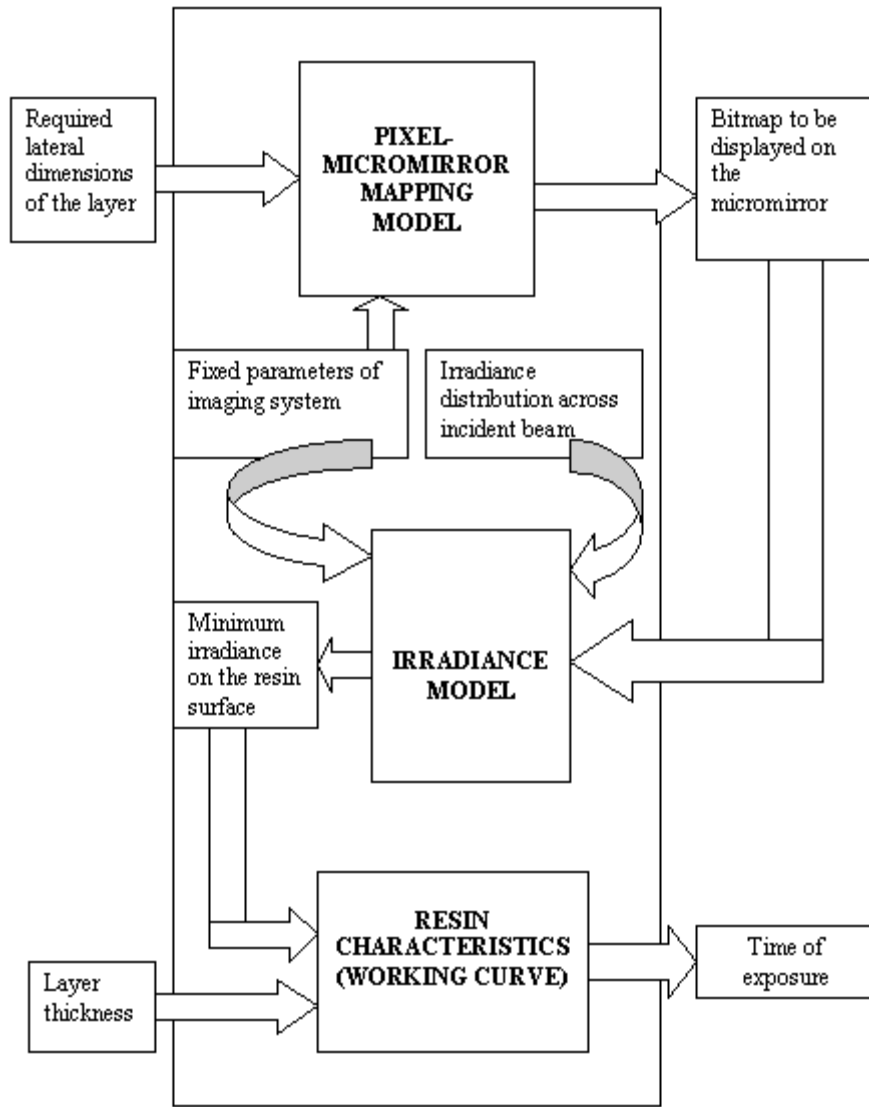


Figure 2.6 Detailed structure of Inverse Layer cure model [24]

The Pixel mapping model is executed in the following steps:

1. Step 1: Mesh the intended layer with points

The intended layer is meshed with points. The denser these points, the better the representation of the layer.

2. Step 2: Snap the points on this mesh to the closest pixel on the resin in the Pixel-micromirror mapping database

The Pixel-micromirror mapping database relates the micromirrors on the DMD with the points on the resin surface. Every mesh point is snapped to the closest resin point from the Pixel-micromirror mapping database

3. Step 3: From the Pixel-micromirror mapping database, determine the locations of the micromirrors on the DMD to be turned “ON”

Since the Pixel mapping database creates a one-to-one correspondence between the micromirrors on the DMD and the points on the resin surface, it can be applied in reverse to look up the micromirrors corresponding to the points on the resin surface.

4. Step 4: Generate the bitmap so that the micromirrors (obtained in Step 3) are turned “ON”

When a monochrome bitmap is supplied to the DMD, every pixel on the bitmap controls one and only one micromirror on the DMD. If a bitmap pixel is white, the corresponding micromirror is switched “OFF”. If the bitmap pixel is black, the corresponding micromirror is switched “ON”. From the locations of the micromirrors on the DMD that are to be turned “ON”, the required monochrome bitmap is generated.

This bitmap is then run through the Irradiance model to obtain the irradiance across the aerial image that will be formed when the bitmap is imaged onto the resin surface. The irradiance at the point receiving the minimum irradiance is computed. From the resin characteristics (experimentally determined), the time of exposure required for the entire exposed area to cure down to a depth of one layer thickness is computed. Thus, the outputs of the Inverse layer cure model are the bitmaps to be displayed on the DMD and the times of exposure.

Thus, this Inverse Layer Cure Model set out the process planning method for Limaye's MP μ SLA. The process planning method for curing a certain layer of given geometrical part was summarized in five steps:

1. Meshing the layer with data points
2. Snap the data-points to the resin points on the database
3. Generate the bitmap to be displayed
4. Use the Irradiance model to determine the minimum irradiance on the layer
5. Determine the time of exposure using the Exposure Threshold Cure model (Beer Lambert's law) [36].

2.2.3.2 Multi-objective process planning method for MP μ SLA

Based on the primary process planning method – Inverse Cure Layer Model for curing one single layer, Dr. Limaye completed and improved the entire process planning method for building a 3D part.

In 2007, he presented a more sophisticated process planning method to build a part with constraints on dimensions, surface finish and build time [1] as shown in Figure 2.7.

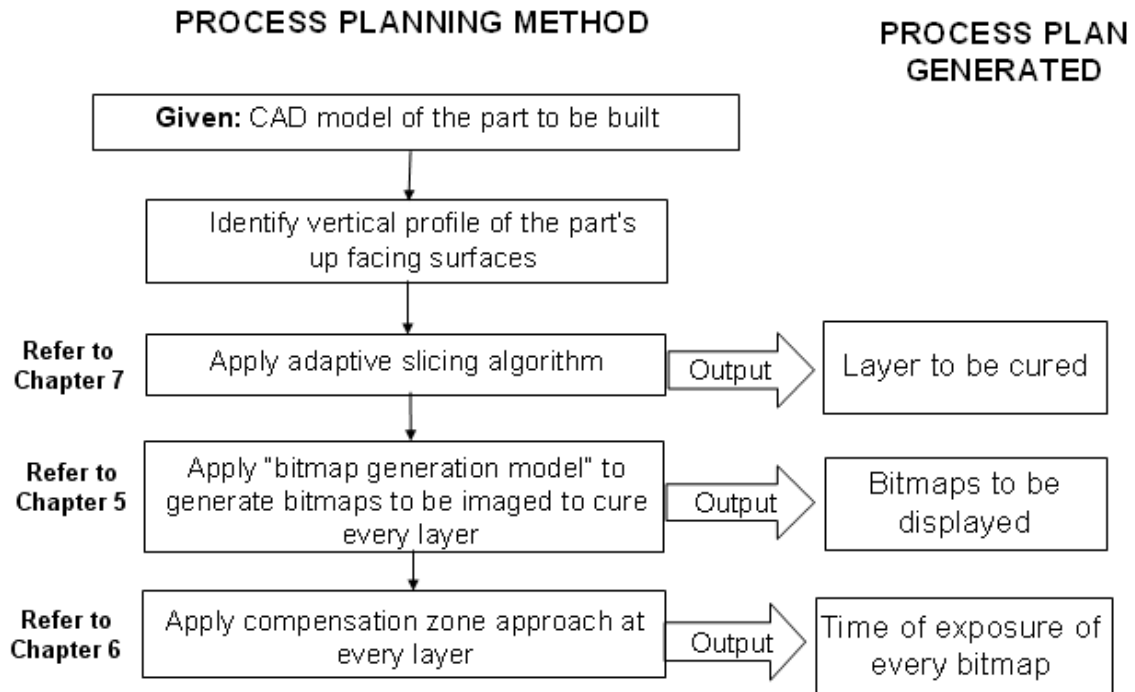


Figure 2.7 Process planning method for MP μ SLA [1]

Limaye formulated an adaptive slicing algorithm that slices a CAD model so as to obtain the required tradeoff between build time and surface finish of up facing surfaces of the part. This slicing algorithm models the trade off as a compromise Decision Support Problem (cDSP) [37] and then solves the cDSP by using a gradient projection algorithm.

In order to model the irradiance distribution on the resin surface when a given bitmap is displayed, Limaye formulated a multi scale modeling approach, which allows the computationally intensive task of computing image formation through ray tracing to be manageable. The bitmap generation method uses the Pixel Image database (referred as “Pixel-micromirror mapping database” in Section 2.2.3.1) to do just the opposite, i.e., generate the bitmap to be displayed on the DMD in order to irradiate a given area on the resin surface.

Furthermore, Limaye presented and validated two new theories: the transient nature of curing of layer and the non-additive nature of exposure if the waiting time between two consecutive exposure doses is significant. The transient layer cure model was formulated which models layer curing as a transient phenomenon. The loss of energy from the bottom surface of a part being built due to diffusion of reactive species and oxygen molecules was quantified as a diffusion factor, which is demonstrated to be determined primarily by the time the cured layers sit in the vat before receiving a second dose of exposure (i.e, waiting time). The non-additive nature of exposure was thereby shown to be a function of waiting time between two consecutive doses of exposure. These theories were used to compute the print through that occurs when a multi-layered part is cured. Limaye developed a compensation zone approach as a method to avoid the print through errors and build parts with accurate down-facing surfaces.

As a summary, the process planning method first slices the parts using an adaptive slicing algorithm. The sliced part is built using Irradiance model and Compensation zone approach. The process planning method was demonstrated on a test part with quadratic up facing and down facing surfaces.

2.2.4 Development of Projection-based μ SLA Adapted to Large Surface and Microstructure Fabrication for Human Body Application

In 2007, Choi, Jae-Won presented a projection-based μ SLA [25], which is composed of a DMD as the pattern generator, mercury lamp as the light source, optics, and opto-mechanics, etc. He fabricated various microstructures using UV (UltraViolet) curable resin. His DMD-based μ SLA consists of the light source part, light delivery part, pattern generation part, image-formation part, stacking part, etc, as shown in Figure 2.8.

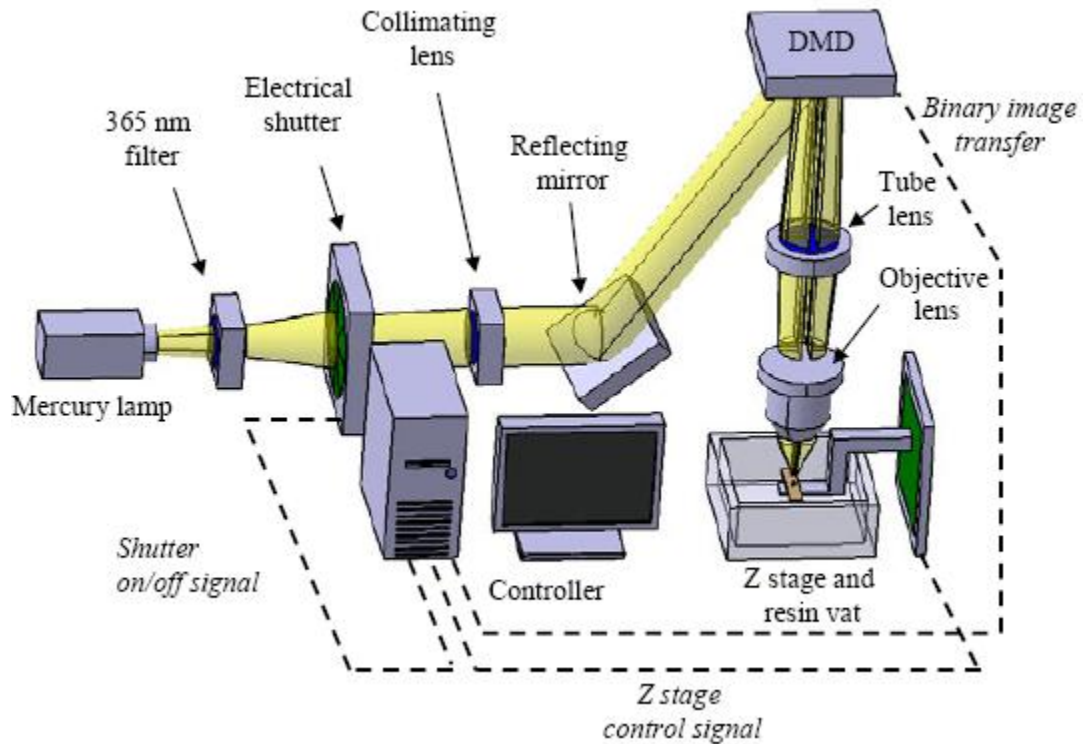


Figure 2.8 Schematic of the DMD-based μ SLA [25]

In Figure 2.8, light is illuminated into the DMD, which is patterned as binary image data; patterned light is focused, and then exposed resin is cured. Exposure is maintained for the given time by an electric shutter. To refresh a new resin surface, the Z stage is moved downward and upward again at the specific position. The final micro structure is produced by conducting these consecutive processes for all layers.

The process planning method developed by Choi [25] is unique in terms of bitmaps generation method and layer stacking part.

1. Bitmap generation method

To generate a bitmap for curing a single layer, being different from Limaye's optics-based Inverse Layer Cure Model (refer to Section 2.2.3.1), Choi's method is directly based on topology as below.

In Choi's research, the binary image is generated from the STL file. For example, Figure 2.9 shows a 3D model of STL file, and Figure 2.10 shows a 3D model of sliced section file consists of more than one closed loops with serial points in each layer.

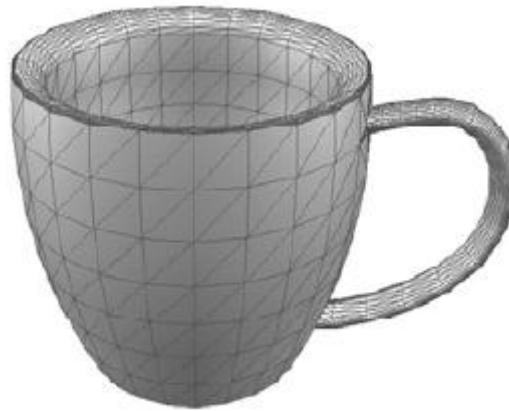


Figure 2.9 the 3D model of STL file [25]

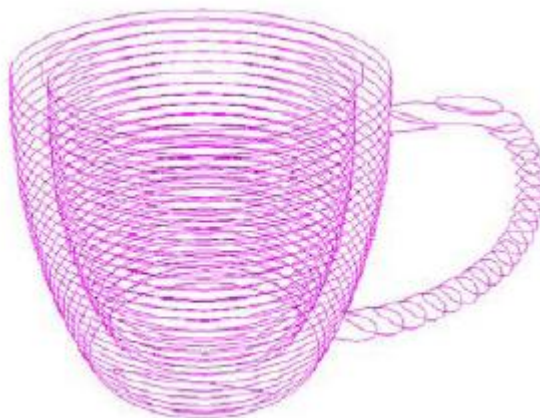


Figure 2.10 the 3D model of sliced section file [25]

The binary image is finally generated from the sliced 2D section data. The algorithm of the binary image generation according to the number of closed loops, together with their topologies, is shown in Figure 2.11. The algorithm starts with the calculation of the number of surrounding loops about each loop. If the number of loops is only one, it can be simply painted black. But if there are more than two loops, the loop has to be painted black or white according to the number of its surrounding loops. The number of surrounding loops can be calculated by counting the number of null sets according to the relative complement among loops, where each loop is regarded as a region set. In Figure 2.11, n , L_i (and L_j), and $n(L_i)$ represent the number of loops in each layer, the region set of the current loop, and the number of surrounding loops about certain loop, including itself. L_j^c denote the complement set of the region set of L_j . Using the calculated number of surrounding loops, the image is generated by painting it black when the number is odd and white when the number is even from the outer loop to inner loop.

```

For (i=1;i<=n;i++)
    For(j=1;j<=n;j++)
        If( $L_i \cap L_j^c = \Phi$ )
            n(Li)++;
Case n(Li)
    1 : Paint Black Image with the given region
    2 : Paint White Image with the given region
    3 : Paint Black
    4 : Paint White
    .....

```

Figure 2.11 Pseudo code for bitmap generation [25]

Figure 2.12 shows an example of binary image generation, and the number of surrounding loops (i.e, null sets) for loop 1 (L_1), loop 2 (L_2), loop 3(L_3), and loop 4 (L_4) are $n(L_1) = 1$, $n(L_2) = 2$, $n(L_3) = 2$, and $n(L_4) = 3$, respectively.

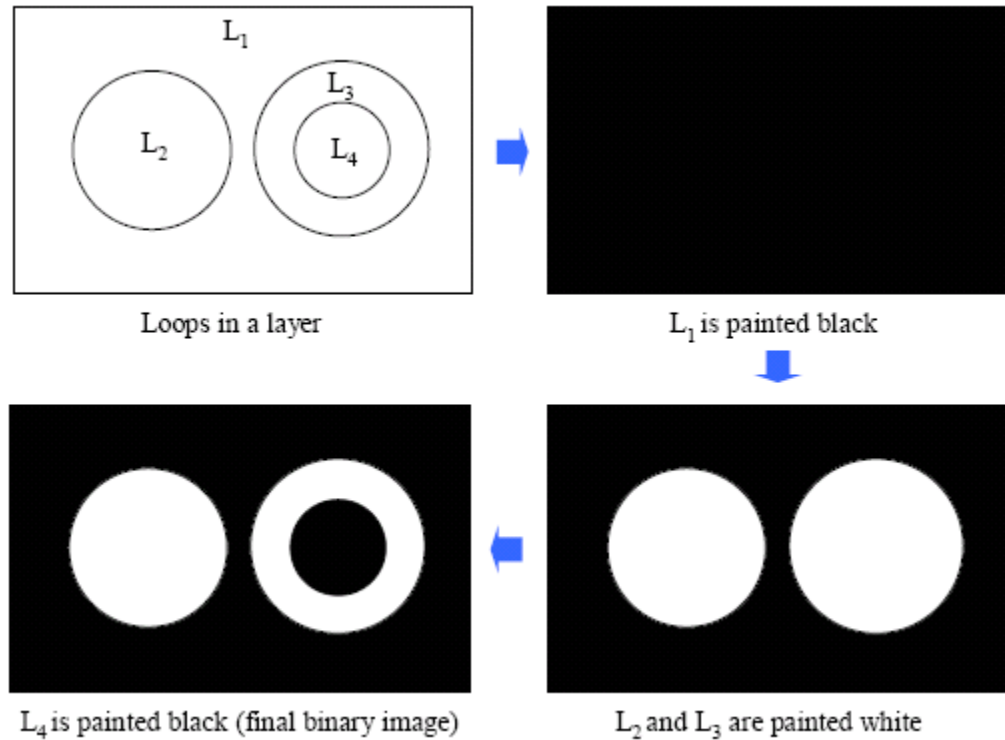


Figure 2.12 Example of binary bitmap generation [25]

2. Layer stacking part

The process data in the DMD-based μ SLA is a binary image file, i.e, bitmap, generated from the STL file as presented above. After the process data is generated from these sliced data, every layer is cured by synchronization of a shutter, a DMD, and a Z stage. A platform, which is the mechanical structure for mounting the substrate, is attached on the Z stage, and it is counter-balanced by pneumatic pressure. The Z stage

with the resolution of 100 nm and the repeatability of 100 nm ~ 300 nm are used because it significantly affects fabrication resolution and accuracy.

2.3 Summary and Research Gaps Analysis

As mentioned in Chapter 1, in this research, a mask projection micro stereolithography apparatus (MP μ SLA) adapted to fabricate complex 3D microstructures through transparent substrate is dealt with. Due to the uniqueness of our MP μ SLA, those existing process planning methods aforementioned cannot be directly employed by the author's apparatus. From the author's needs and perspective, various process planning methods for μ SLA and research gaps are summarized in Table 2.1 as below.

Table 2.1 Research Gaps Analysis

<p style="text-align: center;">Benay Sager's method (Section 2.2.2)</p> <p><u>Description:</u></p> <ol style="list-style-type: none">1. Give parameters of geometric profile, scan pattern, layer thickness, resin properties and grid points.2. Find the single key parameter: scan velocities, using least-squares estimation. <p><u>Research Gaps:</u></p> <p>Focus on scanning μSLA. Doesn't address problems for MPμSLA.</p> <ul style="list-style-type: none">➤ Needs a new mathematical formulation of parameter estimation.

Table 2.1 Research Gap Analysis (Continued)
Ameya Limaye's method (Section 2.2.3)

Description:

1. Slice the part into layers using an adaptive slicing algorithm.
2. Mesh each layer with data points
3. Snap the data-points to the resin points on the database
4. Generate the bitmap to be displayed for each layer
5. Apply compensation zone approach to obtain time of exposure for each bitmap

Research Gaps:

1. To generate bitmaps, the “Element Micromirror Mapping” database maps the center of each pixel to a single micromirror. This one-to-one mapping causes undesired blurs in the bitmaps, and a manual step should be performed to smooth bitmaps.

➤ Needs to develop a new method for bitmap generation.

2. Vertical resolution is limited by layer thickness, which is highly confined by resin properties.

➤ Needs an alternative excluding layer additive approach.

Table 2.1 Research Gap Analysis (Continued)
Jae-Won Choi's method (Section 2.2.4)

Description:

1. Generate STL file and sliced data.
2. Produce a binary image file from STL file based on topologies.
3. Cure layers by synchronization of shutter, DMD, and Z stage.

Research Gaps:

1. The layer stacking approach limits vertical resolution significantly.
 - Needs to unleash the vertical resolution by fixing the Z-stage.
2. Cannot cure viscous materials.
 - Needs to develop a process with little viscosity preference.
3. Lack of modeling the image formation and the resultant exposure profile.
 - Needs to model exposure distribution on the substrate.

The various research gaps identified above could essentially be generalized into four distinct gaps as below.

- **Research Gap 1:** Needs to control both the lateral dimensions and vertical thickness of cured part, without recoating by moving Z-stage, so as to unleash vertical resolution, to relax requirement for material viscosity and to reduce the waiting time effects [1] in the resin cure behavior during recoating process.
- **Research Gap 2:** Needs to develop an exposure distribution model, which can take all exposure amount contributed by multiple micromirrors into account for total exposure received by any single pixel on the substrate.

- **Research Gap 3:** Needs a new mathematical formulation of parameter estimation in process planning for the MP μ SLA under consideration, i.e, the TfMP μ SLA.
- **Research Gap 4:** Needs to develop a new method for bitmap generation.

2.4 Research Questions and Hypotheses

As a result of the research gaps identified in Section 2.3, this thesis is mainly an exploratory investigation of the possibilities and capabilities of a new process planning method for the unique TfMP μ SLA in the author's lab. The long-term goal of this research is to develop a mature process planning method for curing complex 3D micro parts through transparent substrate, with the intention of addressing in future work identified shortcomings of current methodologies. The specific goal in this thesis is to develop a feasible process planning method for the TfMP μ SLA through transparent substrate. This will answer the following primary research question: *What is the feasible process planning method for thick film fabrication on fixed flat transparent substrate using TfMP μ SLA?*

Based on this general research thrust, specific research questions have been identified and will be addressed in this thesis. The hypotheses for each of these aspects, as well as the explanations that crystallize the specific interests, are outlined below.

Column Cure Model: First and foremost, let's deal with Research Gap 1 in Section 2.3.

All the existing process planning methods for μ SLA employ slicing algorithms to discretize the geometric profile of part into horizontal layers. The process planning methods based on conventional discretization approach stress on lateral dimensions only. Such discretization requires a mobile Z-stage in vertical direction with layer stacking

control, so as to enable multi-layer additive curing. However, on the one hand, the vertical resolution is significantly limited by translational stages; on the other hand, recoating process can merely handle materials with low viscosity. Therefore, a Column Cure Model is put forward here to use vertical column voxels instead of horizontal slice voxels. By discretizing vertically into column voxels, the author will develop a new process planning method based on the so-called Column Cure Model, which is capable of controlling both the lateral dimensions and vertical thickness simultaneously, without mechanical stages. The new process planning method based on vertical column voxels is able to cure materials with higher viscosity than that based on horizontal layer voxels could do.

The remainder of the research gaps will be addressed in the form of research questions as below.

Research Question 1: How to control the thickness of each column voxel using TfMP μ SLA?

Hypothesis 1: The amount of energy exposure received by each pixel on the substrate can determine the cured height of corresponding column voxel.

Explanation: The resin cure behavior during the SLA fabrication process should be quantitatively modeled to predict the cured shape. SLA curing process can be modeled by using an energy exposure model to control the generated profile of the cured part within the desired limits of accuracy. In the TfMP μ SLA process, energy exposure is the parameter that determines how high a voxel is cured within the vat. Therefore, energy exposure will become the focus of the TfMP μ SLA parameter estimation formulation.

To be specific, a sub-research question could be derived as below from the research question.

Sub-Research Question: How to transform the desired height of each voxel into desired energy exposure for each pixel?

Sub-Hypothesis: The resin working curve, mapping the energy exposure amount to the cured height from the resin characterization experiments, can provide a transfer function that relates cured height with exposure amount.

Explanation: The working curve should incorporate the cured part effects (i.e, the transient curing nature [1]), since the TfMP μ SLA irradiates from under the resin vat. It will be elaborated in Section 3.4 of Chapter 3.

Research Question 2: How to determine the amount of energy exposure received by each pixel on the substrate?

Hypothesis 2: The amount of energy exposure received by a pixel is a summation of linear time accumulation of irradiance provided by each bitmap, which is a subgroup of DMD's micromirrors turned on, to the pixel.

Explanation: This research question will address Research Gap 2 listed in Section 2.3.

Exposure distribution on the substrate is significant in the photopolymerization process. To develop an analytical model of the TfMP μ SLA process planning method, the exposure profile should be quantitatively modeled and computed. The hypothesis here suggests setting up a "One pixel-to-Multiple mirrors" mapping, which could compute the energy exposure profile based on multiple linear accumulations of irradiances from multiple micromirrors.

Research Question 3: How to generate bitmaps and corresponding exposure time for each bitmap, given desired energy exposure for each pixel on the substrate?

Hypothesis 3: Parameter estimation can be used to find a set of bitmaps and exposure time for each bitmap, which minimize the deviation between desired energy exposure and actual energy exposure provided by the sequence of bitmaps.

Explanation: This research question is envisioned to combine Research Gap 3 with Research Gap 4. Hence, related research tasks can be divided into the following two steps.

Step 1: Identify process parameters, and formulate a mathematical problem to estimate key process parameter(s) for the TfMP μ SLA under consideration.

Step 2: Generate bitmaps with process parameters.

2.5 Chapter summary

In this chapter, literature review on typical process planning for μ SLA has been presented, followed by research gaps analysis. According to the research objective in Chapter 1 and research gaps identified in this chapter, the Column Cure Model along with several research questions are put forward with proper hypotheses. These challenges and possible solutions will be investigated in Chapter 3 and Chapter 4.

CHAPTER 3

FOUNDATIONS OF PROCESS PLANNING METHOD FOR TFMP μ SLA

In this chapter, the foundational knowledge required to analytically formulate the TfMP μ SLA process is presented. Foremost, the experimental setup of the TfMP μ SLA in this research is elaborated in Section 3.1. According to the research questions and hypothesis in Chapter 2, a model of process planning system for TfMP μ SLA is developed in Section 3.2, followed by fundamentals and validations of each module in the succeeding sections.

3.1 Introduction of the TfMP μ SLA

3.1.1 Basic setup of the TfMP μ SLA system

The scheme of the TfMP μ SLA system developed originally is illustrated in Figure 3.1.

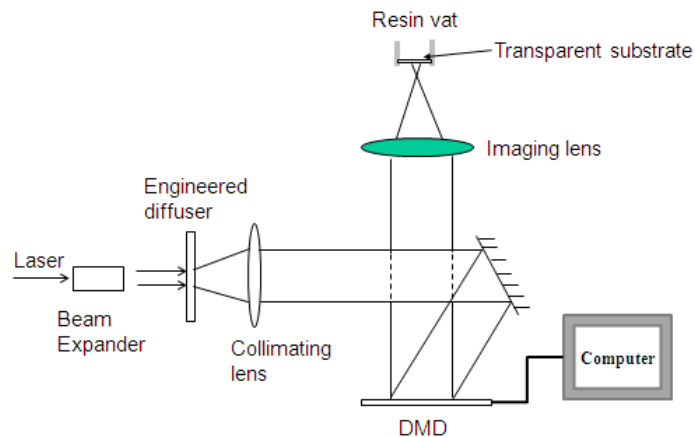


Figure 3.1 Schematic Diagram of the TfMP μ SLA system in this research

The design of the system can be divided into three modules.

Beam conditioning module: This module consists of a Helium-Cadmium UV laser light source from Omnicrome (now, Melles Griot) (Model # 3074-M-X04). The laser emits 38.5mW TEM01 at wavelength of 325nm. A beam expander is placed right after the laser source to expand the laser beam diameter from 1.5mm to 15mm. An Engineered™ Diffuser (micro lens array) is used after the beam expander to homogenize the beam's intensity profile and enlarge the beam diameter to 50 mm. A UV transmitting plano-convex lens with an effective focal length of 150.0 mm is used to collimate the light emerging from the diffuser. A UV coated mirror, mounted on a kinematic mount, directs the laser beam on a dynamic mask.

Imaging module: The Imaging module consists of a dynamic mask, the Digital Micromirror Device, (DMD™), an imaging lens (a UV transmitting Plano-Convex lens with an EFL of 75.0 mm). The DMD is an array of individually addressable, bistable micro mirrors, which can be selectively oriented, to display any bitmap. Every pixel on the bitmap controls one and only one micromirror on the DMD. The micromirrors are 12.65 μm square and the spacing between adjacent micromirrors is 1 μm . The micromirrors in their neutral state are parallel to the DMD chip. In its "ON" state, a micromirror swivels about its diagonal by 12° in one direction and in the "OFF" state, swivels by the same amount in the opposite direction. The DMD™ is a product of Texas Instruments and was sold by Productivity Systems Incorporated (PSI™). The bitmap displayed on the DMD serves as the object for the imaging system. The bitmap is imaged onto the substrate by the imaging lens. The DMD is mounted parallel to the horizontal plane. The object distance, as measured from the center of the pattern to the mid plane of

the imaging lens, was 152 mm and the image distance, measured from the mid plane of the imaging lens to the resin surface, was 132 mm. The radius of curvature of the plano-convex imaging lens is 34.25 mm and the thickness of the lens is 4.4 mm. The refractive index of the lens material is 1.460. The above-mentioned data was used in the ray-tracing algorithm, described in the Section 3.5 “Optical Module”.

Resin vat: The resin vat, as shown in Figure 3.2, is a rectangular container with the base made of a transparent glass slide. This glass slide acts as the substrate over which the film is cured.

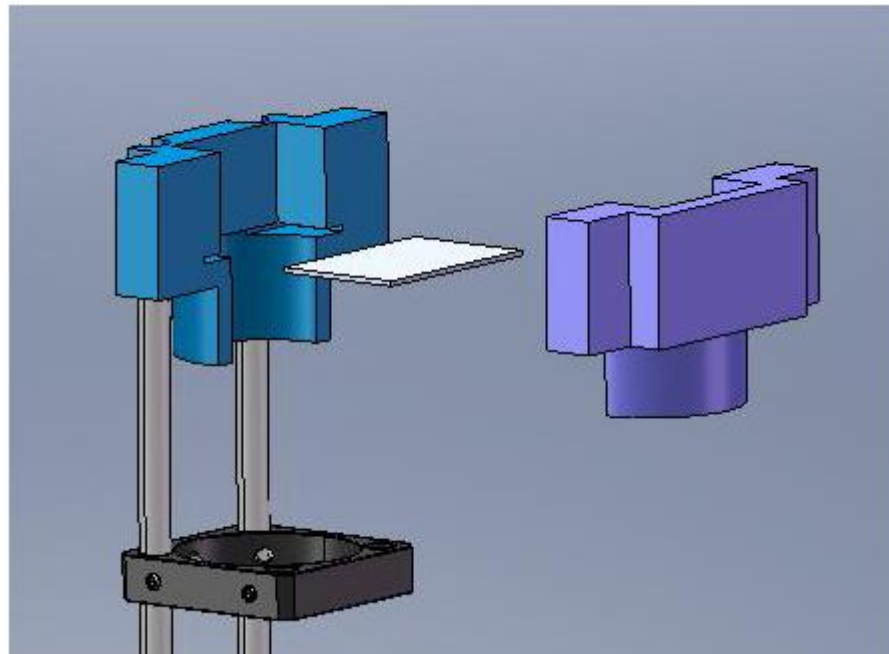


Figure 3.2 Exploded View of the resin vat (designed by Amit S. Jariwala, 2008)

The specifications of the system are presented in Table 3.1.

Table 3.1 Specifications of the TfMP μ SLA system at Georgia Tech

Component	Description	Model/Manufacturer
Laser	Power = 30mW Wavelength = 325nm Beam diameter = 1.5 mm	Omnichrome (Melles Griot)
Beam Expander	Lenes 1: UV Fused Silica Plano-Concave Lenses Effective focal length = -20mm Diameter = 12.7mm Radius of surface 1 = -9.2mm Radius of surface 2 = infinity (plane) Lens thickness = 2.0mm Material refractive index = 1.460 Lenes 2: UV Fused Silica Plano-Convex Lens Effective focal length = 250mm Diameter = 25.4mm Radius of surface 1 = 115.0mm Radius of surface 2 = infinity (plane) Lens thickness = 2.7mm Material refractive index = 1.460	Lens 1: LC4924 Lens 2: LA4158
Engineered Diffuser	Substrate size: 1 x 1", 2mm thick Material: Fused silica Wavelength = 325nm Illumination scatter pattern: Circle Divergence angle: 20 ° (full-width at 90%) Intensity profile at a plane: Flat-top Uniformity within flat-top region: $\pm 10\%$	RPC Photonics Catalog # Customized
Collimating lens	Fused silica Plano convex lens Effective focal length = 150mm Diameter = 50.8mm Radius of surface 1 = 69.0mm Radius of surface 2 = infinity (plane) Lens thickness = 7.8mm Material refractive index = 1.460	Thorlabs Catalog # LA4306-UV
Mirror	Diameter = 25mm. UV Enhanced Aluminum coated	Edmund Optics Catalog # NT45-605

Table 3.1 Specifications of the TfMP μ SLA system at Georgia Tech (Continued)

Component	Description	Model/Manufacturer
DMD	1024 X 768 array of micromirrors Dimension of micromirror = 12.65 μ m square. Spacing between mirrors = 1 μ m	Texas Instruments. Distributed by Prod. Sys Inc.
Imaging Lens	Fused silica Plano convex lens Effective focal length = 75mm Diameter = 25.4mm Radius of surface 1 = 34.5mm Radius of surface 2 = infinity (plane) Lens thickness = 6.7mm Material refractive index = 1.460	Edmund Optics Catalog # LA 4725-UV
Photopolymer resin	PEGDA MW 700 Ec, Dp determined experimentally	Catalog # 455008 Sigma Aldrich

3.1.2 Need to modify the system setup

After our initial tests of curing some simple parts with the basic system setup as described in Section 3.1.1, some problems arose in the equipment setup. First and foremost, we needed a feedback system to ascertain the irradiance projected from the DMD to the transparent substrate. This feedback would enable us to understand and quantify the system's optical performance and make compensations required, if any.

The laser light source is He-Cd UV Laser with 325 nm wavelength. Hence, we selected a UV CCD operating within this range and having the following characteristics:

Model: Sony XC-EU50CE

Black and White Camera with UV sensitivity in the range of 300-420nm

Adjustable shutter speed from 1/125s to 1/10,000s

Manual and automatic gain control

Effective pixels of 752(H) x 582(V) with cell size of 8.6 x 8.3 μ m

This camera is interfaced with the PC by using a frame grabber from CyberOptics Semiconductors. The model number of the frame grabber is Imagination PXC200AL. A BNC cable connector connects the camera to this frame grabber which is installed in the PC. The frame grabber converts the input analog signal from the camera to digital signals for further image processing and analysis through the PC. The camera is powered via the 12V power supply from the PC's power supply box. Figure 3.3 shows the setup with the CCD camera placed in position.

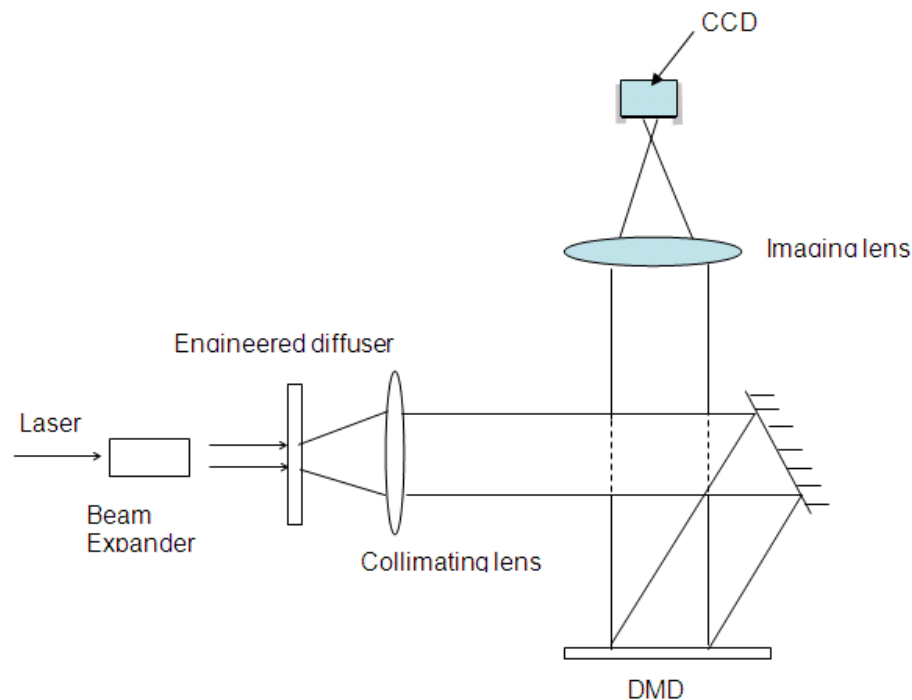


Figure 3.3 using a CCD camera to detect the actual exposure profile on substrate

From our prior experiments, we have observed significant effect of the variations in the irradiance profile on the cured part geometry. Figure 3.4 shows the line profile of

the irradiance captured from the CCD. The irregularities in the irradiance profile are observed very clearly from the graph plot of gray scale values vs pixels on the CCD.

Irradiance line profile plot from CCD

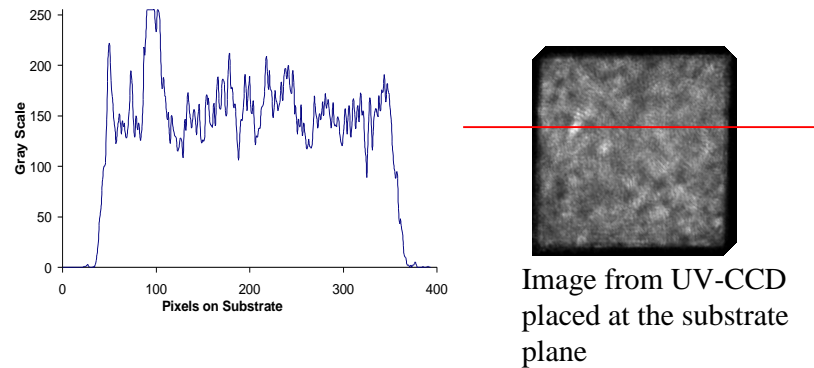


Figure 3.4 irradiance line profile plot from CCD

The effect of these irregularities can be seen on the cured part in Figure 3.5.

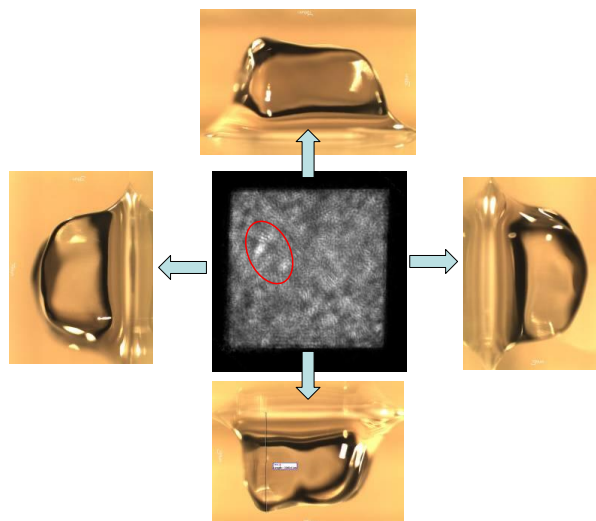


Figure 3.5 effects of irradiance variations on the cured part

From Figure 3.5, we could see that the regions (like the white region within the red circle) that receive higher irradiations cause significant curing heights. Hence, we need to investigate the amount of variation produced in the cured part by the variations in the irradiation profile and try to reduce the actual irradiation variance in the physical setup. This issue is addressed in Section 3.1.3, which details the modification of the experimental setup.

Another significant problem was the inconvenient and inaccurate manual control of displaying the bitmaps. We thought about developing a control software using LabVIEW by ourselves. After a further exploration, we discovered that the DMD software itself could display a series of bitmaps with a precision of 1 millisecond automatically. Thus, in the succeeding experiments, we are free from the difficulty in controlling the bitmaps to display for certain time. Moreover, we could use more bitmaps in the process plans in order to improve the accuracy in the mathematical module as well as in the cured parts (See Chapter 4).

3.1.3 Modified experimental setup

In the process of addressing the need in section 3.1.2, we noticed in the experiments that the exposure profile on the substrate varies if we rotate the diffuser to different angles. Based on the initial setup as presented in Section 3.1.1, the experimental setup is finally improved by adding a rotating device to the diffuser as shown in Figure 3.6; therefore by rotating the diffuser, the irradiance profile is smoothed out over time.

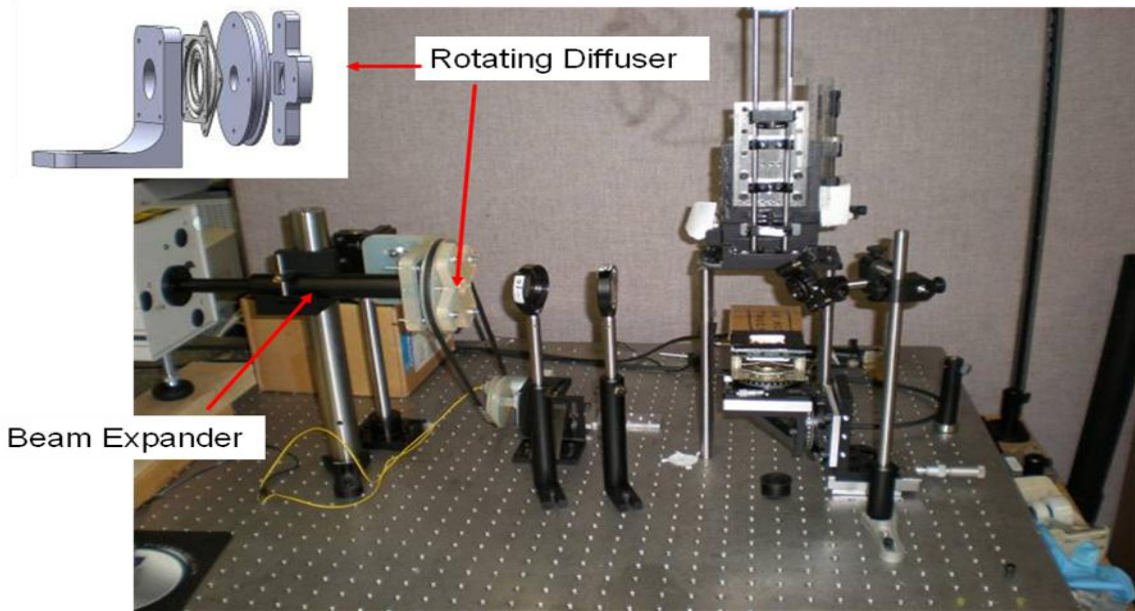


Figure 3.6 modified experimental setup - TfMP μ SLA

As presented in Section 3.1.2, we investigated the exposure profile on the substrate captured by a CCD camera. Figure 3.7 compares the substrate exposure profile in the previous system using a static diffuser with that in the current system using a rotating diffuser. It is clear that the exposure profile with rotating diffuser is more uniform with fewer speckles.

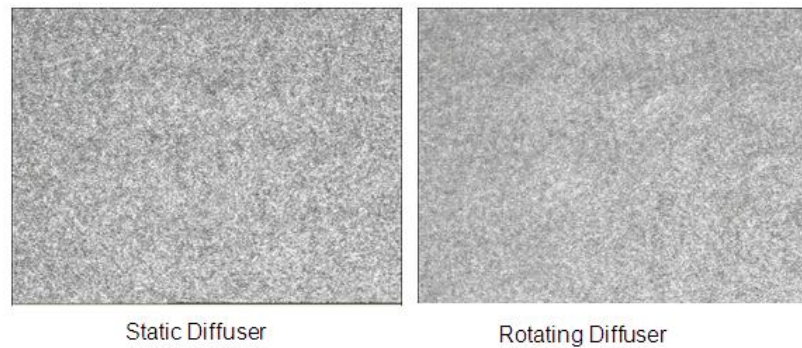


Figure 3.7 a more uniform exposure profile on the substrate obtained by rotating diffuser

A grayscale plot from CCD camera, taking an average of 300 images captured within 60 seconds, is shown in Figure 3.8. Obviously, the improved system with a rotating diffuser can produce a much more uniform exposure profile on the substrate.

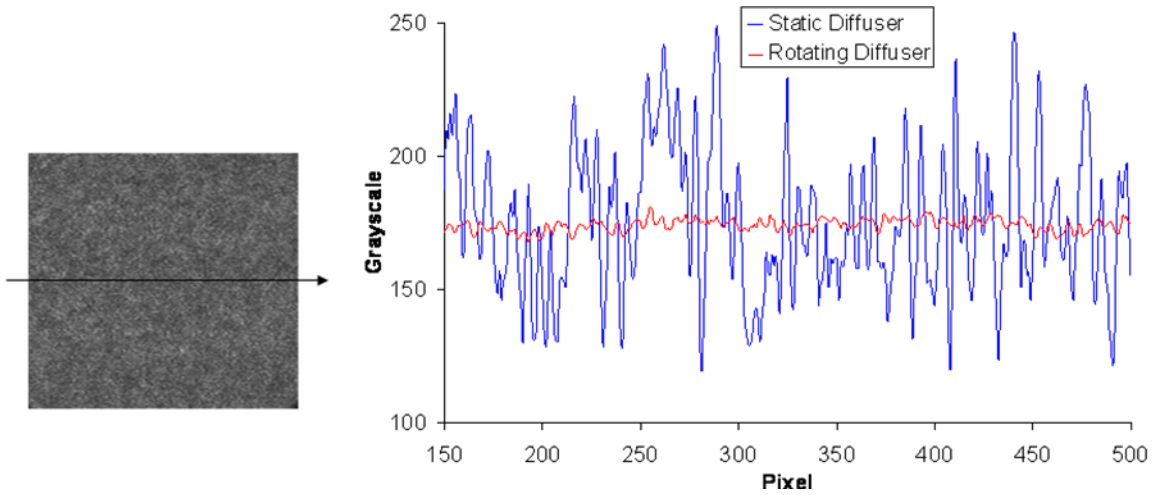


Figure 3.8 Grayscale plots of the exposure profiles obtained by static and rotating diffuser

The grayscale plots in Figure 3.8 are statistically compared in Table 3.2. It is concluded that by rotating the diffuser, the actual exposure profile on the substrate is more smooth and even. The TfMP μ SLA setup has been improved greatly in terms of the optical performance.

Table 3.2 Comparison of exposure profile in original and current systems

Experimental setup	Average of the grayscales	Standard Deviation of the grayscales
orginal (with static diffuser)	175	28
current (with rotating diffuser)	174	2

3.2 Modelling the Process Planning Method for TfMP μ SLA

Any manufacturing process involves a number of process parameters; however it is difficult for a user to choose appropriate process values for fabricating parts with particular requirements. This necessitates the development of a process planning method for any manufacturing process.

A process planning method computes the values to be assigned to process variables in order to fabricate a part with the required properties. Judicious selection of process parameter values entails modeling their effects on the fabricated part's properties. In case of the TfMP μ SLA, the process data is a binary image file, which is a sequence of bitmaps with certain display time for each bitmap. In order to use TfMP μ SLA to fabricate microparts, a process planning method has to be developed. This necessitates the identification of the process parameters and modeling their effect on the cured part's properties.

In order to address the research questions inherited from research gaps identified in Chapter 2, a model of process planning method for curing microparts with the required geometric profile using TfMP μ SLA is formulated.

Corresponding to the research questions in Section 2.4, the model of process planning method is modularized into geometrical, chemical, optical, mathematical, and physical modules. Concurrently, process parameters are identified for each module. An overview of the intended process planning system including primary process parameters is shown as in Figure 3.9.

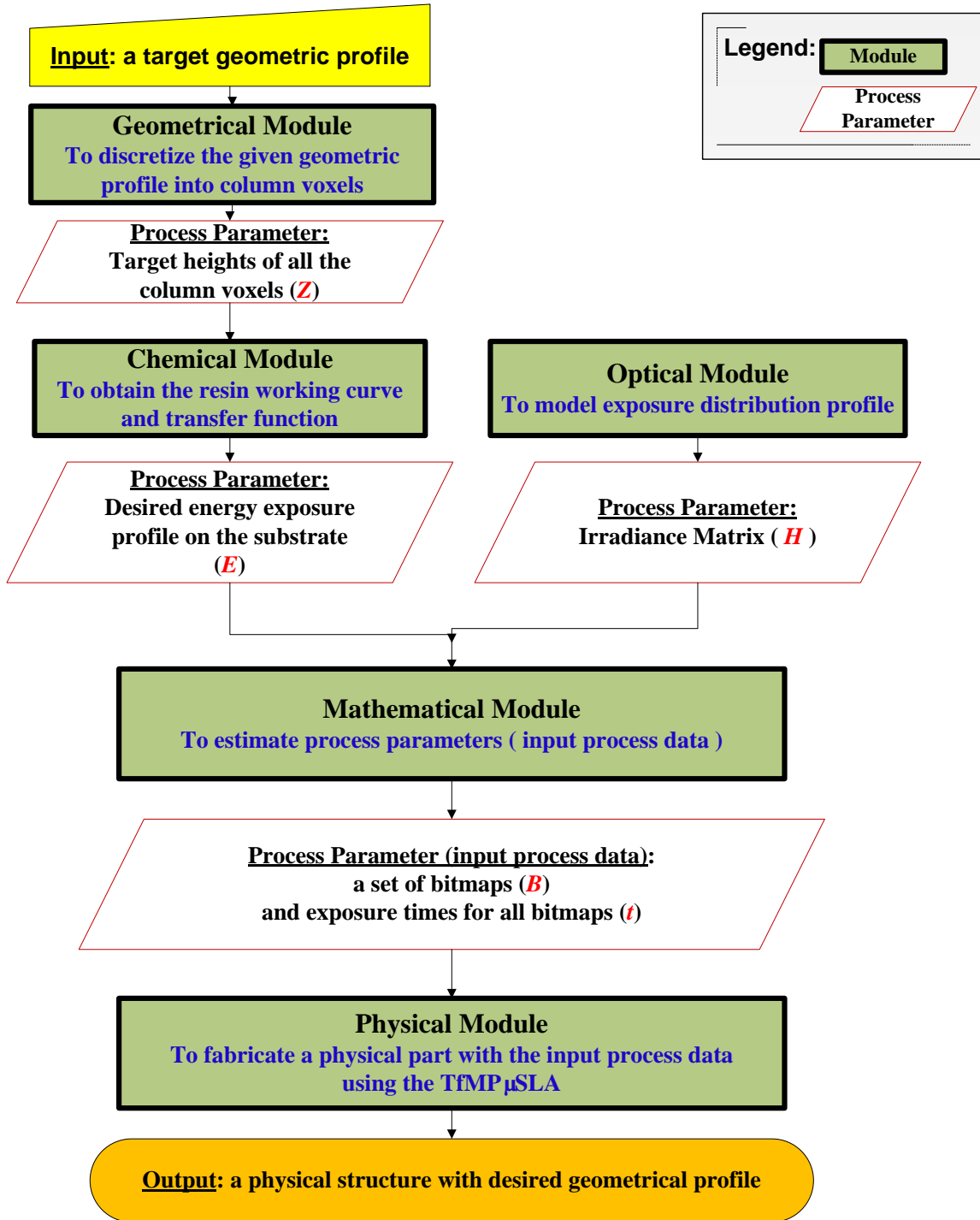


Figure 3.9 Model of the Process Planning System for TfMP μ SLA

3.3 Geometrical Module

As shown in Section 3.2, the input to the process planning system is a target topology. A geometrical module will be developed in this section, to discretize the topology for the sake of digital fabrication using TfMP μ SLA. The module will address Research Gap 1: Needs to control both the lateral dimensions and vertical thickness of cured part, without recoating by moving Z-stage.

As presented in Section 2.4, we have decided to use vertical discretization, based on which the process planning method is likely to address all the aforementioned issues concurrent with moving Z-stage and recoating process, as well as to control both the lateral and vertical dimensions.

3.3.1 Developing the Geometrical Module

Based on the Column Cure Model in Section 2.4, the geometrical module aims to discretize the given geometrical profile of a part into vertical (Z-direction) columns. The build orientation is assumed to have been determined and transformed as the Z direction before using the vertical discretizing procedure.

To achieve a vertical partition, two things need to be determined. One is the cross-section of each column, that is, pixel on the X-Y plane (i.e. substrate in our TfMP μ SLA). The other is the height of each column in vertical direction, i.e. Z-direction.

(1) Discretizing the X-Y plane (substrate) into pixels

There are primarily two factors determining the size of pixels.

Firstly, a pixel should correspond to the image on the substrate of a micromirror on the DMD. According to the simulation of irradiance distribution of micromirror using ray-tracing method (refer to Section 3.5), we identified that the influence area of a

micromirror is roughly within $10\ \mu\text{m} \times 10\ \mu\text{m}$. Figure 3.10 shows the simulation results of irradiation profiles from the center micromirror and one edge micromirror. The two profiles demonstrate that the most intensively irradiated area by a single micromirror is generally $10\ \mu\text{m} \times 10\ \mu\text{m}$. Hence, the size of pixel is better to be multiples of $10\ \mu\text{m} \times 10\ \mu\text{m}$, so that we could control the irradiance profile on the substrate conveniently and accurately by turning on / off some micromirrors. Essentially speaking, the DMD resolution along with the optical setup are dominant factors to determine the size of a pixel on the substrate, since we cannot achieve a sub-micromirror resolution by using substrate pixel smaller than the image of one micromirror.

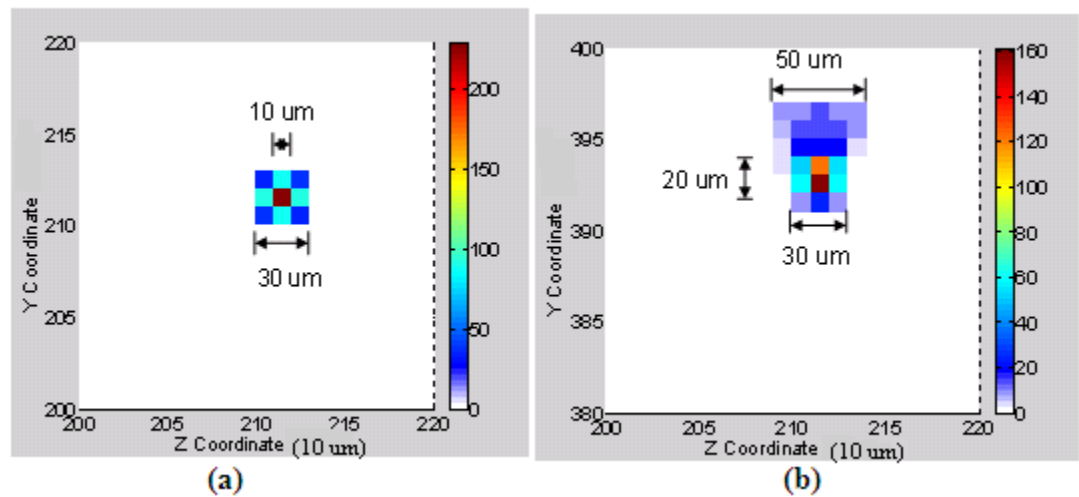


Figure 3.10 (a) Irradiation on the flat substrate from center micromirror; (b) Irradiation on the flat substrate from an edge micromirror

Secondly, the pixel size has significant impacts in the resolution of discretizing the geometric profile into columns. The error caused by this geometric profile partition is case sensitive, i.e., for different geometric profiles different levels of error would be

induced even for the same sampling size. In general, there are two discretizing approaches: uniform discretizing and adaptive discretizing. Uniform discretizing is the simplest approach for discretizing a plane into pixels with equal size. In this research, a uniform discretization is employed, however, adaptive discretization method is recommended for future work to decompose the volumes more accurately.

It is a compromising issue in determining the pixel size. If the pixel is smaller, one obtains a more smooth discretized geometric profile. It may however require much more computation time and enormous space to generate and store the irradiance database in order to obtain a larger irradiance matrix corresponding to the denser mesh of smaller pixels. On the other hand, if the pixel is bigger, the irradiance database is achievable, but one may end up with a part having a larger staircase effect.

The computer configuration in this research allowed using a pixel size of $10\ \mu\text{m} \times 10\ \mu\text{m}$, which is also the smallest area size according to one micromirror's illumination area. Consequently, it is decided that the geometrical module discretizes the substrate equally into $10\ \mu\text{m} \times 10\ \mu\text{m}$ pixels.

Nevertheless, it is desired to achieve smaller pixels in future work to improve the accuracy of the process planning method. The optical setup should be adjusted. To be specific, an optical setup with smaller magnification factor or even a demagnification setup could be considered to enable a smaller illumination area by each single micromirror on the DMD. Meanwhile, a more capable computer is necessary to generate a larger database corresponding to the smaller pixels on the substrate.

(2) Determining the height of each column

Given a geometrical profile, the dimension in vertical direction may vary for different points within a pixel on the substrate. Either an overall average of the heights or the height of the middle point in a pixel could be used as the height of the corresponding column. It is simpler to take the middle point height as that of the column; hence the geometrical module determines the height of each column by using the middle point values.

The geometrical module is illustrated in Figure 3.11.

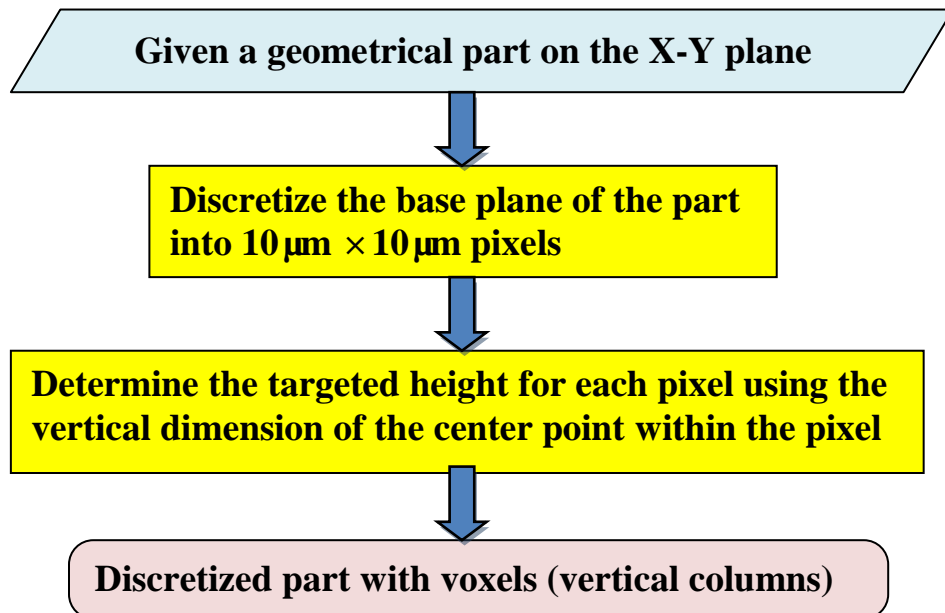


Figure 3.11 the flowchart of the geometrical module

3.3.2 Application Scope of the Geometrical Module

The geometrical module can not only be used to discretize an entire targeted geometrical part into vertical columns for the TfMP μ SLA, but also can be applied to

generate process data (bitmaps and exposure time for each bitmap) for curing each single layer on conventional MP μ SLA with movable Z-stage. In the latter case, the targeted geometrical part is firstly sliced into coarse layers, and then each layer is discretized into vertical columns using the geometrical module. Each single layer is thus regarded as a desired topology for the TfMP μ SLA, and the process planning method for TfMP μ SLA can be applied to cure each single layer. The mixed use of horizontal slicing and vertical discretization will reduce the staircase effect significantly compared with using slicing method only.

In this manner, a new process planning method for the conventional MP μ SLA is envisioned here: apply the process planning method, which is developed for the TfMP μ SLA in the thesis, for each single layer curing until the completion of the part. That is a combination of the novel process planning method in this thesis and the conventional recoating method by moving Z-stage. This hybrid process planning method could be used to cure more accurate and complex parts with MP μ SLA.

3.4 Chemical Module

The chemical module intends to transfer the targeted heights of all the discretized column voxels of a part into a desired energy profile. Before developing the chemical module, the underlying chemistry for photo-polymerization which occurs in curing a stereolithography resin is elucidated. Then a lump chemical module is developed to predict the curing characteristics of a resin. The module will answer Research Question 1: *How to control the thickness of each column voxel using TfMP μ SLA?*

3.4.1 Underlying chemistry of resin curing

A comprehensive photo-polymerization model is developed in Goodner and Bowman (2002) [51]. Based on the three primary reaction mechanisms occurring during the polymerization: initiation, propagation, and termination, the model also incorporates both primary radical termination and inhibition. It schemes the photo-polymerization process using seven equations as shown in Figure 3.12.

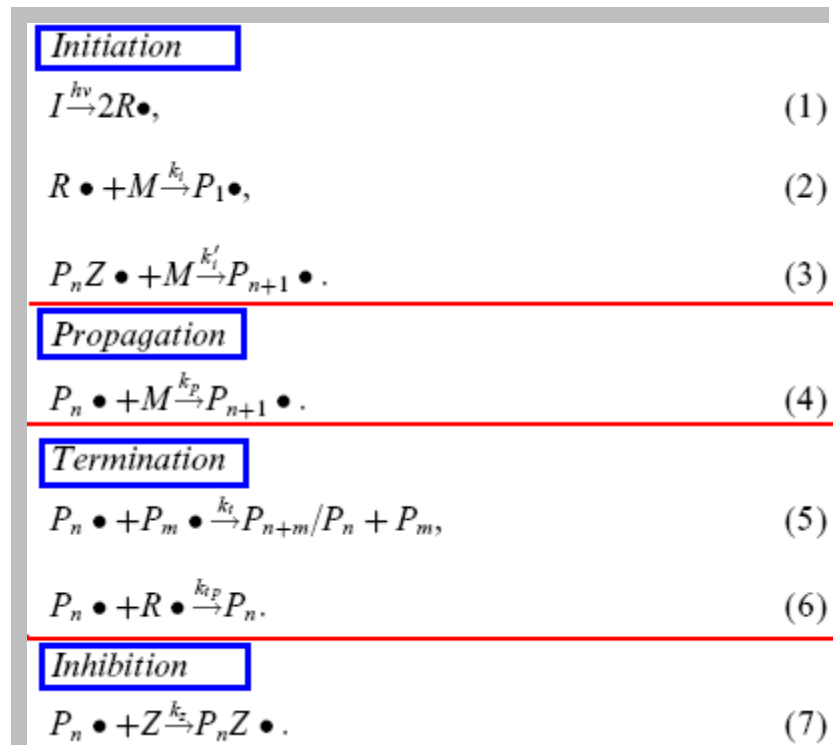


Figure 3.12 the scheme of the photo-polymerization process [51]

In this reaction mechanism in Figure 3.12, Eq. (1) is the photolysis of initiator, I , to give two primary radicals, $R\bullet$

The second step of initiation is the chain initiation process, shown by Eq. (2). In this reaction, a primary radical reacts with monomer, M , to form a growing polymer chain one repeat unit in length, P_1 : The rate of this reaction is determined by the kinetic constant for chain initiation, k_i .

A second type of chain initiation is given by Eq. (3): reinitiation of inhibited chains. In this reaction, an inhibited chain, P_nZ ; reacts with monomer to reform an actively growing chain. The kinetic constant for reinitiation, k_i' will in general be different from k_i ; in fact, the value of k_i' in most systems is either considerably lower (several to many orders of magnitude) than k_i or is considered to be zero.

The propagation reaction is represented by a single reaction (4), and the kinetic constant for propagation is k_p .

Chain termination occurs through two different mechanisms. Bimolecular termination (5) occurs when two growing radical chains come together and react to form dead polymer; this reaction can either occur by combination (forming one polymer chain) or disproportionation (forming two chains). While the mode of termination significantly affects the molecular weight in linear polymer-forming systems, the polymerization kinetics in crosslinked systems, which are predominant in commercial photopolymer applications, are not influenced significantly by the termination mode. Thus, the bimolecular termination reaction will be lumped into a single reaction having kinetic constant k_t . The second termination mechanism is primary radical termination (6), in which a primary radical reacts with a growing polymer chain to form dead polymer. The kinetic constant for this process, k_{tp} , will in general be different from the bimolecular k_t ,

as the two reactions have different chemistry and different species mobilities involved in the termination process.

The last reaction occurring during polymerization is chain inhibition (7). In this process, an inhibitor species, Z , such as molecular oxygen or an intentionally added inhibitor, reacts with a growing chain to form a relatively unreactive species. The kinetic constant for this reaction is k_z .

To be specific, commercial SLA resins are a mixture of the monomer and photoinitiator [53]. Under the light illumination, the photoinitiator absorbs the incident photons and generates radicals. The radicals react with the monomer molecules to form larger reactive molecules. These larger reactive molecules, in turn, have the ability to react with other monomers and form longer reactive molecules. The reactive molecules will keep growing until two of them meet together and form a stable polymer chain. The solidified polymer structure will eventually be constructed by the cross-linking of those polymer chains.

3.4.2 Modeling the chemical resin cure behavior

The chemical resin cure behavior during the μ SLA fabrication process should be modeled quantitatively to predict the cured shape. There exist mainly two kinds of models: one is the exposure threshold model, and the other is the degree of cure (DOC) threshold model.

3.4.2.1 Exposure Threshold Model

The basic exposure threshold model is presented in Jacobs (1992) [41]. It assumes that the depth of cure is proportional to the logarithm of exposure and assumes the threshold model of resin cure.

Suppose that irradiance, H (mW/cm^2), is incident on the resin surface for a duration, t (second). It would supply an exposure by Equation 3.1.

$$E = H \cdot t \quad (\text{mJ}/\text{cm}^2) \quad (3.1)$$

This energy would get attenuated as it enters the resin, according to the Beer Lambert's law. The exposure at a depth, z (μm), is given by Equation 3.2, where D_p (μm) denotes the depth of penetration for light propagation in chemical resin (a measure of attenuation of radiation).

$$E_z = E \cdot \exp(-z / D_p) \quad (\text{unit: mJ}/\text{cm}^2) \quad (3.2)$$

Curing occurs at all points where energy exposure is greater than or equal to, E_c , which represents the threshold exposure value. The thickness of the part cured, C_d , will thus be given by Equation 3.3.

$$C_d = D_p \cdot \ln(H \cdot t / E_c) \quad (3.3)$$

3.4.2.2 Degree of Cure (DOC) Threshold Model

Yanyan Tang (2005) put forward a novel stereolithography cure process model; this is the degree of cure (DOC) threshold model [52]. Dr.Tang firstly formulated the scanning SLA cure process model, which is a set of coupled partial differential equations describing mass and energy transport during the curing process, including exposure and dark reaction in one model. Then she employed differential photocalorimetry (DPC) to characterize the photopolymerization kinetics, thus a comprehensive kinetic model is parameterized. Also, the thermal and physical properties of the resin material should be characterized.

With the kinetic parameters determined, material properties evaluated, and laser and process parameters recorded in the part building process, the SL cure process model established previously was solved using the finite element method with the software package FEMLAB. Through part fabrication and measurement, it was found that a certain degree of cure (DOC) contour outlines the built part within minimal error. For this reason, the SL cure process model established and solved earlier has been referred to as a “DOC threshold model” when used to predict the fabricated part shape and dimensions.

Obviously, the DOC threshold model incorporates the chemical reaction, the resin kinetic characteristics, as well as the thermal and diffusion effects into the cure model, which predicts more accurately the cured shape and dimensions during the scanning SLA process. The major difference between the simplified exposure threshold model and a complex SL cure process model, like the DOC threshold model, is shown in Figure 3.13, where MW represents molecular weight, and CD denotes cure degree.

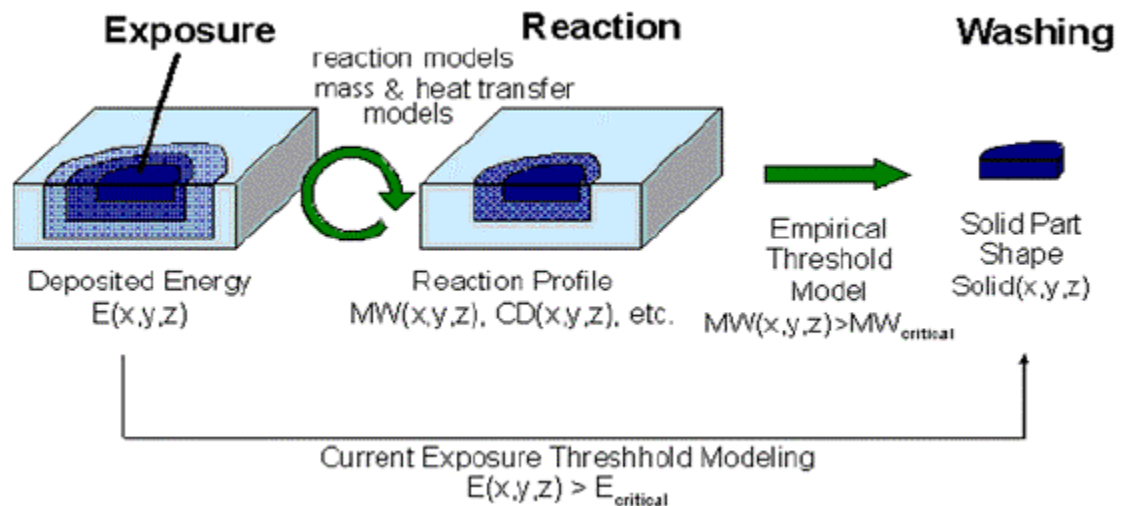


Figure 3.13 Exposure Threshold model VS. Complex SL Cure Process model [52]

3.4.3 Developing the Chemical Module

Before developing the chemical module, we should determine which resin cure model to be used for the TfMP μ SLA process planning. The DOC threshold model is more accurate, however it doesn't apply in our TfMP μ SLA process, since Tang Yanyan's model (2005) was focused on scanning stereolithography process that is far different from the TfMP μ SLA. Unfortunately, for the time being, there is no available resin cure model similar to DOC threshold model that accounts for chemical mechanisms well for MP μ SLA process. A comprehensive MP μ SLA curing process model, which includes chemical reaction and kinetics as well as heat and mass transfer, will be recommended for future work.

In this section, we will develop the chemical module by improving the traditional Exposure Threshold model in hope that it can model the resin cure process well and predict the cured shape accurately enough.

3.4.3.1 TfMP μ SLA's Resin Cure Model

Based on the traditional exposure threshold model [41] and transient layer cure model [1], we formulate a new resin cure model which quantitatively connects the exposure amount with the cured height during the TfMP μ SLA process for any pixel on the substrate.

For a point p_i , energy exposure $E(p_i)$ is given by $E(p_i) = H(p_i) t$, where t is the exposure time at this point. According to the threshold model presented in Section 3.4.2.1, a resin point is cured if and only if the exposure received by this point is greater than the threshold exposure of polymerization E_c .

The variation in exposure with depth in the resin follows the Beer Lambert's law of absorption. So, the exposure at a height z in the resin is given as Equation 3.4.

$$E(p_i, z) = E(p_i)e^{-z/D_p} \quad (3.4)$$

Again, if $E(p_i, z) \geq E_c$, the resin will cure at the point p_i . So, the depth to which the resin will cure at a point p_i receiving irradiance $H(p_i)$, when exposed to irradiation for a time t , is given by Equation 3.5.

$$C_d(p_i) = D_p \cdot \ln(H(p_i) \cdot t / E_c) \quad (3.5)$$

The model in Equation 3.5 is based on an assumption that the attenuation of radiation through a cured layer is the same as that through uncured resin. It does not count the effects of radiation through a cured part, which is in solid phase. Limaye & Rosen (2007) have observed experimentally that the attenuation through a cured layer is significantly less than that through the liquid resin [43]. Thus, the depth of penetration for a cured layer (solid part) D_{pS} is expected to be different from that for the liquid resin D_{pL} . The layer cure model developed by Limaye & Rosen (2007) by modeling the layer curing as a transient phenomenon is described as below.

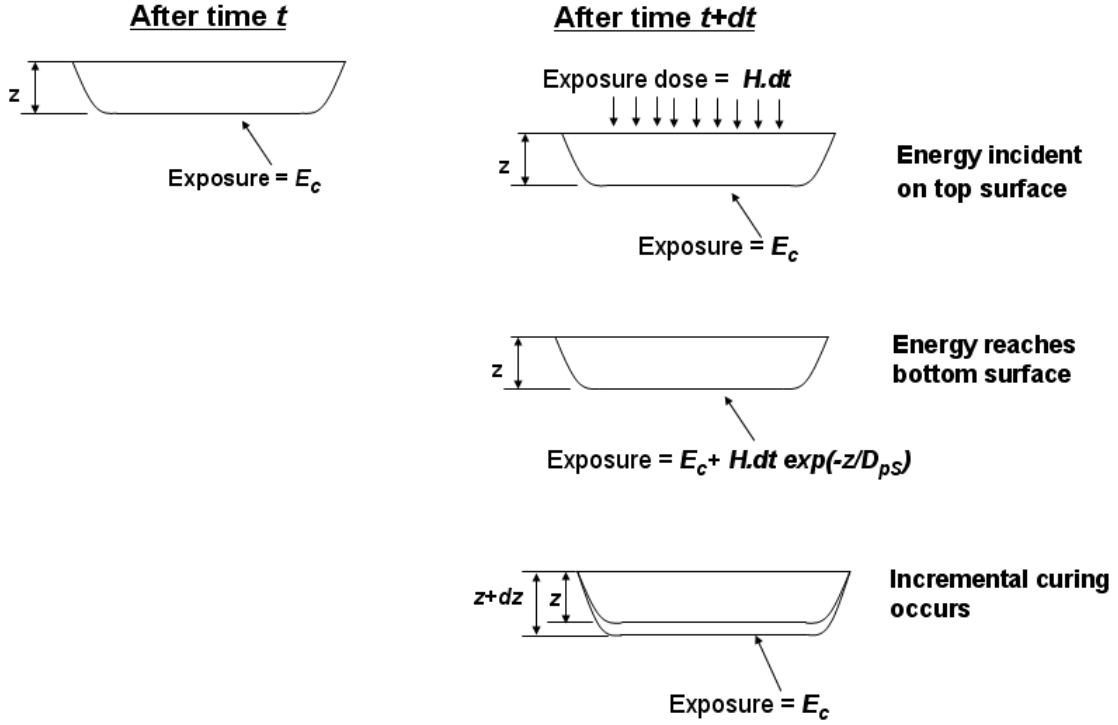


Figure 3.14 Modeling resin curing as a transient phenomenon [43]

Suppose that, as shown in Figure 3.14, the thickness of the film cured after time t is equal to z . The exposure at the bottom surface of this film is equal to E_c . At time $t+dt$, the next dose of energy equal to $H \cdot dt$ will be incident on the top of the cured film. This energy will get attenuated following the Beer Lambert's law of attenuation as it would pass through the cured layer of thickness z and the energy reaching its bottom surface would be $H \cdot dt \exp(-z/D_{ps})$. Here, it will add up with E_c , the energy already at the bottom of the film and cause an incremental curing equal to dz . This incremental curing will be given by Equation 3.6.

$$dz = D_{pL} \ln \left[1 + \frac{dE \cdot \exp(-z/D_{ps})}{E_c} \right] \quad (3.6)$$

In Limaye (2007), Equation 3.6 was solved numerically to obtain the relationship between the depth of cure (z) and the amount of exposure (E). However, his solution could only account for those resins for which the rate of radiation attenuation through cured resin is negligible compared to that through uncured resin.

Instead of using numerical integration, here we derived a novel closed-form solution to the resin cure model as a transient process, i.e, Equation 3.6. The deduction of the solution is described in Figure 3.15.

Since $\frac{dE \exp(-z / D_{ps})}{E_c} \ll 1$, so we can use Taylor series :

$$\ln\left[\frac{dE \exp(-z / D_{ps}) + E_c}{E_c}\right] = \ln\left[1 + \frac{dE \exp(-z / D_{ps})}{E_c}\right] = \frac{dE \exp(-z / D_{ps})}{E_c} - \frac{1}{2} \left(\frac{dE \exp(-z / D_{ps})}{E_c}\right)^2 \dots$$

omitting the higher - order terms, like $(dE)^2$, $(dE)^3$, we have

$$\ln\left[\frac{dE \exp(-z / D_{ps}) + E_c}{E_c}\right] \approx \frac{dE \exp(-z / D_{ps})}{E_c}$$

hence, the working curve function is approximated as below :

$$dz \approx D_{pL} \cdot \frac{dE \exp(-z / D_{ps})}{E_c}$$

Figure 3.15 Deduction of a closed-form solution to the resin cure model as a transient process

In Figure 3.15, after applying Taylor series expansion and omitting the higher order terms, Equation 3.6 can be further simplified into Equation 3.7.

$$dz \approx D_{pL} \cdot \frac{dE \cdot \exp(-z / D_{ps})}{E_c} \quad (3.7)$$

The improved resin cure model, which is named as the TfMP μ SLA's resin cure model, as shown in Equation 3.8, is obtained after solving the ordinary differential equation above.

$$z(E) \approx D_{pS} \cdot \ln\left(\frac{D_{pL}}{D_{pS}} \cdot \frac{E}{E_c} + 1 - \frac{D_{pL}}{D_{pS}}\right) \quad (3.8)$$

In Equation 3.8, z , E denotes the cured height and exposure on a substrate pixel during the TfMP μ SLA process, respectively. The parameters D_{pL} , D_{pS} and E_c are to be determined experimentally in the following resin characterization.

In Limaye (2007), the non-additive nature of exposure was investigated since the waiting time between two consecutive exposure doses is significant. The diffusion effect was thus considered into the MP μ SLA resin cure model, because there existed significant waiting time between two consecutive bitmaps due to the recoating procedure. In our TfMP μ SLA, bitmaps are displayed continually and the switching time is negligible. Hence the diffusion effect as described by Dr.Limaye is not included in our resin cure model. Nevertheless, we managed to reduce the waiting time for a pixel on the substrate to receive a subsequent dose of exposure. In particular, we enable the additive nature of exposure by continuously curing each column voxel. Therefore, a particular constraint will be imposed in the subsequent process planning module – mathematical module. It requires that the output of the mathematical module, i.e, the generated sequence of bitmaps should be downsizing; so as to ensure that the curing of each column voxel will not be interrupted. Such a continual growing manner can reduce greatly the waiting time for each substrate pixel during the resin curing.

3.4.3.2 Resin Characterization – Working Curve

To illustrate the resin characterization, we are taking the Huntsman SL-5510 resin as sample material. Please note that the material resin used in our research is actually a biomaterial hydrogel PEGDA MW 700, not the SL-5510 resin; however, the resin characterization process is the same. The values of E_c and D_p have been specified by the resin manufacturer to be 8.9 mJ/cm^2 and 0.122 mm respectively. Research on MP μ SLA systems has shown that the experimentally observed values of E_c and D_p differ from their values specified by the manufacturer (Bertsch et al., 2000, Farsari et al., 2000, Hadipoespito, 2003). So, the resin needs to be characterized experimentally to obtain the real working curve of SL-5510 resin in our TfMP μ SLA.

The following experiments are performed to determine the unknown parameters in Equation 3.8, which are D_{pL} , D_{pS} and E_c . A thin film is cured on the TfMP μ SLA by exposing it to radiation for different time durations. By varying the time of exposure, the radiant energy received by the film is varied. Thus a series of data points is observed, that is the thickness of the cured film against the exposure received by the film as shown in Figure 3.16. Fitting these data points into the TfMP μ SLA resin cure model (i.e, Equation 3.8), the values of E_c , D_{pS} and D_{pL} are found to be 4.0 mJ/cm^2 , 0.015 mm and 0.011 mm , respectively, which is fairly different from the manufacturer's specified value.

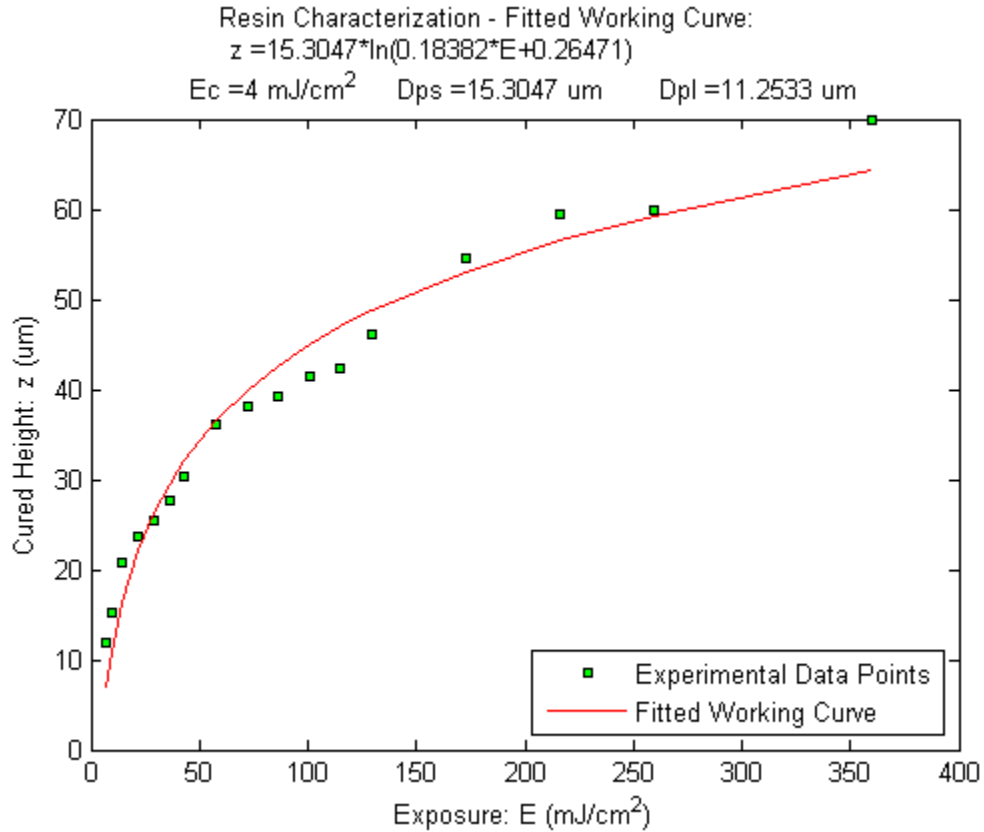


Figure 3.16 Working curve of Huntsman 5510 resin with the TfMP μ SLA system

3.4.3.3 Chemical Module Developed

With the TfMP μ SLA resin cure model formulated in Section 3.4.3.1 and resin characterization experiments prepared in Section 3.4.3.2, the chemical module is ready to transfer the target discretized geometrical profile of a part into a desired exposure energy profile. The flowchart of the chemical module is presented in Figure 3.17.

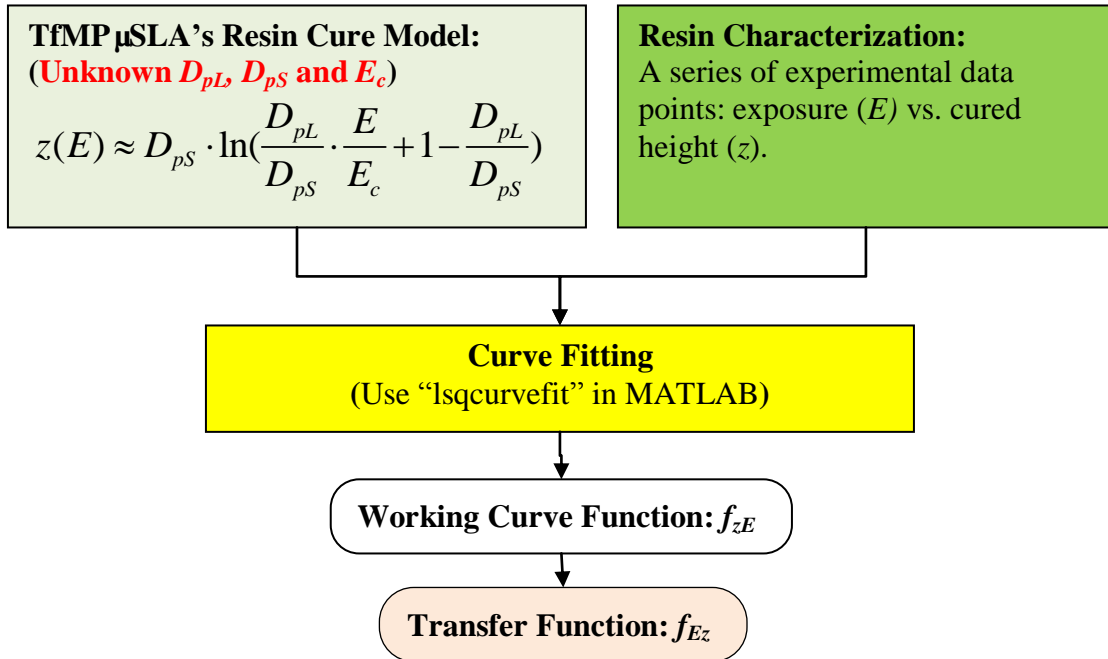


Figure 3.17 the flowchart of the chemical module

As shown in Figure 3.17, through resin characterization experimentation, a series of data points can be obtained, providing a relationship between the amount of exposure (E) and the curing height (z) on the substrate in the TfMP μ SLA system. By fitting the data points into the resin cure model as described in Equation 3.8, the resin parameters D_{pL} , D_{pS} and E_c can be determined yielding a minimum residual norm. The least-squares curve fitting function “lsqcurvefit” in MATLAB is used to solve the curve fitting problem. Appendix A presents the MATLAB code in the chemical module.

By substituting the known values of D_{pL} , D_{pS} and E_c into Equation 3.8, a working curve function f_{zE} (as shown in Equation 3.9), which maps the variable (E) to the cured height (z) is available to predict the cured height on any substrate pixel. Note that for $E <$

E_c , the liquid resin wouldn't get cured, therefore the cured height $z = 0$. The working curve function is finally as shown in Equation 3.9.

$$z = f_{zE}(E) = \begin{cases} 0, & \text{for } E < E_c; \\ D_{pS} \cdot \ln\left(\frac{D_{pL}}{D_{pS}} \cdot \frac{E}{E_c} + 1 - \frac{D_{pL}}{D_{pS}}\right), & \text{for } E \geq E_c \end{cases} \quad (3.9)$$

Theoretically, the transfer function f_{Ez} can be obtained by inverting f_{zE} . However, note that in Equation 3.9 for $z = 0$, E could be any value smaller than E_c . To form a function, we artificially assign a single zero value to E for $z = 0$. Thereby, the transfer function f_{Ez} is obtained as Equation 3.10.

$$E = f_{Ez}(z) = \begin{cases} 0, & \text{for } z = 0 \\ E_c \cdot \frac{D_{pS}}{D_{pL}} \cdot \left[\exp(z / D_{pS}) + \frac{D_{pL}}{D_{pS}} - 1 \right], & \text{for } z > 0 \end{cases} \quad (3.10)$$

The final outputs of the chemical module are the resin working curve function f_{zE} and the transfer function f_{Ez} . Herein, the chemical module has been developed to transfer the desired height (z) of each column voxel into the desired exposure amount (E) on the corresponding substrate pixel.

3.5 Optical Module

According to Hypothesis 2 in Section 2.4, the amount of energy exposure received by a pixel on the substrate is a summary of linear time accumulation of irradiance provided by each contributing micromirror during the TfMP μ SLA process. Therefore, Research Question 2 consists of two sub-problems: one is the irradiance profile, the other the exposure time. Obviously, the irradiance profile, which is also called as ‘‘exposure distribution profile’’ on the substrate by the DMD, should be quantified

foremost; and the part of computing exposure time will be addressed in the mathematical module.

In this section, the optical module aims to model the irradiance (mW/cm^2) profile on the resin substrate by micromirrors of the DMD. The module will partially but essentially address Research Question 2: *How to determine the amount of energy exposure received by each pixel on the substrate?*

3.5.1 Ray-tracing method

The irradiance distribution on the resin depends upon the energy distribution across the light beam incident on the bitmap of DMD and upon the optical aberrations caused by the imaging lens. The irradiance distribution across the beam incident on the DMD is assumed to be uniform and the value is measured using a radiometer. This irradiance is one of the inputs to the optical model. The ray tracing algorithm is adopted from Limaye & Rosen (2007), so as to characterize the system's optical performance in terms of number of rays. Figure 3.18 shows the schematic of the ray tracing algorithm for projection of light rays from DMD onto flat substrate.

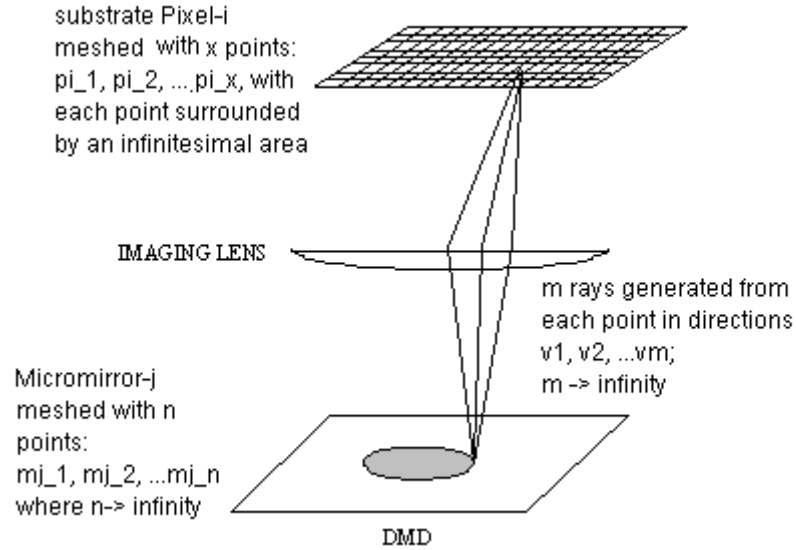


Figure 3.18 Schematic of ray tracing algorithm [43]

When a micromirror on the DMD is imaged onto the resin surface, all rays emanating from all points on the micromirror are directed onto the resin surface by the imaging lens. Every ray irradiates the infinitesimal area centered at the point where it intersects the resin substrate. Each micromirror, say *Micromirror j*, on DMD can be assumed to be composed of n number of points: $m_{j_1}, m_{j_2}, \dots, m_{j_n}$ where $n \rightarrow \infty$. Since a collimating lens is used in conjunction with the diffuser, the light beam incident on the DMD is fairly collimated with a divergence angle of less than 1 degree. To take into account the effect of the minor divergence, a cone of rays is emitted from each micromirror point. $v_t (v_1, v_2, \dots, v_m, \text{ where } m \rightarrow \infty)$ represents the direction vector in which the rays are emitted from the point on the DMD. The substrate pixel, say *Pixel i*, can be assumed to be composed of x number of points $p_{i_1}, p_{i_2}, \dots, p_{i_x}$, where $x \rightarrow \infty$. Each pixel is 10um-by-10um, the same size as in the geometrical module. Refer to Figure 3.18.

We introduce a function, δ which evaluates whether a particular ray from *Micromirror j* will strike an infinitesimal area centered on a given point on the substrate *Pixel i* or not. For example, $\delta(m_{js}, v_t, p_{ik})$ will determine whether the ray originating from the point m_{js} on *Micromirror j* in the direction of vector v_t will strike an infinitesimal area centered on point p_{ik} on *Pixel i*. If the ray does strike the infinitesimal area surrounding point p_{ik} , then $\delta(m_{js}, v_t, p_{ik}) = 1$. Else, $\delta(m_{js}, v_t, p_{ik}) = 0$.

The function δ is evaluated by adopting the exact ray tracing procedure as explained in (Smith, 1996). In an exact ray trace the path of every ray is traced through the lens, and the coordinates where it intersects the image plane are determined. The imaging system parameters are used in the evaluation of the function δ .

The number of rays striking a pixel, say *Pixel i* (p_i) on the resin substrate by a micromirror, say *Micromirror j* (m_j), N_{ij} will be given by the Equation 3.11.

$$N_{ij} = N(p_i, m_j) = \sum_{s=1}^n \sum_{t=1}^m \sum_{k=1}^x \delta(m_{js}, v_t, p_{ik}) \quad (3.11)$$

Since the irradiance at a point on the substrate is proportional to the number of rays striking that point, the irradiance on *Pixel i* (p_i) by *Micromirror j* (m_j), H_{ij} , can be given in Equation 3.12.

$$\begin{aligned} H_{ij} &= c \cdot N_{ij} / (\text{pixel area}) = c \cdot N_{ij} / (10\mu\text{m} \times 10\mu\text{m}) \\ &= c \cdot N(p_i, m_j) / (10^{-6} \text{cm}^2) \\ &= 10^6 \cdot c \cdot \sum_{s=1}^n \sum_{t=1}^m \sum_{k=1}^x \delta(m_{js}, v_t, p_{ik}) \end{aligned} \quad (3.12)$$

Where,

H_{ij} = irradiance on "Pixel i" by "Micromirror j"

unit: mW/cm²

c = power of a single ray, constant

unit: mW

By the ray-tracing method, a database storing numbers of rays irradiated on each substrate pixel from each micromirror on the DMD in the TfMPSLA is generated.

3.5.2 Calculation of single ray power

The constant c in Equation (3.7), which is the power of single ray, is calculated with the following step. Using a radiometer, the average irradiance across the beam can be measured. Let the average irradiance be H_{av} (mw/cm²). The number of rays striking an area of 1 cm² on the resin substrate will be given by extrapolating the number of rays irradiated on a small area, which is handy by using the resultant database from ray-tracing. So, the number of rays, N_{av} (/cm²), corresponding to an irradiance of H_{av} can be obtained. The constant c is thus determined to be H_{av}/N_{av} (mw).

The MATLAB code used to calculate the irradiation carried by single ray is listed in the Appendix B. In the code, the number of rays on 160*160 um² area is counted and extrapolated onto a 1 cm² area.

3.5.3 Irradiance Matrix

The resultant irradiance database from the ray-tracing method actually consists of enormous independent matlab mat-files. Each mat-file contains the numbers of rays irradiated on all the pixels on the substrate by certain single micromirror of the DMD. The database establishes “one-to-multiple” mapping relations: “one micromirror-shine onto-multiple pixels” and “one pixel-irradiated by-multiple micromirrors”. Such “one-to-multiple” irradiance manner will be utilized as a fundamental principle in the mathematical module while generating bitmaps and exposure time vector. The mathematical module will use parameter estimation method to minimize the deviation

between the desired and the actual exposure energy profile. Foremost, an irradiance matrix should be ready for the sake of executing the mathematical module.

The irradiance matrix, written as H , embodies all the mapping relationships between DMD micromirrors and resin substrate pixels. The typical element of H is H_{ij} (refer to Equation 3.12), denoting the element of row i and column j , where row i corresponds to the i^{th} pixel and column j corresponds to the j^{th} micromirror. The number of rows of H equates with the number of all the pixels on the resin substrate. Similarly, the number of columns of H is equal to that of all the micromirrors of the DMD part.

The MATLAB code used to create the irradiance matrix from the database generated by ray-tracing method is attached in Appendix B.

3.5.4 Optical Module Developed

The optical module has been developed to output the irradiance matrix. As a summary, the flowchart of the optical module is given in Figure 3.19.

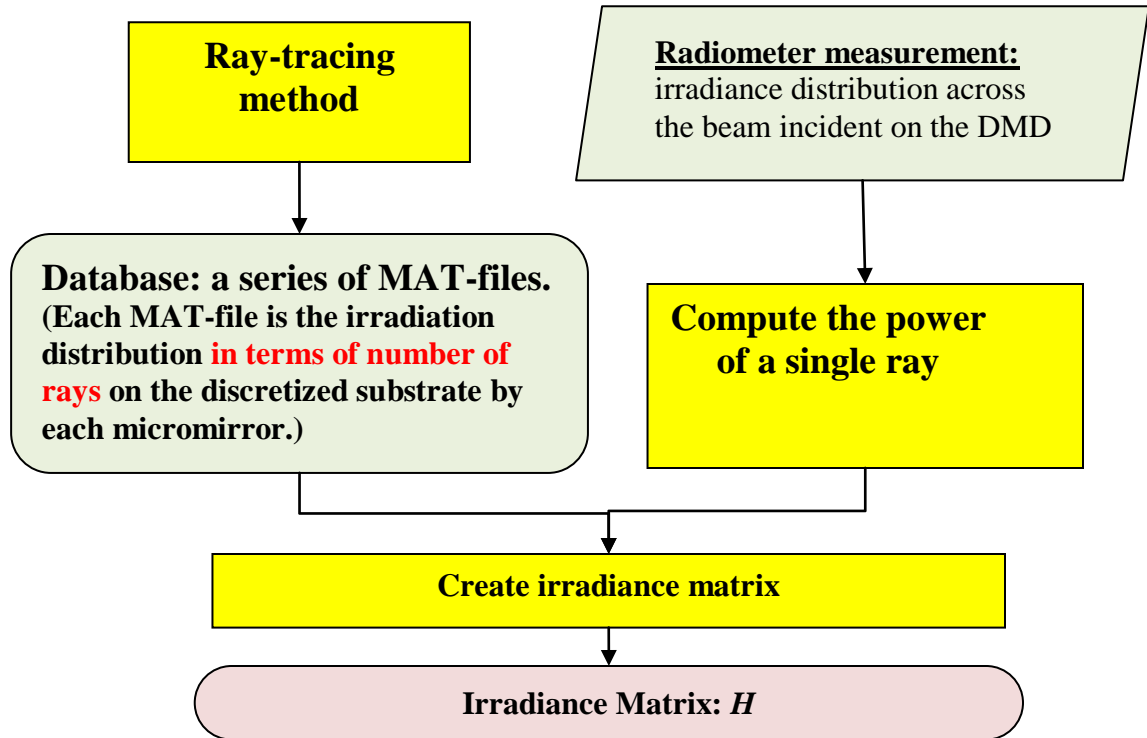


Figure 3.19 the flowchart of the optical module

3.5.5 Analysis of the ray-tracing density effect

The optical module primarily adopts the ray-tracing method, which solves the irradiation problem by repeatedly advancing idealized narrow beams called rays through the system by discrete amounts n and m as described in Figure 3.18. Again, n is the number of discretized points of each micromirror on the DMD, and m is the number of discretized rays originating from the same point on each micromirror. Ideally, a perfect model of the system's optical behavior will be achieved if n and m are at infinity. However, we could only assign some fairly small values to n and m due to the limitation in computation time and data storage. Small n and m mean that a few rays are used

corresponding to a sparse sampling, while the so-called dense sampling uses much more rays.

The effect of the sampling density in ray-tracing method is analyzed by comparing two cases which have different sampling densities in the ray-tracing system. In the sparse ray-tracing case, $n = 9$, $m = 121$; while in the dense ray-tracing case, $n = 81$, $m = 225$.

In each case, the ray-tracing method traced the rays emitted from 421×421 micromirrors onto 301×301 pixels. We investigated the exposure profile on the center line of 200 pixels on the substrate irradiated by 161 micromirrors on the center of DMD. An irradiance matrix, H , were generated in each case. The exposure profile within a unit time (1 second) is shown in Figure 3.20. Figure 3.20(a) shows the exposure profile generated by the sparse ray-tracing, Figure 3.20(b) the exposure profile generated by the dense ray-tracing.

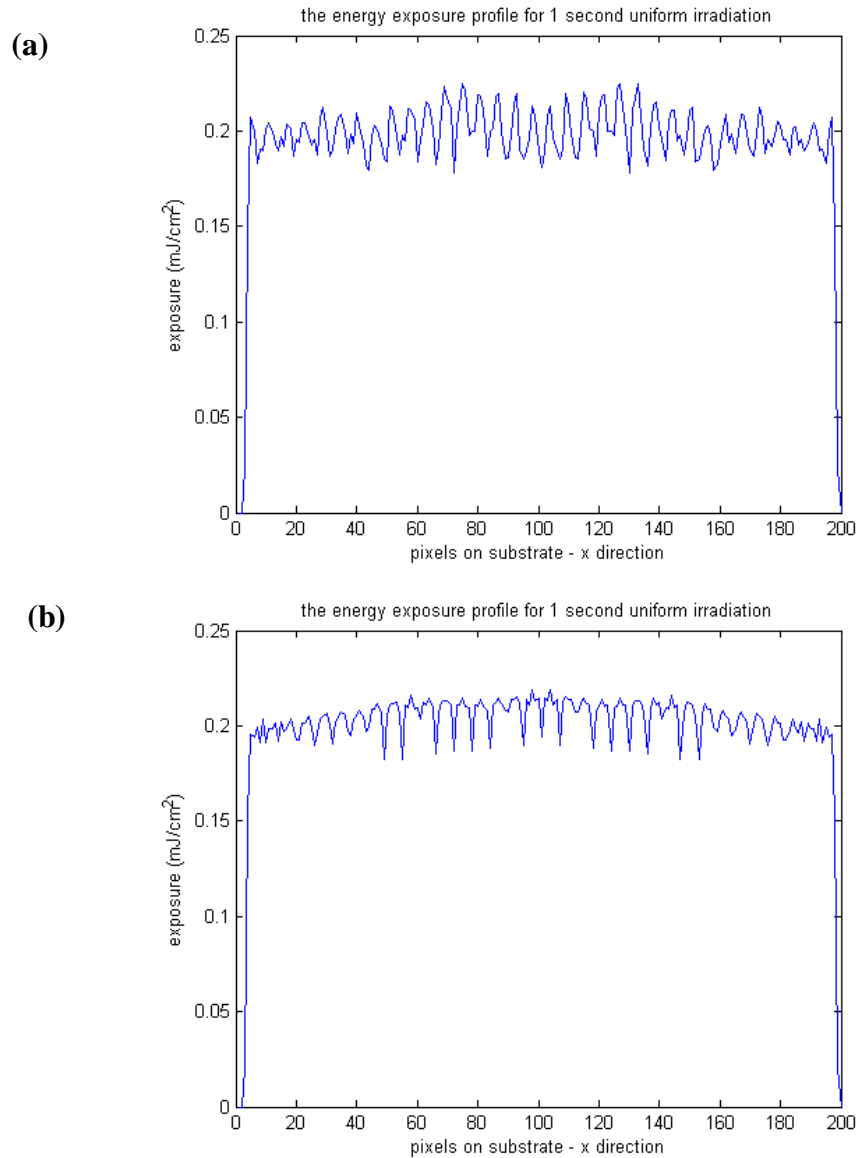


Figure 3.20 (a) the exposure profile for 1 second generated by the sparse ray-tracing; (b) the exposure profile for 1 second generated by the dense ray-tracing

In Figure 3.20, note that the sparse ray-tracing produced many unwanted sharp jags, compared with a flatter profile generated by the dense ray-tracing. It is clear that dense ray-tracing could yield a relatively more smooth exposure profile, which conforms better to the anticipated uniform exposure on the substrate. Figure 3.21 provided a

statistic depiction of the irradiation distribution on the substrate using box plot. On each box, the central mark is the median, the edges of the box are the 25th and 75th percentiles, the whiskers extend to the most extreme data points not considered outliers, and outliers are plotted as red cross mark individually. Apparently, the distribution of exposure dose simulated by the dense ray-tracing is more compact and uniform.

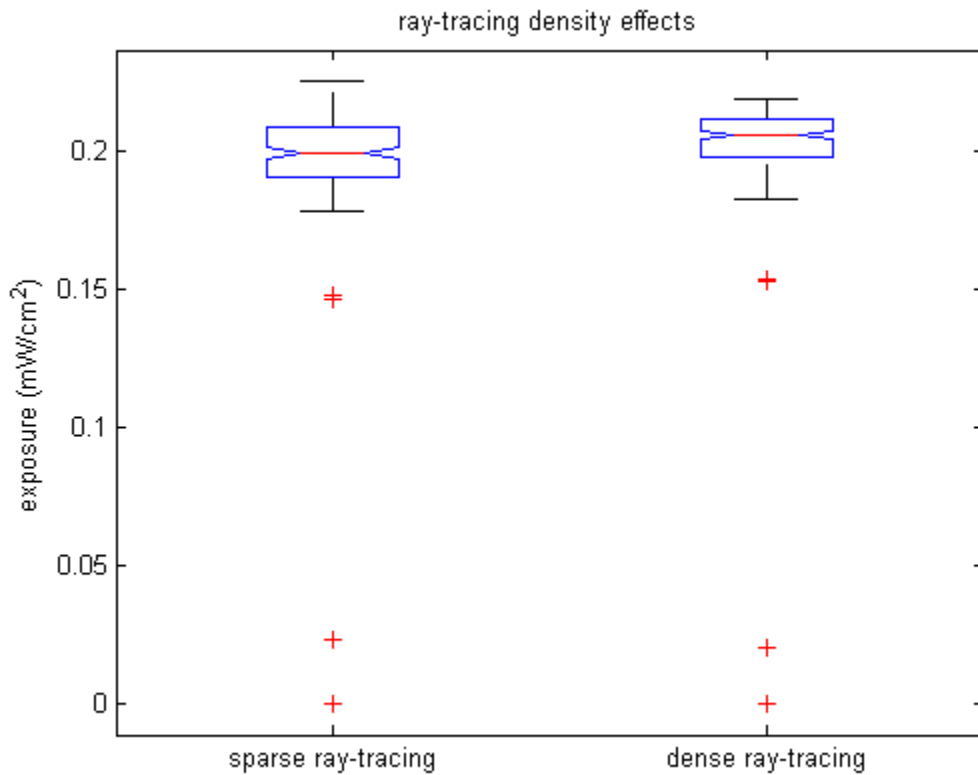


Figure 3.21 box plot of the irradiation distribution generated by the sparse and dense ray-tracing

Furthermore, to demonstrate the ray-tracing density effect, we used the irradiance matrix generated by the two ray-tracing systems of different sampling densities to do process plans for curing a 2.5D geometric profile as shown in Figure 3.22.

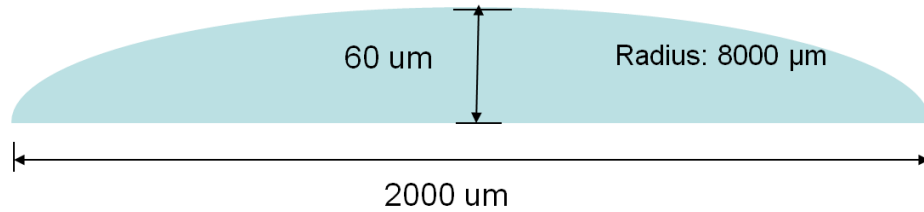


Figure 3.22 the target geometric profile in demonstrating the ray-tracing density effect

Implementing the process planning system proposed in Section 3.2, we applied the chemical working curve presented in Section 3.4.3.2 to get the desired energy exposure profile E_0 . Then we estimated the energy exposure profile E using the irradiance matrix H output by the optical module. 40 bitmaps were generated for each process plan. And the estimated exposure profile E is the total exposure dose contributed by all the 40 bitmaps. Note that the irradiance matrix H varies with the ray-tracing density. Figure 3.23 is the resultant exposure profiles using H from both sparse ray-tracing and dense ray-tracing.

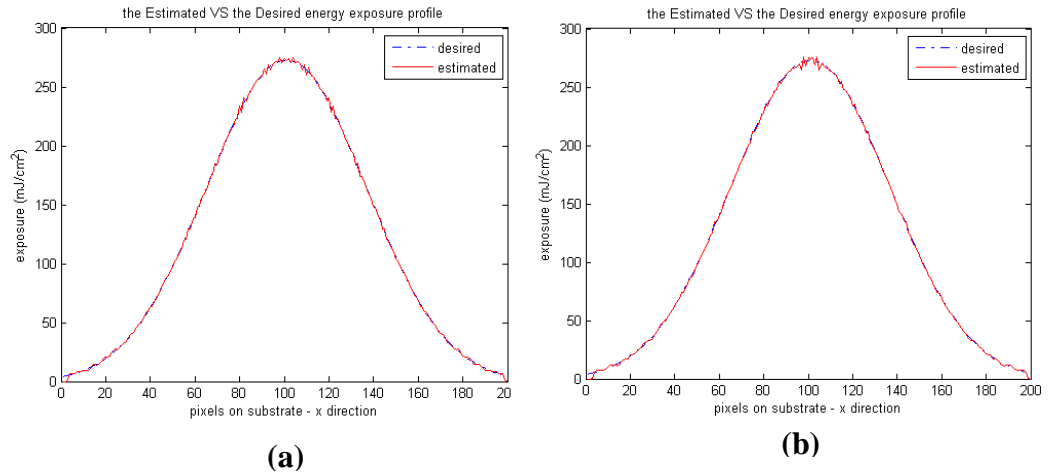


Figure 3.23 energy exposure profile estimation with (a) sparse ray-tracing (b) dense ray-tracing

Both dense and sparse ray-tracing were able to provide a reasonable estimation of the energy exposure profile in the process planning system. However, there was some discrepancy in terms of the deviation between the desired and estimated energy exposure. Table 3.3 shows the ray-tracing density effect in energy exposure profile estimation during the process plan. Column 4 is the RMS value (root mean square) of the energy deviations. The dense ray-tracing resulted in a smaller deviation than the sparse ray-tracing. However, the difference is not too much.

Table 3.3 Effect of the sampling density in the ray-tracing method

Ray-tracing density	n	m	RMS($E-E_0$) (mJ/cm ²)
Sparse	9 (3×3)	121 (11×11)	1.658
Dense	81 (9×9)	225 (15×15)	1.543

It is concluded that by increasing the ray-tracing density, the optical module can output a more uniform exposure profile as expected, which would improve the process planning system's performance in minimizing the deviation between the desired and estimated energy exposure profiles. Nevertheless, it is acceptable to use a seemingly small ray-tracing density, like the aforementioned sparse ray-tracing with $n = 9$ and $m = 121$. It won't have too much influence if the computation environment cannot sustain a too dense ray-tracing. In this thesis, a ray-tracing with $n = 81$ and $m = 225$ is adopted in the TfMP μ SLA process plan.

3.6 Chapter summary

In Chapter 3, the setup of the TfMP μ SLA under consideration is introduced. Following the model of the process planning system prepared in Section 3.2, so far the geometrical module, chemical module and optical module have been developed (refer to Figure 3.9). The geometrical module has explained the Column Cure Model presented as proposed in Section 2.4. The chemical module discloses a relationship between the cured heights and the exposure dose by modeling resin cure behavior analytically and characterizing resin experimentally. The chemical module validates Hypothesis 1, establishing a foundation for testing the remaining hypotheses, which will be evaluated in the mathematical module presented in Chapter 4.

Moreover, the optical module quantifies the irradiance amount from every DMD micromirror onto every substrate pixel. The irradiance matrix, H , prepares for a mathematical representation of Hypothesis 2 in Chapter 4.

CHAPTER 4

MATHEMATICAL MODULE

With the desired energy exposure profile, E , evaluated in the chemical module, and irradiance matrix, H , determined in the optical module, the mathematical module will be established in this chapter, in order to generate the input process data for the TfMP μ SLA – a sequence of bitmaps and respective time of exposure. The mathematical module will primarily answer Research Question 3, which is related to producing the process data; nevertheless, it also virtually addresses the second part of Research Question 2, which involves computing the exposure time. In general, all the research questions in the thesis will have been addressed after this chapter.

In Section 4.1, a new mathematical formulation of parameter estimation in process planning for the TfMP μ SLA is presented. The mathematical algorithms to solve the problem formulated are proposed in Section 4.2, including optimization and clustering. Developing the mathematical module, the flowchart as well as MATLAB codes are presented in Section 4.3. Validation and analysis is presented in Section 4.4 and 4.5, shedding light on the capability of the mathematical module.

4.1 Mathematical Formulation

To illustrate the mathematical formulation of parameter estimation in process planning for the TfMP μ SLA, an example will be given in Section 4.1.1. Section 4.1.2 will define, quantify and formulate the practical problem into a mathematical problem.

4.1.1 TfMP μ SLA parameter estimation formulation example

The basic idea of the proposed process planning method will be explained in the context of Figure 4.1. The geometrical profile of the part of interest in the parameter estimation formulation can be discretized as a cluster of voxels along which the exposure value should be equal to the desired exposure. The cross-section of a voxel on the substrate (X - Y plane) is called as pixel. By specifying the shape and size of these pixels, the surface finish of the cured outline can be controlled. For the pixels on this substrate, the goal is to minimize the deviation between the exposure received from DMD and the desired exposure. The surface we are interested in is the sphere surface. Since pixels are cured as a result of DMD projection, the goal is to estimate the exposure patterns (bitmaps) and exposure time for each bitmap pattern that will satisfy the least squares minimization.

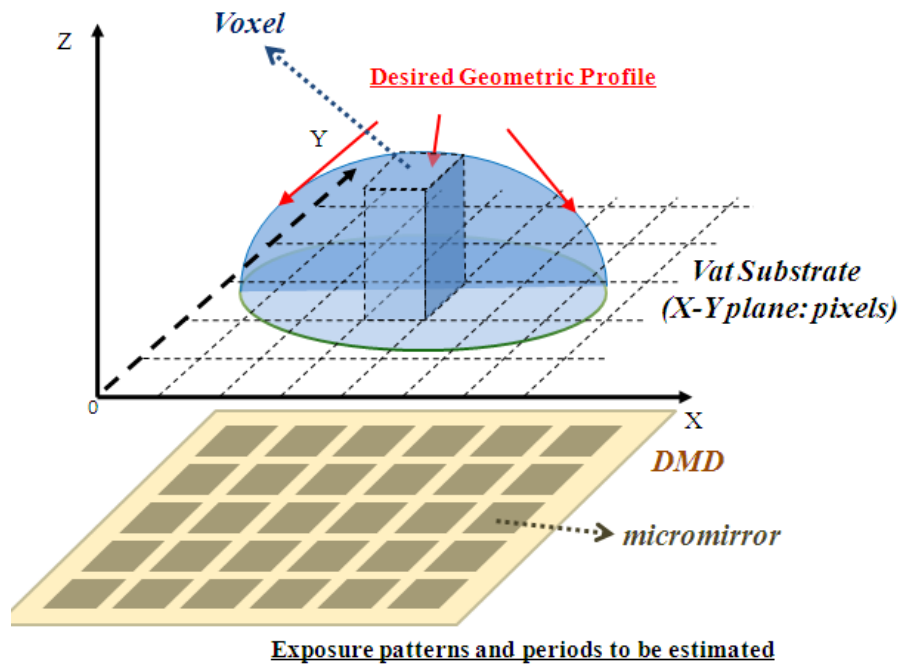


Figure 4.1 TfMP μ SLA parameter estimation formulation example

4.1.2 Problem formulation – optimizing z

Taking the example in Section 4.1.1, we formulate the parameter estimation problem in the following steps.

The initial problem can be represented as following:

Problem 1

Input:

A desired geometrical profile: $z_0 = G_0(x, y)$ and TfMP μ SLA system

Output:

An estimated geometric profile by the process planning method $z = G(x, y)$

Objective:

To minimize deviation between $z_0 = G_0(x, y)$ and $z = G(x, y)$

To solve the problem, we discretize the plane of the substrate into $10\mu\text{m} \times 10\mu\text{m}$ pixels in the geometrical module developed in Chapter 3. Let the substrate be a mesh of $N_x \times N_y$ pixels, where N_x and N_y are the numbers of pixels in X -direction and Y -direction respectively, as shown in Figure 4.1. The entire mesh of pixels will be formulated as a vector. We define 2-norm distance between cured profile and geometrical profile as our optimization objective. Note that $2\text{-norm}(x)$ is the Euclidean length of a vector x : $\|x\| = \text{sqrt}[x_1^2 + x_2^2 + \dots + x_n^2]$, where n is the length of x .

Then the problem 1 can be translated to problem 2:

Problem 2

Input:

A desired geometrical profile: z_0 (z_0 is a vector with size $N = N_x \times N_y$)

Output:

An estimated geometric profile by the process planning method (z is also a vector with size N)

Objective:

$$\min_z \| z - z_0 \|$$

The desired geometrical profile z_0 can be transferred to the desired exposure E_0 in the chemical module developed in Chapter 3. The cured height of z due to an exposure dose of E can be obtained by using the working curve function f_{zE} (see Equation 3.9).

Then the problem 2 can be translated to problem 3:

Problem 3

Input:

A desired geometrical profile: z_0 (z_0 is a vector with size N)

The chemical module (refer to Section 3.4)

Output:

An estimated exposure profile on the substrate E (E is a vector with size N)

Objective:

$$\min_E \| f_{zE}(E) - z_0 \|$$

The exposure E on pixels of substrate is decided by the exposure time T of micromirrors on the DMD. The formula for this relationship comes from the optical module developed in Chapter 3. The optical module outputs an irradiance matrix H ,

which provides all the mapping relationships between DMD micromirrors and resin substrate pixels in the TfMP μ SLA.

Exposure energy is linearly accumulative both temporally and spatially. For a single pixel on the substrate, the exposure energy received by the pixel is an addition of each dose of exposure from any single micromirror that has irradiated on it. In total, exposure for each pixel on the substrate is a weighted sum of the irradiance from all micromirrors on the DMD, where the “weights” are exposure time for each micromirror. The equation is as below in Equation 4.1.

$$E = f_{ET}(T) = HT \quad (4.1)$$

In Equation 4.1, T is a vector with size M (number of micromirrors on the DMD used in the TfMP μ SLA), representing the exposure time of each micromirror, and H is a matrix with size $N \times M$ from the optical module. Now the problem is transformed to:

Problem 4

Input:

A desired geometrical profile: z_0 (z_0 is a vector with size N)

The chemical module (refer to Section 3.4)

The optical module (refer to Section 3.5)

Output:

An estimated exposure time T of each micromirror on DMD in the TfMP μ SLA

(T is a vector with size M)

Objective:

$$\min_{T \geq 0} \| f_{zE}(f_{ET}(T)) - z_0 \|$$

This is a constrained large scale optimization problem. But it's not the end. Actually the exposure time T is controlled by a series of black-white bitmaps. The white pixel on the bitmap means that the corresponding micromirror is OFF and the black pixel on the bitmap means that the corresponding micromirror is ON. The exposure time is decided by the aggregate display time of all the bitmaps. For the purposes of this work, we denote the number of bitmaps as K . The K bitmaps are denoted as Equation 4.2.

$$B_i = \{B_i^{(j)} \mid B_i^{(j)} \in \{0,1\}, 1 \leq j \leq M\}, \text{ where } 1 \leq i \leq K \quad (4.2)$$

where $B_i^{(j)}$ denote the j -th pixel of the i -th bitmap, and the value “0” represent black pixel, while “1” white pixel. Each pixel in the bitmap corresponds to a micromirror on the DMD.

The display time of each bitmap is $t_i, 1 \leq i \leq K$.

Thus

$$T = \sum_{i=1}^K t_i B_i = Bt \quad (4.3)$$

where

$$B = [B_1, B_2, \dots, B_K], t = [t_1, t_2, \dots, t_K]^T, B \text{ is } M \times K \text{ and } t \text{ is } K \times 1.$$

Note that B is a sequence of downsizing bitmaps. In other words, the size of a bitmap is no bigger than its previous one if any. The reason has been explained at the end of Section 3.4.3.1 in the chemical module. During the TfMP μ SLA process, each micromirror, once turned on, is supposed to be “on” for desired duration continuously rather than intermittently. This requirement imposes the following constraints: $B_m^{(j)} \leq B_n^{(j)}$, for all j , where $1 \leq m \leq n \leq K$. The K -th bitmap is the last bitmap to be displayed on the DMD.

The problem comes to the following.

Problem 5 (Geometric profile optimization problem – Optimize z problem)

Input:

A desired geometrical profile: z_0 (z_0 is a vector with size N)

The chemical module (refer to Section 3.4)

The optical module (refer to Section 3.5)

Output:

1. K bitmaps:

$$B = [B_1, B_2, \dots, B_K], B \text{ is } M \times K$$

2. The display time of each bitmap:

$$t = [t_1, t_2, \dots, t_K]^T, t \text{ is } K \times 1$$

Objective:

$$\min_{B^{(j)} \in \{0,1\}, t \geq 0} \| f_{zE}(f_{ET}(B \times t)) - z_0 \|$$

Constraints:

$$B_m^{(j)} \leq B_n^{(j)}, \forall j, \text{ and } 1 \leq m \leq n \leq K$$

4.1.3 Problem formulation – optimizing E

In Problem 5 in Section 4.1.2, the function f_{ET} is linear, but the transfer function f_{zE} is nonlinear, which would increase the computation complexity significantly. It will be difficult to solve Problem 5 directly. An alternate problem formulation, which is much easier to solve, is desired. From the chemical module, we could see that z and E are

monotonically related. The more exposure energy received, the higher the resin cured.

Hence we transform the optimization target from z_0 to E_0 , where $E_0 = f_{Ez}(z_0)$. Refer to

Equation 3.6 for the transfer function f_{Ez} . It comes to Problem 6:

Problem 6 (Energy exposure optimization problem – Optimize E problem)

Input:

An energy exposure profile: E_0 (E_0 is a vector with size N)

The optical module (refer to Section 3.5)

Output:

1. K bitmaps:

$$B = [B_1, B_2, \dots, B_K], B \text{ is } M \times K,$$

2. The display time of each bitmap:

$$t = [t_1, t_2, \dots, t_K]^T, t \text{ is } K \times 1$$

Objective:

$$\min_{B^{(j)} \in \{0,1\}, t \geq 0} \| f_{ET}(B \times t) - E_0 \| \text{ where } E_0 = f_{Ez}(z_0)$$

Constraints:

$$B_m^{(j)} \leq B_n^{(j)}, \forall j, \text{ and } 1 \leq m \leq n \leq K$$

The objective in Problem 6 is linear already, however with the constraints imposed, it is still too complex to solve. We try to reduce the whole problem to several small problems to further simplify the problem. Then it is decomposed into two subproblems.

Subproblem 6.1 (Estimate exposure time for each micromirror: T)

Input:

An energy exposure profile: E_0 (E_0 is a vector with size N)

The optical module (refer to Section 3.5)

Output:

An estimated exposure time T of each micromirror on DMD in the TfMP μ SLA

(T is a vector with size M)

Objective:

$$\min_{T \geq 0} \| f_{ET}(T) - E_0 \| \quad \text{where } E_0 = f_{Ez}(z_0), f_{ET}(T) = HT$$

Subproblem 6.2 (Bitmap grouping to obtain bitmaps B and exposure time t)

Input:

An estimated exposure time T of each micromirror on DMD in the TfMP μ SLA

(T is a vector with size M)

Output:

1. K bitmaps:

$$B = [B_1, B_2, \dots, B_K], B \text{ is } M \times K,$$

2. The display time of each bitmap:

$$t = [t_1, t_2, \dots, t_K]^T, t \text{ is } K \times 1$$

Objective:

$$\min_{B^{(j)} \in \{0,1\}, t \geq 0} \| T - B \times t \|^2$$

Constraints:

$$B_m^{(j)} \leq B_n^{(j)}, \forall j, \text{ and } 1 \leq m \leq n \leq K$$

Subproblems 6.1 and 6.2 are the final two problems we need to solve. To illustrate, for curing a sphere surface as shown in Figure 4.1, suppose there are $N = 300 \times 300 = 90000$ pixels on the substrate, and $M = 151 \times 151 = 22801$ micromirrors on the DMD. We can see that it is a complex large-scale optimization problem:

$$H : N \times M = 90000 \times 22801$$

$$T : M \times 1 = 22801 \times 1$$

$$B : M \times K = 22801 \times K$$

To solve the large-scale problem, algorithms are proposed in the next section.

4.2 Proposed Algorithms

In last section, we formulated the problem into two subproblems, which could be identified as one linear regression problem and one clustering problem. The least-squares optimization algorithm and K -means clustering algorithm are proposed and used to solve the two problems, respectively.

Subproblem 6.1 can be explained as a simple bound constrained optimization problem in Equation 4.4.

$$\min_{x \in \Omega} f(x) \quad \Omega = \{x \in R^N \mid L_i \leq (x)_i < U_i\}$$

where,

$$f(x) = f(T) = \frac{1}{2} \|HT - E_0\|_2^2 \tag{4.4}$$

$$L_i = 0 \quad U_i = +\infty$$

We utilize the optimization toolbox in MATLAB to solve this problem. The detail of the algorithm will be introduced in Section 4.2.1.

Subproblem 6.2 is hard to be solved directly since the number of variables $M \times K$ is very big. We exploit K -means clustering algorithm [54] to solve it. M elements of T are clustered into K clusters; the average value of each cluster is obtained and sorted in the ascending order as shown in Equation 4.5.

$$\bar{T}_i \quad :1 \leq i \leq K \quad (4.5)$$

Then the value of t and B are specified as following in Equation 4.6.

$$t_i = \begin{cases} \bar{T}_i & i = 1 \\ \bar{T}_i - \bar{T}_{i-1} & 2 \leq i \leq K \end{cases} \quad (4.6)$$

$$B_i^{(j)} = \begin{cases} 0 & \bar{T}_i < T_j \\ 1 & \bar{T}_i \geq T_j \end{cases}$$

The details of the clustering algorithm will be introduced in Section 4.2.2.

4.2.1 Optimization

MATLAB provides a solver “lsqin”, which can solve bound constrained least-squares problem as Subproblem 6.1. Figure 4.2 shows a brief introduction of “lsqin”.

Optimization Toolbox

lsqin

Solve constrained linear least-squares problems

Equation

Solves least squares curve fitting problems of the form

$$\min_x \frac{1}{2} \|Cx - d\|_2^2 \quad \text{such that} \quad \begin{aligned} A \cdot x &\leq b \\ Aeq \cdot x &= beq \\ lb &\leq x \leq ub \end{aligned}$$

where C , A , and Aeq are matrices and d , b , beq , lb , ub , and x are vectors.

Figure 4.2 brief introduction of “lsqin” (MATLAB help document)

When the problem given to “lsqlin” has only upper and lower bounds; i.e., no linear inequalities or equalities are specified, and the matrix C has at least as many rows as columns, the default algorithm is the large-scale method. This method is a subspace trust region method based on the interior-reflective Newton method [55]. Each iteration involves the approximate solution of a large linear system using the method of preconditioned conjugate gradients (PCG).

According to the function of “lsqlin” in MATLAB, it is qualified to solve Subproblem 6.1, in which the variable T is bounded between 0 and positive infinity. Furthermore, the number of pixels is larger than that of the micromirrors, which means the size of matrix H satisfies the requirement by “lsqlin”.

4.2.2 Clustering Algorithm

K -means is one of the simplest unsupervised learning algorithms that solve the well known clustering problem. The procedure follows a simple and easy method to classify a given data set into a certain number of clusters (assume k clusters).

The main idea is to define k centroids, one for each cluster. These centroids should be placed in a cunning way because different locations would cause different total intra-cluster variances. So, the better choice is to place them as far away from each other as possible. The next step is to take each point belonging to a given data set and associate it to the nearest centroid. When no point is pending, the first step is completed and an initial grouping is done. At this point we need to re-calculate k new centroids as centers of the clusters resulting from the previous step. After we have these k new centroids, a new binding has to be done between the same data set points and the nearest new centroid. A loop has been generated. As a result of this loop we may notice that the k centroids

change their location step by step until no more changes are observed. In other words centroids do not move any more.

Finally, this algorithm aims at minimizing an objective function, in this case a squared error function. The objective function is shown in Equation 4.7.

$$J = \sum_{k=1}^K \sum_{i=1}^n \|x_i^{(k)} - c_k\|^2$$

where, $\|x_i^{(k)} - c_k\|^2$ is a chosen distance measure between a data point $x_i^{(k)}$ and the cluster center c_k (4.7)

The algorithm is composed of the following steps:

1. Place K points into the space represented by the objects that are being clustered.

These points represent initial group centroids.

2. Assign each object to the group that has the closest centroid.

3. When all objects have been assigned, recalculate the positions of the K centroids.

4. Repeat Steps 2 and 3 until the centroids no longer move. This produces a separation of the objects into groups from which the metric to be minimized can be calculated.

A drawback of the K -means algorithm is that the number of clusters k is an input parameter. An inappropriate choice of k may yield poor results. Hence, we should observe the intra-cluster variance and adjust the value of k to ensure an appropriate clustering. One of the advantages is that the k -means algorithm assumes the variance an appropriate measure of cluster scatter. This assumption agrees very well with the objective in Subproblem 6.2.

We'd like to exploit the K -means clustering for our problem as following: M elements of T are clustered into K clusters, corresponding to K bitmaps. In this case, the objective of using K -means algorithm is to minimize the intra-cluster variance in Equation 4.7. This equation is actually the square of the objective function in Subproblem 6.2. Hence, by solving Equation 4.8 using K -means algorithm, Subproblem 6.2 is addressed.

$$V = \sum_{i=1}^K \sum_{T_j \in S_i} (T_j - \bar{T}_i)^2$$

where S_i is the i^{th} -cluster with \bar{T}_i as the average exposure time value (4.8)
 T_j is the exposure time for the j^{th} -micromirror in the vector T

To obtain a sequence of downsizing bitmaps subject to the constraints in Subproblem 6.2, the average value of each cluster is sorted in an ascending order as shown in (4.9).

$$T_j: 1 \leq j \leq M \xrightarrow{\text{Clustering}} \bar{T}_b: 1 \leq b \leq K$$

$$\xrightarrow{\text{Sort ascending}} \bar{T}_i \leq \bar{T}_{i+1}, 1 \leq i \leq K-1$$
(4.9)

Then the value of exposure time t_i and bitmap B_i ($i = 1, 2, \dots, K$) are computed as in Equation 4.10 and 4.11. Refer to Equations 4.2-4.3 for the details of symbols.

$$t_i = \begin{cases} \bar{T}_i & i=1 \\ \bar{T}_i - \bar{T}_{i-1} & 2 \leq i \leq K \end{cases}$$
(4.10)

$$B_i^{(j)} = \begin{cases} 0 & \bar{T}_i < T_j \\ 1 & \bar{T}_i \geq T_j \end{cases}, \forall j, 1 \leq j \leq M, \text{ and } 1 \leq i \leq K$$
(4.11)

where $B_i^{(j)}$ denote the j^{th} -pixel in i^{th} -Bitmap

4.3 Developing the mathematical module

During the development of the mathematical module, we experienced a transition from 2.5D process planning method to 3D process planning method. Since the process planning method for 2.5D curing involves much fewer variables (i.e, pixels and micromirrors) in the mathematical formulations, the research started with it to gain an initial understanding of the functionality and capability of the mathematical module, along with an initial experiment for curing a simple 2.5D part as presented in Section 4.3.1. After that, the research advanced into the process planning method for large-scale and more complex 3D geometric parts, which was elaborated in Section 4.3.2. A capable and mature mathematical module is finally established in Section 4.3.3.

4.3.1 The initial 2.5D process planning method

The 2.5D process planning method focused on the cross-section profile of the target part, instead of the entire geometrical profile. Hence, we input only the cross-section profile of the 2.5D geometric part into the geometric module, and obtained a vector of discretized column voxels to approximate the cross-section profile. Then following the problem formulations in Section 4.1, we solved Problem 6 to generate bitmaps and exposure time for each bitmap. At the stage of 2.5D process planning, Subproblem 6.1 was treated as an inequality constrained linear least-squares problem rather than as a bound constrained linear least-squares problem proposed in Section 4.2, and Subproblem 6.2 was solved by observing the histogram of T - the vector of each micromirror's exposure time and grouping the micromirrors manually into bitmaps according the distribution of T . This is different from the clustering algorithm proposed in Section 4.2 either. An illustrative example is presented in Section 4.3.1.1.

4.3.1.1 Illustrative example: curing a curve feature

Figure 4.3 shows the desired shape for curing a curve feature. It is a half cylinder, and we are going to observe the cross-section, which is an arc.

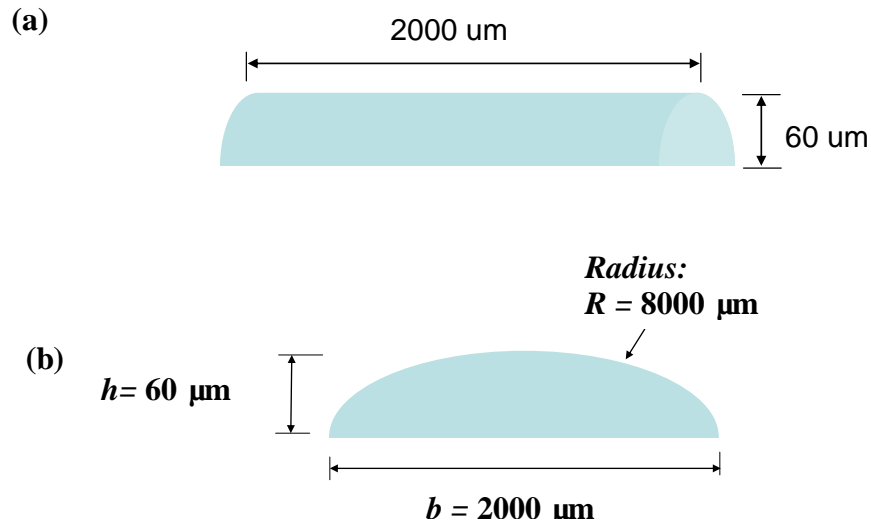


Figure 4.3 (a) The CAD model (desired cured shape); (b) The cross-section view of the desired cured shape for example: curing a curve feature

The resin used with the TfMP μ SLA system in the initial test was the Vantico Huntsman SL-5510 resin. This is a common stereolithography resin used extensively to cure SLA parts. The resin working curve has been presented in Section 3.4.3.2.

After optimizing the energy exposure profile, the desired and estimated energy exposure profile is plotted in Figure 4.4. It is observed that the estimated energy profile is not as smooth as desired and has some zero irradiation pixels on the edges (see the

leftmost pixels on the x-axis in Figure 4.4). Consequently, some edge effects as well as jags in the profile of the cured part would appear.

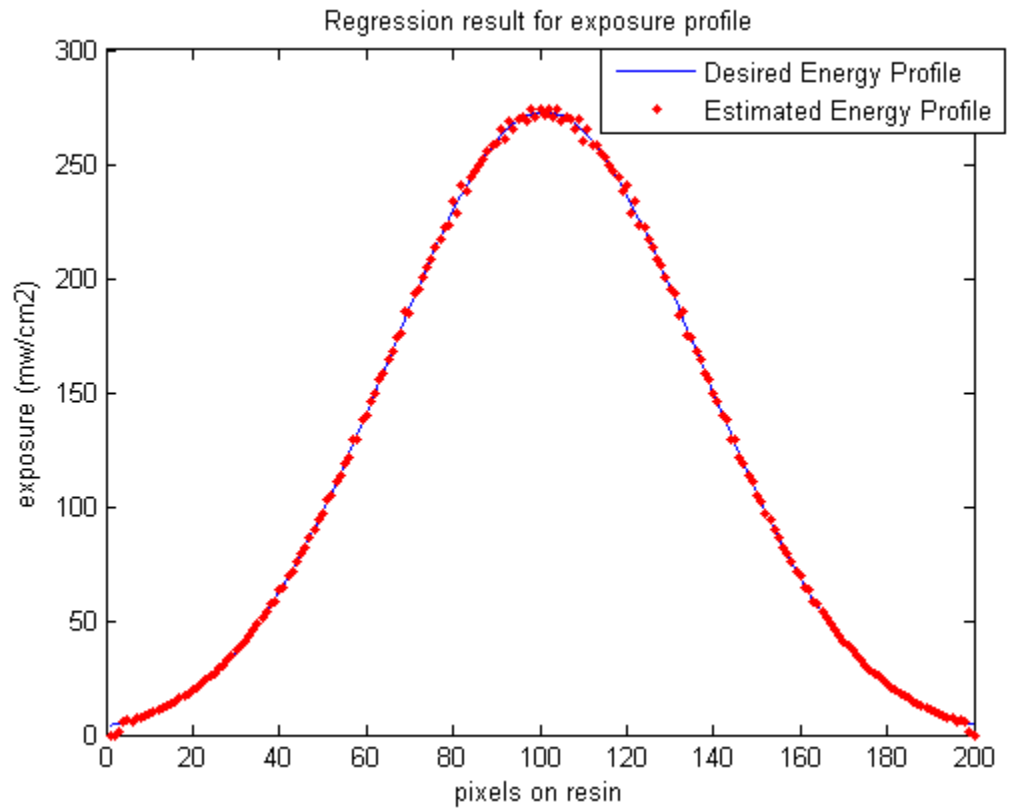


Figure 4.4 optimizing E for example: curing a curve feature

Figure 4.5 and Figure 4.6 show the bitmaps series for the DMD and the experimental results, respectively.

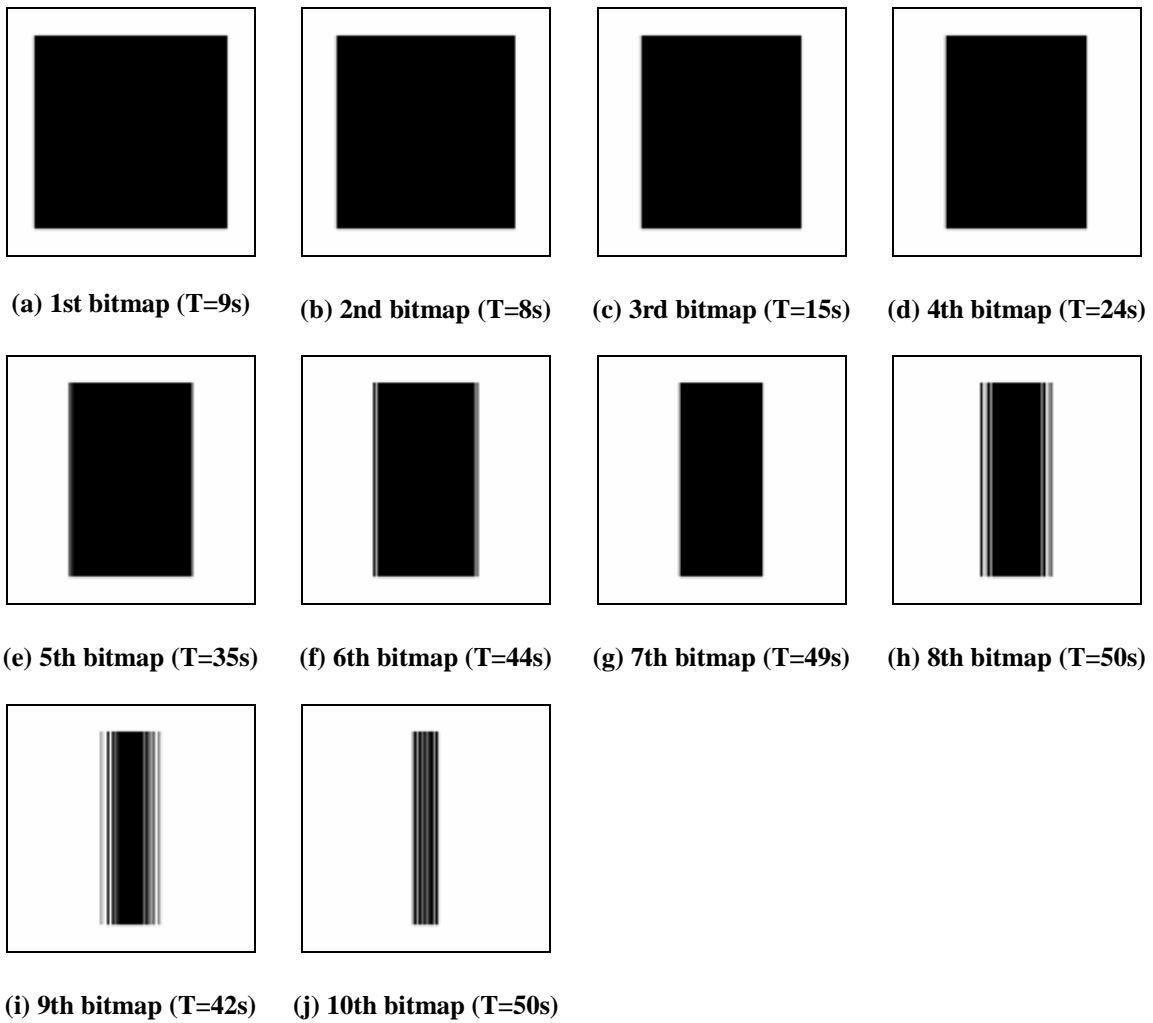


Figure 4.5 Bitmaps displayed on DMD for example: curing a curve feature

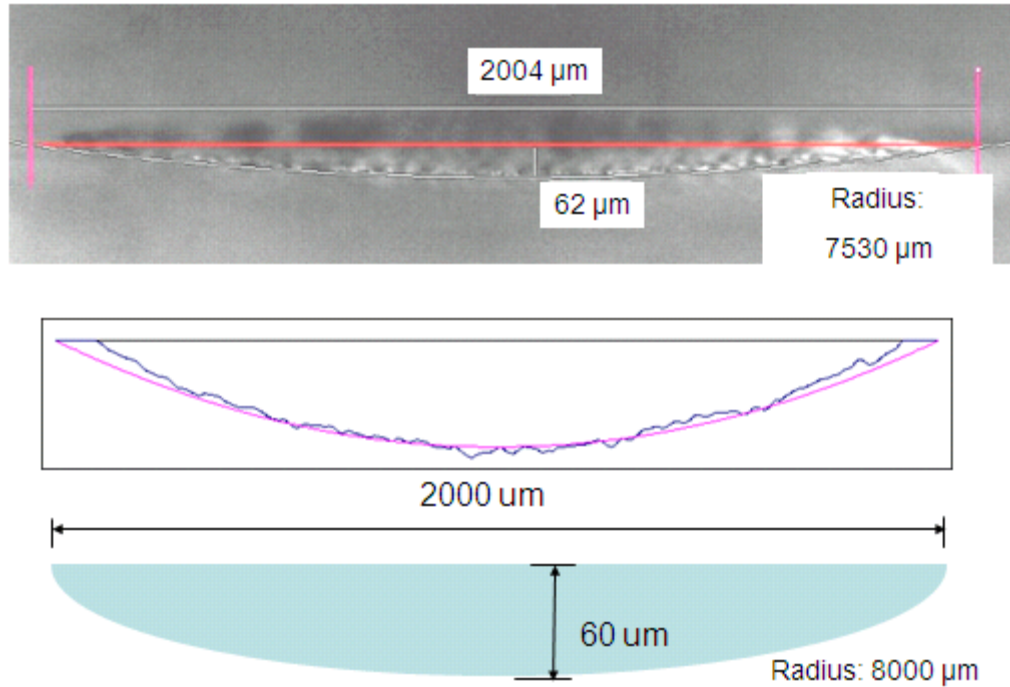


Figure 4.6 Cured shape from experiments for example: curing a curve feature

In Figure 4.6, the top picture shows the cured part, the middle plot is the surface plot using Talysurf, and the bottom graph is the desired geometric profile. In the Talysurf plot, the blue profile is the actual cured profile, while the pink curve is the desired profile. The Talysurf measurement of the cured surface profile indicates that the edges were deficient. We will investigate the edge effect further in next section.

Comparison of the cured part and the desired shape in Figure 4.3(b) is shown in Table 4.1. The cured shape dimensions of the cross-section from the experiment are very close to the desired dimensions.

Table 4.1 Comparison on dimensions of desired part and part from experiments – curve feature

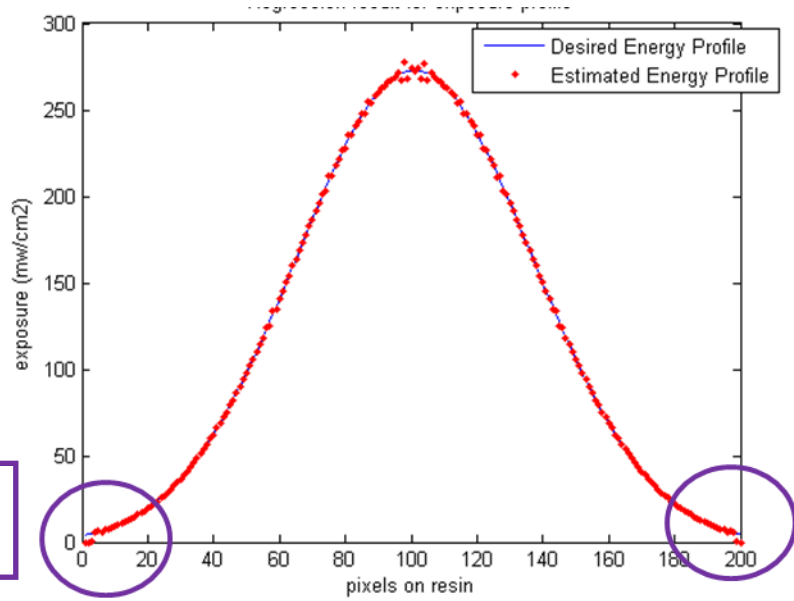
Dimension	Desired (um)	Cured (um)	Percent Error (%)
h	60	62	3.33
R	8000	7530	5.88
b	2000	2004	0.20

4.3.1.2 Need to improve the process planning method

As to the 2.5D process planning system itself, the initial test also indicated that further experimentation and analysis was needed in order to improve this process planning system. The lack of exposure dose at edge pixels, for example, suggests that we need to include more micromirrors into the process planning system. In the illustrative example above, while curing a curve feature, we used 161 micromirrors to irradiate on the 200 pixels which formed the cross-section of the intended part. However, the estimated energy exposure profile as shown in Figure 4.7(a) indicated that the edge pixels didn't receive as much exposure dose as desired at all. Those underdosed pixels accounted partially for the undercured edges in the experimental result as shown in Figure 4.6. Another cause of the edge deficiency is postulated to be the oxygen diffusion effects in the resin curing.

**(a) :
Original
process plan**

**Edge pixels:
deficient exposure**



**(b):
Improved
process plan**

**Edge pixels:
sufficient exposure**

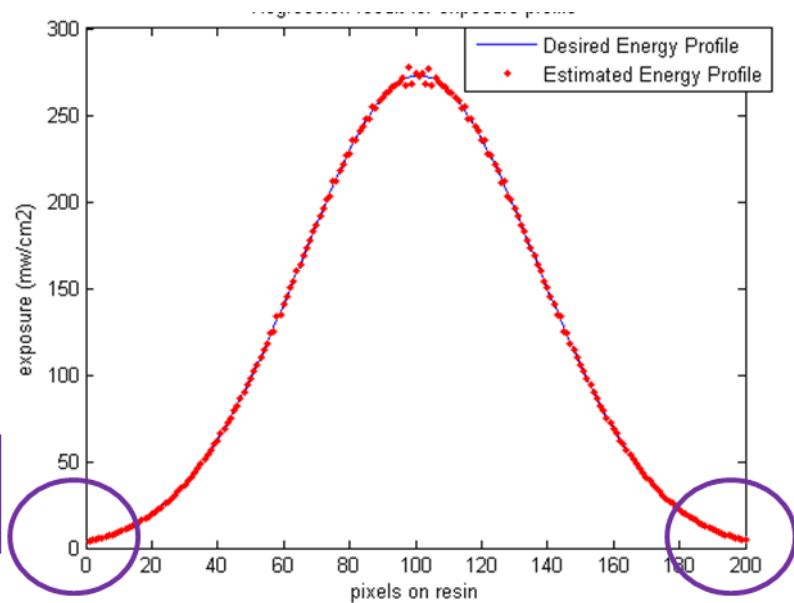


Figure 4.7 edge pixels get better irradiation with more micromirrors

To address the underdosed edge pixels, we need to improve the process planning method, in particular the mathematical module, so as to include more micromirrors into

the energy exposure profile optimization. Thus, the additional micromirrors would irradiate on the edge pixels and contribute to the exposure required by the pixels. Figure 4.7(b) shows the estimated energy exposure profile whose edge pixels already received approximately the desired dose, with 6 more micromirrors added to the process parameters.

Herein, one question may come up: why did we take meticulous efforts in determining the number of micromirrors used in the mathematical optimization? What is the matter if we give some arbitrary number of micromirrors and let the mathematical module itself to compute and “remove” the unnecessary micromirrors? To remove micromirrors simply means to assign zero exposure time to the unwanted micromirrors. Obviously, it could be more convenient to remove undesired micromirrors automatically than to add desired micromirrors manually.

Back to the previous case for curing a curve feature, 6 more micromirrors were added successfully to the process plan to enable edge pixels better exposure. After that we did try adding 2 more micromirrors. However, these additional 2 micromirrors didn't work at all and worse still it resulted in an unbounded solution at infinity because the constraints were not restrictive enough. Therefore, we had to be very careful while adding even one or two more micromirrors while using the 2.5D process planning system.

Totally speaking, the incapacity of the initial mathematical module in our original 2.5D process planning system to solve problem with more micromirrors, not only prevented an effective way of optimizing energy exposure at edge pixels, but also disabled a 3D process planning system in which a much larger scale problem is expected to be solved. Thereby, we need to improve the process planning system to solve a large scale problem. Section 4.3.2 meets the demand.

4.3.2 Improving the process planning method

As required in Section 4.3.1, a 3D process planning method is highly desired to solve large scale process planning problem. Recalling Section 4.2, we have actually presented the algorithms applicable for 3D process planning system in details. Essentially, the basic ideas of both the original 2.5D and current 3D process planning systems are the same as schemed in Section 3.2. The comparisons made in Table 4.2 as below aims to shed light on how the process planning method was improved.

Table 4.2 original 2.5D process planning system vs current 3D process planning system

items		2.5D process planning system	3D process planning system
Geometrical module		input: cross-section profile	input: entire geometric profile
Chemical module		same	
Optical module		same	
Mathematical module	optimization	1. medium-scale algorithm 2. output: exposure time for a line of micromirrors corresponding to the cross-section profile	1. large-scale algorithm 2. output: exposure time for all the micromirrors corresponding to the entire geometric profile

Table 4.2 original 2.5D process planning system vs current 3D process planning system (Continued)

items		2.5D process planning system	3D process planning system
Mathematical module	clustering	1. manual grouping 2. output: Intermediate 1D bitmaps with 1 line of pixels corresponding to the line of micromirrors. Note: the 1D bitmaps will be extended into final 2D bitmaps.	1. automatic clustering using <i>K</i> -means algorithm 2. output: final 2D bitmaps and exposure time

From the comparison in Table 4.2, it is obvious that the 3D process planning system is more advanced and mature. The main factor leading to the successful transition from 2.5D to 3D is the improvement of the mathematical module, especially in the optimization algorithm, which was once the bottleneck issue as discussed in Section 4.3.1.2.

As presented in Section 4.2.1, we used “lsqin” solver in MATLAB to solve Problem 6.1 – the energy exposure profile optimization problem. Please be noted that in Figure 4.2 there are different ways of imposing constraints while using “lsqin”. One type of constraint is inequality constraint, the other bound constraint. To be specific, in Subproblem 6.1, the optimization problem is subject to the constraint “ $T \geq 0$ ”, which could be imposed to the solver either as inequality constraints “ $-T \leq 0$ ” or as bound

constraints “ $0 \leq T \leq \infty$ ”. Mathematically, these two constraints are equivalent; however implementally they are totally different while using “lsqin” in MATLAB.

Initially in the 2.5D process planning system, we used the inequality constraint “ $-T \leq 0$ ”, to solve the problem (MATLAB code shown in Figure 4.8). In Figure 4.8, T_j is actually the exposure time T for each micromirror, H_{ij} is the irradiance matrix H , E_i denotes the desired exposure profile E_0 .

```
A = -1 * eye(size(Hij));
B = zeros(Hij_Row,1);
%Ax<=B i.e, x>=0
... (non-negatvie exposure time values for each micromirror)
[Tj,ResNorm,Res] = lsqin(Hij,Ei,A,B);
```

Figure 4.8 MATLAB code to solve the exposure profile optimization problem in 2.5D process plan

Unfortunately, once inequality constraints are imposed, the “lsqin” solver could use medium-scale algorithm only, which can solve only simple 2.5D problems. That is why sometimes even adding one or two more micromirrors would induce unbounded solutions. At the stage of 2.5D process planning, it seemed difficult for MATLAB to solve the problem with a “ 200×160 ” irradiance matrix involving 200 pixels on the cross-section and 160 micromirrors, not to mention solving a 3D problem where a “ $200^2 \times 160^2$ ” irradiance matrix with 200^2 pixels and 160^2 micromirrors may be encountered. Actually speaking, for the 3D process planning, the size of the irradiance matrix could be even larger.

I tried using large-scale algorithm to solve the linear least squares problem, but it didn't work due to the inappropriate constraints. Finally, I found that the large-scale algorithm can handle bound constraints only. That is to say, we should use bound constraints ($0 \leq T \leq \infty$), rather than inequality constraint. Modified code is shown in Figure 4.9. It is the right code we developed in the 3D process planning system.

```
options = optimset('LargeScale', 'on', 'MaxIter', 20000, 'TolFun', 10e-16);
[Tj,ResNorm,Res,output] = lsqlin(Hij,Ei,[],[],[],[],zeros(Hij_Column,1),Inf*ones(Hij_Column,1),[],options);
```

Figure 4.9 MATLAB code to solve the exposure profile optimization problem in 3D process plan

Now that the original 2.5D process planning system was upgraded to the current 3D process planning system, generally speaking, the 3D process planning system is referred as the TfMP μ SLA process planning system in the thesis. Case study of the TfMP μ SLA process planning system will be presented in CHAPTER 5 to do further test.

4.3.3 The mathematical module developed

It should be noted that no matter 2.5D or 3D, the underlying mathematical formulations are identical. Apparently, the process planning system finally developed in the thesis, which is for 3D curing on TfMP μ SLA, is inclusive and complete already, capable of generating process plans for 2.5D curing too.

As a summary, our process planning method solves Problem 6, which aims to optimize energy exposure E and is decomposed into two subproblems 6.1 and 6.2. The flowchart of the mathematical module optimizing E in two steps is schemed in Figure

4.10. MATLAB codes using the algorithms in Section 4.2 are developed (refer to Appendix C).

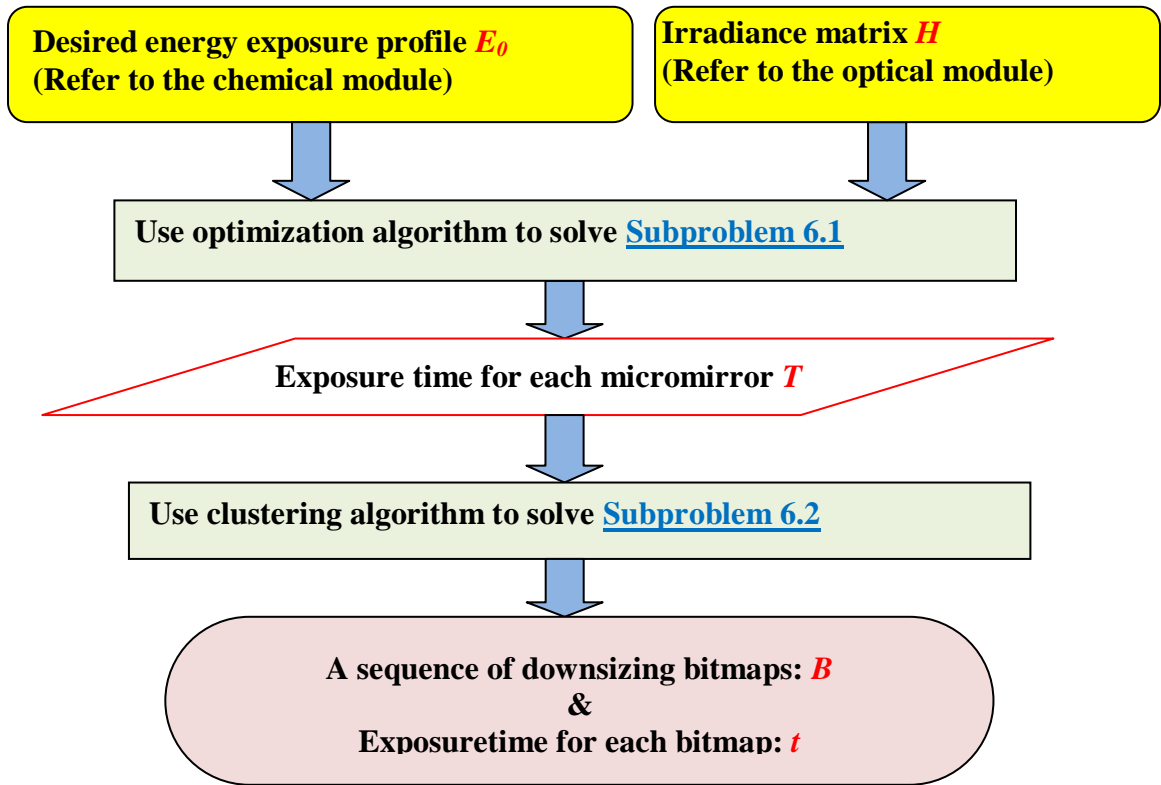


Figure 4.10 the flowchart of the mathematical module

4.4 Validating the mathematical module

Taking the example in Section 4.1.1, the desired spheric surface is discretized into voxels as shown in Figure 4.11. The X - Y plane is discretized into $10\ \mu\text{m} \times 10\ \mu\text{m}$ pixels. Proportionally, we also scale down the vertical (Z -direction) dimensions to a unit of $10\ \mu\text{m}$. Hence, all the X - Y - Z dimensions are in the unit of $10\ \mu\text{m}$, instead of $1\ \mu\text{m}$. The actual

dimensions of the desired geometric profile are: base diameter 3000 μm , and the central height 400 μm .

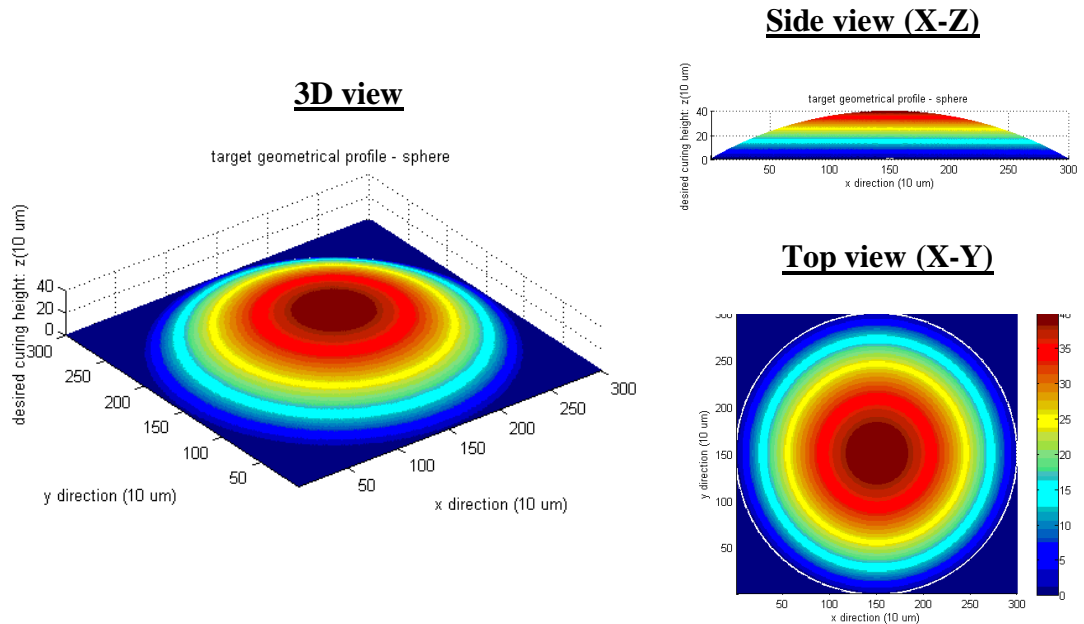


Figure 4.11 the desired geometric profile (discretized) for validating the mathematical module

To run the mathematical module, we also need the outputs from both optical module and chemical module. An irradiance matrix H is ready after implementing the optical module with the real configuration and parameters of the TfMP μSLA system. Assume that we use PEGDA hydrogel material to cure the desired geometric profile. The chemical module outputs the working curve function f_{zE} (working curve presented in Figure 4.12) and transfer function f_{Ez} . There are several points off the fitted working curve at lower exposure area; however the experiments would be done within the fitted area.

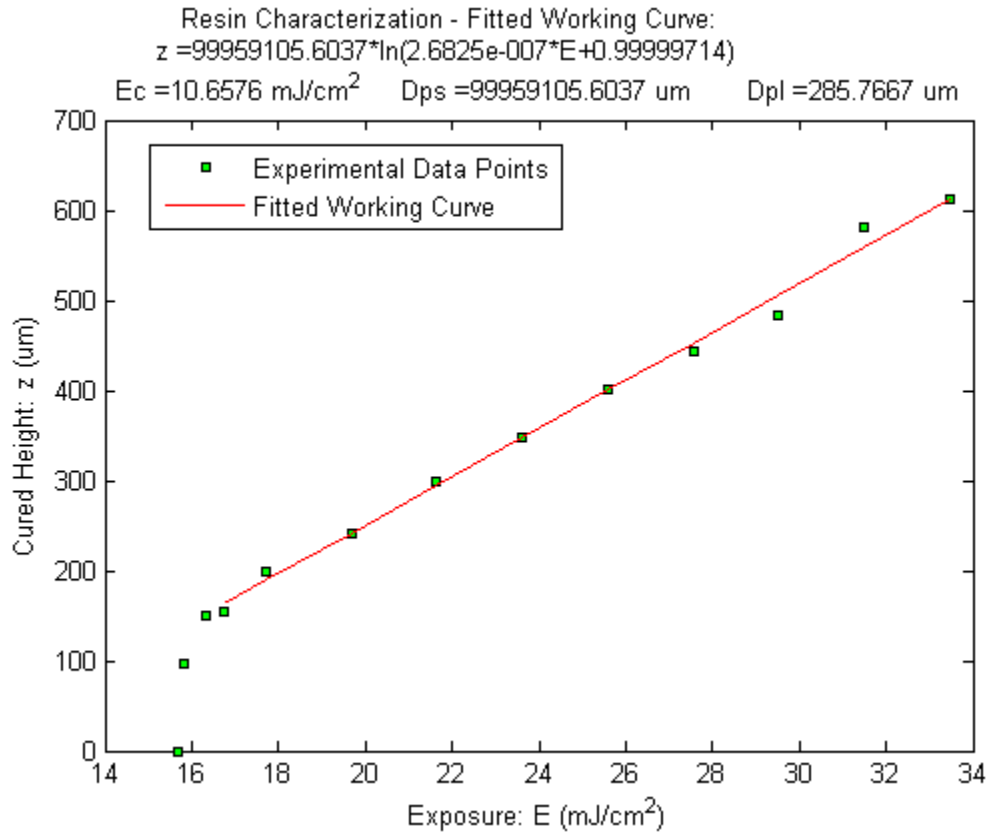


Figure 4.12 resin working curve used in validating the mathematical module

We run through the mathematical module to generate bitmaps and respective exposure time for curing the sphere surface. The output process parameters are shown in Figure 4.13. For example, the title “Bitmap_001_10.2s” means that the bitmap right above it is the first bitmap to project on the DMD during the TfMPSLA process, and the exposure time is 10.2 seconds. Totally 24 bitmaps were obtained.

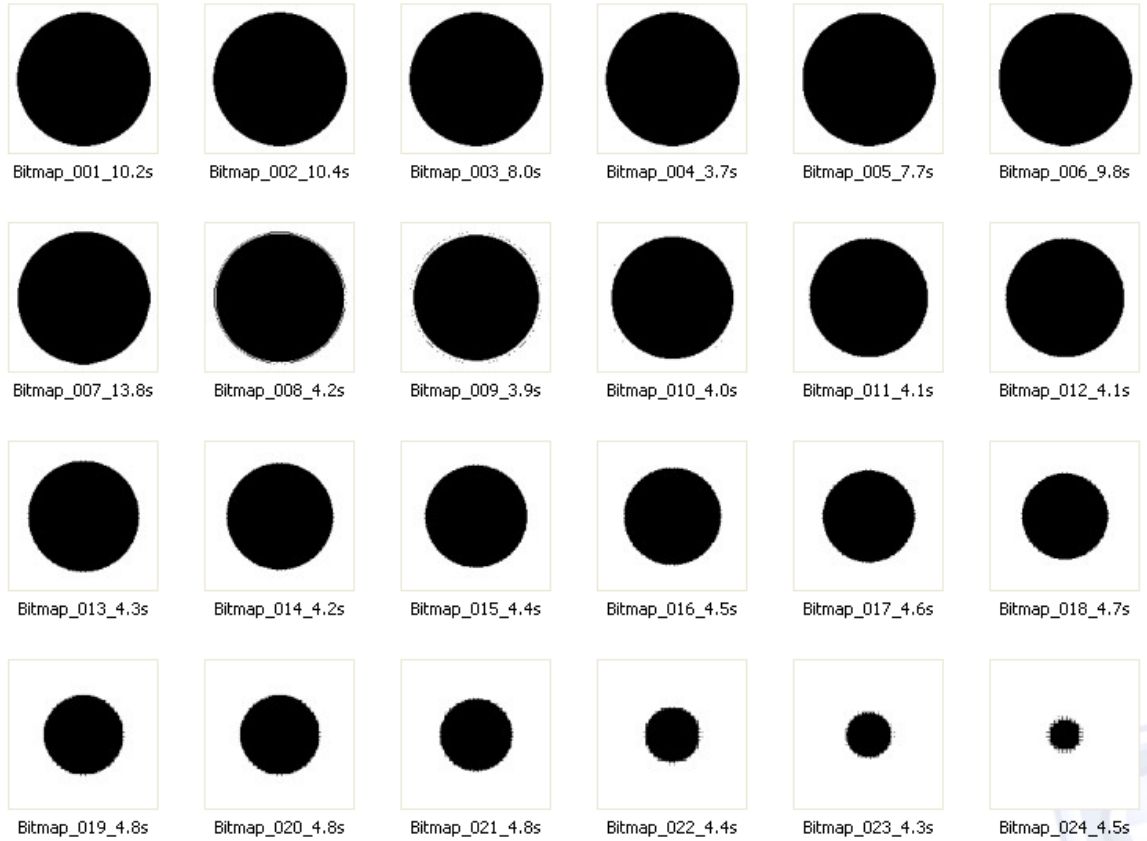


Figure 4.13 resultant bitmaps and exposure time from the mathematical module

At first glance of the resultant bitmaps, it makes sense that all the bitmaps are circular, which agrees pretty well with the expected spherical surface. In some sense, this validates the mathematical module in terms of cross-section agreement.

Comparing the desired energy exposure with the estimated energy exposure (as shown in Figure 4.14), we find that the mathematical module, which employs linear least-squares solver and clustering algorithms to solve the two subproblems 6.1 and 6.2, has been successful in achieving the total objective in Problem 6. That is, the mathematical module is proved to be able to minimize the deviation between the desired (E) and

estimated energy exposure (E_0), i.e, norm ($E - E_0$). The root-mean-square (RMS) value of the error to measure the absolute deviation between E and E_0 is defined as Equation 4.12.

In this example, $RMS (E - E_0)_{abs}$ is 0.8389 mJ/cm^2 .

$$RMS(E - E_0)_{abs} = \frac{\text{norm}(E - E_0)}{\text{sqrt}(N)} \quad (\text{unit: mJ / cm}^2), \text{ where } N : \text{length of } E_0 \quad (4.12)$$

The absolute error represented in Equation 4.12 is not concrete enough to disclose how much the deviation is. Hence, the RMS value of relative error is calculated as in Equation 4.13. Here, $RMS (E - E_0)_{rel}$ is 5.14%.

$$RMS(E - E_0)_{rel} = \frac{\text{norm}(\text{abs}(E - E_0) / \text{abs}(E_0))}{\text{sqrt}(N)}, N : \text{length of } E_0, \text{ excluding } 0 \text{ values} \quad (4.13)$$

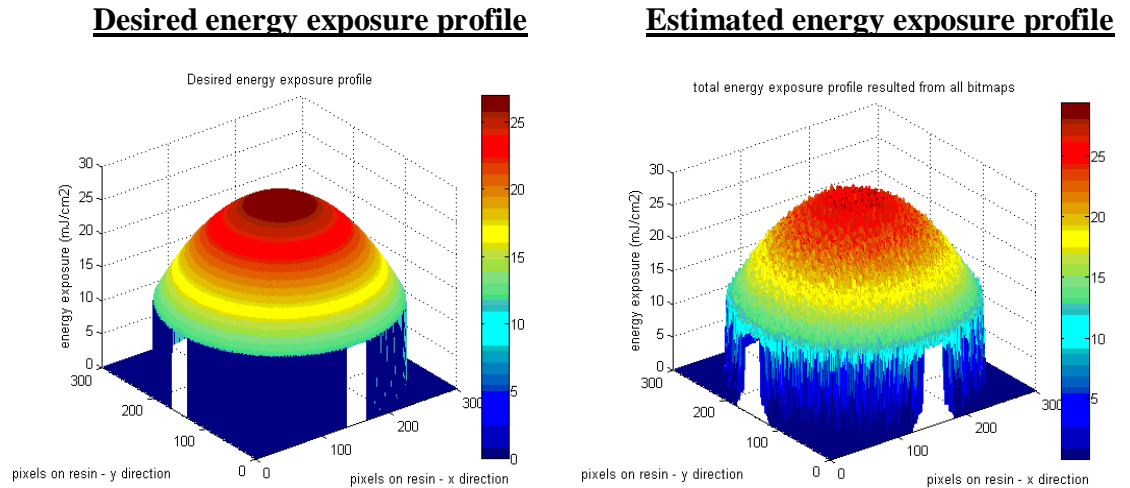


Figure 4.14 desired energy exposure vs estimated profile returned by the mathematical module

Although the mathematical module is validated in terms of estimating the energy exposure profile, it is still necessary to prove that it can optimize the simulated geometric profile as well. We simulated the curing process in the mathematical module by converting the estimated exposure profile to geometric profile with the function f_{zE} . The estimated exposure profile is a sum of energy exposure contributed by all the bitmaps in Figure 4.13. The simulated geometric profile is shown in Figure 4.15.

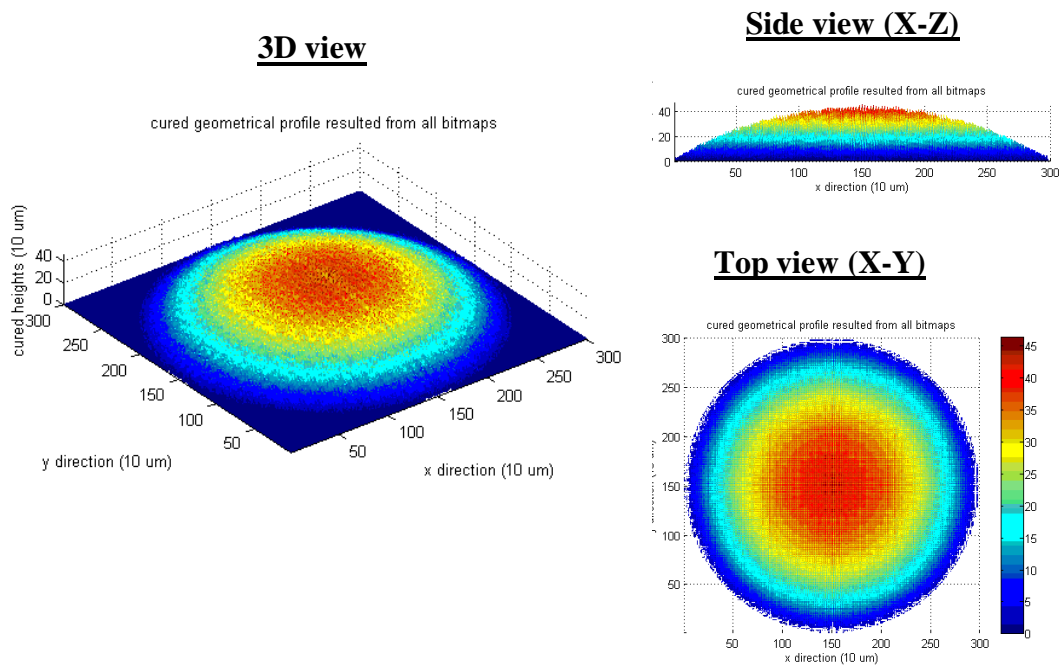


Figure 4.15 the estimated geometric profile returned by the mathematical module

The residuals between the estimated (z) and desired voxels' heights (z_0) are shown in Figure 4.16, which is a three-dimensional shaded surface from the components in $(z - z_0)$ on the X-Y mesh of pixels. The simulated geometrical deviations result mostly from the

incompleteness in resin working curve function f_{zE} in the chemical module and sampling errors in the geometrical and optical modules; hence the roughness shown in Figure 4.16 would not be completely expected in real cured parts. The simulated geometrical errors aim to merely provide an estimation of the process quality.

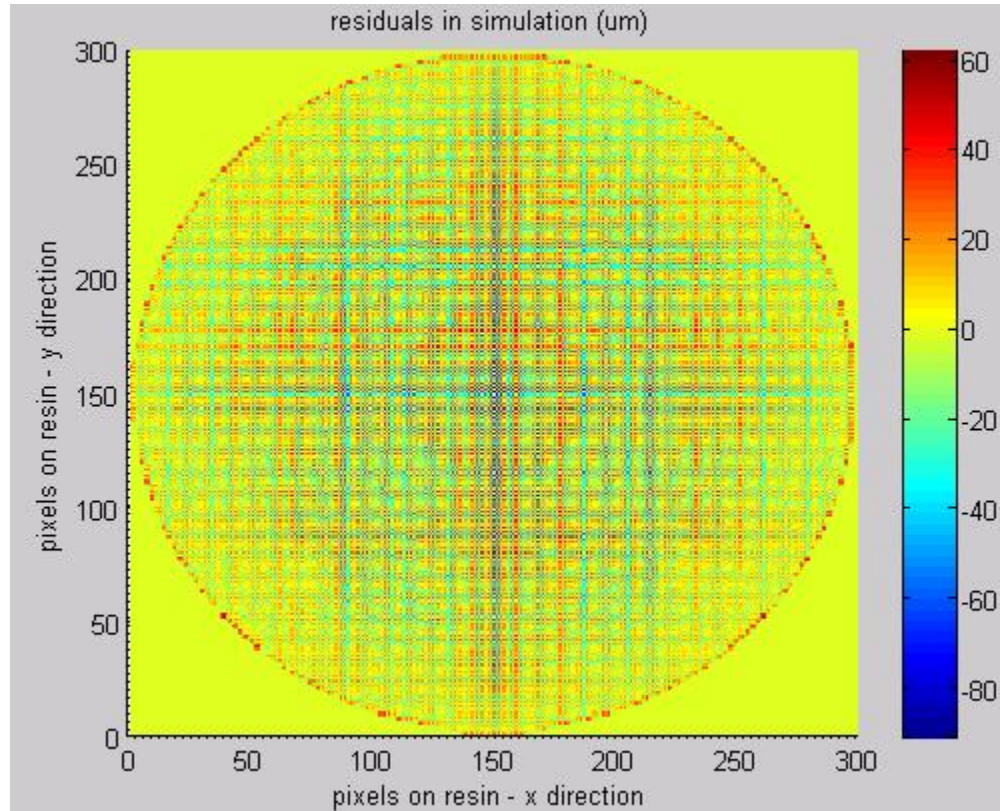


Figure 4.16 the residuals between the estimated and desired geometric profile

In some sense, the residuals represent profile roughness. The estimated surface is quite rough compared with the desired geometric profile. To visually quantify the deviation between z and z_0 , we borrow the definition of R_a , which is an arithmetic average of the profile roughness as shown in Equation 4.14.

$$R_a(z - z_0) = \frac{1}{N} \sum_{i=1}^N |z(i) - z_0(i)| \quad (\text{unit: } \mu m), \text{ where } N : \text{length of } z_0 \quad (4.14)$$

In Figure 4.16, the residuals range between [-90.96 μm , 62.25 μm], and the “roughness” value R_a is 11.19 μm .

Another measure of the deviation between z and z_0 is root-mean-squares (RMS) as Equation 4.15.

$$RMS(z - z_0) = \frac{\text{norm}(z - z_0)}{\text{sqrt}(N)} \quad (\text{unit: } \mu m), \text{ where } N : \text{length of } z_0 \quad (4.15)$$

In this example, the value of RMS ($z - z_0$) is around 16.09 μm .

Totally speaking, the $R_a(z - z_0)$ and RMS ($z - z_0$) values disclose that the mathematical module would yield a resolution of 10~20 μm in vertical (Z) dimension.

It is clear from Figure 4.15 and Figure 4.16 that the profile shape and dimensions obtained by the mathematical module very closely matches the desired dimensions (refer to Figure 4.11). Thus, we have validated the hypothesis that parameter estimation can be used to find a set of bitmaps and exposure time, which minimizes the deviation between desired and estimated energy exposure profiles, thus to minimize the deviation between the desired and estimated geometric profiles. The errors observed in the dimensions are expected to have their origins in the problem formulation and algorithms, while the least-squares optimization step induced much more errors than the clustering step did. More discussions about the algorithms will be presented in Chapter 6.

4.5 Analyzing the mathematical module

Some analysis about the mathematical module will be presented in this Section. Section 4.5.1 will discuss about the influence of the number of bitmaps used while optimizing the energy exposure profile. Section 4.5.2 will investigate Problem 5, i.e.,

“Optimize z problem”, formulated in Section 4.1.2, and compare it with the so-called “Optimize E problem” (see Problem 6).

4.5.1 Effects of the number of bitmaps

As mentioned in Section 4.2.2, the number of clusters K , i.e, the number of bitmaps, is an input parameter for the K -means algorithm. We have to specify how many bitmaps are expected to generate before running the mathematical module. Obviously, the more bitmaps used in the process plan, the smaller deviation resulted in Subproblem 6.2. We are interested in investigating the effects of the number of bitmaps. How good or bad is it to use 10~25 bitmaps for the TfMP μ SLA process plan?

We will continue to use the same example in Section 4.4, where we specified $K = 25$ as the number of clusters. Actually we obtained 25 bitmaps, while the first bitmap’s exposure time is almost 0 second. That is why we omit it and finally used 24 bitmaps for curing the sphere surface.

We will assign the clusters’ number K several different values to study the effects of the number of bitmaps. The pictures of the estimated geometric profile using different numbers of bitmaps are shown in Appendix D. The number of bitmaps is directly related to the clustering quality in Sub Problem 6.2, thereby we observe the root-mean-squares (RMS) of the deviation between the exposure times provided by all bitmaps ($B \times t$) (Equation 4.3) and the resultant exposure time T in Subproblem 6.1. Equation 4.16 defines the RMS ($T - Bt$), which embodies the objective of Subproblem 6.2.

$$RMS(T - Bt) = \frac{\text{norm}(T - B \times t)}{\text{sqrt}(M)} \quad (\text{unit: } s) \quad (4.16)$$

where, M is the length of T ; and $B^{(j)} \in \{0,1\}, t \geq 0$

To measure the effects of the number of bitmaps in the estimated exposure profile and geometric profile, we also use deviation values defined as in Equation (4.6) ~ (4.9). The comparison of effects is shown in Table 4.3 and Figure 4.17. The column of module running time in Table 4.3 is the computer running time of the whole mathematical module to implement the process planning method with the study parameter K , while all other conditions remain the same.

Table 4.3 effects of the number of bitmaps

K	RMS ($T-Bt$) (s)	RMS ($E-E_0$) _{abs} (mJ/cm ²)	RMS ($E-E_0$) _{rel} (%)	$R_a(z-z_0)$ (μm)	RMS ($z-z_0$) (μm)	time (s)
5	5.924	1.471	9.164	26.119	35.280	40.891
10	2.613	0.960	5.864	14.058	19.915	45.266
15	1.812	0.884	5.417	12.316	17.604	48.094
20	1.407	0.858	5.245	11.671	16.770	51.391
25	1.024	0.839	5.138	11.193	16.087	54.297
30	0.908	0.835	5.115	11.104	15.966	55.250
35	0.862	0.833	5.106	11.065	15.919	59.063
40	0.719	0.829	5.085	10.968	15.769	58.906
50	0.540	0.826	5.067	10.880	15.650	62.250
60	0.489	0.825	5.064	10.866	15.632	66.313
80	0.369	0.823	5.052	10.819	15.563	79.625
100	0.274	0.822	5.046	10.791	15.525	92.391

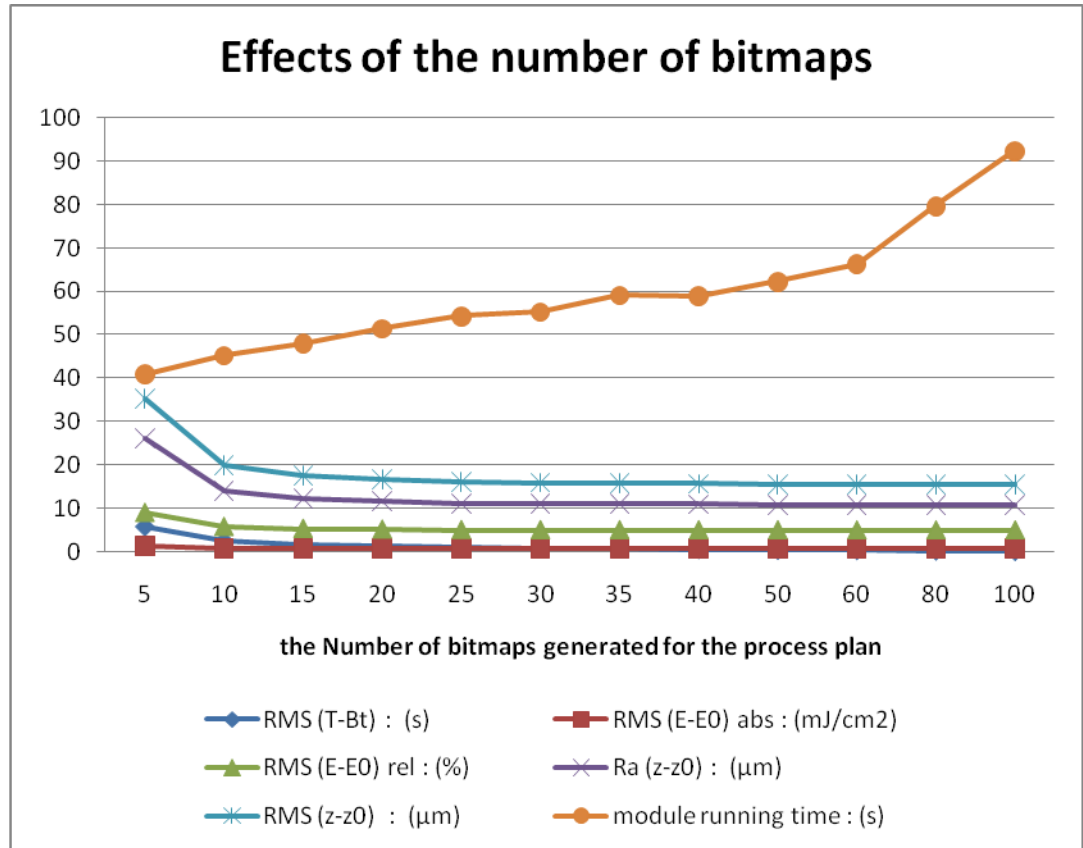


Figure 4.17 the effects of the number of bitmaps

It is clear from Figure 4.17 that the time required to run the mathematical module increases with the number of bitmaps in general. The observation of running time sheds some light on the clustering algorithm efficiency. When the number of bitmaps K is 100, the running time is still acceptable. Note that we couldn't increase K arbitrarily, say 500, it would probably induce "Out of memory" errors in MATLAB due to the limitation of the k -means algorithms. Fortunately, from the plots of root-mean-squares of the deviations, we could see that tens of bitmaps can be good enough to yield a process plan with considerably smaller errors. Taking a tradeoff between the difficulty in displaying a large number of bitmaps and the accuracy in the estimated geometric profile, we usually

use 25 bitmaps for the TfMP μ SLA process plan. Of course, it is subject to change with the actual shape, dimensions and complexity of the geometric profile to be cured.

4.5.2 Optimize z vs Optimize E

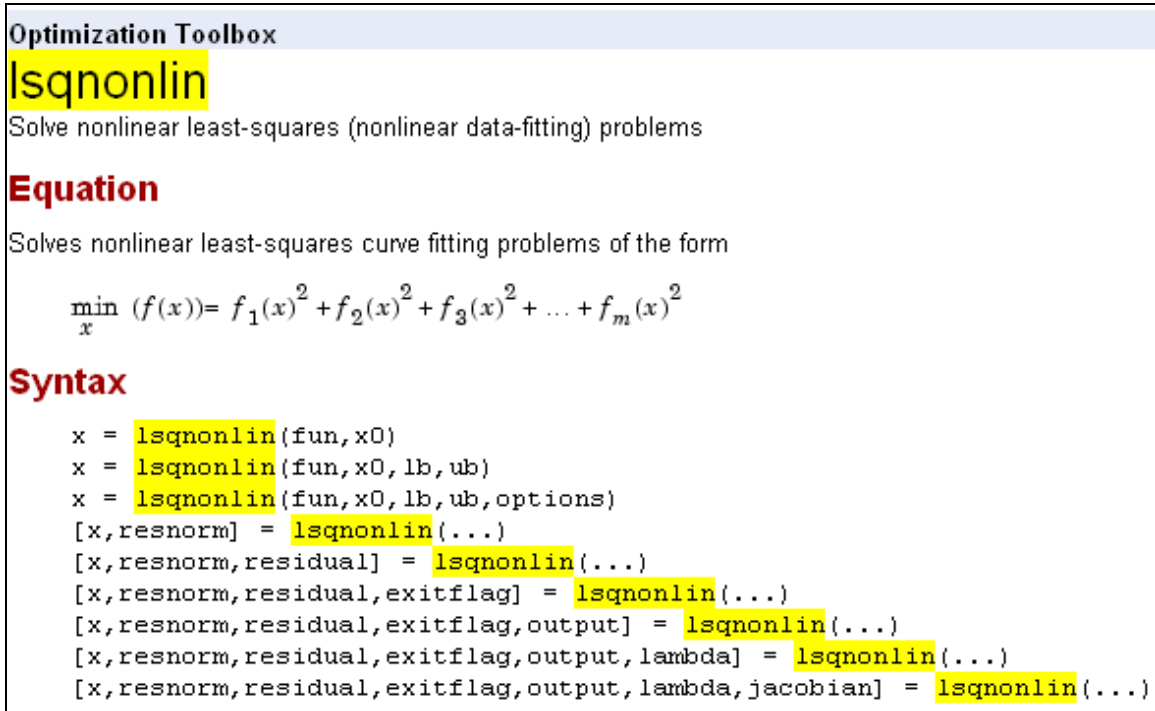
The mathematical module developed in the thesis is based on Problem 6 formulated in Section 4.1.3, and aims to solve it, that is, to solve the “optimize E ” problem. Tracing back to Problem 5 in Section 4.1.2, the so-called “optimize z ” problem, we find it quite complicated due to the nonlinear objective function. That is why we resorted to the alternative – “optimize E ” as in the mathematical module. However, in this section, we are interested in trying to solve Problem 5, i.e, “optimize z ” directly and compare it with our current mathematical module. This section will first investigate solutions to Problem 5 and then study the differences between “optimize z ” and “optimize E ”.

4.5.2.1 Solving the “optimize z ” problem

The only difference between the “optimize z ” problem (see Problem 5) and the “optimize E ” problem (see Problem 6) is the objective function. Similarly, we will use the 2-stage method as in the “optimize E ” problem to solve the “optimize z ” problem. That is, use appropriate bound constrained least-squares algorithms to calculate exposure time for each micromirror first, and then use the same clustering method to group the micromirrors into bitmaps.

The only change in the algorithms is that instead of using “lsqlin” to solve the first-step optimization problem, “lsqnonlin” will be employed in MATLAB to optimize z . A brief introduction of the function “lsqnonlin” is shown in Figure 4.18. By default

“lsqnonlin” chooses the large-scale algorithm. This algorithm is a subspace trust region method and is based on the interior-reflective Newton method.

The image shows a screenshot of the MATLAB help document for the 'lsqnonlin' function. The document is titled 'Optimization Toolbox' and 'lsqnonlin'. It describes the function as solving nonlinear least-squares (nonlinear data-fitting) problems. It includes an 'Equation' section with the formula $\min_x (f(x)) = f_1(x)^2 + f_2(x)^2 + f_3(x)^2 + \dots + f_m(x)^2$. The 'Syntax' section lists various ways to call the function, such as `x = lsqnonlin(fun, x0)`, `x = lsqnonlin(fun, x0, lb, ub)`, and `[x, resnorm, residual, exitflag, output, lambda, jacobian] = lsqnonlin(...)`.

Optimization Toolbox

lsqnonlin

Solve nonlinear least-squares (nonlinear data-fitting) problems

Equation

Solves nonlinear least-squares curve fitting problems of the form

$$\min_x (f(x)) = f_1(x)^2 + f_2(x)^2 + f_3(x)^2 + \dots + f_m(x)^2$$

Syntax

```
x = lsqnonlin(fun, x0)
x = lsqnonlin(fun, x0, lb, ub)
x = lsqnonlin(fun, x0, lb, ub, options)
[x, resnorm] = lsqnonlin(...)
[x, resnorm, residual] = lsqnonlin(...)
[x, resnorm, residual, exitflag] = lsqnonlin(...)
[x, resnorm, residual, exitflag, output] = lsqnonlin(...)
[x, resnorm, residual, exitflag, output, lambda] = lsqnonlin(...)
[x, resnorm, residual, exitflag, output, lambda, jacobian] = lsqnonlin(...)
```

Figure 4.18 brief introduction of “lsqnonlin” (MATLAB help document)

The corresponding matlab code to solve the “optimize z” problem is presented in Appendix E.

With the code developed, we solved some sample “optimize z” problems, which however were only medium-scale problems. For instance, we could only do process plan for a sphere surface with bottom radius of 1000 μm , but we failed to do a larger surface, say with the bottom radius of 2000 μm . Note that we have done process plan in Section 4.4 for curing a sphere surface with the bottom radius of 3000 μm successfully.

Some limitations were observed using the “optimize z ” method to generate process plans for TfMP μ SLA curing. The nonlinear least-squares solver used in “optimize z ” requires much more memory in MATLAB; hence “Out of memory” errors pop up frequently, disabling us from solving the “optimize z ” problems. Worse still, the maximum variable size allowed by the “lsqnonlin” solver used in “optimize z ” is much smaller than the “lsqlin” solver used in “optimize E ”. Consequently, the “optimize z ” method could only handle a comparatively small geometric part with much fewer pixels on the substrate than the “optimize E ” method could. If we increased the number of pixels and micromirrors needed for curing a larger part on the substrate, an error would come out as “Maximum variable size allowed by the program is exceeded”. This is unfortunately a fatal flaw inherent in our current “optimize z ” method using “lsqnonlin” in MATLAB. Future improvement on the mathematical model and related algorithms is recommended.

4.5.2.2 Comparing “optimize z ” with “optimize E ”

The method of “optimize z ” is not mature and capable enough. Though we prefer to employ the “optimize E ” method as in the mathematical module developed previously, we may still be curious to know what differences there are between using “optimize z ” and “optimize E ” to do process plan for curing the same geometric profile. To illustrate it, we are going to do process plan for curing the same sphere surface as shown in Figure 4.19, with the two different approaches.

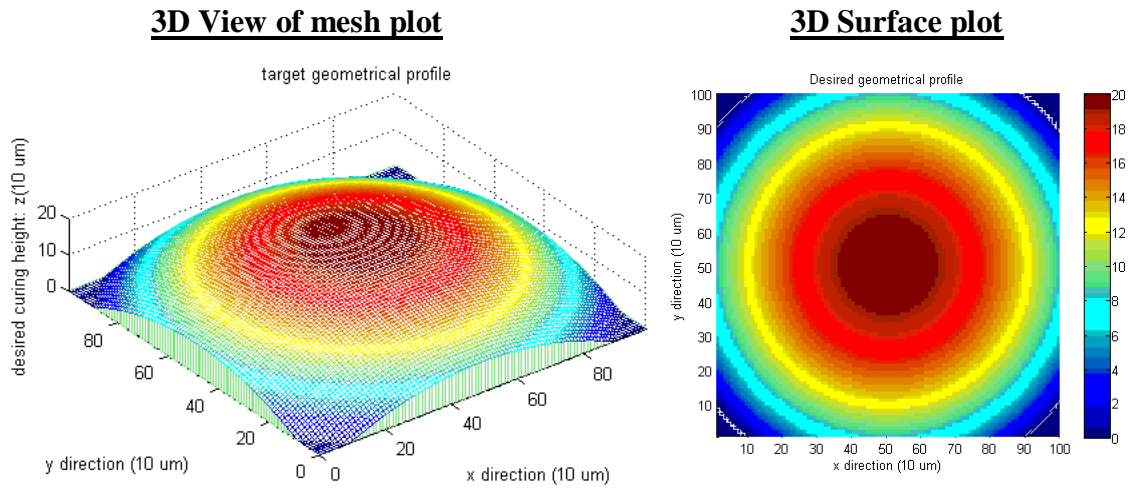


Figure 4.19 Desired geometric profile – example in comparing “optimize z ” with “optimize E ”

For each method, 25 bitmaps were obtained for curing the sphere surface. Figure 4.20 shows the bitmaps and exposure time generated by the “optimize E ” method. Similarly, those generated by the “optimize z ” method are shown in Figure 4.21. It is clear from the resultant bitmaps and exposure time that the two methods generate quite different input process data for the TfMP μ SLA system.



Figure 4.20 bitmaps and exposure time generated by the “optimize E ” method

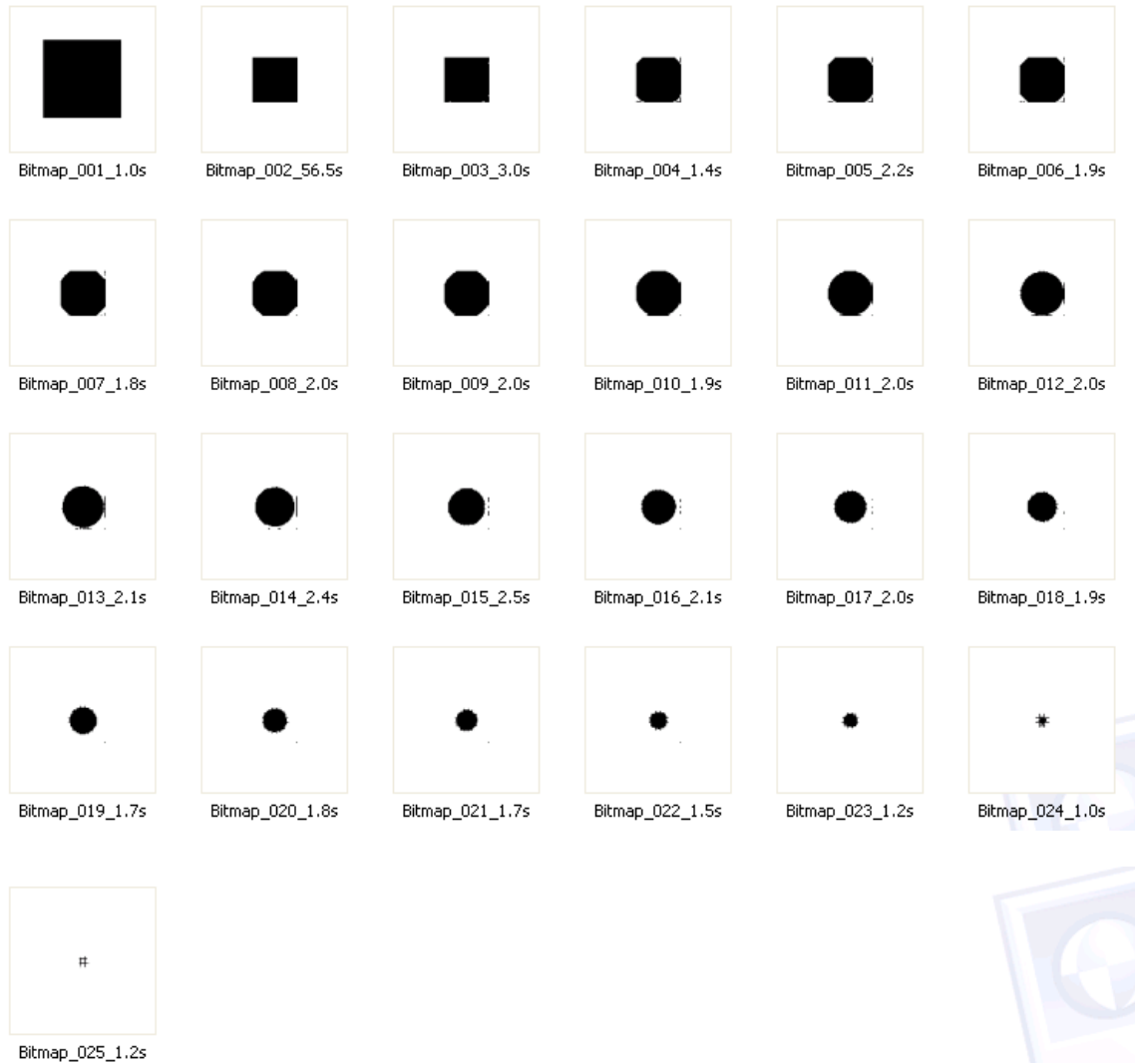


Figure 4.21 bitmaps and exposure time generated by the “optimize z ” method

A comparison is made in Table 4.4. The “module running time” column reveals that the computation time and complexity of the nonlinear problem “optimize z ” is far more than that of the linear problem “optimize E ”. The “RMS $(E-E_0)_{abs}$ ” (see Equation 4.12) column shows that the “optimize E ” method output smaller deviations between the desired and estimated energy exposure profile, while the rightmost two columns demonstrate that the “optimize z ” method produced smaller deviations between the

desired and estimated geometric profile. The comparison results are consistent with the two different objectives in Problem 5 and Problem 6.

Table 4.4 compare the results from “optimize z ” and that from “optimize E ”

Methods	module running time (s)	RMS $(E-E_0)_{abs}$ (mJ/cm ²)	$R_a(z-z_0)$ (μm)	RMS $(z-z_0)$ (μm)
optimize z	135	1.863	12.115	15.228
optimize E	12	0.749	12.215	15.455

One main concern of the process planning method is to get a geometric profile as close enough as possible to the desired geometric profile. Though the method “optimize z ” seems to generate a more accurate geometric profile, it wins over the method “optimize E ” just by a narrow margin: 0.1 μm in terms of $R_a(z-z_0)$ (refer to Equation 4.14) and 0.227 μm in terms of RMS $(z-z_0)$ (refer to Equation 4.15). Considering the tradeoff among algorithms efficiency, complexity, capability and accuracy inherent in the two methods, we conclude that the “optimize E ” method, based on which the mathematical module was developed in the thesis, is more feasible in the TfMP μSLA process planning system.

4.6 Chapter summary

In this Chapter, a mathematical formulation of the TfMP μSLA process planning method is presented, so as to address Research Question 2 and 3. The function f_{ET} (refer to Equation 4.1) provides a mathematical description of Hypothesis 2, based on which the

TfMP μ SLA parameter estimation is formulated. Thus, Hypothesis 2 and 3 are mathematically associated. The mathematical module is demonstrated to be valid through an example problem. Observing an acceptable RMS value of deviations between desired exposure profile and estimated exposure profile resulted from f_{ET} , Hypothesis 2 is demonstrated to be able to estimate the amount of energy exposure on a pixel by linearly accumulating irradiance amounts provided by all contributing micromirrors. During the validation of the mathematical module, a desired set of bitmaps and exposure time for each bitmap were obtained by solving the parameter estimation problems, thus Hypothesis 3 is validated.

Though Hypothesis 2 and 3 have been demonstrated to be valid by modeling and simulation, physical validations are still desired to show that the process planning method does work in the real world. Chapter 5 will verify further the process planning method as well as all the hypotheses experimentally.

CHAPTER 5

PHYSICAL MODULE - EXPERIMENTAL VALIDATION

This chapter presents the physical module, which aims to implement the process plans generated by the process planning system physically. The main role of this physical module is experimental case study and validations.

5.1 Validation strategy for the TfMP μ SLA process planning method

To validate the TfMP μ SLA process planning method developed in the thesis, we will implement the method in three applications of curing different parts, and compare the cured parts with the desired parts quantitatively in terms of dimensions and qualitatively in terms of profiles. Section 5.2 presents these experimental case studies. Sources for dimensional errors and profile errors are analyzed in Section 5.3 and suggestions for future work to reduce those errors are also presented in order to improve the process planning method.

Three illustrative examples to cure desired geometric profiles of parts are chosen to validate the process planning method individually; nevertheless, they together will meanwhile also demonstrate the temporal repeatability and capability in micro fabrication (refer to Table 5.1).

The first illustrative example is to cure a spherical surface on a cylinder base. It serves as an initial investigation and simple validation of the process planning method. The geometric profile is pretty straightforward with primarily circular cross-sections, and the process data, i.e., the bitmaps, are expected to be circles intuitively. Therefore, it is straightforward to verify the bitmaps generated by the process planning method at first

glance; and the exposure time for each bitmaps can be validated by measuring the cured parts.

The second illustrative example is to cure a part of microchannels as introduced in Chapter 1. Being different from the first example, the example can investigate the process planning method in curing sharp edge features. Apart from validating the method, it primarily aims to explore the possibility of applying the TfMP μ SLA technology to microfluidics area.

Furthermore, to broaden the application area, which can be applied to a real field, array-type complex 3D microstructures, an array of micro lens is to be cured as the third illustrative example. Besides, the example will demonstrate the spatial repeatability in the process.

While implementing the process planning method in each of the examples, all the hypotheses put forward for developing the method in Section 2.4 will be validated. To be specific, in each example, according to the geometrical module, the target CAD model of a part is discretized into column voxels, which will validate the Column Cure Model. The chemical module outputs a working curve function and transfer function mapping the desired geometric profile into the desired energy exposure profile, providing an input to the succeeding mathematical module. By validating the mathematical module, Hypothesis 1 is also simultaneously validated. The mathematical module adopting Hypothesis 2 and 3 can be validated by observing the generated bitmaps shapes as well as the cured parts dimensions and profiles.

As a summary, the validation strategy is presented in Table 5.1.

Table 5.1 Validation strategy of the TfMP μ SLA process planning method

Example	To Validate the Hypotheses			Spatial Repeatability	Temporal Repeatability	Geometric Shapes	Other Purposes
	1	2	3				
1	√	√	√			spherical	An intuitive and straightforward validation
2	√	√	√	√		sharp edge	To explore the application potentiality in microfluidics area
3	√	√	√	√		spherical	To explore the application potentiality in micro-optics area.
All together	√	√	√		√	features: step, curve	

5.2 Applying the TfMP μ SLA process planning method

Using the modules formulated and validated in Chapters 3 and 4, it is now possible to present a process planning method to cure a 3D TfMP μ SLA part. In this section, the process planning method is described and its implementation to cure some test parts is demonstrated following the validation strategy presented in Section 5.1.

The TfMP μ SLA process planning method is as shown in Figure 5.1.

Given: a CAD model of the part to be built.

1. Apply the geometrical module to obtain a discretized part with vertical column voxels. It will output a vector of all the voxels' desired heights, z_0 .
2. Apply the chemical module to obtain the resin working curve function f_{zE} , and the transfer function f_{zE} . The transfer function f_{zE} serves to transfer z_0 to the desired energy exposure profile E_0 , which is in the same size with z_0 .
3. Apply the optical module to obtain the irradiance matrix H .

4. Apply the mathematical module, plug in all the parameters obtained from the modules above, and specify the number of bitmaps to be generated, the final machining data input to the TfMP μ SLA setup will be generated to cure the whole part.
5. Build part.

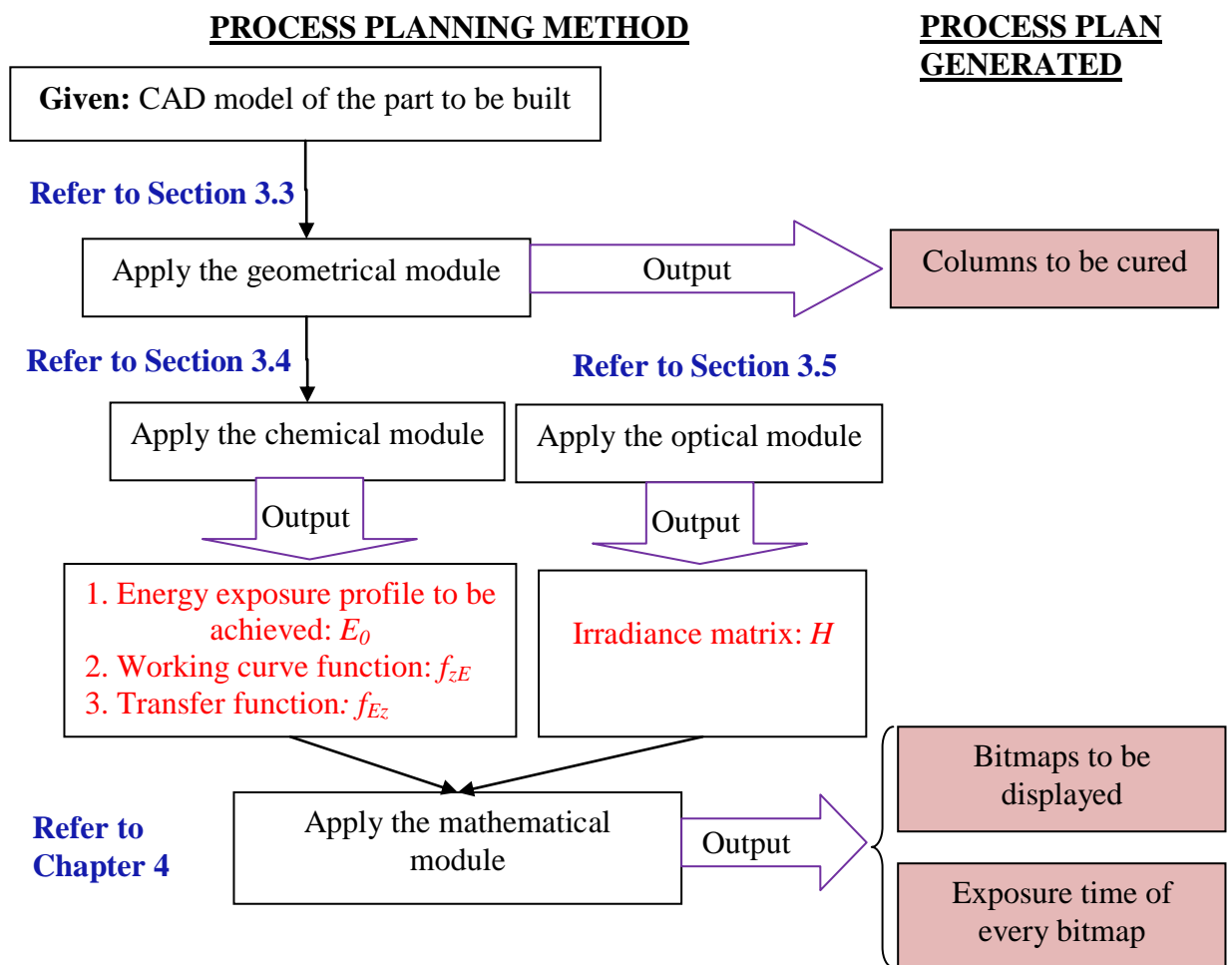


Figure 5.1 Process planning method for Thick-film Mask Projection micro Stereolithography

In this section, the process planning method in Figure 5.1 is applied on three test parts. In Sections 5.2.1 – 5.2.3, three different test parts are discretized using the geometrical module presented in Section 3.3, to obtain the desired geometric profile. The same chemical resin, a biomaterial hydrogel - PEGDA MW 700 (vendor: Sigma-Aldrich) is used in curing all the three parts. By applying the chemical module presented in Section 3.4, the working curve and its function “ $z = f_{zE}(E)$ ” (refer to Equation 3.9) is as shown in Figure 5.2. The transfer function f_{Ez} is simply an inverse function of f_{zE} for $z > 0$, and zero for $z = 0$. Refer to Equation 3.10.

Please note the two distinct sections of the working curve in Figure 5.2, one is the so-called “low area” corresponding to the cured heights smaller than 180 μm ; while the other called “high area” refers to the section with cured heights larger than 180 μm . There are very large changes in values of D_{pS} and D_{pL} from the two segments of the working curve. From the resin cure model developed in Section 3.4.3.1, it is known that if D_{pS} is much larger than D_{pL} , the working curve tends to be linear. Hence, the changes of the values in the higher area indicate a more linear resin cure behavior. The underlying reasons for the piecewise curing characteristics still need further investigation and probably cooperation work from the Chemical Engineering collaborators if applicable.

In the following case studies, we intend to cure parts of desired heights within “high area” only, to simplify the process planning system a little bit. Nevertheless, a recommendation for curing parts lower than 180 μm using this hydrogel, is simply to use the corresponding working curve function $f_{zE} = z_n(E)$ and parameters like E_{cn} , D_{psn} and D_{pln} as shown in Figure 5.2.

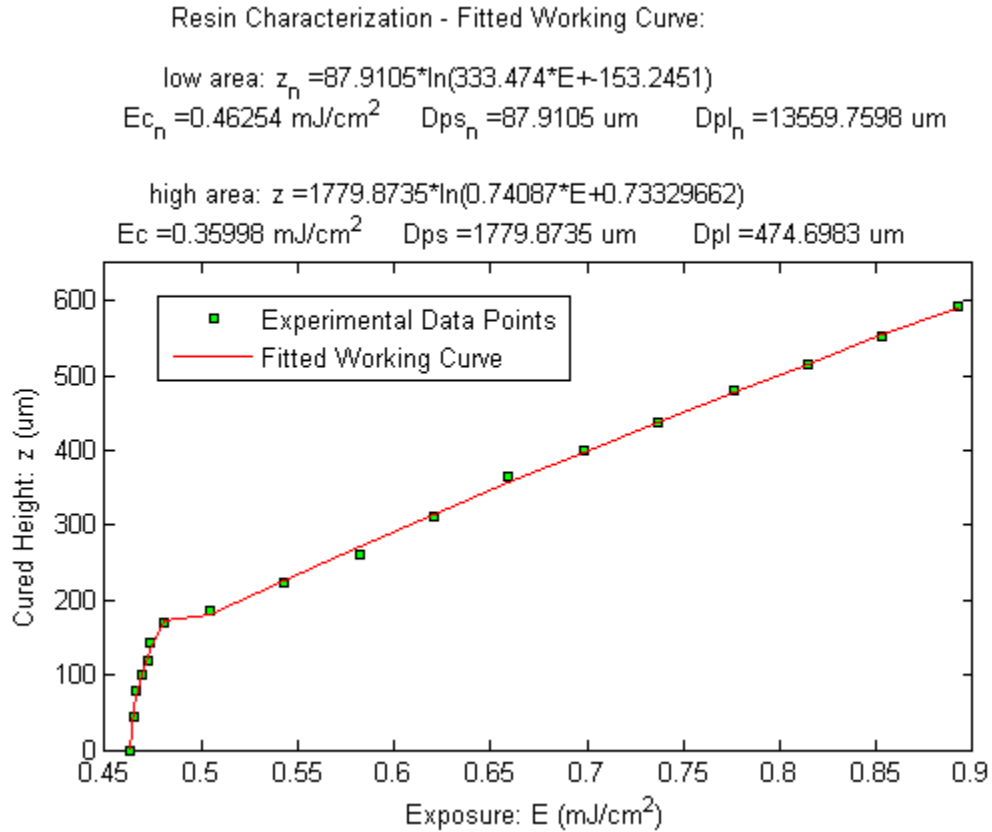


Figure 5.2 working curve for the chemical resin PEGDA MW 700

As to the optical module, one thing to point out is that we used a ray-tracing method with $n = 81$ and $m = 225$ in the TfMP μ SLA process plans as presented in Section 3.5. The output irradiance matrix H is used in all the three test cases below.

Different target geometric profiles are transferred by the chemical module to different desired energy exposure profiles. Use the desired energy exposure profile and irradiance matrix as inputs to the mathematical module. In each case study, 25 bitmaps are generated to be imaged onto the resin substrate in order to cure the test part using the mathematical module, presented in Chapter 4. Simultaneously, the exposure time of each bitmap is also computed by the mathematical module.

The parts are built on the TfMP μ SLA system by using the generated process plans. The display of the bitmaps is controlled by Discovery 1100 Controller (Texas Instruments) with the accuracy of 1 millisecond.

The built parts are presented separately in Sections 5.2.1 – 5.2.3 and their geometric shapes are compared to the required geometry.

5.2.1 Case 1: curing a spherical profile on a cylinder base

Figure 5.3 shows the desired shape for Case 1, which is a part of sphere sitting on a cylinder base. The diameter of the cylinder base is 3000 μm and the thickness of the cylinder is 250 μm . The top of the spherical surface to the bottom of the cylinder is 450 μm .

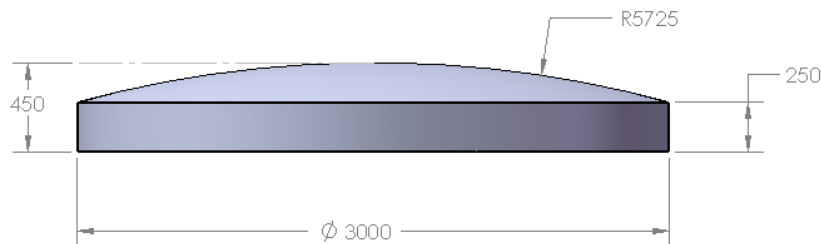


Figure 5.3 CAD model (desired cured shape) for Case 1: curing a spherical profile on a cylinder

From the chemical module results as shown in Figure 5.2, the desired energy exposure profile for the given geometry can be calculated by applying the transfer function f_{E_z} . Figure 5.4 shows the desired exposure profile for Case 1. Please note that the units on the X and Y axis are pixels, which are 10 μm .

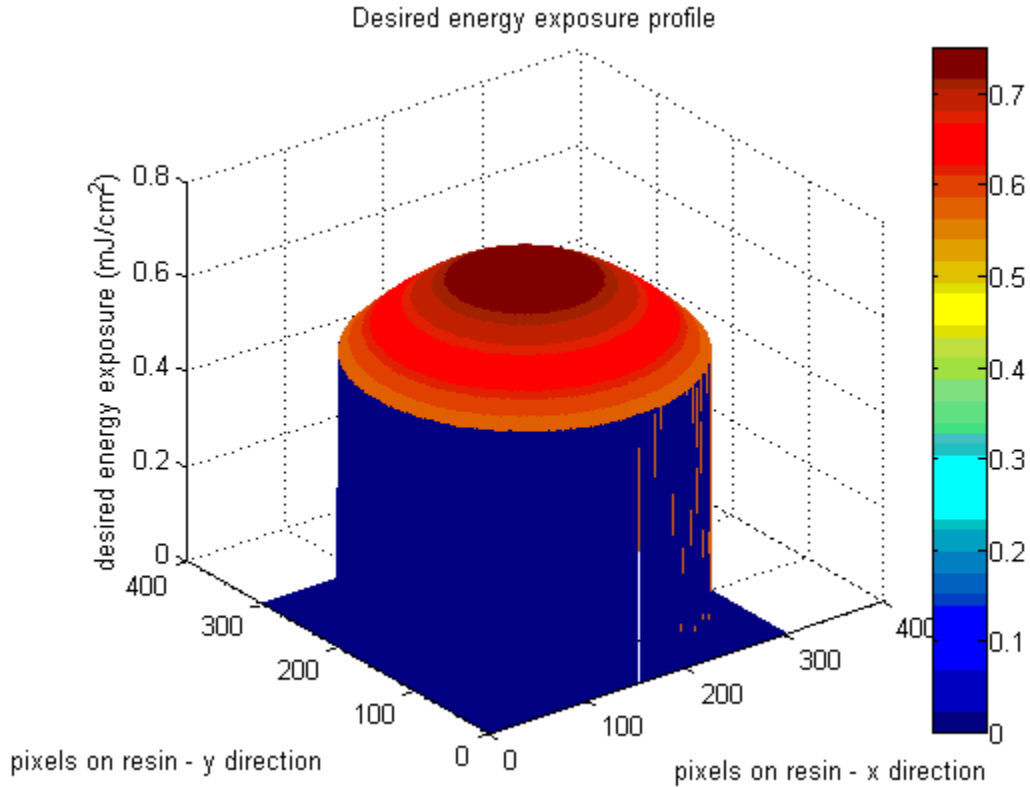


Figure 5.4 desired energy exposure profile for Case 1: curing a spherical profile on a cylinder

After running the mathematical module, the bitmaps with the times of exposure are obtained. Figure 5.5 shows the results. The title “Bitmap_002_11.0s”, for example, means that the bitmap right above it is the second bitmap to project on the DMD during the TfMP μ SLA process, and the exposure time is 11.0 seconds. Totally 25 bitmaps were obtained. However, the resultant exposure time of the first bitmap is zero, so actually speaking only 24 bitmaps count. It makes sense that the first square bitmap should be displayed for zero seconds, because the required profile is a cylinder base which should be circular.

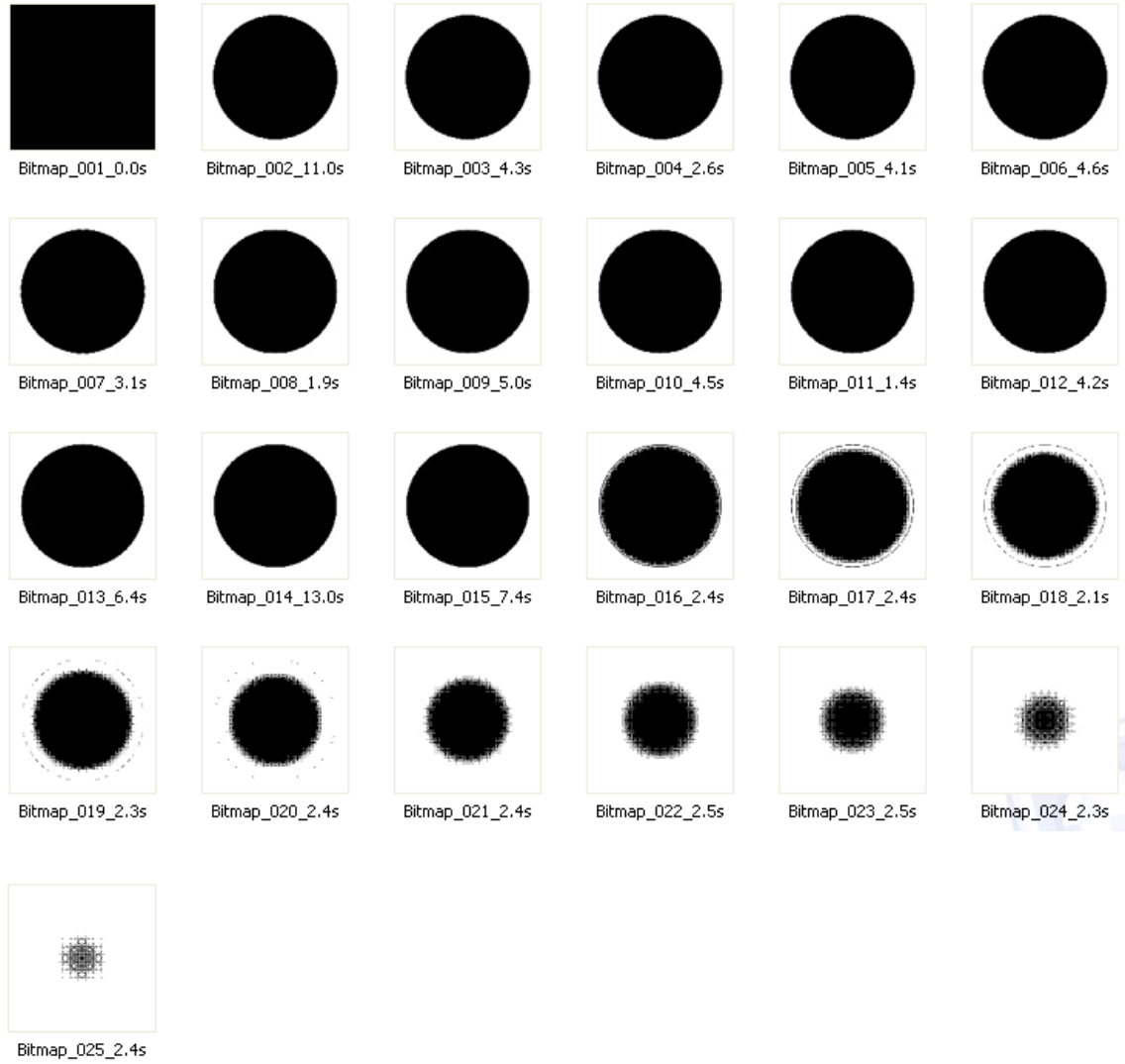


Figure 5.5 Bitmaps displayed on DMD for Case 1: curing a spherical profile on a cylinder

Using the above bitmaps, the estimated energy exposure profile is obtained as shown in Figure 5.6. The RMS value of relative error is calculated as in Equation (4.7). Here, $\text{RMS } (E-E_0)_{rel}$ is 5.816%. This error results mostly from discretization of the micromirrors on the DMD and the sampling errors in ray tracing. Again, please note that the units are in pixels.

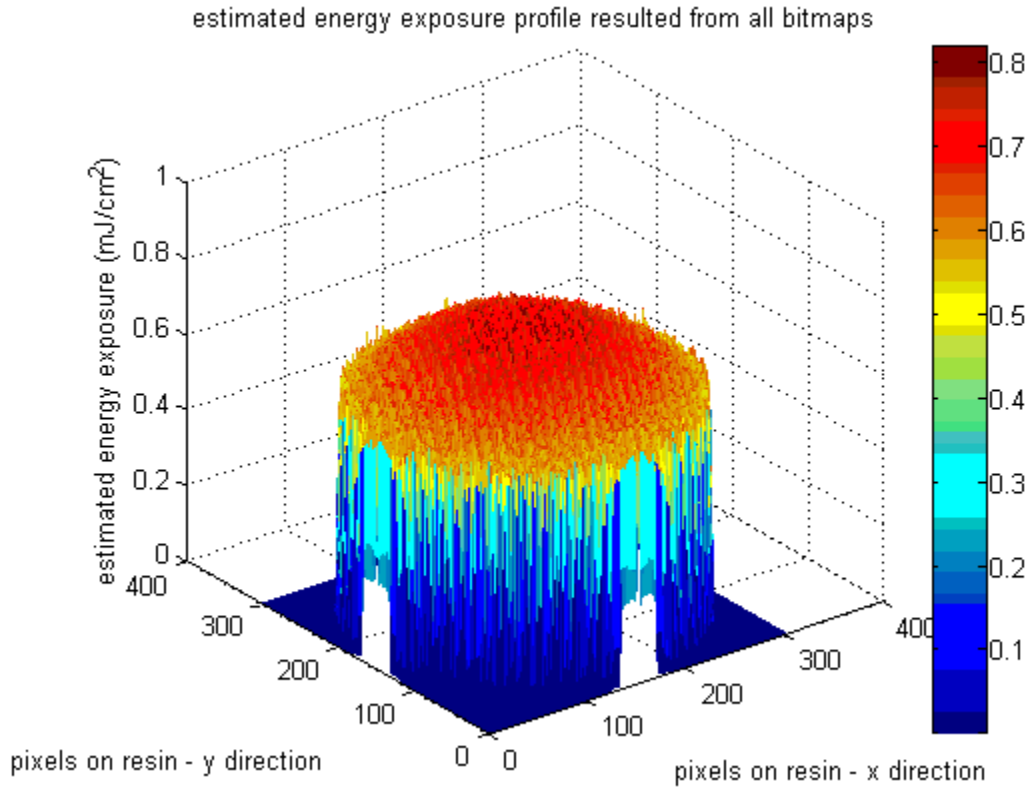


Figure 5.6 estimated energy exposure profile for Case 1: curing a spherical profile on a cylinder

Figure 5.7 shows the experimental results obtained after using the 25 bitmaps as shown in Figure 5.5. The blue profile outlines the desired part shape.

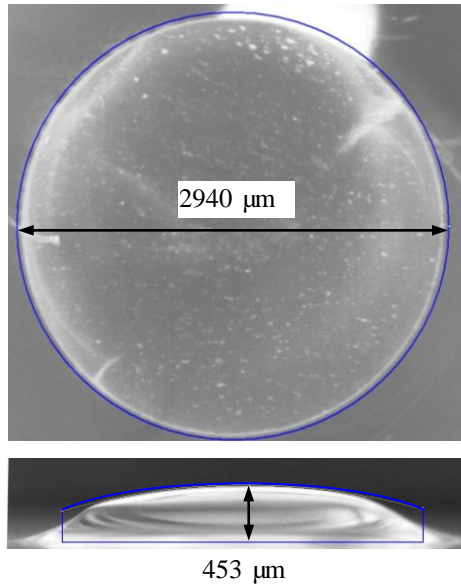


Figure 5.7 TfMP μ SLA part built for Case 1: curing a spherical profile on a cylinder

The dimensional errors on the overall dimensions are compared in Table 5.2. The error in diameter is better than that of 2.5% in Limaye’s master’s thesis [24]. Moreover, the circular shape achieved is much better than the somewhat elliptic shape cured in [24]. Though Limaye used a different resin material and this comparison may not be fair, it could be concluded that the process planning method developed in this thesis is at least not worse than his.

Table 5.2 Comparison on dimensions of desired and cured part – spherical profile on cylinder base

Dimension	Desired (um)	Cured (um)	Percent Error (%)
diameter of the cylinder base	3000	2940	2.00
maximum height	453	450	0.67

5.2.2 Case 2: curing microchannels

Considering the example problem in Section 1.3, we'd like to test the capability of fabricating microchannels with the TfMP μ SLA method. The CAD model of a part with micro channels is shown in Figure 5.8 (a). In this part, there are 3 micro channels with depths of 200 μm and widths of 300 μm . The height of the walls of the micro channels is 450 μm and the height of the base of the micro channels is 250 μm . The walls between the micro channels are 500 μm wide. The front view of the part is shown in Figure 5.8 (b).

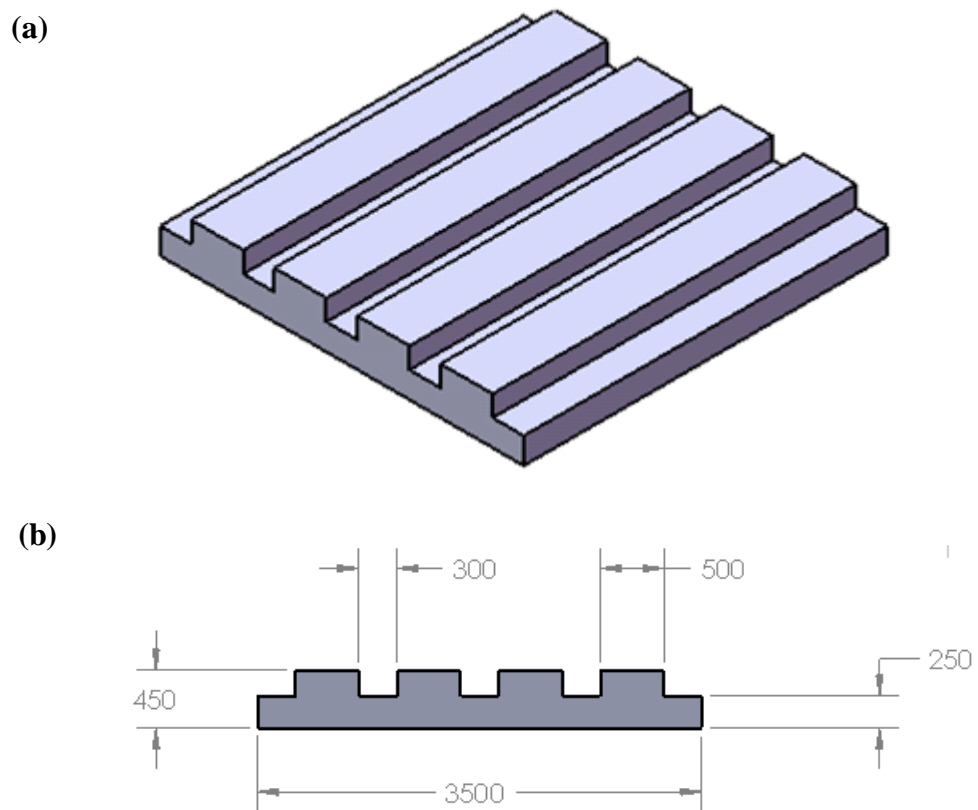


Figure 5.8 CAD model for Case 2: curing a part of microchannels (a) desired part (b) desired dimensions

Figure 5.9 shows the 25 bitmaps generated from the mathematical module.

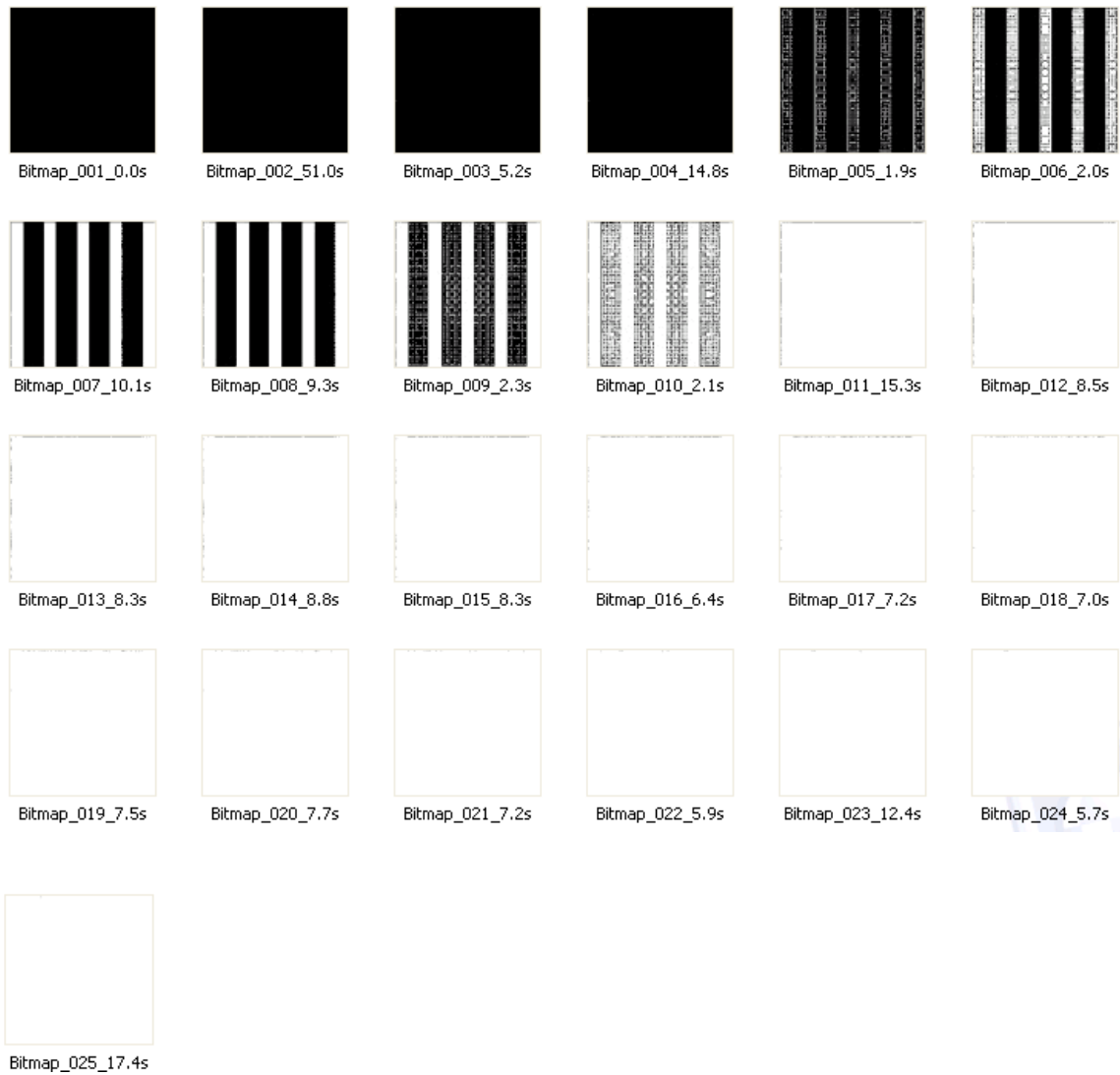


Figure 5.9 Bitmaps displayed on DMD for Case 2: curing a part of microchannels

In Figure 5.9, Bitmaps 11 – 25 are almost blank with only some edge pixels on the top and left. This is because the linear least squares solver computed out some comparatively larger exposure time values for those pixels at the first stage of solving Subproblem 6.1, which is energy exposure profile optimization. The point here is that due to the mathematical computation tolerance and errors, speckles and even strips are

sometimes unavoidable in the resultant bitmaps. Though they appear inconsistent with the desired geometric profile, they are normal in mathematics and acceptable in physical curing. The ugly but reasonable bitmaps actually contribute to the energy exposure profile optimization and have no bad impacts on the cured part. For instance, in this case, despite the seemingly “abnormal” bitmaps, the exposure profile is still appropriately estimated and the RMS $(E-E_0)_{rel}$ is 4.444%. The estimated exposure profile plot is shown in Figure 5.10.

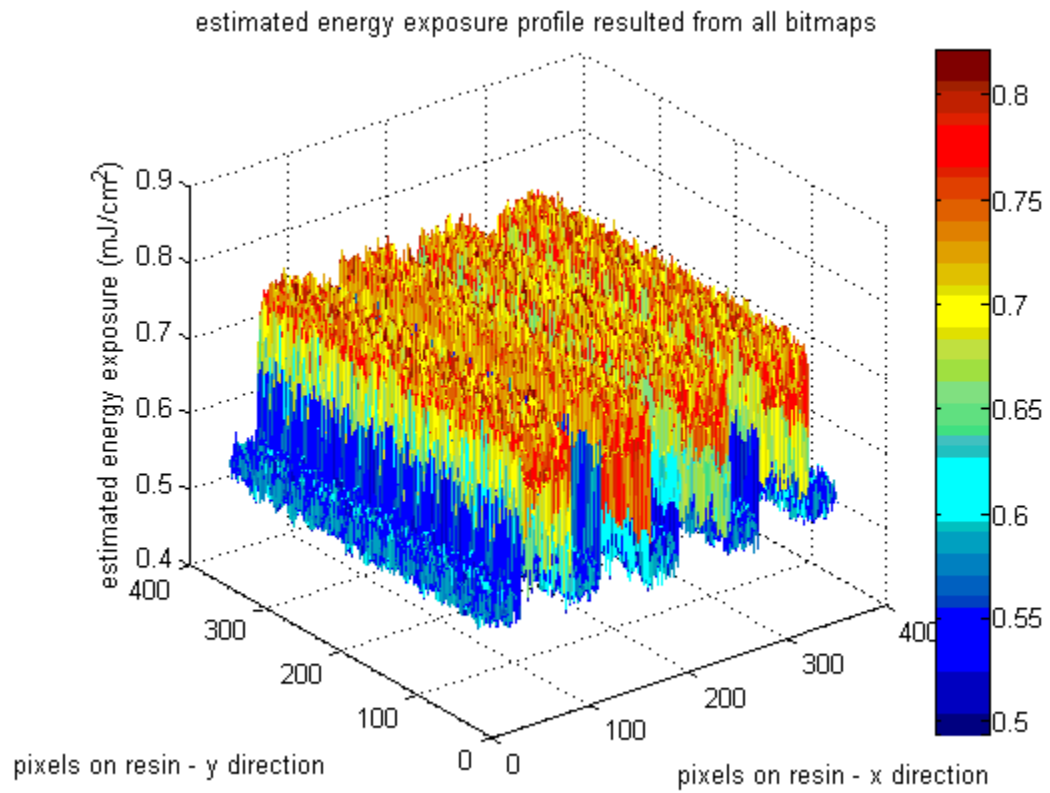


Figure 5.10 estimated energy exposure profile for Case 2: curing a part of microchannels

The cured shape from the experiment for Case 2 is shown in Figure 5.11. Figure 5.11(a) is the top-view of the cured part, which shows the lateral dimension of the micro channels. Figure 5.11(b) is the front-view of the cured part, which shows the vertical dimensions of the channels. Please note that the front-view is a little skewed, due to an in-plane incline angle (approximately 8°) between the cured part and the glass substrate. That is, the side of the cured part didn't exactly align with the substrate side; however, to measure the side profile of the cured part, we had to put the substrate side on the measure table. The blue lines in Figure 5.11 show the edges of the desired geometry.

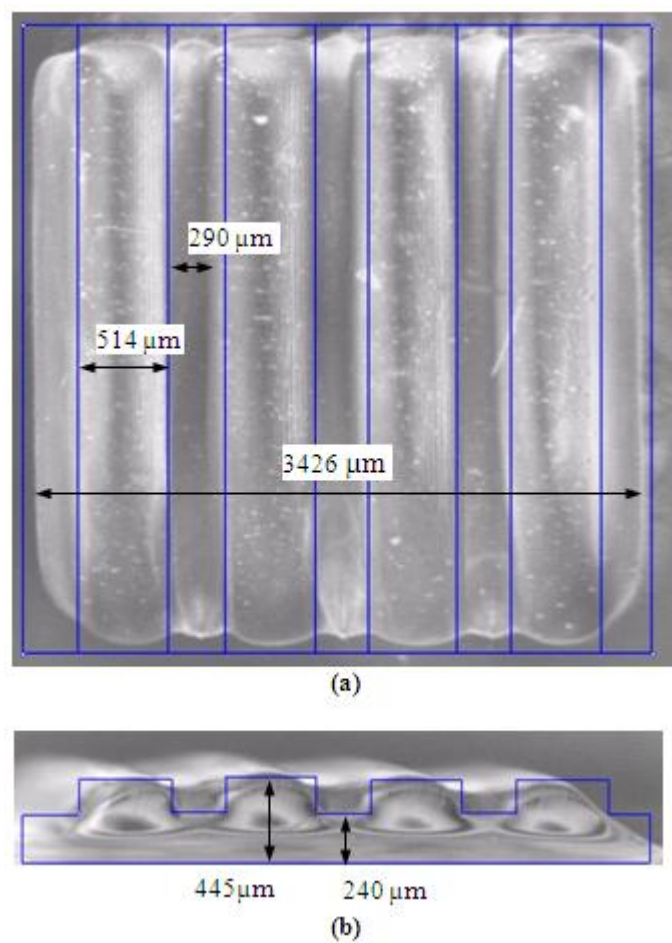


Figure 5.11 TfMP μ SLA part built for Case 2: curing a part of microchannels

The dimensions shown in Figure 5.11 are average values of multiple measurements. For example, to measure the width of grooves, we measured the width at three different locations within the same groove, and then averaged them to obtain a value as the groove width.

A comparison of the cured part and the desired shape is shown in Table 5.3.

Table 5.3 Comparison on dimensions of desired and cured part – microchannels

Dimension	Desired (um)	Cured (um)	Percent Error (%)
Groove depth	200	205	2.50
Groove width	300	290	3.33
Wall width	500	514	2.80
Overall height	450	445	1.11
Overall length	3500	3426	2.11

5.2.2.1 Dimensional errors analysis

In Table 5.3, although the dimensional errors on the overall dimensions are shown to be less than 5%, the possible error sources should be quantified to demonstrate that the percent errors are eligible and acceptable. Errors for this case are analyzed as below by tracing through each module in the process planning method.

1. Firstly, the geometrical module discretized the CAD model of microchannels into column voxels with cross-sections of $10\mu\text{m} \times 10\mu\text{m}$ square pixels. Since all the pixels align with the walls and grooves completely and the surfaces of the microchannels are flat, there is no error introduced by the geometrical module.
2. Secondly, in the chemical module, there were some regression residuals, while fitting the experimental data into the resin cure model. Hence, the functions f_{zE} and f_{Ez} could introduce errors during the transformation between

the desired geometrical profile and the desired energy exposure profile. The error could be estimated by calculating the RMS values of the residuals for the working curve as shown in Figure 5.2. The residuals norm denoted as *resnorm*, is 760.1833 (μm^2), and there are totally 18 data points. The RMS value is the square root of (*resnorm*/18), which is $\pm 6.5 \mu\text{m}$. Hence, the vertical dimensional error introduced by the chemical module is estimated as $\pm 6.5 \mu\text{m}$. As to the lateral dimensional errors, for those dimensions involving edges, each edge would lack roughly 1 pixel ($10 \mu\text{m}$) due to the oxygen diffusion effects. For dimensions including two edges, say the overall length of the microchannels part, the error range due to oxygen diffusion effect is estimated as ($-20 \mu\text{m}$).

3. In the optical module, given a uniform irradiance incident on the DMD, some variations in the irradiance profile were however observed in the simulation. Those variations probably have origination in the sampling errors in ray-tracing as analyzed in Section 3.5.5. For all the experiments presented in this chapter, the irradiance incident on the substrate was measured to be 7.757×10^{-3} (mW/cm^2), while the optical module output a simulation of the irradiance profile of all the pixels on the substrate as shown in Figure 5.12.

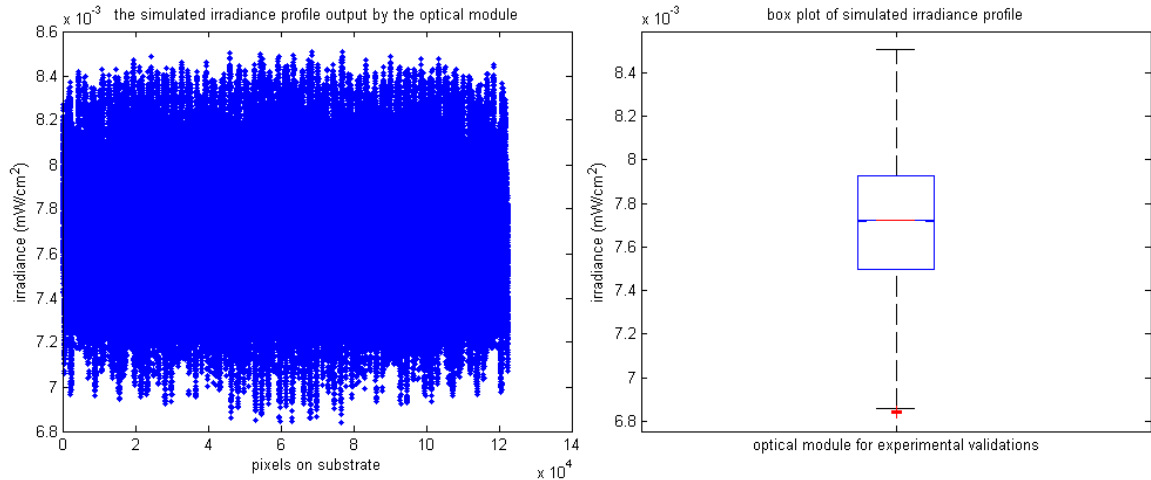


Figure 5.12 the simulated irradiance profile on the substrate

In Figure 5.12, the average irradiance values simulated is 7.721×10^{-3} (mW/cm²), which is very close to the actually measured value. The standard deviation is 0.305×10^{-3} (mW/cm²). In the physical setup, the actual irradiance profile captured by the CCD camera also presented some variations which are consistent with the simulated profile. Therefore, it is postulated that the errors introduced by the optical module is negligible.

4. The mathematical module can simulate the geometrical profile and compute the deviations between the desired and estimated column voxels' heights (see Equation 4.14). In this case, the value of $R_a(z-z_0)$ is 24.2 μm , which could be regarded as the vertical dimensional errors introduced by the mathematical module.

As to the lateral dimensional errors, since the mathematical module optimization energy exposure profiles over a grid of 10 μm -by-10 μm pixels, there are some transition pixels, like the pixels on the edges and those between

channel walls and grooves. The linear least-squares solver would assign some intermediate values to the transition pixels resulting in a smooth transition of geometric features, rather than sharp jumps to a different feature. Hence, a lateral dimensional error of 1~2 pixels would come out for edges as well as the width of channels and walls. In the case, from the simulated geometric profile as shown in Figure 5.13, we didn't observe edge effects, but some incline features were observed rather than sharp step features which could influence the width of channels and overall length by twice $\pm 20\mu\text{m}$ due to both the sides of lateral dimensions would be influenced by transition pixels.

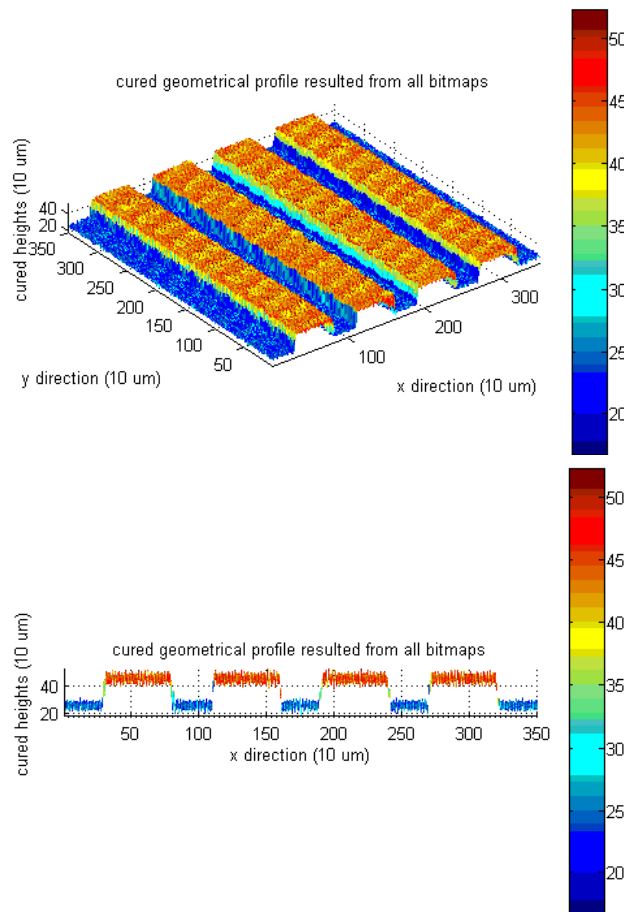


Figure 5.13 Simulated geometric profile: microchannels

5. Measurement errors

Please note that the measurement errors could also be significant due to the optical measurement methodology.

The measurement system comprised of a Nikon microscope with a USB digital camera from Motic Cam mounted with a C-mount on the microscope eyepiece. The cured parts were viewed using this microscope imaging system. The pictures taken by the camera were analyzed using the camera software (Motic Images Plus 2.0) designed for measuring images from the microscope. This software was calibrated for various magnifications prior to using it.

There are two sources of error in this measurement system. These are pixel resolution and the error in selecting the object edge (human error). The resolution of the system is $4\mu\text{m}$ per pixel for measurement at 2X magnification. The human error was not quantified, though its effect was reduced by taking average of multiple readings for the same object under consideration.

Since it is difficult to identify the edges, especially in the top view with blurred areas and shadows, the human error due to a subjective way of selecting the measured object is estimated to be ± 2 pixels corresponding to $\pm 8\mu\text{m}$ for vertical dimensions, and ± 4 pixels corresponding to $\pm 16\mu\text{m}$ for lateral dimensions due to both edges.

Table 5.4 Error analysis for curing microchannels

		Lateral Dimensions			Vertical Dimensions	
Error Sources & Levels (μm)	Geometrical module	0			0	
	Chemical module	-20 (for overall length)			± 6.5	
	Mathematical module	± 40			± 24.2	
	Measurement	± 16			± 8	
	Total range	± 56 ([-76, 56] for overall length)			± 39	
		Groove width	Wall width	Overall length	Groove depth	Overall height
Desired Dimensions (μm)		300	500	3500	200	450
Estimated range (μm)		244-356	444-556	3424-3556-	161-239	411-489
Actual Dimensions (μm)		290	514	3426	205	445
Actual Error percent (%)		3.33	2.8	2.11	2.5	1.11

As a summary, the dimensional errors are analyzed as shown in Table 5.4. The error range is fairly large, however that could be the maximum error for the worst case using the process planning method. Actually, we didn't see large deviations from the desired dimensions; instead, the actual dimensions of cured microchannels are close to the center of the ranges, resulting in pretty small error percents. The reason is probably that the errors sources offset each other to some extent reducing the observed errors.

5.2.2.2 Profile errors analysis

As to the profile errors, it is noteworthy that in Figure 5.11 the front view shows that the channels' walls are not vertically sharp. The channels of the cured part are inclined and not exactly perpendicular to the base as in the desired profile. These profile errors are expected from the optical module in the process planning system. Essentially speaking, it is the physical setup that determines the optical module, so as to induce the errors in the process plan. The current system setup was designed for a higher optical magnification than that required to cure the experimental parts. This causes blurring of the image resulting from a single micro-mirror and thus loss of precise control over the cured part. These blurring further limits the accuracy obtained from the process planning

method. Hence, instead of the desired cured shape of perfectly vertical walls, the process planning method generates inclined channel walls. To address this problem, the setup should be adjusted to obtain an appropriate optical setup with desired magnification factor.

5.2.3 Case 3: curing micro lens array

Figure 5.14(a) shows the CAD model of a micro lens array. The front-view of the CAD model is shown in Figure 5.14(b).

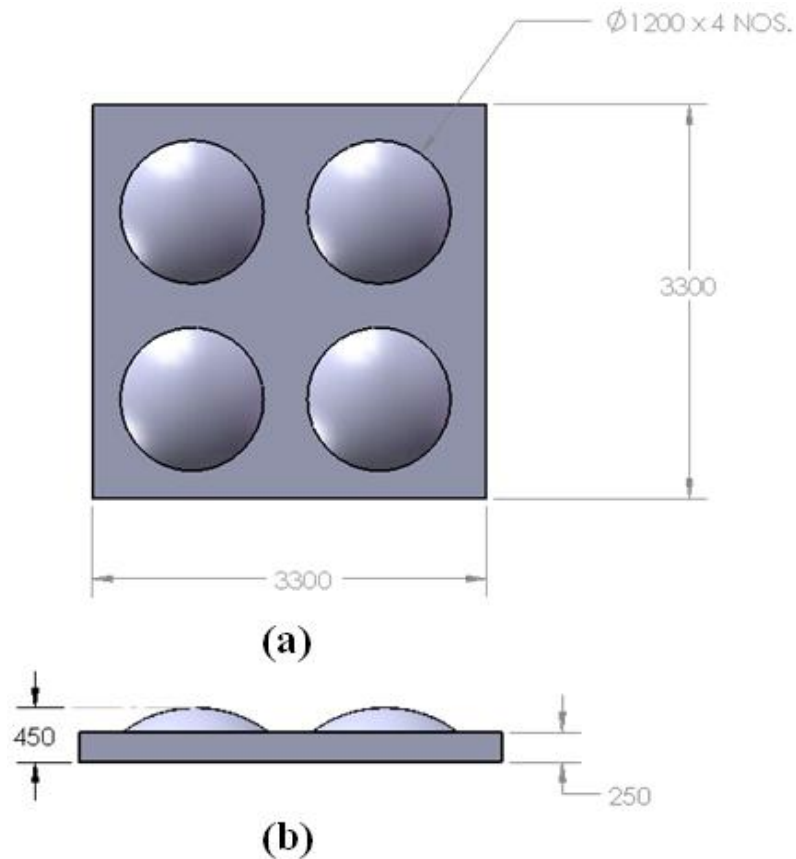


Figure 5.14 CAD model for Case 3: curing a micro lens array (a) top view (b) front view

After applying the mathematical module, the bitmaps displayed on the DMD were produced. All the 25 bitmaps are shown in Figure 5.15.

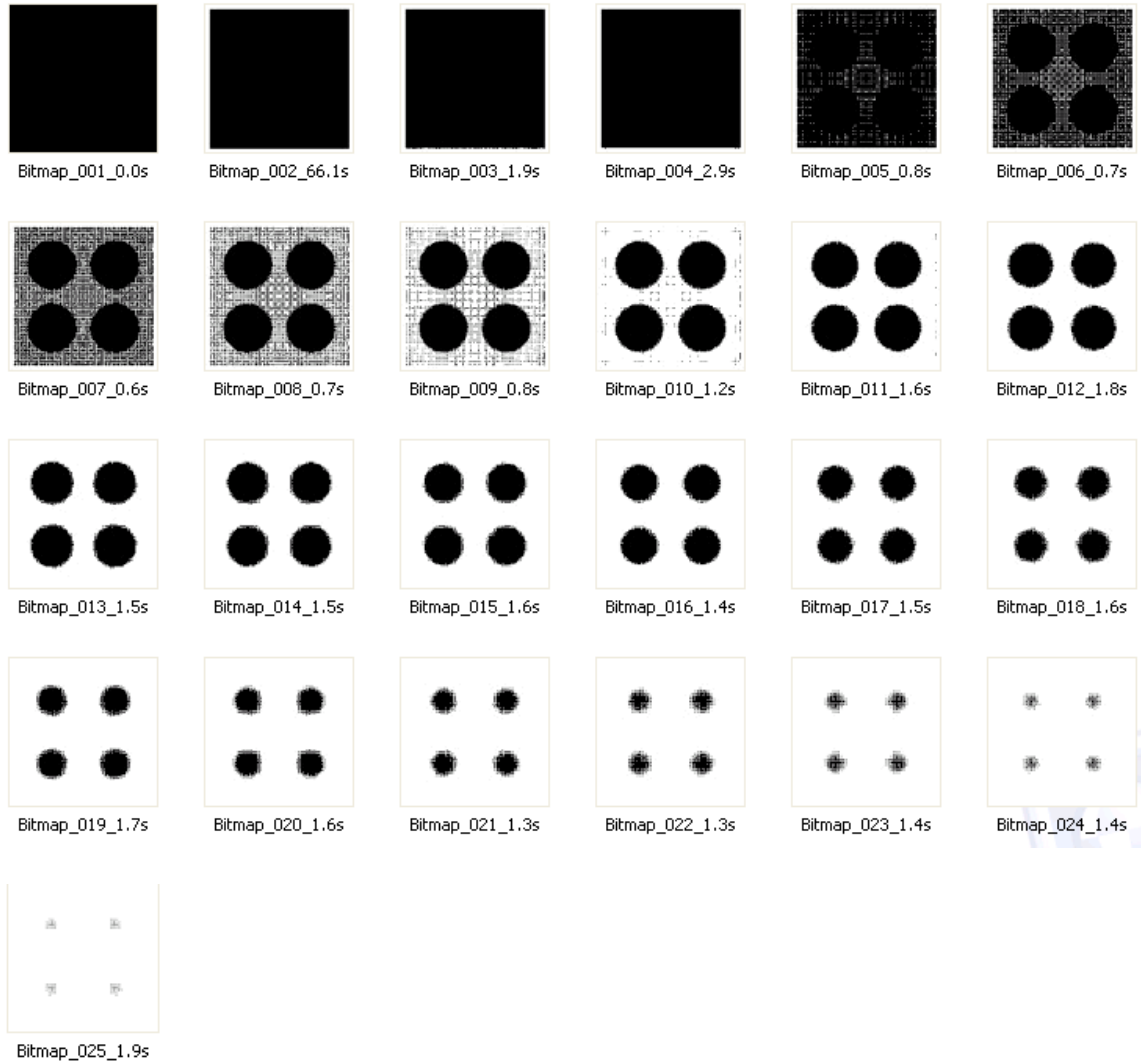


Figure 5.15 Bitmaps displayed on DMD for Case 3: curing a micro lens array

The estimated exposure profile plot is shown in Figure 5.16. The RMS $(E-E_0)_{rel}$ is 3.83%.

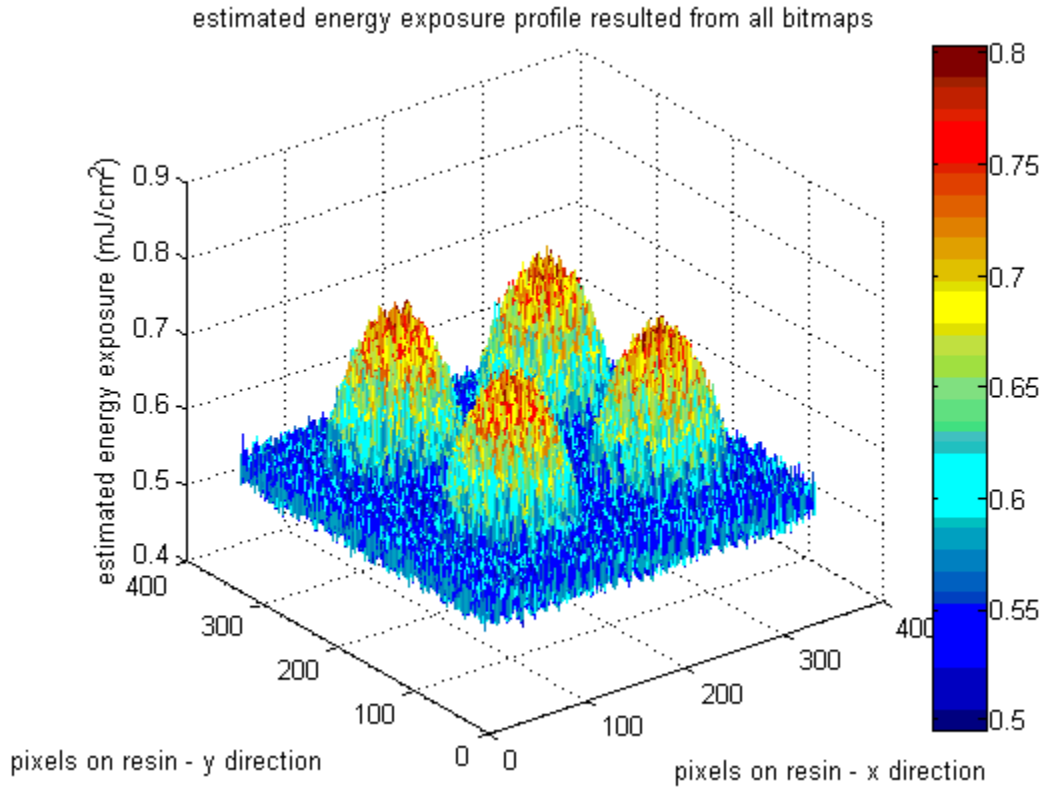


Figure 5.16 Estimated exposure profile for Case 3: curing a micro lens array

Figure 5.17 shows the cured part from the experiments. The measurement of the diameter of each individual micro lens was performed by slicing the cured part and precisely focusing the microscope on the profile required to be measured.

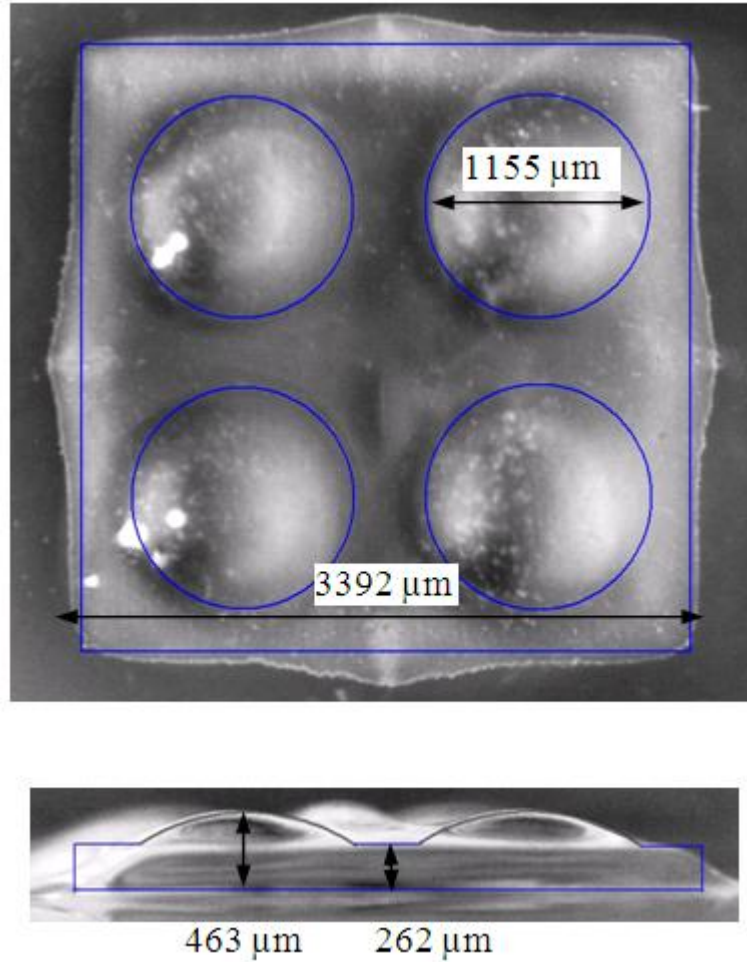


Figure 5.17 TfMP μ SLA part built for Case 3: curing a micro lens array

5.2.3.1 Dimensional errors analysis

A similar dimensional error analysis as in Section 5.2.2.1 is conducted for this case. The range of the maximum errors due to the vertical partition of the spherical surface in the geometrical module is estimated as $[-3\mu\text{m}, 4\mu\text{m}]$. The mathematical module obtained that the value of $R_a(z-z_0)$ is $21.1\ \mu\text{m}$. All the other errors are identical as in Section 5.2.2.1.

The summary of dimensional errors analysis as well as a comparison of the cured part and the desired shape is as shown in Table 5.5.

Table 5.5 Error analysis and comparison on dimensions – micro lens array

		Lateral Dimensions		Vertical Dimensions	
Error Sources & Levels (μm)	Geometrical module	0		[-3, 4]	
	Chemical module	-20 (for overall length)		± 6.5	
	Mathematical module	± 40		± 21.1	
	Measurement	± 16		± 8	
	Total range	± 56 ([-76, 56] for overall length)		[33, 40]	
		Diameter of lens	Overall length	Base height	Overall height
Desired Dimensions (μm)		1200	3300	250	450
Estimated range (μm)		1144-1256	3224-3356	217-290	417-490
Actual Dimensions (μm)		1155	3392	262	463
Actual Error percent (%)		3.75	2.79	4.8	2.89

As shown in Table 5.5, the errors in vertical dimensions, especially in base height are relatively larger. Since the part is cured on a transparent substrate and measurements of vertical heights are performed from the base of the glass substrate, a hazy image on the other side of the measured datum can be observed from the reflections produced from the transparent substrate. Hence, the hazy image would interfere in the measurements, leading to more errors.

Besides, the actual dimension of the overall length exceeds the estimated range in Table 5.5. This is because that the square base swelled outward. A possible cause of the protrusions in the square base is residual stresses, which however is not modeled in the process planning method.

In Table 5.6, we validated the spatial repeatability by comparing the diameters of all the four lenses as shown in Figure 5.17. The standard deviation is about $8 \mu\text{m}$, which mainly results from the machine error due to the pixel resolution in the measurement software and human error while measuring the objects.

Table 5.6 Validating the spatial repeatability

	Top Left lens	Top Right lens	Bottom Left lens	Bottom Right lens	Average	Standard Deviation
Diameter (μm)	1176	1155	1156	1165	1163	8.5

5.2.3.2 Profile errors analysis

Ideally, a profilometer should be used to measure the lenses' surface profiles and surface roughness. In our experiments, we didn't do this since the main concern in the validation is lateral and vertical dimensions. In future work, surface profile and finish should be considered into the process planning method. One noteworthy profile error is the protrusions of the square base. The simulated geometric profile as shown in Figure 5.18 has no such protrusions at all. Thus, possible causes of the protrusions are curing shrinkage and residual stresses, which however are not incorporated into the process planning method. From the measured dimension of overall length and estimated range in Table 5.5, it is estimated that the error due to curing shrinkage and stresses is about 1%.

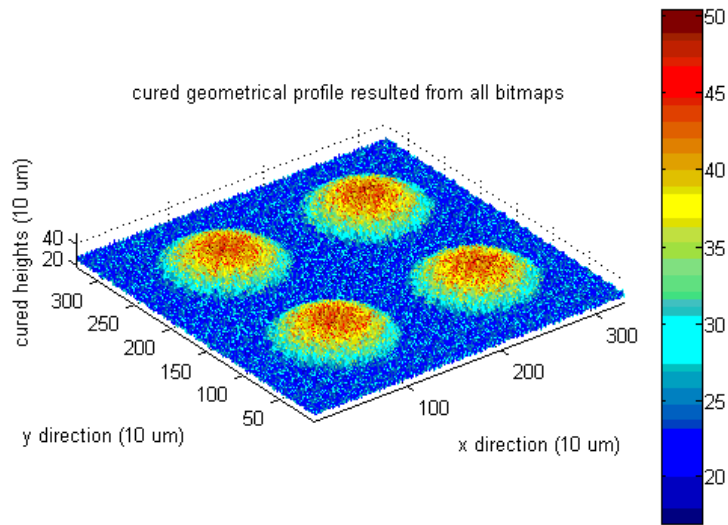


Figure 5.18 Simulated geometric profile: micro lens array

5.2.4 Summary

In this section, three illustrative examples were tested and errors were estimated to evaluate the process planning method critically. Error ranges were estimated for lateral dimensions and vertical dimensions respectively. Maximum errors are estimated as 60 μm for lateral dimensions and 40 μm for vertical dimensions, which errors are fairly large. However in the cured parts, smaller errors were observed than estimated ranges, indicating that some errors offset yielding a smaller observed error. Hence, the process planning method is still valid in curing parts with acceptable dimensions and shapes.

Furthermore, the process planning method could be evaluated by comparing with that developed by Dr. Limaye for his MP μSLA . First of all, he cured a solid circle [24] which is comparable with Case 1 as presented in Section 5.2.1. The error percent in the circle diameter is 2.5%, which is larger than the value of 2% as shown in Table 5.2. Also, an obvious distortion was observed in the cured circle part by Limaye [24], while the top view of the spherical surface is pretty circular and better than the somewhat elliptical shape in [24]. In the cured arrow part [24], the maximum observed percent error for lateral dimensions using Limaye's layer cure model is about 10%, which is much larger than that of 3.75% observed in Table 5.4 and Table 5.5. Vertical dimensions were not the research focus in Limaye's master thesis [24], but they were addressed with much effort in his PhD dissertation [1]. A sample part of down-facing surface was cured in [1]; however there were no explicit measurements and evaluation of the vertical thickness. As to the lateral dimensions, a maximum error of approximately 150 μm was observed, which is larger than that of 92 μm in Table 5.5. It might be not a fair comparison due to the different resin material and different illustrative geometric profiles Limaye used.

However, it is still believed that the process planning method developed in this research is at least not worse than the existing method.

By simulations, it seemed that the mathematical module is responsible for half of the errors. Hence, more efficient mathematical module should be established to improve the process planning method. Prior to that, it is highly recommended that an optical setup with smaller magnification factor be built to reduce the pixel size. Also, it will be worthwhile to understand further the chemical resin behavior and to improve the accuracy of the working curve.

A more general and complete error analysis will be presented in Section 5.3, aiming to draw attentions to all details that could influence the accuracy of the process planning method.

5.3 Error analysis of the TfMP μ SLA process

In Section 5.2, the errors on the lateral and vertical dimensions of the cured parts are shown to be within 5%. Apart from the quantified dimensional errors, the noticeable edge effects become another type of error, which is called as profile error. The profiles of the cured parts presented in Figure 5.7, Figure 5.11 and Figure 5.17 respectively in the three cases above, can be seen to be having some observable edge deficiencies. Therefore, error analysis of the TfMP μ SLA process is presented in this section, in order to identify the error sources and shed light on future research efforts for improving the process accuracy.

In general, two fundamental factors limiting the spatial resolution of TfMP μ SLA system are the physical-chemical characteristics of the chemical resin and optical resolution of the projected image.

To trace out the process error sources, we need to review the model of the TfMP μ SLA process planning system. Section 3.2 introduced the model, which is divided into several process planning modules in the thesis. It is believed that the error sources lie with the modeling loss. According to the modeling loss depiction [56], the TfMP μ SLA process planning model loss is reviewed as below to find out the error sources.

There are four primary sources of differences between the results of the modeling of the TfMP μ SLA process planning system and the behavior of the real TfMP μ SLA. These are depicted in Figure 5.19.

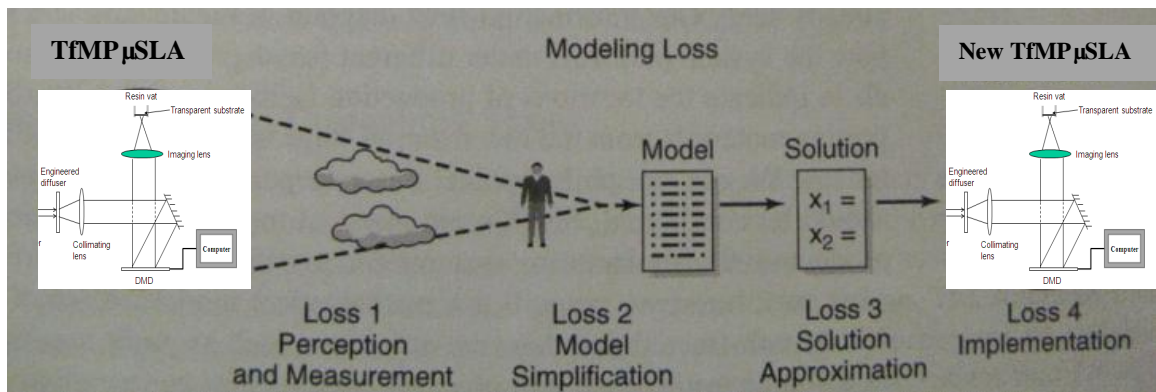


Figure 5.19 TfMP μ SLA process modeling loss [56]

First, we have an imperfect view of the TfMP μ SLA process because of our own limited knowledge and experiences. We see only a portion of the real system that we view through a cloud of perception and measurement error. Thus, we could not construct an exact replica even if we so desired. The loss at this stage is referred as “Loss 1: perception and measurement” in Figure 5.19. It consists of several concrete error sources, which will be elaborated in the sub Section 5.3.1.

Second, we extract the essence of our image of the TfMP μ SLA system to construct a simplified model of the reality. This is to keep the model understandable and manageable within the available time and cost resources. The best model will generally be the simplest model that adequately replicates the reality, according to the so-called parsimonious principle of model building. In Figure 5.19, “Loss 2: model simplification” is identified at this stage. Section 5.3.2 will present the specific error sources imbedded in this type of loss.

The final model may be established through the iterative process of hypothesizing a model form, building the model, and then inputting experimental or empirical data and comparing model and actual outcomes. “Loss 3: solution approximation” is produced at the stage of solving the model, and “Loss 4: implementation” is induced while implementing the model physically. Sections 5.3.3 - 5.3.4 will elaborate on the error sources for modeling Loss 3 and 4 respectively.

5.3.1 Modeling Loss 1: perception and measurement

In terms of perception, the main imperceptible area currently is the chemical realm, especially the resin cure behavior including the resin cure kinetics, oxygen inhibition effect, curing shrinkage and residual stresses. In Section 3.4, the chemical module presents some necessary chemical knowledge relating to the photopolymerization process, however it is not sufficient. One big concern in the profile errors is the edge effects, which probably result from the oxygen inhibition effects. Also the curing shrinkage and residual stresses could also have significant impacts on the cured profiles. The epistemic motivations recommend considerable future work to investigate and quantify these chemical effects.

In terms of measurement, there are mainly two types of measurement needed in the TfMP μ SLA system. One is the measurement of illumination on the substrate, and the other is the measurement of profile. A radiometer and CCD camera are used to measure the irradiance in the optical module, and a microscope is mainly used to measure the profile heights in both the resin characterization in the chemical module and in measuring the cured parts in the physical module. Both illumination measurement and surface metrology are critical to process control in TfMP μ SLA research and curing of parts. Currently, we have some difficulty in measuring the profile thickness as indicated in the pictures of the cured parts in the aforementioned cases. A more advanced 3D surface profiler is needed to improve the measurement capability and precision.

5.3.2 Modeling Loss 2: model simplification

In this research, several simplifications are made to model the TfMP μ SLA process.

1. Optical module

A first-order ray-tracing method is used to model the exposure profile on the substrate. Neither optical aberrations nor diffraction are included in the optical module. It was validated in Limaye (2007) that geometric optics can be used to model the image formation by the MPSLA system. This simplification is acceptable, though errors would originate in the neglected aberrations and diffraction effects. To reduce the errors, a higher order ray-tracing method could be adopted to replace the current first-order one.

2. Chemical module

So far we have assumed that the resin cure behavior doesn't change with irradiation pattern, i.e., bitmap displayed on the DMD. However, with every bitmap

displayed, the exposure pattern is likely to change the curing characteristics of the resin, especially in that different patterns correspond to different topologies which may be impacted by the curing shrinkage, residual stresses and oxygen effects in different degrees. The variations in resin behavior caused by bitmap patterns are called bitmap pattern effects, which can be specifically called bitmap size effects and bitmap shape effects.

Also, it is assumed that the resin doesn't cure in the lateral direction. Thus, we could quantitatively connect the exposure dose with the cured height in vertical direction in the model.

The two assumptions above about resin cure behavior simplify the resin cure model. A TfMP μ SLA resin cure model is formulated in the chemical module (see Section 3.4). Bitmap pattern effects, especially, bitmap size effects were observed in our experiments to have sometimes induced lower cured heights than desired; thereby, compensation is needed to reduce the dimensional errors. Besides, the edge effects in cured profiles suggest that the resin cure model used in the research turns out to be still an oversimplification, even though it has included the cured part effects. A more rigorous analytical model of resin cure behavior, including oxygen diffusion effects should be developed, in the hope that the profile errors could be reduced.

5.3.3 Modeling Loss 3: solution approximation

Due to the computation capability available, sometimes approximated solutions are used in the process planning model. These solution approximations will induce errors in the process. The error sources in the solution approximations are identified as below.

1. Geometrical module

In the geometrical module, we approximate the desired geometric profile of the part with discretized column voxels, whose lateral cross-sections correspond to $10\mu\text{m}\times 10\mu\text{m}$ pixels on the substrate. The geometric profile approximation will induce staircase effects in the cured profile. Smaller pixels, like pixels with size of $1\mu\text{m}\times 1\mu\text{m}$, could reduce the errors greatly. However, it requires a lot of memory to store the irradiance database mapping the exposure amounts from every DMD micromirrors to every substrate pixels. If possible, it is worthwhile to reduce the pixel size so as to reduce the staircase effects and improve the process accuracy.

2. Optical module

Ideally, an infinite number of rays should be used to model the exposure profile perfectly. However it is infeasible due to the computation and storage limitations, hence a finite number of rays are used to approximate the exposure profile. The so-called ray-tracing density effects have been discussed in Section 3.5.5.

3. Mathematical module

In the problem formulations, since z and E are monotonically related, we solve “optimize E ” problem instead of the “optimize z ” problem. The approximation errors are compared in Section 4.5.2. It is concluded that the error induced by this approximation is not so significant.

Further, while solving the “optimize E ” problem (see Problem 6 in Chapter 4), we use a 2-step method to solve the two subproblems. In this solution, we approximate the exposure time for each micromirror with a sum of every bitmap’s exposure time. Hence, an error would come out by this approximation. The so-called effects of the number of bitmaps are discussed in Section 4.5.1. It is shown that usually 25 bitmaps are good

enough in the process. More bitmaps could be generated and used since there is no physical limitation for displaying many bitmaps. Besides, it is found that the first-step method, i.e., the linear least squares algorithm, is responsible for more of the estimation errors than the second-step method. Some inherent errors of the least-squares algorithm are inevitable; hence what we could do is to establish a more advanced mathematical model and solve it with more sophisticated algorithms.

5.3.4 Modeling Loss 4: implementation

While implementing the TfMP μ SLA process, either objective system errors or subjective operational errors are influencing the process accuracy. The following errors lurking in the implementation are introduced.

1. System errors – DMD discretization

The DMD consists of an array of discretized and independent micromirrors. The micromirror array works like a mask to write patterns onto substrates through reflections. For each mirror, on/off reflection is selected based on the pattern information. The proper beams reflected off the selected mirrors are irradiated onto the substrate for patterning. All the micromirror controller does is digitally control the light reflection off the micromirrors. Figure 5.37 shows the irradiance profile on the substrate from one unit micromirror. Note that in our system, the size of each micromirror is $12.6\mu\text{m} \times 12.6\mu\text{m}$, and space between adjacent micromirrors is $1\mu\text{m}$. For such a $13.6\mu\text{m} \times 13.6\mu\text{m}$ center micromirror on the DMD, the size of the irradiation area on the substrate is shown to be $30\mu\text{m} \times 30\mu\text{m}$ in Figure 5.20(a). The influence area of one micromirror could even be larger if the mirror is off the optical axis and at the edges as shown in Figure 5.20(b). Obviously, the smaller a unit micromirror is, the smaller its corresponding irradiation

area is, and the more control we could have in directing the pattern onto the substrate precisely.

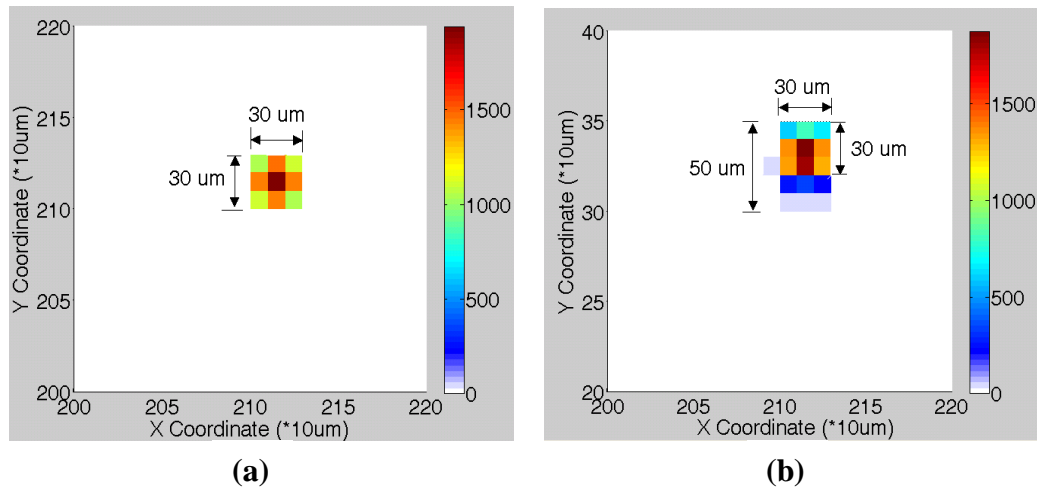


Figure 5.20 (a) Irradiation on the flat substrate from center micromirror; (b) Irradiation on the flat substrate from one edge micromirror

Therefore, the operation of micromirror based TfMP μ SLA has some inherent accuracy limitation due to the DMD discretization resolution, which is a big limiting factor to the micro-sized applications. To address the DMD discretization effects, one may refer to Shih-Hsuan Chiu, et al (2008), which pointed out that if a rescaled micro-sized image generated from DMD is directly used for fabricating the micro-part, the error will be large. In that study, Chiu et al suggested a photomask auto-correction method to remain the original photomask with high resolution. They installed a set of optical lenses for reducing the photomask size and employed the image processing technology for automatic calibration of the photomask size.

It is recommendable to learn from Chiu's group work and modify our TfMP μ SLA with some photomask correction components. Besides, to achieve a sub-pixel resolution, one could also refer to Zhi Chou et al (2008), which presented an optimization based method for mask image planning. For each pixel of the bitmap pattern, instead of simply determining an "ON" or "OFF" state (corresponding to a black or white pixel), they calculated its gray scale value for achieving the best part quality. A commercial DLP or LCD projector supporting at least 256 different gray scale levels was used, rather than a DMD. Actually speaking, the TfMP μ SLA process planning method developed in this thesis could be conveniently adjusted to a TfMP μ SLA system based on DLP or LCD projector with 256 gray scale levels. Firstly, the micromirror on DMD is changed to be a pixel on the projector. Then, based on the current mathematical module, after clustering algorithm is applied, for each cluster, one would assign every pixel gray scale level proportionally with the difference between its actual exposure time and the cluster's smallest exposure time value, instead of assigning all the pixels with "0" (corresponding to "black" pixel). Also, the exposure time for each bitmap is determined by the smallest exposure time value of each cluster, not the average exposure time value anymore (see Equation 4.7 and 4.8). Equation 5.2-5.3 presents how to generate the bitmaps and respective exposure time.

$$B_i^{(j)} = \frac{255}{T_i^u - T_i^l} \cdot (T_j - T_i^l), \forall j, \text{ and } 1 \leq i \leq K$$

where $B_i^{(j)}$ denote the j^{th} -pixel in i^{th} -Bitmap (5.1)

T_i^u, T_i^l denote the upper and lower bound of the i^{th} -cluster, respectively

$$t_i = \begin{cases} T_i^l & i = 1 \\ T_i^l - T_{i-1}^l & 2 \leq i \leq K \end{cases} \quad (5.2)$$

It could be envisioned that by intelligently manipulating pixels' gray scale values in a cluster, the exposure levels can be varied to a higher resolution within a column voxel. This can reduce the estimation errors in the energy exposure profile optimization.

2. Incorrect alignment of the optical components

The beam expander, diffuser, collimating lens, the imaging lens and the DMD are aligned only manually. Hence, some errors might come up if the system is not appropriately aligned.

3. Errors introduced by the post-cure cleaning operations

Every cured part is submerged in resin. Cleaning should be done to remove the excess resin surrounding the cured part. A variation in the time for which the part was dipped in the alcohol bath and variations in manual operations are likely to cause some random errors in the cured part dimensions.

5.4 Chapter summary

In this Chapter, the results of experimental investigation conducted to illuminate the capabilities of the TfMP μ SLA process planning system were reported. Here, the biomaterial hydrogel PEGDA MW 700 was used as the test material, and three different parts were cured. The cured geometric profiles agree with the desired parts shape well, and the errors on the lateral and vertical dimensions of the cured part were estimated to be within 8%. Results for the cured parts showed some significant edge effects, which should be one of the future research concerns. Error analysis is presented to shed light on the TfMP μ SLA process planning error sources and directs future research efforts towards improving the process accuracy.

The case of curing microchannels shows that the TfMP μ SLA process planning system falters at curing sharp vertical walls due to the edge effects and optical setup, hence the current system is not fairly competitive in microchannels fabrication compared with other existing mature technology. However, the cured part looks promising, demonstrating great potentiality. Hopefully by improving the TfMP μ SLA system, the technology could become a candidate in microfluidics fabrication.

The case of curing micro lens array is pretty good, implying that it is feasible in micro lens fabrication. In future, the dimensional errors and profile errors need still to be reduced, and smaller lens are expected to be able to be cured with this system. Also, curing micro lens with other material resins will be tested to extend further the application areas.

By using the process data generated by the TfMP μ SLA process planning method developed in the thesis, the illustrative examples cured parts with desired shapes and acceptable dimensions. It is demonstrated in this Chapter that the energy exposure profile could determine the geometrical profile, validating Hypothesis 1. Also, the exposure profiles achieved by displaying sets of downsizing bitmaps validate Hypothesis 2. The bitmaps whose shapes are consistent with the desired geometric profiles and the exposure times controlling the parts' dimensions rightly, together validate Hypothesis 3.

CHAPTER 6

CLOSURE AND RECOMMENDATIONS

This final chapter of the thesis serves to bring together the understanding and findings presented throughout the entire document. To achieve this, the research questions posed in Chapter 2 are answered by testing the proposed hypotheses in Section 6.1. In addition, the second section outlines specific achievements and contributions of this work. As with any research, however, the limitations of the work conducted must be considered; these are outlined in the third section of this chapter. Thoughts about areas of potential interest and progress are outlined in future work section – the fourth section.

6.1 Answering the research questions (Evaluation of Hypotheses)

A number of research hypotheses were put forth in Chapter 2 with the intention that they would be investigated through the research reported in this thesis. Each of those hypotheses, along with its research question, is now revisited and evaluated in light of the results reported in previous chapters.

The purpose of this research is to develop a process planning method for TfMP μ SLA to obtain dimensionally accurate parts. The core step of curing dimensionally accurate parts is to be able to feed the TfMP μ SLA system accurate process data - a series of accurate bitmaps with accurate exposure durations. The research focus in this work is to obtaining the accurate input processing data for TfMP μ SLA system. The research objective stated in Chapter 1 is restated here:

“To develop a process planning method to generate input process data – a series of bitmaps and respective exposure time for the TfMP μ SLA, so as to cure dimensionally accurate parts.”

This objective is broken down into research questions and hypotheses are proposed for each of them. The validity of the proposed hypotheses is evaluated in this section.

Before coming up with the research questions and hypotheses, we presented in Section 2.4 of Chapter 2 that a process planning method based on column voxels will be developed in the thesis. Thereby, first and foremost, the solution of vertical discretization should be evaluated before testing the research hypotheses.

Evaluating the Column Cure Model: In Section 2.4 and 3.3, the reasons for vertical discretization are explained in terms of the TfMP μ SLA methodology. The geometrical module is established on the basis of column voxels, which will be built by the succeeding process planning modules so as to restore the entire geometric profile. By discretizing the geometric profile vertically into column voxels, the author has developed a new process planning system capable of controlling both the lateral dimensions and vertical thickness simultaneously, without horizontal layers' recoating process anymore. In this TfMP μ SLA process, all columns get cured continuously till the desired heights. The process of curing a part using this system is analytically modeled as the “Column cure model”. It is different from the conventional process - “Layer cure model” [24].

In Chapter 5, a close agreement is observed in the dimensions of the cured parts from the TfMP μ SLA process planning system and the dimensions of the desired geometric profile, to which the fidelity of the geometrical module is valid. Thus, the

vertical discretization has been used successfully to partition the given geometric profile for the TfMP μ SLA system. Thus, the Column Cure Model has been tested and has been found to be valid.

Research Question 1: How to control the thickness of each column voxel on fixed transparent substrate using TfMP μ SLA?

Hypothesis 1: The amount of energy exposure received by each pixel on the substrate can determine the cured height of corresponding column voxel.

Evaluating the hypothesis: In Section 3.4, the chemical module is developed to output the working curve function f_{zE} and the transfer function f_{Ez} , relating the cured heights (z) of column voxels and energy exposure amount (E) on corresponding pixels. Transferring a target geometric profile to a desired energy exposure profile, the energy exposure profile becomes the focus of the TfMP μ SLA parameter estimation formulation. In Chapter 4, the mathematical module is developed to optimize the energy exposure profile. The so-called “optimize E ” method is validated by an exemplificative process plan in Section 4.4 and by physical experiments curing several parts successfully in Chapter 5. Furthermore, the comparison between “optimize E ” and “optimize z ” made in Section 4.5.2 demonstrates that the hypothesis of determining the cured heights in terms of energy exposure dose is valid.

Research Question 2: How to determine the amount of energy exposure received by each pixel on the substrate?

Hypothesis 2: The amount of energy exposure received by a pixel is a summation of linear time accumulation of irradiance provided by each bitmap, which is a subgroup of DMD’s micromirrors turned on, to the pixel.

Evaluating the hypothesis: In Section 3.5, the optical module is developed to output an irradiance matrix H . Each row of H represents the irradiance on a certain pixel from all micromirrors, while each column of H denotes the irradiance onto all pixels by a single micromirror. Let T denote the vector of exposure time of each micromirror, then the product $H \times T$ yields a vector of energy exposure dose received by each pixel on the substrate. The function f_{ET} (refer to Equation 4.1): “ $E = f_{ET}(T) = H \times T$ ” is actually a mathematical description of Hypothesis 2.

The method of estimating the exposure profile using f_{ET} is employed in the mathematical formulation as presented in Chapter 4. By developing the process planning system based on the energy exposure profile optimization using the function f_{ET} for curing dimensionally accurate parts, Hypothesis 2 has been validated.

Hypothesis 2 could be validated simultaneously with Hypothesis 3, since they are mathematically associated. We still would like to provide a separate validation of it by an experimental observation as below.

The primary thing to validate is to show that the irradiance matrix H resulted from the optical module can approach the real irradiance profile on the substrate. To be straightforward, let's use one bitmap to show that the irradiance on one pixel can be determined by a summation of irradiances from all contributing micromirrors. In this scenario, a part of microchannels with 7 grooves is the desired geometric profile. Accordingly, the desired shape of the bitmap is similar to the desired geometric profile due to the geometrical optics principles. A bitmap is generated by our process planning method. When the bitmap is displayed on the DMD as shown in Figure 6.1 (a), we measured the irradiance profile (mW/cm^2) on the substrate by the CCD camera as shown

in Figure 6.1(b). The irradiance profiles of 3 different lines on the substrate are selected for measurement and comparison. The three lines are denoted as Line 1, 2 and 3 in Figure 6.2. Meanwhile, the irradiance provided by the bitmap - a subgroup of micromirrors turned on, is computed by the function f_{ET} : Irradiance = $f_{ET}(T) = H T$, where T is a vector with all values of 1 second to calculate the irradiance value (mW/cm^2) which by definition is energy exposure amount within one second. A comparison of the actual irradiance values measured by CCD camera with the computed values using Hypothesis 2 is shown in Figure 6.2.

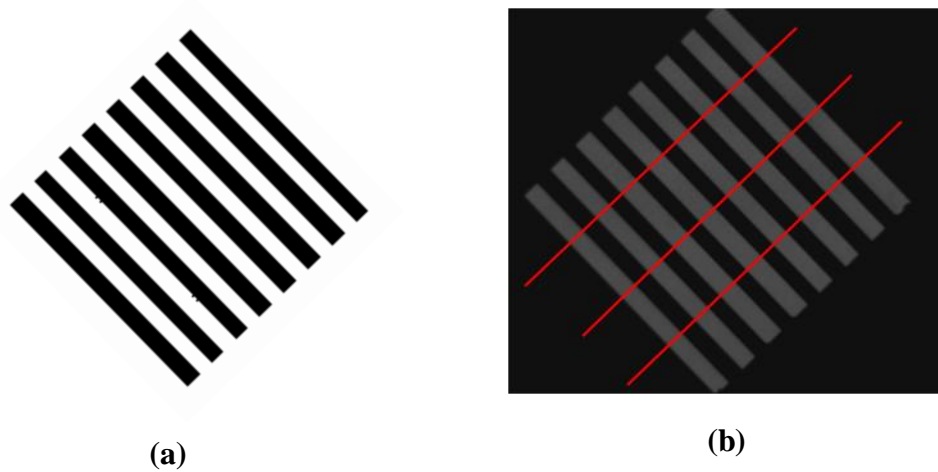


Figure 6.1 Validating Hypothesis 2 (a) bitmap displayed on the DMD (b) irradiance profile on the substrate

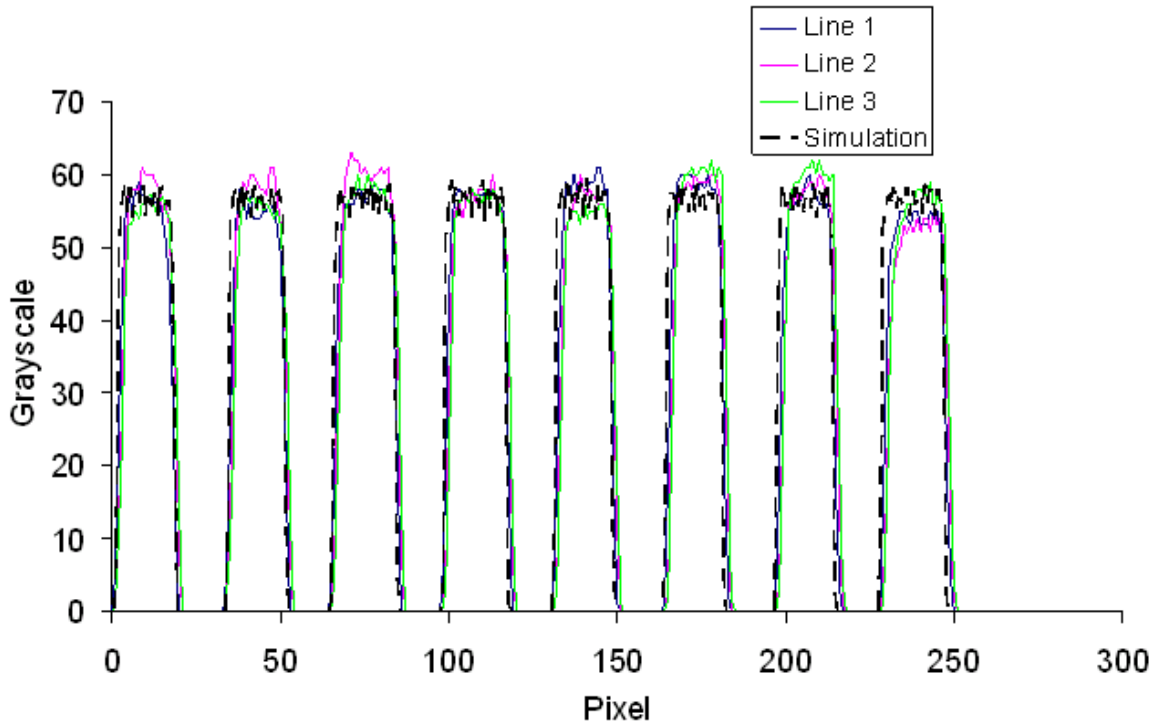


Figure 6.2 Irradiance on pixels consistent with estimated values

It is clear from Figure 6.2 that the irradiance values on each pixel of the 3 arbitrarily selected lines match closely with the simulated values by the function f_{ET} underlying Hypothesis 2. Herein, Hypothesis 2 is validated.

Research Question 3: How to generate bitmaps and corresponding exposure time for each bitmap, given desired energy exposure for each pixel on the substrate?

Hypothesis 3: Parameter estimation can be used to find a set of bitmaps and exposure time for each bitmap, which minimize the deviation between desired energy exposure and actual energy exposure provided by the sequence of bitmaps.

Evaluating the hypothesis: Again, the bitmaps and corresponding exposure time forms the so-called input process data to the TfMP μ SLA system. In Chapter 4, the mathematical module is developed to generate the input process data in two steps:

1. Solve subproblem 6.1

- Use a linear least-squares solver to compute T - the exposure time for each micromirror. Refer to Equation 4.4.

2. Solve subproblem 6.2

- Use the kmeans clustering algorithm to cluster T and group micromirrors into a series of downsizing bitmaps. Refer to Equations 4.2 - 4.3 and Equations 4.10 – 4.11.

Section 4.4 validates the capability of the mathematical module in producing accurate bitmaps and exposure time for curing a spherical surface. Furthermore, by applying the process data on the TfMP μ SLA setup, dimensionally accurate parts are cured in Chapter 5, thereby validating Hypothesis 3.

6.2 Contributions

Process planning literatures available for the conventional laser scanning stereolithography and existing mask projection stereolithography allow a manufacturer to build prototypes by gradually building up layers of solidified photopolymerizable resin. These literatures can't be directly extended to thick film mask projection micro stereolithography (TfMP μ SLA) because the characteristics of this system are considerably different. For example, the parameter estimation formulation of the process planning in the case of TfMP μ SLA is a completely different process from that achieved by laser scanning [35], due to the distinct nature of irradiation of the resin surface and curing characteristics of a resin.

The existing process planning methods for mask projection stereolithography however have limitations in terms of the minimum thickness of the resin layers due to viscosity and surface tension. The TfMP μ SLA process planning system developed in the

thesis does not have such limitations because it does not require the resin to be layered. The UV laser patterns projected on the photopolymer resin substrate forming the lateral (x - y) dimensions while the exposure time for each bitmap controls the thickness (z) of the cured profile. The entire x - y - z stages are not moving at all, thus little possibility exists of the structure collapsing.

The primary contributions of this work are in the realm of analyzing the TfMP μ SLA process and explaining it in mathematical terms. The following are the contributions of the thesis to the field of TfMP μ SLA:

1. It has been shown that the method of discretizing the target geometric profile vertically into column voxels can be satisfactorily used to cure micro stereolithography parts with TfMP μ SLA system. Compared with the horizontal layer cross-section STL files, this unconventional partition method indicates an alternative process planning method for stereolithography. It could even be embedded into the conventional layer additive manufacturing process. As envisioned in Section 3.3.3, a hybrid process planning method, utilizing the TfMP μ SLA process planning method to cure each layer as well as following the conventional recoating method by moving Z-stage, could be used to cure more accurate and complex parts with MP μ SLA.
2. The TfMP μ SLA's resin cure model provided a closed-form solution to the layer-curing model [1] as a transient process, which was previously solved numerically and limited for those resins for which the rate of radiation attenuation through cured resin is negligible compared to that through uncured resin. This model eliminates the limitation in Limaye's model [1] and furthermore enables a more

accurate resin cure model than the conventional exposure threshold model simply based on the Beer Lambert law.

3. The effect of the ray-tracing density on the process planning system has been investigated. This investigation can be extended to other mask projection stereolithography process planning system using a ray-tracing method to obtain the irradiation profile.
4. An exposure profile model has been presented, which can take into account all exposure amounts contributed by multiple micromirrors to compute the total exposure received by any single pixel on the substrate.
5. A new mathematical model of parameter estimation in the TfMP μ SLA process planning system is formulated.
6. Meanwhile, a new method for bitmap generation is developed. The mathematical module enables the user of a TfMP μ SLA system assign the number of bitmaps and will automatically generate a series of bitmaps as required. The application of the clustering algorithm automates the process planning in great part.
7. The effects of the number of bitmaps used in the TfMP μ SLA process planning system has been quantified and will enable the manufacture to cure more accurate parts.
8. Besides the “optimize E ” method adopted in the process planning system in the thesis, an alternative method “optimize z ” is also investigated, in hope of shedding light on the potential of improving the process planning system by testing some other models and algorithms.

6.3 Scope and limitations of this research

This thesis is mainly focused on the development and implementation of the process planning method for the TfMP μ SLA. Some of the developed process planning method, such as the resin working curve incorporating cured part effect and the algorithms for generating bitmaps and exposure times for each bitmap can also be extended for process plan in other MP μ SLA, like MP μ SLA on a curved substrate. Furthermore, all these can be even reduced to cure each single layer in conventional MP μ SLA with movable Z-stage, by regarding each single layer as the intended topology in our TfMP μ SLA.

In case of very sophisticated topology, say topology with holes, shells or dents, the process planning method cannot cure it due to the vertical discretizing approach in the geometrical module. In this case, some column voxels are not solid, for instance some have some slits or cracks. However, the process planning method intends to cure every column voxel from bottom up, hence no gap or broken points can be achieved within the voxel. So, the scope of this work is limited strictly to cure geometrical parts which can be discretized into solid vertical columns with no dent or hole.

Furthermore, some limitations with the process planning method are discussed as below.

1. The Geometrical Module

The build orientation is an important issue in rapid manufacturing. It is however beyond the scope of the present thesis. It is assumed that the build orientation has been determined and transformed as the Z direction before using the discretizing procedure.

Shrinkage and laser beam compensation are some other issues that must be properly addressed for the manufacturing processes.

To use the process planning method on the TfMP μ SLA, the targeted topology is required to be able to be oriented in the way that the bottom is flat and then the topology could be discretized into solid vertical columns. Thereby the process planning method itself is not omnipotent in terms of geometrical limitations. To some extent, the process planning method could be modified to cure complex geometrical profiles without flat bottom. In that case, the substrate is not necessarily flat and can be changed to fit the bottom shape of the intended part. Accordingly, the optical module should have its ray-tracing part modified to incorporate the new optical path, thus an updated irradiance database will be available for curing the specific part.

2. The Chemical Module

A limitation in the chemical module is that it doesn't actually incorporate the oxygen diffusion effect into the working curve. As a result, the discrepancy observed in the working curve plotted using the TfMP μ SLA system cannot be explained as regards to the oxygen diffusions that occur in the resin. In order to compensate for that, it is required in the mathematical module that the generated sequence of bitmaps should be downsizing so as to ensure a continuous non-stop curing of each column voxel. Thus, there is only negligible waiting time between each two consecutive bitmaps and the diffusion effect is reduced. Even with this negligible waiting time, the oxygen diffusion effect remains significant and destructive in the edges of the cured parts. Further research on this area is desired.

3. The Optical Module

The optical module assumes that the laser beam irradiation on the DMD is uniform, thus that a uniform meshing of the DMD micromirrors can be employed in ray tracing and also each ray can be assigned the same power value. This assumption absolutely requires that the exposure profile on the DMD be uniform in the physical setup. In our TfMP μ SLA, the beam expander and rotating diffuser are added, and the optical system is adjusted to ascertain that an acceptably uniform exposure profile is achieved.

A limitation in the optical module is that it doesn't work as desired if the laser irradiation on the DMD is uneven. If the irradiation profile cannot be even, one possible solution is impose some weights on micromirrors to make the modeled optical performance as close to the reality as possible. For strongly irradiated area, meshing of the corresponding micromirrors could be denser, and vice versa. Totally speaking, the optical module developed in the thesis is for evenly-distributed exposure, which is also the most common case. Even so, it can be modified to work for those cases where laser beam irradiation is not uniform.

Another limitation in the optical module is the ray-tracing density. We just compared two densities: one is the sparse ray-tracing with $n = 9$ and $m = 121$; the other is ray-tracing with $n = 81$ and $m = 225$. A minor difference was observed in the comparison, but what if n and m are increased further to some much larger numbers? Will there be still only a minor difference? Perhaps a significant difference will be observed if we have a large enough density in ray-tracing. If the computation environment permits, it could be worthwhile to increase the ray-tracing density further to investigate the effects.

4. Mathematical module

In developing the mathematical module, first and foremost, building a good mathematical model (i.e, appropriate formulation) of the problem is highly critical, because the mathematical model inherently determines the computation complexity and accuracy. Proper objective(s) and sufficient constraints account for a robust model. Sometimes, even stating the same constraints in a different way could change the algorithms needed significantly (refer to Section 5.1.4.3). The mathematical module developed in this thesis sets up a two-stage model consisting of one linear least-squares model with bounded constraints (refer to Sub Problem 6.1) and one clustering model (refer to Sub Problem 6.2), and solves it with “lsqin” solver in MATLAB and “kmeans” algorithm. Although it has been validated to be able to output a feasible process plan, the undercured edge pixels (so-called “edge effects”) and rough surface still indicate that some improvement of the mathematical module is desired to eliminate edge effects and enable achievement of a range of surface finish and accuracy requirements.

First, let’s discuss about the energy exposure optimization problem (Subproblem 6.1) at the first stage of the mathematical module. It was modeled as a linear least squares problem with bound constraints. Unfortunately, such formulation is usually impossible to yield a smooth profile. There will be always some pixels in the target edges that have to be underdosed and some pixels in the critical features that have to be overdosed. No special treatments on the target edges and/or critical features pixels are incorporated either in the objective function or in the constraints. Therefore, the linear least squares algorithm in Subproblem 6.1 treats all pixels equally, inducing unavoidably lower exposure dose than desired here and higher exposure dose than desired there, resulting in jagged edges in cured geometric profile. Especially for some of the edge pixels, the

inadequate exposure dose they received was usually even lower than the critical exposure E_c ; consequently they didn't get cured, bringing about the edge deficiency effects.

To address this issue, a suitable objective function can be added to the formulation. In particular, for each edge, a penalty function can be specified related to the exposure dose received by the pixels in that edge. The penalty function assigns a value to the exposure dose received by each pixel in the corresponding edge. Typical penalty functions may have a value proportional to the exposure dose received by all edge pixels. A more sophisticated objective function could be obtained when the penalty is equal to the absolute deviation of the exposure dose received from a desired exposure dose. Since higher doses in edges are always preferred to lower doses, for pixels in these edges the penalty function is generally one-sided, i.e., only deficits under the desired exposure dose are penalized in the objective function. Since large deviations from the desired exposure dose are considered to be much more important than small deviations, a much more frequently used alternative is to use a weighted least squares objective function, aiming to penalize jags and edge effects simultaneously.

In our current mathematical module, the main error source is the first-stage problem, i.e, the energy exposure optimization problem (refer to Subproblem 6.1). Hopefully the improved energy exposure optimization problem incorporating edge effects and profile jags would reduce the errors significantly.

As to the clustering algorithm, although it can be proved that the procedure will always terminate with a feasible solution, the K -means algorithm does not necessarily find the optimal configuration, corresponding to the global objective function minimum. The algorithm is also significantly sensitive to the initial randomly selected cluster

centers. The *K*-means algorithm can be run multiple times to reduce this effect. If necessary, some other powerful clustering algorithms may be exploited, such as Fuzzy *c*-means clustering and QT clustering algorithms.

6.4 Future work

The following directions for future work have been identified, from the view of bolstering confidence in the modules and process planning methods presented in this thesis.

1. Geometrical Module

The geometrical module used uniform column discretization to partition the geometrical part profile. If the column size is computed based on the local geometry, the staircase effect can then be controlled to a user-specified tolerance level. An adaptive column discretization could be better for complex 3D profiles.

There have been lots of efforts on improving the slicing algorithms to obtain accurate and smooth part surface. Various adaptive algorithms have been developed to identify features, contours and layer thickness for layer additive manufacturing methods. Sophisticated algorithms to discretize geometrical profiles into column voxels were however not a concern in this thesis because the research issue was only to make a choice between horizontal discretization and vertical discretization, so as to enable a feasible systematic process planning for the TfMP μ SLA under consideration. Apparently advanced algorithms are necessary to obtain accurate geometrical profiles, we could borrow the existing research achievements on slicing algorithms and modify them into required “columning” algorithms.

As a future work, volume decomposition and adaptive column capabilities can be added in order to partition part geometry into small, independent columns based on the local geometry and pre-specified required smoothness requirement, to enable accurate, 3D process planning.

Moreover, some automated software to discretize computer aided design (CAD) models into columns may be developed for the TfMP μ SLA. This is somewhat an analogue to softwares that generate STL files for layer-based additive manufacturing. Then it would be more convenient for the user to generate desired voxels' heights and input the geometric data into the TfMP μ SLA process planning system built on MATLAB platform.

2. The Chemical Module

MP μ SLA curing process is a coupled mass and energy balance problem, involving chemical reaction, heat transfer and mass transfer. In this thesis, we assume that the empirical working curve from resin characterization embodies how the chemical reaction, the resin cure kinetic characteristics, oxygen inhibition effect and shrinkage effect as well as the diffusion and thermal effects influencing the size, shape and properties of parts fabricated by TfMP μ SLA. However, the chemical module may still be somewhat an oversimplification of the resin cure process.

The working curve based on the exposure threshold model can get improved by including resin cure kinetics and the oxygen inhibition effect. Dr.Tang [52] put forward a DOC (Degree of Curing) threshold model, which was proved more accurate than the exposure threshold model. It may shed some light on the TfMP μ SLA resin curing model.

Also, cooperation with the chemical engineering group would be helpful to address this problem.

3. The Optical Module

The ray-tracing method used in the optical module could be improved by adopting a better discretization method, increasing the meshing density as well as imposing some intensity distribution weights on the DMD micromirrors. Hence, the simulated irradiance profile on the substrate would agree better with that in physical reality.

Improvements could also result from using higher order ray tracing, instead of simple first-order ray tracing.

4. The Mathematical Module

The problem of formulating the TfMP μ SLA process plan resembles to a large extent a problem of designing a treatment plan for irradiation modulated radiation therapy (IMRT). In particular, the problem of designing an optimal radiation density profile in the patient, which is often referred to as the fluence map optimization problem, can be an excellent analogue to the energy exposure profile optimization problem (Optimize E) in Chapter 4.

In IMRT treatment plan, the goal of the fluence map optimization problem is to design a radiation treatment plan that delivers a specific level of radiation, a so-called prescription dose, to the targets, while on the other hand sparing critical structures by ensuring that the level of radiation received by these structures does not exceed some structure-specific tolerance dose. The dose calculation function [61] as described in Figure 6.3 is pretty similar to the energy exposure calculation Equation 4.1.

Finally, let P_{ij} denote the dose received by voxel j from beamlet i at unit intensity. We can then express the radiation received by each voxel as a linear function of the radiation intensities x as follows:

$$D_j(x) = \sum_{i \in N} P_{ij} x_i \quad j \in V.$$

Figure 6.3 the dose calculation function [61]

The so-called “beamlet”, a discretized part of the beam, could be regarded as an analogue of micromirror. In a typical application of IMRT treatment plan [61], 1,232 beamlets were generated to adequately cover the target structures, which were discretized into a voxel grid with 126,000 voxels. This generated approximately 96,000 nonzero P_{ij} 's in a sparse matrix of size 1,232 by 126,000. From the numbers in the application example, we could see the TfMP μ SLA and IMRT optimization problems are also comparable in terms of large scale and computation complexity.

Herein, one recommendation for future work is to explore the existing research accomplishments in IMRT influence map optimization, and to learn from them. Numerous literatures (like Romeijn et al, 2006 and Gino J. Lim, et al, 2008) dedicated to formulating and solving such IMRT fluence map optimization problems have been found in both medical physics and operations research areas. It is worthwhile to do the literature study, which may help us establish a more sophisticated process plan model and develop some more computationally efficient algorithms so as to improve the dimension accuracy and surface finish of curing in TfMP μ SLA system.

5. The Physical Module

Firstly, further validation of computed process plans will be performed using larger and more complex parts.

Secondly, we can think of an adaptive multiple-exposure stereolithography scheme that monitors and corrects the fabricated structures iteratively in real time within the field of view of the TfMP μ SLA system. In Figure 6.4, the input of the system is the target topology, and the output is given by the measured structure after fabrication. The transfer function depends on the illumination by the DMD on the substrate, the response of the photopolymer resin, further steps like proportional transfer by rinse and drying, and other variables in the TfMP μ SLA system. After a first fabrication and characterization step, the input data (bitmaps and exposure times) can be varied to get closer to the desired topology. This approach is based on the assumption that the complete process sequence is repeatable.

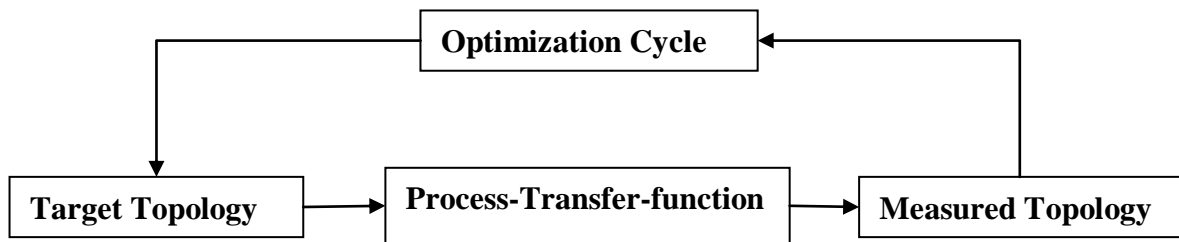


Figure 6.4 Optimization cycle for improving the fabricated topology

APPENDIX A

CODE FOR RESIN WORKING CURVE

In this section, the MATLAB code used to execute curve fitting in the chemical module described in Section 3.4.3 of Chapter 3 is presented. Note that it is example code for Vantico Huntsman SL-5510 resin. The experimental data is subject to change with the specific resin used.

(1) MATLAB code for the TfMP μ SLA Resin Cure Model

(MyFunction_WorkingCurve.m)

```
%% TfMPSLA resin cure model, also the Working curve function:
% Developed by Xiayun on July 26,2008

%% Cured Height (Cd) Vs. Ec, Dps(cured solid part's Dp), Dpl(liquid
resin's Dp)
% Dp means "Depth penetration"

%%x(1) = Ec, x(2) = Dps, x(3) = Dpl
function Cd = MyFunction_WorkingCurve(x, E_data)
Cd = x(2)*log(x(3)*E_data/x(2)/x(1) + 1 - x(3)/x(2));
```

(2) MATLAB code for working curve fitting

(WorkingCurve_Fitting_MyFunction_0.m)

```
%% objectives of the code
... 1. fitting experiment data from resin characterization...
... into the analytical resin cure model in TfMPuSLA,
... so as to determine unknown parameters in fzE(E)
... (i.e, MyFunction_WorkingCurve.m)
... 2. inverse the working curve function fzE(E)...
... to obtain the transfer function fEz(z)
%% run on Jan 16,2009

clc;
clear all;
format long;

%% Experimental Data (subject to actual experimental data)
% Here is the example experiment data (July27,2008)
% H:laser power used in resin characterization: mw/cm^2
```

```

H = 0.2064;

% time: time (seconds)
time = [170
160
150
140
130
120
110
100
95
85
]';

% Edata: exposure
E_data = H*time;

% observed data of cured height: Cd (um)
Cd_data = [611.4583333
581.6666667
482.4166667
443.53
401.8055556
348.5555556
299.8055556
241.4444444
199.9722222
154.2833333
]';

%% Curve Fitting
%%x(1) = Ec, x(2) = Dps, x(3) = Dpl
% Starting guess (initial value)
% x0 = [1;1;1]
% x0 = [12.7;2150;400]
% x0 = [12;4000;350]
% x0 = [12;6350;330]
% x0 = [12;1e4;320]
% x0 = [12;1e5;320]
% x0 = [12;1e6;320]
% x0 = [12;1e7;320]
x0 = [12;1e8;320]
% x0 = [12;1e9;320]
% x0 = [12;1e10;320]
% x0 = [12;1e11;320]

%defines a set of lower and upper bounds on the design variables in x
so
% that the solution is always in the range lb<=x<=ub
lb = [0;0;0] % lowerbound
% ub = [13;1e3;1e3]
ub = []

```

```

%curve fitting
[x,resnorm,residual,exitflag,output] =
lsqcurvefit(@MyFunction_WorkingCurve,x0,E_data,Cd_data,lb,ub),
Ec = x(1);
Dps = x(2);
Dpl = x(3);
Cd_fitted = MyFunction_WorkingCurve(x,E_data);

%% Plot working curve fzE(E):E->z
% note: residual = observed data - fitted data
figure
% plot(E_data,Cd_data,'k+',E_data,Cd_fitted,'-ro',E_data,residual,'-
.b',...
% E_data,zeros(length(E_data)),'k-')
plot(E_data,Cd_data,'ks','MarkerEdgeColor','k','MarkerFaceColor','g',
'MarkerSize',3)
hold on
plot (E_data,Cd_fitted,'-r')

% h = legend('Experimental Data Points','Fitted Working
Curve',strcat('Residuals (resnorm = ',num2str(resnorm),')'),'zero-
thickness line',4);
h = legend('Experimental Data Points','Fitted Working Curve')
set(h,'Interpreter','none')

txt_title=char('Resin Characterization - Fitted Working
Curve:',strcat('z =
',num2str(x(2)), '*ln(',num2str(x(3)/x(2)/x(1)), '*E+',num2str(1-
x(3)/x(2)), ')'),...
strcat('Ec = ',num2str(x(1)), ' mJ/cm^2 Dps = ',num2str(x(2)), '
um Dpl = ',num2str(x(3)), ' um'));
title(txt_title)

xlabel('Exposure: E (mJ/cm^2)'), ylabel('Cured Height: z (um)')
hold off

%% inverse MyFunction_WorkingCurve fzE(E): E -> z
% to obtain the transfer function fEz(z):z -> E
syms z z_sym
digits(15)
% E_sym and EE are the same expression acutally...
... E_sym is used for displaying title in the figure...
... EE is saved and to be loaded in the function: func_Ez.m
E_sym = vpa(finverse(MyFunction_WorkingCurve(x,z)));
EE = vpa(finverse(MyFunction_WorkingCurve(x,z_sym)));
save ('TransferFunction-fun_Ez.mat','EE','Ec','Dps','Dpl');

figure
plot(Cd_fitted,E_data, '-r')
E_string=char(E_sym);
title({'Transfer function: target cure height z -> required exposure
E';'';...
['f_E_z ',': E = ',E_string]})

xlabel('Cured Height: z (um)'), ylabel('Exposure: E (mJ/cm^2)')

```


(3) MATLAB code to implement the transfer function $f_{Ez}(z)$ to get the required

exposure profile (func_Ez.m)

```
function E = func_Ez(z)
% (updated on Jan 16, 2009)

%load the transfer function: E=f(z) obtained from the chemical module
%Note: EE, Ec, Dps, Dpl are included in the MAT-file
load ('TransferFunction-func_Ez.mat');
% E = subs(EE, z);
%% copy the parameter "EE" in 'TransferFunction-func_Ez.mat'...
...and change the symbol "z_sym" into z(i) as below

length_z = length(z);
E = zeros (length_z, 1);
for i = 1 : length_z
    if z(i) > 0
        E(i) = 3828116.41992384*exp(.100004397485814e-7*z(i)) -
3828104.82691021;
    end
end
clear i;
```

APPENDIX B

CODE FOR THE OPTICAL MODULE

In this section, the MATLAB code used in the optical module in Section 3.5 of Chapter 3 is presented.

(1) MATLAB code to calculate the irradiance carried by a single ray

In the code, the number of rays on $160*160\mu\text{m}$ area are counted and extrapolated onto 1 cm^2 .

```
clear all
load 'otherdatabase\DMD6_3_150allon.mat'

nresin = 421;

coarse=16;
mod1=mod(210,coarse);

nresin=2*(int16(210/coarse));

irradiance_body_coarse=zeros(nresin,nresin);

for i=1:1:nresin
    for j=1:1:nresin
        for ii=1:1:coarse
            for jj=1:1:coarse

irradiance_body_coarse(i,j)=irradiance_body_coarse(i,j)+irradiance_body
(coarse*(i-1)+ii+mod1,coarse*(j-1)+jj+mod1);
            end
        end
    end
end

save
(strcat('otherdatabase\DMD6_3_150allon_coarse',int2str(coarse),'.mat'),
'irradiance_body_coarse');

irr=0.05*6*0.8; %mW/cm2
pix_ray=max(max(irradiance_body_coarse)) %number of rays per coarse
pixel
```

```

numpix_cm=10*10/(coarse*0.01)^2; %number of pixels per cm2
irr_ray=irr/(pix_ray*numpix_cm)

```

(2) MATLAB code to create the irradiance matrix H . (Create_IrradianceMatrix.m)

Note:

1. The variables “nPixel” and “nMirror” are equal to those in the initial meshing while doing ray-tracing.

2. The irradiance matrix is still in the unit of ray. The matrix will be multiplied by the single ray power in the mathematical module to be a real “irradiance” matrix.

```

%%Objective: to get irradiance matrix [Pixel on Resin, Micromirror],
save
%%it as IrradianceMatrix.mat file
%%updated on Jan 9,2009

clc;
clear;

%mesh resin substrate into nResin-by-nResin pixels
nPixel = 421;
%mesh DMD's effective region into nMirror-by-nMirror micromirrors
nMirror = 151;

% %%compute irradiance matrix:
IrradianceMatrix[Pixel_Index,Micromirror_Index]
for i = 1:1:nMirror
    i
    for j = 1:1:nMirror

        %conver micromirror matrix (i,j) to array with index:
Mirror_Ind
        Mirror_Ind = (i-1)*nMirror + j;

        %load the database corresponding to micromirror(i,j)
load(strcat('database\database', (int2str(i)), '.',
(int2str(j)), '.mat'));
for m = 1:nPixel
    for n = 1:nPixel

```

```
                                %conver resin's pixel matrix (m,n) to array with
index: Pixel_Ind
                                Pixel_Ind = (m-1)*nPixel + n;
                                IrradianceMatrix(Pixel_Ind, Mirror_Ind) =
sparse(database(m,n));
                                end
                                end

                                clear database;

                                end
end

save('IrradianceMatrix.mat','IrradianceMatrix')
```

APPENDIX C

CODE FOR THE MATHEMATICAL MODULE

In this appendix, the MATLAB codes developed in the mathematical module are presented. This appendix is referred in Chapter 4.

1. run_all.m

Description: Top-level code to run the mathematical module, including the geometrical module and optical module. Note that the chemical module is not integrated into it, but it should run before this code to provide some necessary input, like func_zE.m and func_Ez.m.

Note: the top-level parameters are subject to change according to the application.

```
%% Call run_all.m to run the program
... Large Scale Optimization for Mask Projection MicroStereolithography
... updated on Jan 9, 2009
% All we need to change is the parameters "expt" and "numCluster"

clc;
clear all;
close all;

%% top-level parameters
%title of the resluted file folder: result\ "expt"
expt = 'sphere';

result_folder = strcat('result/', expt);
global result_folder;
mkdir(result_folder);

%number of pixels, micromirrors in x and y directions...
... involved in the algorithms
... 1 pixel = 10um
nPixelx = 300;
nPixely = 300;
nMirrorx = 151;
nMirrory = 151;

%power of a single ray (mw), obtained from the optical module
Power_Ray = 8.0275e-011;
```

```

%number of bitmaps to be generated for the process planning
numCluster = 25;

%% creat geometrical profile: obtain discretized voxel hights
%call the function to creat geometry
z_xy = createSphere([1:nPixelx]', [1:nPixely]');
z = z_xy(:);
save('VoxelData.mat', 'z');

figure;
% meshz(z_xy/10);
% axis([0,nPixelx,0,nPixely,0,max(z)]);
surf(z/10,'EdgeColor','none','Marker','none');
colorbar('location','eastoutside');
axis equal
xlabel('x direction (10 um)'),ylabel('y direction (10
um)'),zlabel('desired curing height: z(10 um)'),
% title(['target geometrical profile - sample ',expt];''(1pixel =
10um)');
title('target geometrical profile - sample ');
saveas(gcf, sprintf('%s/Desired_Geometry.fig', result_folder));

%% run the mathematical module, including optimization and clustering
begin_time = cputime;
run_optimization(expt, nPixelx, nPixely, nMirrorx, nMirrory, Power_Ray);
run_clustering(expt, numCluster);
elapsed_time = cputime - begin_time;

```

2. run_optimization.m

Description:

- 1) Called by “run_all.m”.
- 2) First-step problem solver. Call the function “solveOPT.m”.

```

function run_optimization(expt, nPixelx, nPixely, nMirrorx, nMirrory,
Power_Ray)
%%updated on Jan 18,2009...
%Plot z
...objective: compute exposure time for each micromirror
    ...to minimize the deviation between the required energy profile
and the actual
% meaning of parameters:
... expt: name of the result folder to save resultant files
... nPixelx: number of pixels in x direction
... nPixely: number of pixels in y direction
... nMirrorx: number of mirrors in x direction
... nMirrory: number of mirrors in y direction
... Power_Ray: power of a single ray (mw)

```

```

%% folder for resulted files: result/**
if(~exist('expt'))
    clc;
    clear all;
    close all;
    expt = 'Geometry';
    result_folder = strcat('result/', expt);
    global result_folder;
    mkdir(result_folder);
end

result_folder = strcat('result/', expt);

%% Get Hij for this given profile
%load the overall irradiance matrix first
load('IrradianceMatrix.mat');

%mesh resin into nPixelMax-by-nPixelMax pixels
nPixelMax = 421;
nPixelAll = nPixelMax^2;
%mesh DMD into nMirrorMax-by-nMirrorMax micromirrors
nMirrorMax = 151;
nMirrorAll = nMirrorMax^2;

%% Given geometrical profile to cure: Px,Py corresponds to pixel ranges
in
%%x, y direction,respectively
nPixel = nPixelx * nPixely;

iPixelMid = ceil(nPixelMax/2);
Px = [ceil(iPixelMid - nPixelx/2) : ceil(iPixelMid - nPixelx/2) +
nPixelx - 1]';
Py = [ceil(iPixelMid - nPixely/2) : ceil(iPixelMid - nPixely/2) +
nPixely - 1]';

%% Map given profile to potential subgroup of micromirrors: Mx, My
%%corresponds to micromirrors array in x,y direction,respectively
nMirror = nMirrorx * nMirrory;

iMirrorMid = ceil(nMirrorMax/2);
Mx = [ceil(iMirrorMid - nMirrorx/2) : ceil(iMirrorMid - nMirrorx/2) +
nMirrorx - 1]';
My = [ceil(iMirrorMid - nMirrorory/2) : ceil(iMirrorMid - nMirrorory/2) +
nMirrorory - 1]';

%% Extract rows of total H (i.e, pixels for particular profile)
indPixel = reshape([1:nPixelAll]', nPixelMax, nPixelMax)';
Hi_Ind = indPixel(Py, Px);

%% Extract columns of total H (i.e, micromirrors needed for particular
profile)
indMirror = reshape([1:nMirrorAll]', nMirrorMax, nMirrorMax)';
Hj_Ind = indMirror(My, Mx);

%% Extract matrix from total H

```

```

% %power of a single ray (mw)
%irradiance: mw/cm2
H = IrradianceMatrix(Hi_Ind(:),Hj_Ind(:))*Power_Ray*1e6;
H = reshape(H, nPixel, nMirror);

%% Get Ei: converted geometry profile Zi to Ei using working curve
%'VoxelData.mat' contains all discretized voxels' height
load('VoxelData.mat');
E = func_Ez(z);

%% -----
%%-----Regression-----
%%-----

%%% Solve
[T] = solveOpt(H, E, zeros(nMirror,1),Inf*ones(nMirror,1));

%% Save

save(sprintf('%s/E.txt', result_folder), 'E', '-ASCII');
save(sprintf('%s/Time.txt', result_folder), 'T', '-ASCII');

save(sprintf('%s/data.mat', result_folder), 'H', 'z', 'E', 'T',
'nPixelx', 'nPixely', 'nMirrorx', 'nMirrory', 'Px', 'Py', 'Mx', 'My', ...
'nMirrorMax', 'nPixelMax');

%% -----
%%-----
%%% figures
%%-----

figure;
z0 = reshape(z, nPixely, nPixelx);
surf(z0/10, 'EdgeColor', 'none', 'Marker', 'none');
colorbar('location', 'eastoutside');
xlabel('pixels on resin - x direction'), ylabel('pixels on resin - y
direction'), zlabel('desired voxels hights (um)'), title('Desired
geometrical profile')
saveas(gcf, sprintf('%s/Geometry_Desired.fig', result_folder));

figure
M = func_zE(H * T);
M = reshape(M/10, nPixely, nPixelx);
surf(M, 'EdgeColor', 'none', 'Marker', 'none');
colorbar('location', 'eastoutside');
xlabel('pixels on resin - x direction'), ylabel('pixels on resin - y
direction'), zlabel('cured height (um)'), title('Optimization result for
geometrical profile')
saveas(gcf, sprintf('%s/Geometry_Optimized.fig', result_folder));

figure
surf((M - z0), 'EdgeColor', 'none', 'Marker', 'none');

```



```

colorbar('location','eastoutside');
xlabel('pixels on resin - x direction'),ylabel('pixels on resin - y
direction'),zlabel('difference between desired voxels heights and
optimization result'),title('residual in optimaztion (um)')
saveas(gcf, sprintf('%s/relative_residual_in_Optimization.fig',
result_folder));

figure
surf( abs(M - z0)./abs(z0), 'EdgeColor', 'none', 'Marker', 'none');
colorbar('location','eastoutside');
xlabel('pixels on resin - x direction'),ylabel('pixels on resin - y
direction'),zlabel('relative error rate after
optimization'),title('relative residual in optimaztion')
saveas(gcf, sprintf('%s/relative_residual_in_Optimization.fig',
result_folder));

```

3. run_all.m

Description: Called by “run_optimization.m”.

```

function x = solveOpt(A, B, low, up)
% Solve min ||Ax - B||, low <= x <= up
% A: irradiance matrix (H)
% B: required energy (E)
% x: exposure time for each micromirror
%(updated on Jan 17,2009)

global result_folder;

tol = 1e-10;
maxit = 5000;

% Solve via lsqlin in Matlab
display('lsqlin');
options = optimset('LargeScale', 'on', 'MaxIter', maxit, 'TolFun',
tol);
[x] = lsqlin(A,B,[],[],[],[],low, up, [],options);

```

4. run_clustering.m

Description:

- 1) Called by “run_all.m”.
- 2) Second-step problem solver. Call the function “kmeans.m”.

```

function run_clustering(expt, numCluster)
%%updated on Jan 18,2009
% Plot z

```

```

... objective: cluster micromirrors with similar exposure time into
bitmaps
%%"expt" is partial title of the result folder
... "numCluster" is equal to the number of bitmaps

%% 2-D BITMAP_GENERATOR File created by Yanjun Zhao on Nov.8, 2008
if(~exist('expt'))
    clc;
    clear all;
    close all;
    expt = 'Geometry';
end
begin_time = cputime;
%% -----given parameters: Tj (Exposure time of each
micromirror)
% load 'H', 'z', 'E', 'T', 'Px', 'Py', 'Mx', 'My', 'nMirrorMax'
data_folder = strcat('result/', expt);
load(sprintf('%s/data.mat',data_folder));
bmp_folder = strcat(data_folder, '/bmp');
mkdir(bmp_folder);

nMirror = nMirrorMax;

nMirrorx = length(Mx);
nMirrory = length(My);
nPixelx = length(Px);
nPixely = length(Py);

E_real = zeros(size(E));
z_real = zeros(size(z));
%% -----
--
% -----Clustering T (TOE_Bitmaps is displaying time of
bitmaps)--
%%call the function "kmeans" to cluster micromirrors
%let j=idx_Tj(i) means T'(i) belongs to the jth cluster
[idx_Tj, mu_Tj] = kmeans(T', numCluster);

Tj_new = mu_Tj(idx_Tj)';
Tj_new = reshape(Tj_new, nMirrorx, nMirrory);

%%sort average time of each cluster in ascendent order
%T_Cluster_mu: average exposure time for each cluster of micromirrors,
%i.e, T_Cluster_mu: exposure time of each bitmap
%note: um_Tj(idx_mu) is ascending
[T_Cluster_mu, idx_mu] = sort(mu_Tj, 'ascend');
%Time of Exposure of bitmaps
Time_Bitmaps = diff([0, T_Cluster_mu]);%exposure time for each bitmap
%% -----
--
% ----- Grouping Bitmaps -----
----
% Group of micromirrors on DMD corresponding to each cluster:
Cluster_On_Off

```

```

figure;
for i = 1 : numCluster
    diffu = Time_Bitmap(i);

    %initialize Micromirror_On_Off matrix: all mirrors off("1"->"off")
    mirror = ones(nMirrory, nMirrorx);
    ind = (Tj_new - diffu > -1e-8);
    mirror(ind) = 0;
    Tj_new = Tj_new - diffu;

    E_real(:) = E_real(:) + H * diffu * ind(:);
    z_real(:) = func_zE(E_real(:));
    meshz(reshape(z_real, nPixely, nPixelx));
    axis([0,nPixelx,0,nPixely,0,max(z)*1.1]);
    xlabel('pixels on resin - x direction');ylabel('pixels on resin - y
direction');zlabel('cured heights (um)');
    M(i) = getframe(gcf);

    mirror_all = ones(nMirror,nMirror);
    mirror_all(My, Mx) = mirror;

    %%Save bitmaps and corresponding exposure time data
    mirror_all_set{i} = mirror_all;
    imwrite(mirror_all, sprintf('%s/Bitmap_%03d%.1fs.bmp', bmp_folder,
i, Time_Bitmap(i)), 'bmp');
end
clusterTime = cputime - begin_time;

% movie(M);
movie2avi(M, sprintf('%s/movie.avi', data_folder));

% save figure
surf(reshape(z_real/10, nPixely,
nPixelx), 'EdgeColor', 'none', 'Marker', 'none');
colorbar('location', 'eastoutside');
% mesh(reshape(z_real/10, nPixely, nPixelx));
axis equal
xlabel('x direction (10 um)'),ylabel('y direction (10
um)'),zlabel('cured heights (10 um)'),title('cured geometrical profile
resulted from all bitmaps')
saveas(gcf, sprintf('%s/Geometry_Clustered.fig', data_folder));
%% Calculate residual
resClusterA = norm(z_real - z);
resClusterR = resClusterA / norm(z);
save(sprintf('%s/Residuals_in_Clustering.txt',
data_folder), 'resClusterA', 'resClusterR', '-ASCII');
save(sprintf('%s/clusterHistory.mat', data_folder), ...
'mirror_all_set', 'Time_Bitmap', 'z_real', 'clusterTime',
'resClusterA', 'resClusterR');

```

5. kmeans.m

Description: Called by “run_clustering.m”.

```

%% Clustering algorithm: kmeans

function [R, M] = kmeans(X, K, seed)
%KMEANS: K-means clustering
% idx = KMEANS(X, K) returns M with K columns, one for each mean.
Each
%     column of X is a datapoint. K is the number of clusters
% [idx, mu] = KMEANS(X, K) also returns mu, a row vector, R(i) is the
%     index of the cluster datapoint X(:, i) is assigned to.
% idx = KMEANS(X,K) returns idx where idx(i) is the index of the
cluster
%     that datapoint X(:,i) is assigned to.
% [idx,mu] = KMEANS(X,K) also returns mu, the K cluster centers.
%
% KMEANS(X, K, SEED) uses SEED (default 1) to randomise initial
assignments.

if ~exist('seed', 'var'), seed = 1; end

%
% Initialization
%
[D,N] = size(X);
% if D>N, warning(sprintf('K-means running on %d points in %d
dimensions\n',N,D)); end;

M = zeros(D, K);
Dist = zeros(N, K);
M(:, 1) = X(:,seed);
Dist(:, 1) = sum((X - repmat(M(:, 1), 1, N)).^2, 1)';
for ii = 2:K
    % maximum, minimum dist
    mindist = min(Dist(:,1:ii-1), [], 2);
    [junk, jj] = max(mindist);
    M(:, ii) = X(:, jj);
    Dist(:, ii) = sum((X - repmat(M(:, ii), 1, N)).^2, 1)';
end

% plotfig(X,M);
X2 = sum(X.^2,1)';
converged = 0;
R = zeros(N, 1);
while ~converged
    distance = repmat(X2,1,K) - 2 * X' * M + repmat(sum(M.^2, 1), N, 1);
    [junk, newR] = min(distance, [], 2);
    if norm(R-newR) == 0
        converged = 1;
    else
        R = newR;
    end
    total = 0;
    for ii = 1:K
        ix = find(R == ii);
        M(:, ii) = mean(X(:, ix), 2);
        total = total + sum(distance(ix, ii));
    end
end

```

```

% plotfig(X,M);
%   fprintf('Distance %f\n', total);
end
% pause; close all;
return

function plotfig(x,M),
    figure; plot(x(1,:),x(2:,:), 'go', 'MarkerFaceColor','g',
'LineWidth',1.5); hold on; plot(M(1,:),M(2:,:), 'rx', 'MarkerSize',12,
'LineWidth',2);
    w = 2.15; h = 2;
    for k=1:size(M,2),
        rectangle('Position',[M(1,k) M(2,k) 0 0]+w*[-1 -1 +2 +2],
'Curvature',[1 1], 'EdgeColor','r', 'LineWidth',2);
    end;
    xlim([floor(min(x(1,:))) ceil(max(x(1,:)))]);
    ylim([floor(min(x(2,:))) ceil(max(x(2,:)))]);
return

```

APPENDIX D

STUDYING THE EFFECTS OF THE NUMBER OF BITMAPS

In this appendix, the pictures of estimated geometric profile resulted from different numbers of bitmaps are presented. Since the target profile is a spherical surface, we just show the side views of estimated profile in X - Z dimensions, which clearly disclose the effects of the number of bitmaps. This appendix is referenced in Section 4.5.1 of Chapter 4.

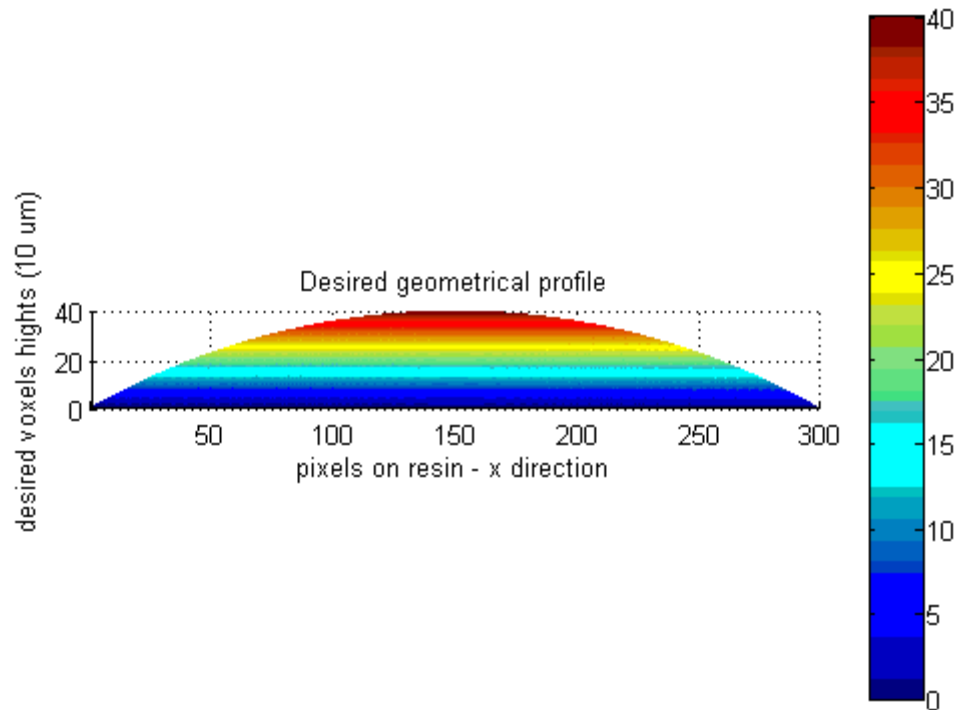


Figure D.1 Desired geometric profile (side view – XZ dimensions)

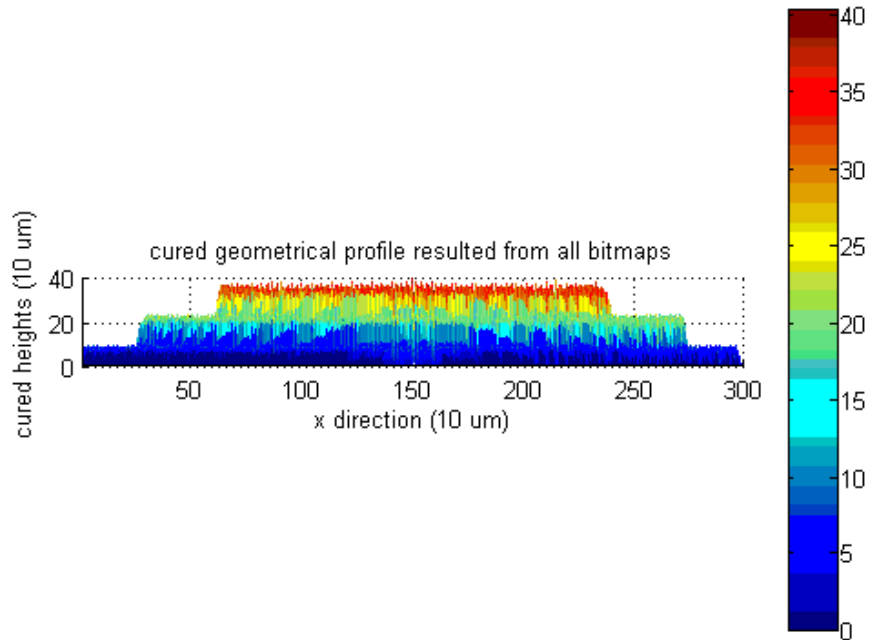


Figure D. 2 Estimated geometric profile resulted from 5 bitmaps (side view – XZ dimensions)

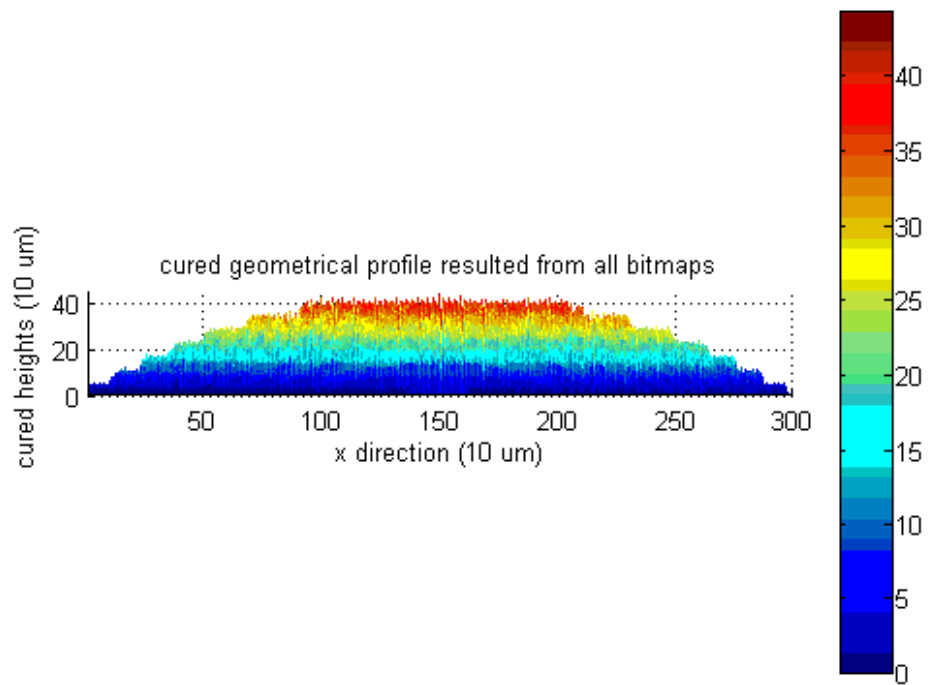


Figure D. 3 Estimated geometric profile resulted from 10 bitmaps (side view – XZ dimensions)

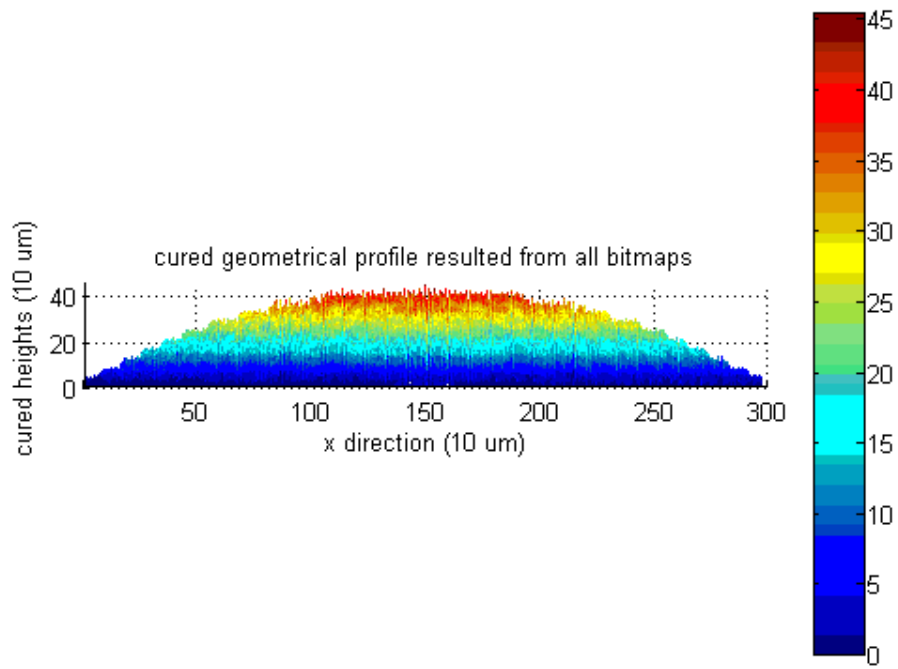


Figure D.4 Estimated geometric profile resulted from 15 bitmaps (side view – XZ dimensions)

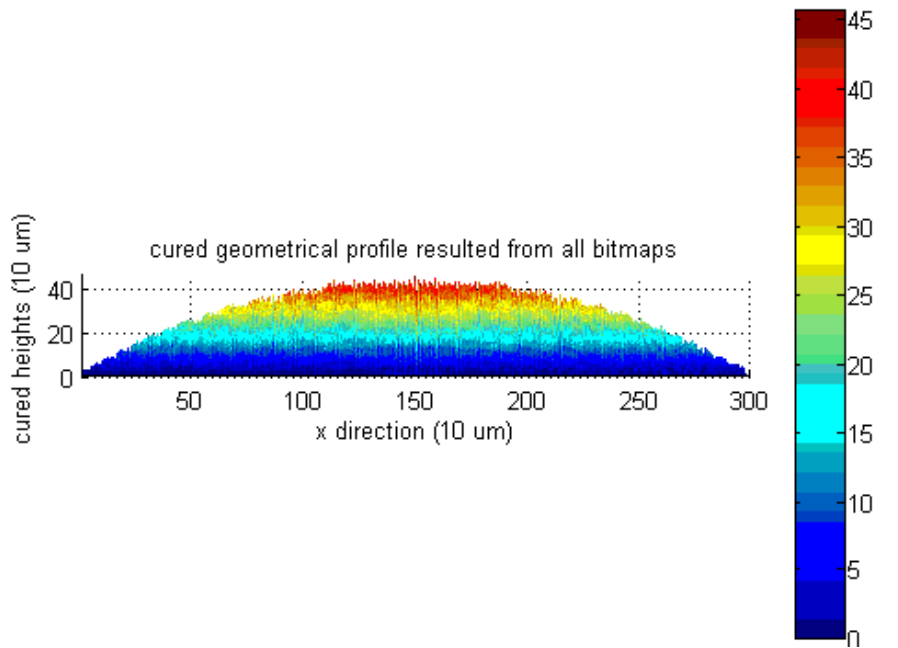


Figure D.5 Estimated geometric profile resulted from 20 bitmaps (side view – XZ dimensions)

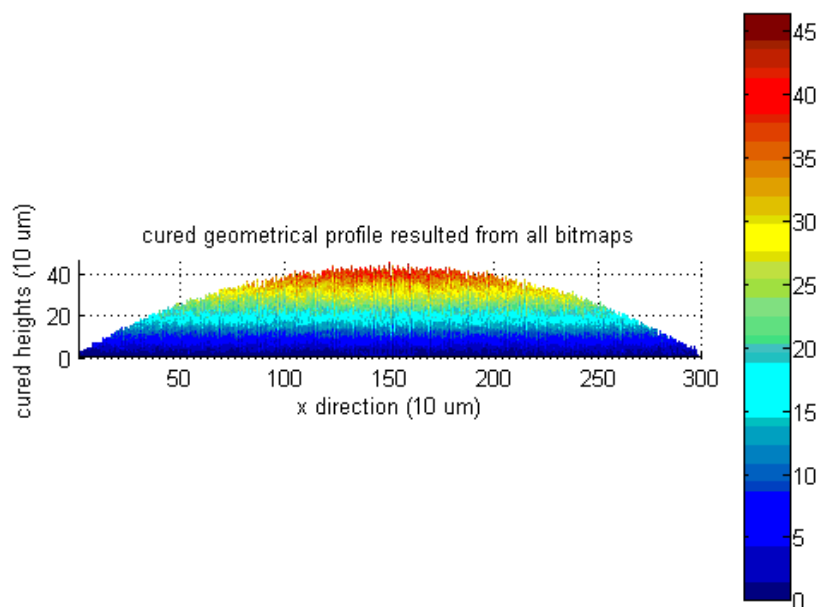


Figure D.6 Estimated geometric profile resulted from 25 bitmaps (side view – XZ dimensions)

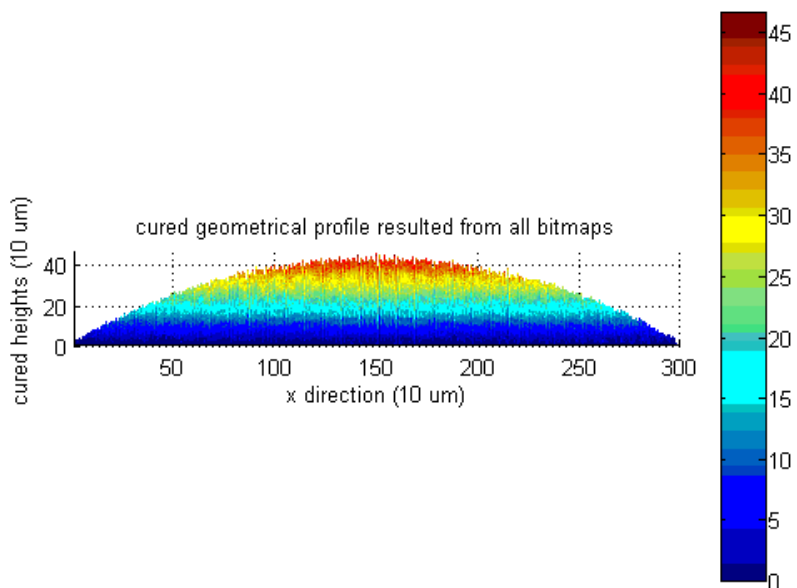


Figure D.7 Estimated geometric profile resulted from 30 bitmaps (side view – XZ dimensions)

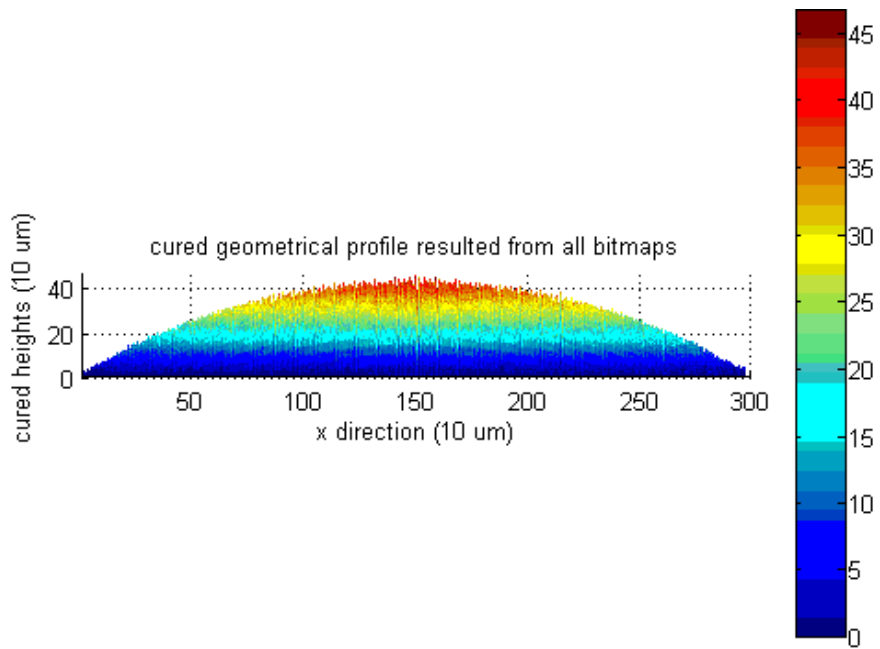


Figure D.8 Estimated geometric profile resulted from 50 bitmaps (side view – XZ dimensions)

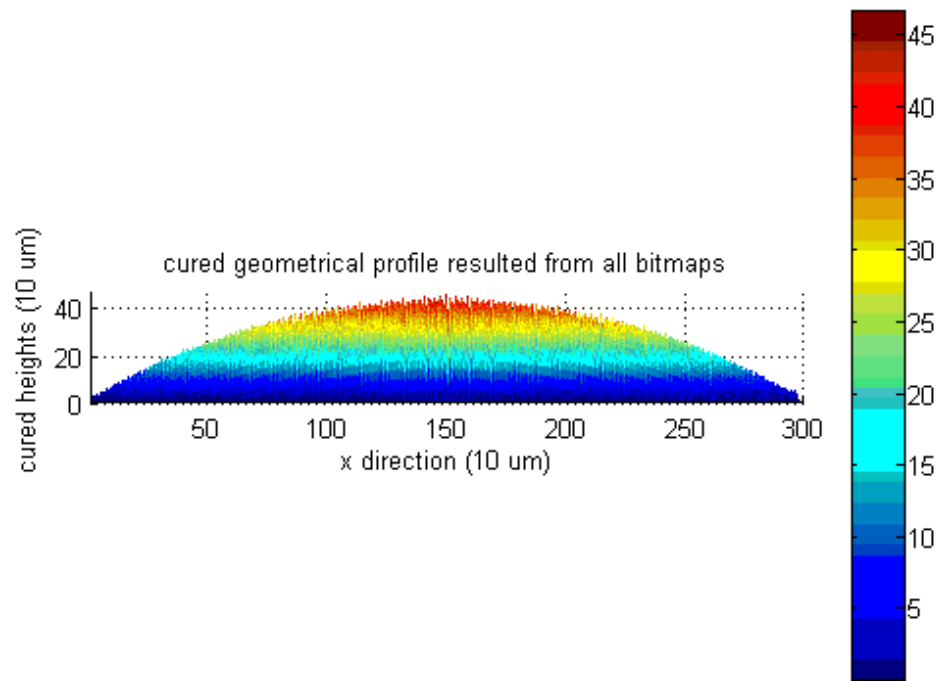


Figure D.9 Estimated geometric profile resulted from 100 bitmaps (side view – XZ dimensions)

APPENDIX E

CODE AND RESULT FOR “OPTIMIZE Z” PROBLEM

In this appendix, the code used to solve the “optimize z” problem as explained in Section 4.5.2 is presented. This code includes the following:

1. “solveOptZ.m”

(1) Function: solve the nonlinear least-squares optimization problem, with the objective to minimize the deviations between the estimated and desired voxels’ heights: $\min \|z - z_0\|$ as described by “funcLsqz.m”.

(2) Called by “run_optimization.m” as in Appendix D. Note that we should change the function “solveOpt” to “solveOptZ” before running the code.

```
function x = solveOptZ(H, z, low, up)
% Solve min ||func_zE(Hx) - z||, low <= x <= up
global result_folder;
global H;
global z;

tol = 1e-14;
maxit = 20000;
x0 = ones(size(H,2), 1);

% Solve via lsqnonlin in Matlab
display('lsqnonlin');
options = optimset('Jacobian', 'on', 'MaxIter', maxit, 'TolFun',
tol);
[x] = lsqnonlin(@funcLsqZ, x0, low, up, options);
-----
```

2. “funcLsqz.m”

(1) Function: the objective function to be optimized in the “optimize z” problem.

(2) Called by “solveOptZ.m”.

```
function [y, jacob] = funcLsqZ(x)
% func_zE(Hx)
% function y = funcLsqZ(x)

Ec = 11.593;
Dps = 99995602.7076;
Dpl = 302.8253;

global H;
global z;

E = H * x;
a = Dps;
b = Dpl/Dps/Ec;
c = 1 - Dpl/Dps;
y = a*log(b*E + c) - z;

if nargin > 1
    jacob = a * b * H ./ repmat(b*H*x+c, 1, size(H,2));
end
```

REFERENCES

- [1] Ameya Shankar Limaye. (2007). "MULTI-OBJECTIVE PROCESS PLANNING METHOD FOR MASK PROJECTION STEREOLITHOGRAPHY", *PhD dissertation, Georgia Institute of Technology*.
- [2] <http://www.laserproto.com/ServicesProcess.aspx?PageID=5> (Accessed Mar 5, 2009).
- [3] http://www.3dsystems.com/products/sla/ipro/ipro_9000XL.asp (Accessed Mar 5, 2009).
- [4] <http://xlab.me.berkeley.edu/research/microstereolith.htm> (Accessed Mar 5, 2009).
- [5] Ji Soon Choi, H.-W. K., In Hwan Lee, Tae Jo Ko and Dong-Woo Cho (2008) "Development of micro-stereolithography technology using a UV lamp and optical fiber", *The International Journal of Advanced Manufacturing Technology*.
- [6] Ikuta K, Hirowatari K (1993). "Real three-dimensional microfabrication using stereolithography and metal mold". *Proc IEEE International Workshop on Micro Electro Mechanical Systems (MEMS'93)*, pp 42–47.
- [7] Ikuta K, Ogata T, Tsubio M, Kojima S (1996). "Development of mass productive micro stereo lithography (Mass-IH Process)". *Proc of IEEE International Workshop on Micro Electro Mechanical Systems (MEMS'96)*, pp 301–306.
- [8] Ikuta K, Maruo S, Kojima S (1998). "New micro stereo lithography for freely movable 3D micro structure". *Proc IEEE International Workshop on Micro Electro Mechanical Systems (MEMS'98)*, pp 290–295.
- [9] Bertsch A., Bernhard P., Vogt C., Renaud P., (2000). "Rapid prototyping of small size objects", *Rapid Prototyping Journal*, Vol. 6, Number 4, pp. 259-266.
- [10] Bertsch A., Zissi S., Jezequel J., Corbel S., Andre J. (1997) "Microstereolithography using liquid crystal display as dynamic mask-generator", *Microsystems Technologies*, Vol 3 No 2, pp. 42-47.

- [11] Bertsch A., H. Lorenz, P. Renaud (1999) "3D microfabrication by combining microstereolithography and thick resist UV lithography". *Sensors and Actuators* 73: 14-23.
- [12] Bertsch A, Jiguet S, Berhard P, Renaud P (2003) "Microstereolithography: A Review". *Mat Res Soc Symp Proc* 758:L.L.1.1.
- [13] Bertsch A, Jezequel JY, Andre JC (1997) "Study of spatial resolution of a new 3D microfabrication process: the microstereolithography using a dynamic mask-generator technique". *J Photochem Photobiol A* 107:275–281.
- [14] Lee IH, Cho D-W, Lee ES (2004) "Development of microstereolithography systems for the fabrication of three-dimensional micro-structure". *J Korean Soc Precis Eng* 21(2):29–36.
- [15] Lee IH, Cho D-W (2003) "Micro-stereolithography photopolymer solidification patterns for various laser beam exposure conditions". *Int J Adv Manuf Technol* 22(5–6):410–416.
- [16] Lee IH, Cho D-W (2004) "An investigation on photopolymer solidification considering laser irradiation energy in micro-stereolithography". *Micro Syst Technol* 10(8–9):592–598.
- [17] Maruo S, Kawata S (1998) "Two-photon-absorbed near-infrared photopolymerization for three-dimensional microfabrication". *J Microelectromechan Syst* 7(4):411–415.
- [18] Sun H-B, Takada K, Kim M-S, Lee K-S, Kawata S (2003) "Scaling laws of voxels in two-photon photopolymerization nanofabrication". *Appl Phys Lett* 83(6):1104–1106.
- [19] Maruo S, Ikura K (1999) "Movable microstructures made by twophoton three-dimensional microfabrication". *Int Symp Micromechatron Human Sci* 173–178.
- [20] Strickler JH, Webb WW (1991) "Three-dimensional optical data storage in refractive media by two-photon point excitation". *Opt Lett* 16(22):1780–1782.

- [21] Sun H-B, Matsuo S, Misawa H (1999) "Three-dimensional photonic crystal structures achieved with two-photon-absorption photopolymerization of resin". *Appl Phys Lett* 74(6):786–788.
- [22] Pan E-Y, Pu N-W, Tong Y-P, Yau H-F (2003) "Scaffold-like microwell structures fabricated by two-photon-absorption photopolymerization". *J Med Biol Eng* 23(2):79–84.
- [23] Bhuian, B., R. J. Winfield, et al. (2007). "Pattern generation using axicon lens beam shaping in two-photon polymerisation". *Applied Surface Science* 254(4): 841-844.
- [24] Ameya Shankar Limaye. (2004). "DESIGN AND ANALYSIS OF A MASK PROJECTION MICRO-STEREOLITHOGRAPHY SYSTEM", *Master's thesis, Georgia Institute of Technology*.
- [25] Choi, Jae-Won. (2007). "Development of Projection-based Microstereolithography Apparatus Adapted to Large Surface and Microstructure Fabrication for Human Body Application" ", *PhD dissertation, Pusan National University, Korea*.
- [26] <http://www.envisiontec.com/index.php?id=33> (Accessed on Oct 15, 2008).
- [27] http://www.prototypemagazine.com/index.php?Itemid=7&id=39&option=com_content&task=view (Accessed on Oct 15, 2008).
- [28] Erdmann L., Deparnay A., Maschke G., Längle M., Bruner R., (2005) "MOEMS-based lithography for the fabrication of micro-optical components", *Journal of Microlithography, Microfabrication, Microsystems. Vol. 4(4), pp. 041601-1, -5*.
- [29] S. C. H. Thian , J. Y. H. F., Y. S. Wong, H. T. Loh, P. W. Gian and Y. Tang (2008). "Fabrication of microfluidic channel utilizing silicone rubber with vacuum casting." *Microsystem Technologies* 14(8): 1125-1135.
- [30] Su Eun Chung, W. P., Hyunsung Park, Kyoungsik Yu, Namkyoo Park, and Sunghoon Kwon (2007). "Optofluidic maskless lithography system for real-time synthesis of photopolymerized microstructures in microfluidic channels." *Appl. Phys. Lett.* 91.

- [31] Mizukami Y., Rajnaik D., Rajnaik A., Nishimura M. (2002) "A novel microchip for capillary electrophoresis with acrylic microchannel fabricated on photosensor array", *Sensors and Actuators B*, Vol. 81, pp. 202-209.
- [32] Don W. Arnold, L. e. a. (2001). "Microfluidic channel fabrication method." *US Patent 6210986*.
- [33] Itoga, K., J. Kobayashi, et al. (2008). "Second-Generation Maskless Photolithography Device for Surface Micropatterning and Microfluidic Channel Fabrication." *Anal. Chem.* 80(4): 1323-1327.
- [34] David C. Duffy, J. C. M., Olivier J. A. Schueller, and George M. Whitesides (1998). "Rapid Prototyping of Microfluidic Systems in Poly (dimethylsiloxane)." *Analytical Chemistry* 70(23): 4974 -4984.
- [35] Sager, B., and D. W. Rosen (2008). "Use of Parameter Estimation for Stereolithography Surface Finish Improvement." *Rapid Prototyping Journal* Vol 14, 213-220.
- [36] Jacobs P., 1996, "Rapid Prototyping and Manufacturing Fundamentals of StereoLithography", *Society of Manufacturing Engineers*.
- [37] Mistree F., Patel B., Vadde S (1994). "On modeling multiple objectives and multi-level decisions in concurrent design", *Proceedings ASME Design Automation conference*, Vol. 69, Issue 2, pp. 151-161.
- [38] Chatwin C., Farsari M., Huang S., Heywood M., Birch P., Young R., Richardson J., (1998) "UV microstereolithography system that uses spatial light modulator technology", *Applied Optics*, Vol 37 No 32, pp. 7514-22.
- [39] Farsari M., Claret-Tournier F., Huang S., Chatwin C., Budgett D., Birch P., Young R., Richardson J., (2000) "A novel high-accuracy microstereolithography method employing an adaptive electro-optic mask", *Journal of Material Processing Technology* Vol 107, pp. 167-172.
- [40] Hadipoespito G., Yang Y., Choi H., Ning G., Li X., (2003) "Digital Micromirror device based microstereolithography for micro structures of transparent photopolymer and nanocomposites", *Proceedings of the 14th Solid Freeform Fabrication Symposium, Austin Texas*, pp. 13-24.

- [41] Jacobs, P. 1992. Rapid Prototyping and Manufacturing: Fundamentals of StereoLithography. *Society of Manufacturing Engineers*.
- [42] Limaye A., Rosen D. 2004. Quantifying dimensional accuracy of a Mask Projection Micro Stereolithography System. *Proceedings of the 15th Solid Freeform Fabrication Symposium, Austin Texas: 481-492*
- [43] Limaye, A and Rosen, D 2007. Process planning method for mask projection micro- stereolithography, *Rapid Prototyping Journal 13(2): 76-84*
- [44] Mizukami Y., Rajnaik D., Rajnaik A., Nishimura M. (2002) "A novel microchip for capillary electrophoresis with acrylic microchannel fabricated on photosensor array", *Sensors and Actuators B, Vol. 81, pp. 202-209*.
- [45] Monneret S., Loubere V., Corbel S., (1999) "Microstereolithography using dynamic mask generator and a non-coherent visible light source", *Proc. SPIE, Vol 3680, pp. 553-561*.
- [46] Sun C., Fang N., Wu D.M., Zhang X., (2005) "Projection micro-stereolithography using digital micro-mirror dynamic mask", *Sensors and Actuators A, Vol. 121, pp. 113-120*.
- [47] Yoon, S. H. N., S.J. (2005). "Application of laser joining process for elimination of stair steps in steel laminate tooling." *International Journal of Advanced Manufacturing Technology 25(1/2): 154-159*.
- [48] Murakami, T. Y., T.; Kobayashi, G (2006). "Positive direct-mask stereolithography with multiple-layer exposure: layered fabrication with stair step reduction." *Virtual & Physical Prototyping 1(2): 73-81*.
- [49] W. Ma, W. C. B. a. P. H. (2004). "NURBS-based adaptive slicing for efficient rapid prototyping." *Computer-Aided Design 36(13): 1309–1325*.
- [50] Mäkelä A. D. a. I. (1994). "Slicing procedures for layered manufacturing techniques." *Computer-Aided Design 26(2): 119-126*.
- [51] Goodner, M. D. and C. N. Bowman (2002). "Development of a comprehensive free radical photopolymerization model incorporating heat and mass transfer effects in thick films." *Chemical Engineering Science 57(5): 887-900*.

- [52] Tang, Yanyan (2005). "Stereolithography Cure Process Modeling", *PhD dissertation, Georgia Institute of Technology*.
- [53] C. Sun, N. F., D.M. Wu, X. Zhang (2005). "Projection micro-stereolithography using digital micro-mirror dynamic mask." *Sensors and Actuators A(121): 113-120*.
- [54] A.K.Jain, M.N.Murty, and P.J.Flynn (1999), "Data clustering: a review." *ACM Comput. Surv. 31(3):264–323*.
- [55] Coleman, T.F. and Y. Li (1996), "A Reflective Newton Method for Minimizing a Quadratic Function Subject to Bounds on Some of the Variables," *SIAM Journal on Optimization, Vol. 6, Number 4, pp. 1040-1058*.
- [56] Ronald G.Askin, Jeffrey B.Goldberg (2002), "Design and Analysis of Lean Production Systems", John Wiley&Sons,Inc, *Page 44*
- [57] Shih-Hsuan Chiu, S.-H. P., Dien-Chi Wu, Chien-Hung Lin (2008). "A study of photomask correction method in area-forming rapid prototyping system." *Rapid Prototyping Journal 14(5): 285 - 292*.
- [58] Sun, C., N. Fang, et al. (2005). "Projection micro-stereolithography using digital micro-mirror dynamic mask." *Sensors and Actuators A: Physical 121(1): 113-120*.
- [59] Manseung Seo, H. K. (2007). "Lithography upon micromirrors." *Computer-Aided Design 39: 202-217*.
- [60] Chi Zhou, Y. C., Richard A. Waltz (2008). "OPTIMIZED MASK IMAGE PROJECTION FOR SOLID FREEFORM FABRICATION." Proceedings of the ASME 2008 International Design Engineering Technical Conferences and Computers and Information in Engineering Conference.
- [61] Romeijn, H. E., R.K. Ahuja, J. F. (2006). "A new linear programming approach to radiation therapy treatment planning problems." *Operations Research 54(2): 201-216*.
- [62] Gino J. Lim, J. C., and Radhe Mohan (2008). "Iterative Solution Methods for Beam Angle and Fluence Map Optimization in Intensity Modulated Radiation Therapy Planning." *OR Spectrum 30(2): 289-309*.